

[REDACTED]

**Instituut Mijnbouwschade
Groningen**

Cascadeplein 10
9726 AD Groningen

Antwoordnummer 3061
8000 WB Zwolle
0800 44 44 111
www.schadedoormijnbouw.nl
woo@schadedoormijnbouw.nl

Uitsluitend per e-mailbericht:

[REDACTED]

Kenmerk:

[REDACTED]

Datum: 21 mei 2024

Betreft: Uw Woo-verzoek

Geachte [REDACTED]

U heeft op 7 maart 2024 een verzoek ingediend bij het Instituut Mijnbouwschade Groningen (hierna: het Instituut). Middels uw verzoek wenst u informatie op grond van artikel 4.1 van de Wet open overheid (hierna: Woo) te ontvangen.

Uw verzoek

U wenst middels uw Woo-verzoek alle onderzoeken, presentaties, en andere documenten te ontvangen over onderzoek naar schade aan gebouwen door grondbewegingen verricht door de TU Delft. Daarbij denkt u specifiek aan het onderzoek van Paul Korswagen, Jan Rots e.a.

Verder wilt u ook alle documenten ontvangen waarin deze onderzoeken worden besproken binnen het Instituut. Daarbij denkt u specifiek aan de bestuursvergaderingen.

Procesverloop

Om de strekking van uw Woo-verzoek zo duidelijk mogelijk te krijgen heeft op 7 maart 2024 een telefonisch overleg plaatsgevonden tussen u en [REDACTED]

Tijdens dit overleg heeft u een toelichting gegeven op uw Woo-verzoek en is afgesproken dat het Instituut geen (concept)documenten over niet-afgeronde onderzoeken publiceert. Wel verstrekkt het Instituut aan u een overzicht van de niet-afgeronde onderzoeken.

Op 11 maart 2024 heb ik u laten weten dat ik uw verzoek in goede orde heb ontvangen en heb ik aangegeven dat ik uw verzoek binnen vier weken na ontvangst zal beoordelen.

Op 4 april 2024 heb ik de beslistermijn met twee weken verdaagd.

Bij brief van 18 april 2024 is de beslistermijn met uiterlijk twee weken opgeschort in het kader van een zienswijzeverzoek aan een derde belanghebbende.

Op 2 mei 2024 heeft telefonisch overleg plaatsgevonden tussen u en [REDACTED] Tijdens dit overleg is besproken dat het Instituut ook de oude e-mail inbox van oud-bestuurders zou doorzoeken teneinde voor uw verzoek relevante documenten te vinden. Omdat het doorzoeken van oude e-mails op locatie in Den Haag moet

plaatsvinden is afgesproken dat de beslistermijn voor nog eens twee weken is verdaagd. Het Instituut moet daarom voor 17 mei 2024 beslissen op uw verzoek.

Wettelijk kader

Uw verzoek is behandeld als een verzoek op basis van artikel 4.1 de Woo. Voor de relevante artikelen uit de Woo verwijst het Instituut naar bijlage 1.

Besluit

U heeft verzocht om openbaarmaking van alle onderzoeken, presentaties, en andere documenten over onderzoek naar schade aan gebouwen door grondbewegingen verricht door de TU Delft. Verder wilt u ook alle documenten ontvangen waarin deze onderzoeken worden besproken binnen het Instituut.

Ik heb besloten uw verzoek in te willigen met inachtneming van de toepasselijke uitzonderingsgronden. Er zijn uiteindelijk 13 documenten aangetroffen. Deze documenten zijn weergegeven in de inventarislijst. Hiervoor verwijst ik u naar bijlage 2. Zowel in de inventarislijst als in de documenten heb ik opgenomen welke uitzonderingsgrond is toegepast. Daarnaast heb ik besloten aan u een lijst te verstrekken met daarop alle niet afgeronde onderzoeken waar de TU Delft in opdracht van het Instituut nog aan werkt.

Twee van de gevonden onderzoeken zijn reeds openbaar gemaakt. De Woo is niet van toepassing op informatie die reeds openbaar is; om die reden volstaat het Instituut met een verwijzing naar de gevraagde informatie. U kunt het onderzoek 'COMPUTATIONAL MODELLING CHECKS OF MASONRY BUILDING DAMAGE DUE TO DEEP SUBSIDENCE' dat al gepubliceerd is raadplegen via: [AGE 23-10.024 \(schadedoormijnbouw.nl\)](https://schadedoormijnbouw.nl/AGE_23-10.024). Het tweede reeds openbare rapport 'Schade aan gebouwen door diepe bodemdaling en -stijging' kunt u raadplegen via: [20210302-tno-2021-r10325b-img-schade-aan-gebouwen-door-diepe-bodemdalings-en-stijging.pdf \(schadedoormijnbouw.nl\)](https://www.20210302-tno-2021-r10325b-img-schade-aan-gebouwen-door-diepe-bodemdalings-en-stijging.pdf).

Zoekslag

Graag licht ik toe hoe het Instituut heeft gezocht naar documenten die vallen onder de reikwijdte van uw verzoek. Het Instituut heeft eerst uitvraag gedaan bij de afdeling schade expertise en herstel om erachter te komen welke onderzoeken van de TU Delft er zijn; dit heeft geresulteerd in een lijst van onderzoeken. Vervolgens is ook aan deze afdeling gevraagd alle relevante documenten te overleggen en daarbij te zoeken op de termen van de lijst van onderzoeken die door de afdeling schade expertise en herstel is overhandigd. Daarna is het secretariaat van het bestuur verzocht om op dezelfde wijze te zoeken naar relevante documenten en deze te overleggen. Navraag bij het secretariaat leerde dat mogelijkerwijs relevante documenten stonden in de mailbox van oud bestuurders van het Instituut; om die reden is in Den Haag in het archief gezocht. Tot slot heb ik, als uit de documenten bleek dat er bijhorende documenten ontbraken, aan de desbetreffende medewerkers gevraagd deze alsnog naar mij te sturen.

Overwegingen

Algemene overweging

Iedereen heeft het recht om overheidsinformatie op te kunnen vragen zonder daarbij een reden te hoeven aangeven. Dit staat in artikel 1.1. van de Woo. Dit is een belangrijk recht van de burger. Daarbij is het uitgangspunt dat overheidsinformatie openbaar is, tenzij er uitzonderingsgronden zijn die dit beperken. De uitzonderingsgronden staan in hoofdstuk 5 van de Woo. Ik moet hierbij het algemeen belang van openbaarheid afwegen tegen de belangen die de uitzonderingsgronden beschermen. In het algemeen geldt hierbij de regel dat wanneer ik informatie aan u verstrek, het openbaar is voor eenieder. De Woo is niet van toepassing op informatie die al openbaar is.

Algemene uitgangspunten bij toetsing aan de uitzonderingsgronden

De toetsing aan de uitzonderingsgronden verloopt als volgt. Eerst kijk ik of één van de uitzonderingsgronden van toepassing is. Dat doe ik meestal per alinea, soms per zin. Vervolgens

kijk ik wat voor soort uitzonderingsgrond het is. Als het een absolute uitzonderingsgrond is, mag ik de informatie niet verstrekken. Als het een relatieve uitzonderingsgrond is, moet ik een afweging maken tussen het algemene belang van openbaarheid en het specifieke belang dat de uitzonderingsgrond beschermt. Daarbij weegt het belang van openbaarheid zwaar. Als ik informatie weiger, moet ik goed motiveren waarom ik dat doe.

Overwegingen

Het recht op openbaarmaking op grond van de Woo dient uitsluitend het algemeen belang van openbaarheid van publieke informatie voor de democratische samenleving, zoals neergelegd in artikel 2.5 van de Woo. Het komt iedere burger in gelijke mate toe. Daarom kan ten aanzien van de openbaarmaking geen onderscheid worden gemaakt naar gelang de persoon of de bedoeling of belangen van de verzoeker. Bij de te verrichten belangenafweging worden dan ook het algemeen belang van openbaarmaking van de gevraagde informatie betrokken en de door de uitzonderingsgrond te beschermen belangen, maar niet het specifieke belang van de verzoeker bij de kennisname van de informatie.

Toegepaste uitzonderingsgronden

In de documenten 8 t/m 13 heb ik één uitzonderingsgronden toegepast. Hier leg ik het onderstaande aan ten grondslag.

De eerbiediging van de persoonlijke levenssfeer (5.1 lid 2 sub e)

Op grond van artikel 5.1, tweede lid, aanhef en onder e, van de Woo kan ik geen informatie openbaar maken als dit de persoonlijke levenssfeer schaadt en dit belang zwaarder weegt dan het belang van openbaarheid. Het gaat om persoonsgegevens die (indirect) te herleiden zijn tot een persoon zoals namen, (e-mail)adressen, telefoonnummers en functienamen.

In de documenten waarin deze uitzonderingsgrond is toegepast gaat het om gegevens die herleidbaar zijn tot een persoon, zoals onder meer namen, e-mailadressen, functienamen en telefoonnummers. In het kader van goed werkgeverschap vind ik dat het belang van de eerbiediging van de persoonlijke levenssfeer zwaarder moet wegen dan het belang van openbaarheid. Dit ter bescherming van de privacy van de betrokken ambtenaren. Daarbij weegt mee dat het hier niet gaat om het opgeven van een naam aan een individuele burger die met een ambtenaar in contact treedt, maar om openbaarmaking voor eenieder op grond van de Woo. Daarom maak ik deze persoonsgegevens niet openbaar.

Uitgezonderd daarvan zijn de namen van medewerkers van een bestuursorgaan die wegens hun functie in de openbaarheid treden (zie o.a. ABRvS 17 november 2010, ECLI:NL:RVS:2010:BO4235). Gelet hierop is de uitzonderingsgrond niet toegepast bij de namen van de bestuursleden en de directeur van het Instituut. Deze namen worden derhalve openbaar gemaakt.

Wat betreft de namen van de deskundigen zie ik geen aanleiding om voormelde uitzonderingsgrond toe te passen. In dit verband verwijst ik naar de uitspraak van de Afdeling bestuursrechtspraak van de Raad van State van 8 december 2010 (ECLI:NL:RVS:2010:BO6617, AB 2011/55 m.nt. P.J. Stolk).

Bezwaar maken

Mogelijk bent u het niet eens met onze beslissing. U kunt hiertegen bezwaar maken door binnen zes weken na verzending van deze brief schriftelijk een bezwaarschrift in te dienen. U kunt het ondertekende bezwaarschrift sturen naar het Instituut Mijnbouwschade Groningen, Postbus 40009, 8004 DA Zwolle. Uw Woo-verzoek is bij ons geregistreerd onder kenmerk [REDACTED] Het is belangrijk dat u dit nummer in uw bezwaarschrift vermeldt.

Contact

Op onze website www.schadedoormijnbouw.nl kunt u meer lezen over het Instituut Mijnbouwschade Groningen. Met algemene vragen kunt u ons van maandag tot en met zaterdag bereiken van 8.00 tot 17.30 uur op 0800 4444 111. We vragen u het kenmerk van uw Woo-verzoek [REDACTED] bij de hand te houden als u met ons belt.

Hoogachtend,

H.C.D. (Henk) Korvinus
Voorzitter Bestuur Instituut Mijnbouwschade Groningen

Deze brief is met zorg gemaakt en heeft geen handtekening in de ondertekening omdat de brief automatisch is verwerkt.

Bijlage 1 relevante artikelen Woo

Artikel 4.1 Verzoek

1.

Eenieder kan een verzoek om publieke informatie richten tot een bestuursorgaan of een onder verantwoordelijkheid van een bestuursorgaan werkzame instelling, dienst of bedrijf. In het laatste geval beslist het verantwoordelijke bestuursorgaan op het verzoek.

2.

Een verzoek kan mondeling of schriftelijk worden ingediend en kan elektronisch worden verzonden op de door het bestuursorgaan aangegeven wijze.

3.

De verzoeker behoeft bij zijn verzoek geen belang te stellen.

4.

De verzoeker vermeldt bij zijn verzoek de aangelegenheid of het daarop betrekking hebbende document, waarover hij informatie wenst te ontvangen.

5.

Indien een verzoek te algemeen geformuleerd is, verzoekt het bestuursorgaan binnen twee weken na ontvangst van het verzoek de verzoeker om het verzoek te preciseren en is het de verzoeker daarbij behulpzaam.

6.

Het bestuursorgaan kan besluiten een verzoek niet te behandelen, indien de verzoeker niet meewerkt aan een verzoek tot precisering als bedoeld het vijfde lid. In afwijking van artikel 4:5, vierde lid, van de Algemene wet bestuursrecht wordt het besluit om het verzoek niet te behandelen aan de verzoeker bekendgemaakt binnen twee weken nadat het verzoek is gepreciseerd of nadat de daarvoor gestelde termijn ongebruikt is verstrekken.

7.

Een verzoek om informatie wordt ingewilligd met inachtneming van het bepaalde in hoofdstuk 5.

Artikel 5.1 Uitzonderingen

1.

Het openbaar maken van informatie ingevolge deze wet blijft achterwege voor zover dit:

- a. de eenheid van de Kroon in gevaar zou kunnen brengen;
- b. de veiligheid van de Staat zou kunnen schaden;
- c. bedrijfs- en fabricagegegevens betreft die door natuurlijke personen of rechtspersonen vertrouwelijk aan de overheid zijn meegedeeld;
- d. persoonsgegevens betreft als bedoeld in paragraaf 3.1 onderscheidenlijk paragraaf 3.2 van de Uitvoeringswet Algemene verordening gegevensbescherming, tenzij de betrokken uitdrukkelijk toestemming heeft gegeven voor de openbaarmaking van deze persoonsgegevens of deze persoonsgegevens kennelijk door de betrokken openbaar zijn gemaakt;
- e. nummers betreft die dienen ter identificatie van personen die bij wet of algemene maatregel van bestuur zijn voorgeschreven als bedoeld in artikel 46 van de Uitvoeringswet Algemene verordening gegevensbescherming, tenzij de verstrekking kennelijk geen inbreuk op de levenssfeer maakt.

2.

Het openbaar maken van informatie blijft eveneens achterwege voor zover het belang daarvan niet opweegt tegen de volgende belangen:

- a. de betrekkingen van Nederland met andere landen en staten en met internationale organisaties;
- b. de economische of financiële belangen van de Staat, andere publiekrechtelijke lichamen of bestuursorganen, in geval van milieu-informatie slechts voor zover de informatie betrekking heeft op handelingen met een vertrouwelijk karakter;
- c. de opsporing en vervolging van strafbare feiten;
- d. de inspectie, controle en toezicht door bestuursorganen;
- e. de eerbiediging van de persoonlijke levenssfeer;
- f. de bescherming van andere dan in het eerste lid, onderdeel c, genoemde concurrentiegevoelige bedrijfs- en fabricagegegevens;
- g. de bescherming van het milieu waarop deze informatie betrekking heeft;
- h. de beveiliging van personen en bedrijven en het voorkomen van sabotage;
- i. het goed functioneren van de Staat, andere publiekrechtelijke lichamen of bestuursorganen.

3.

Indien een verzoek tot openbaarmaking op een van de in het tweede lid genoemde gronden wordt afgewezen, bevat het besluit hiervoor een uitdrukkelijke motivering.

4.

Openbaarmaking kan tijdelijk achterwege blijven, indien het belang van de geadresseerde van de informatie om als eerste kennis te nemen van de informatie dit kennelijk vereist. Het bestuursorgaan doet mededeling aan de verzoeker van de termijn waarbinnen de openbaarmaking alsnog zal geschieden.

5.

In uitzonderlijke gevallen kan openbaarmaking van andere informatie dan milieu-informatie Voorts achterwege blijven indien openbaarmaking onevenredige benadeling toebrengtaan een ander belang dan genoemd in het eerste of tweede lid en het algemeen belang van openbaarheid niet tegen deze benadeling opweegt. Het bestuursorgaan baseert een beslissing tot achterwege laten van de openbaarmaking van enige informatie op deze grond ten aanzien van dezelfde informatie niet tevens op een van de in het eerste of tweede lid genoemde gronden.

6.

Het openbaar maken van informatie blijft in afwijking van het eerste lid, onderdeel c, in geval van milieu-informatie eveneens achterwege voor zover daardoor het in het eerste lid, onderdeel c, genoemde belang ernstig geschaad wordt en het algemeen belang van openbaarheid van informatie niet opweegt tegen deze schade.

7.

Het eerste en tweede lid zijn niet van toepassing op milieu-informatie die betrekking heeft op emissies in het milieu.

Artikel 5.2 Persoonlijke beleidsopvattingen

1.

In geval van een verzoek om informatie uit documenten, opgesteld ten behoeve van intern beraad, wordt geen informatie verstrekt over daarin opgenomen persoonlijke beleidsopvattingen. Onder persoonlijke beleidsopvattingen worden verstaan ambtelijke adviezen, visies, standpunten en overwegingen ten behoeve van intern beraad, niet zijnde feiten, prognoses, beleidsalternatieven, de gevolgen van een bepaald beleidsalternatief of andere onderdelen met een overwegend objectief karakter.

2.

Het bestuursorgaan kan over persoonlijke beleidsopvattingen met het oog op een goede en democratische bestuursvoering informatie verstrekken in niet tot personen herleidbare vorm. Indien degene die deze opvattingen heeft geuit of zich erachter heeft gesteld, daarmee heeft ingestemd, kan de informatie in tot personen herleidbare vorm worden verstrekt.

3.

Onverminderd het eerste en tweede lid wordt uit documenten opgesteld ten behoeve van formele bestuurlijke besluitvorming door een minister, een commissaris van de Koning, Gedeputeerde Staten, een gedeputeerde, het college van burgemeester en wethouders, een burgemeester en een wethouder, informatie verstrekt over persoonlijke beleidsopvattingen in niet tot personen herleidbare vorm, tenzij het kunnen voeren van intern beraad onevenredig wordt geschaad.

4.

In afwijking van het eerste lid wordt bij milieu-informatie het belang van de bescherming van de persoonlijke beleidsopvattingen afgewogen tegen het belang van openbaarmaking. Informatie over persoonlijke beleidsopvattingen kan worden verstrekt in niet tot personen herleidbare vorm. Indien degene die deze opvattingen heeft geuit of zich erachter heeft gesteld, daarmee heeft ingestemd, kan de informatie in tot personen herleidbare vorm worden verstrekt.

Bijlage 2

Inventarislijst

Nr.	Document	Beoordeling	Woo
1	Presentatie 12 juli 2018	openbaar	
2	Memo TU Delft 16 december 2020	openbaar	
3	Memo TU Delft 23 februari 2021	openbaar	
4	Rapport TU Delft 3 oktober 2022	openbaar	
5	Memo TU Delft 14 oktober 2022	openbaar	
6	Presentatie	openbaar	
7	Presentatie 5 februari 2021	openbaar	
8	Aantekeningen 5 februari 2021	gedeeltelijk openbaar	5.1.2 e
9	Bestuursvergadering 17 december 2020	gedeeltelijk openbaar	5.1.2 e
10	Bestuursvergadering 22 april 2021	gedeeltelijk openbaar	5.1.2 e
11	Bestuursvergadering 8 juni 2023	gedeeltelijk openbaar	5.1.2 e
12	Bijlage bij bestuursvergadering 23 november 2023	gedeeltelijk openbaar	5.1.2 e
13	Bestuursvergadering 23 november 2023	gedeeltelijk openbaar	5.1.2 e

Onderzoek oorzaken schade Groningen

12 juli 2018

Piet van Staalanduin, Karel Terwel, Jan Rots

Aanleiding

- Discussie over de voormalige contour (wel/niet vergoeden schade)
- Review door TU Delft van onderzoeken Arcadis (juli 2016)
- Als buiten contour bevingen niet tot schade aanleiding geven, wat zijn dan wel de oorzaken?
- Dus: *duiden* van de diverse oorzaken van schade aan gebouwen

Onderzoeksvergadering

Wat is de (meest waarschijnlijke) oorzaak of wat zijn (de meest waarschijnlijke) oorzaken van de gemelde schades in het onderzoeksgebied?



Uitvoering

Onderzoeksteam TU Delft: Piet van Staalduin, Karel Terwel, Jan Rots

Deskundigenteam: Huibert Borsje, Karel Terwel, Roel Schipper, Bert Everts, Simon Wijte

Mentoren: Jan Maertens, Johan Blaauwendraad

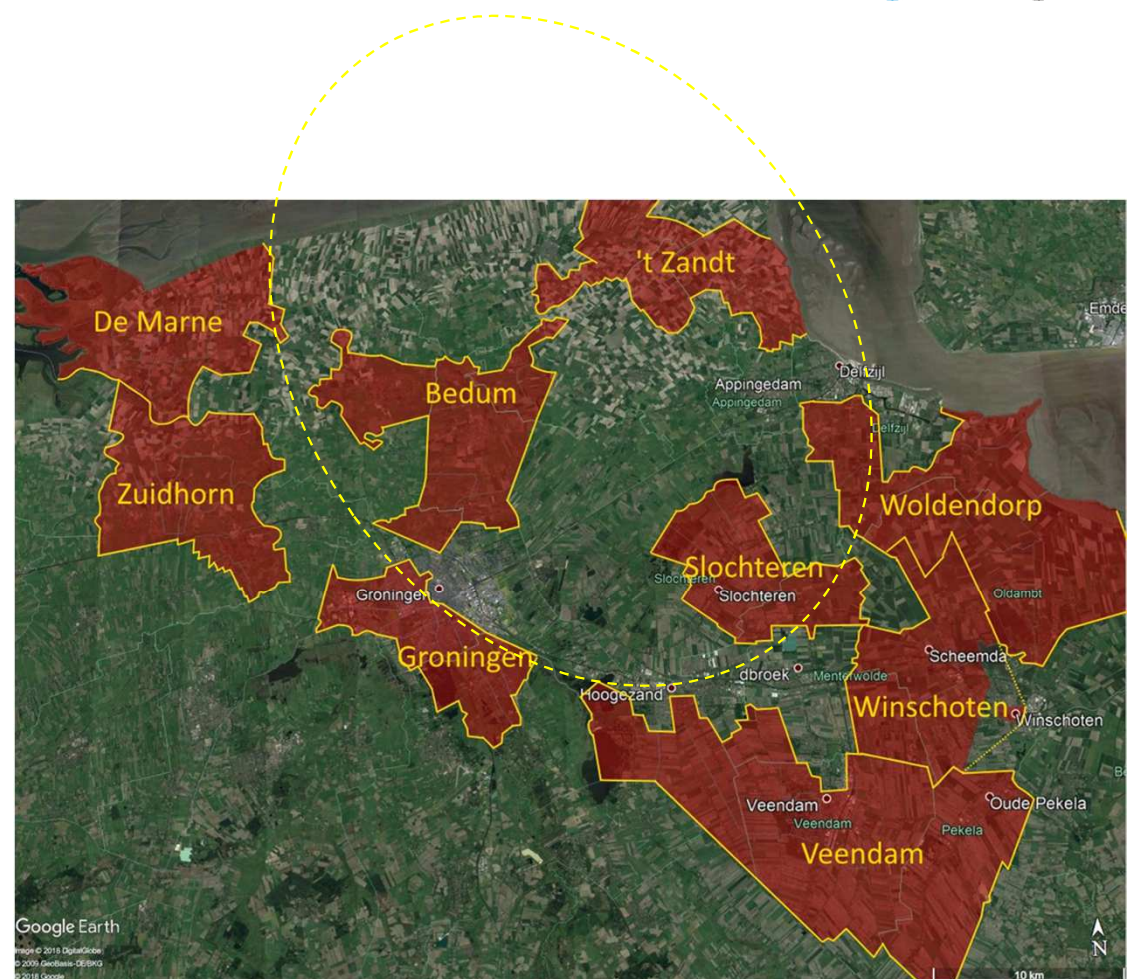
Doelstellingen

1. Duidelijkheid en duiding bieden over de oorzaken en hun invloed op de schade aan gebouwen (*oorzakelijk verband en toerekenbaarheid*)
2. Enkelvoudige oorzaken èn meervoudige oorzaken beschouwen
3. Zo veel mogelijk relevante achtergrondinformatie beschouwen over de schade en over de schadecontext: gebouw, bodem en omgeving
4. Onderzoek ter plaatse uitvoeren waar dit nodig is om onduidelijkheden op te lossen (vooral fundering en bodem)
5. Nieuwe inzichten benutten over het ontstaan van schade door o.m. bevingen

Uitvoering

9 onderzoeksgebieden, 3 binnen de voormalige contour en 6 buiten de voormalige contour

Onderzoek aan de hand van 69 cases, (complexe) schadegevallen, brede variëteit aan gebouwtypen en bouwjaren



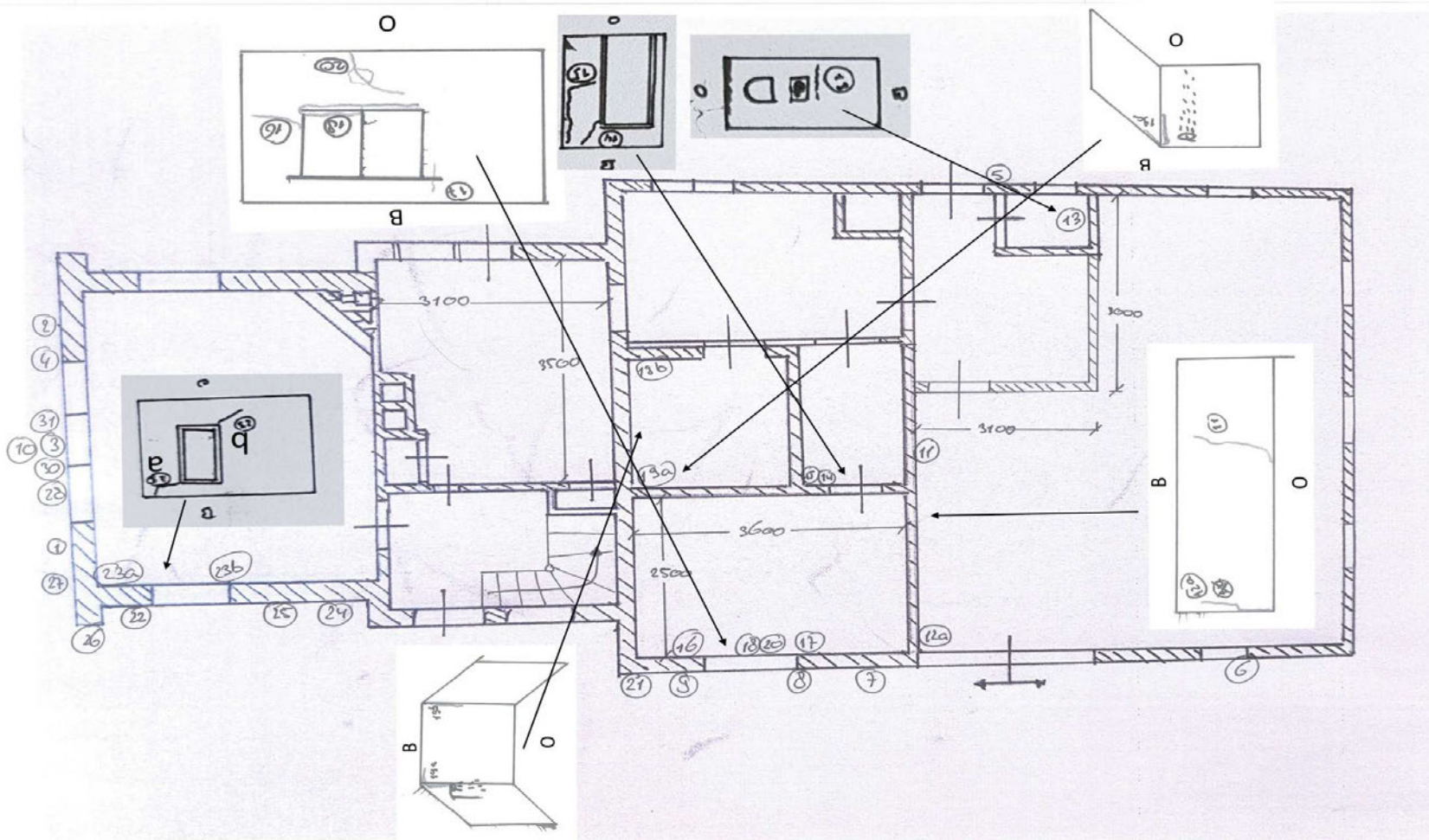
Uitvoering

Startpunt zijn beschikbare schadeopname rapporten

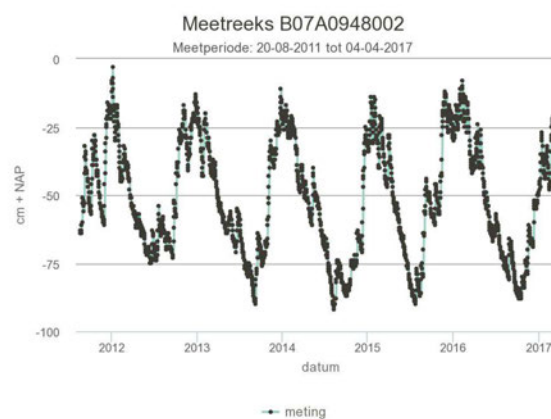
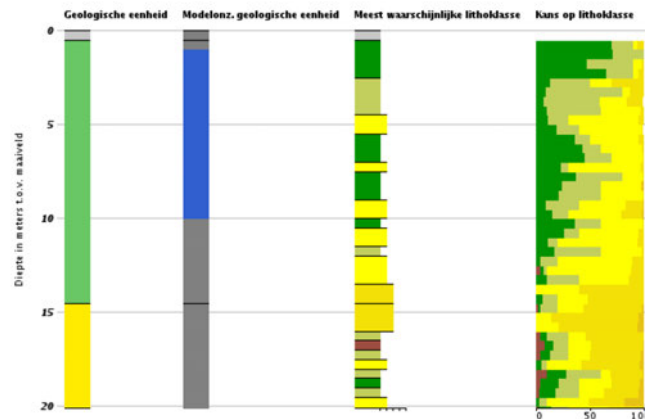
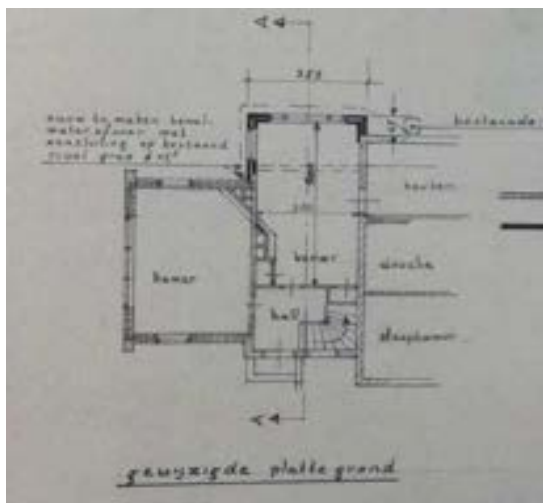
En verder:

- Bronnenonderzoek gebouwen en bodem (bouwdossiers, boringen)
- Inzet van InSAR data (satellietwaarneming) met oog op bodemdaling
- Grond/funderingsonderzoek en zettingsmetingen ter plaatse
- Bepaling invloed alle historische geïnduceerde bevingen (vanaf 1986)
- Oriënterend modelonderzoek naar invloed lichte bevingen op schade

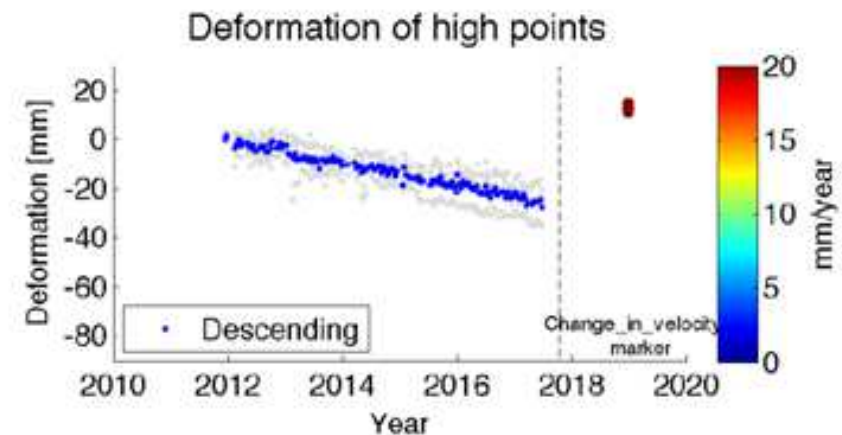
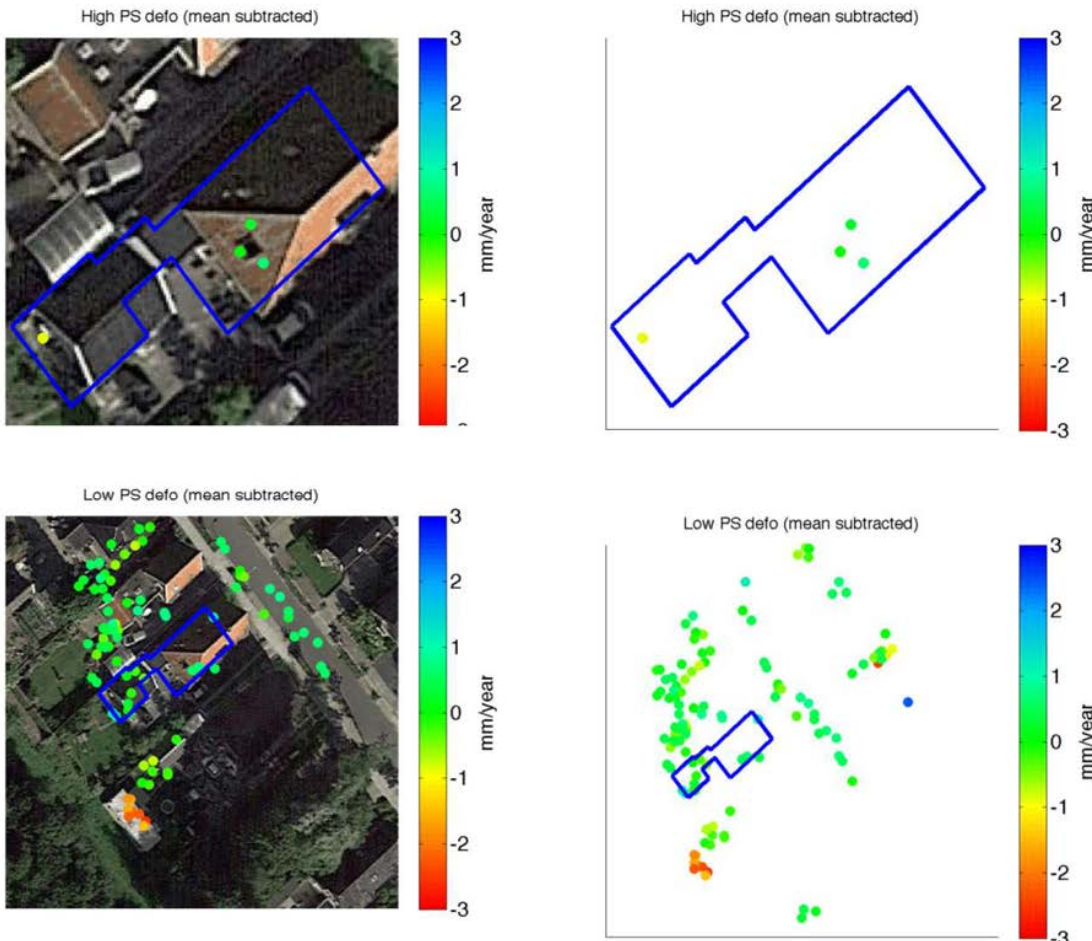
In kaart brengen van schades



Bronnenonderzoek gebouwen

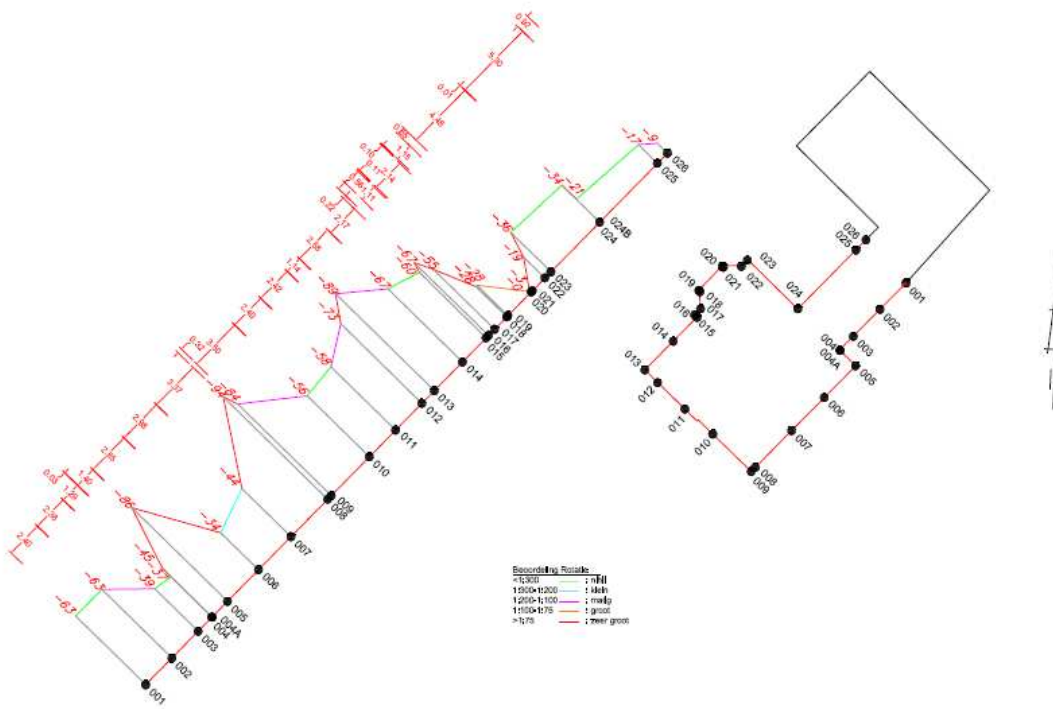


InSAR data



InSAR data geven inzicht in zakkingsgedrag van een pand gedurende de tijd en in zakkingsgedrag van de bodem in de directe omgeving

Aanvullend onderzoek ter plaatse



Lintvoegwaterpassingen (zettingsmetingen)

Aanvullend onderzoek ter plaatse

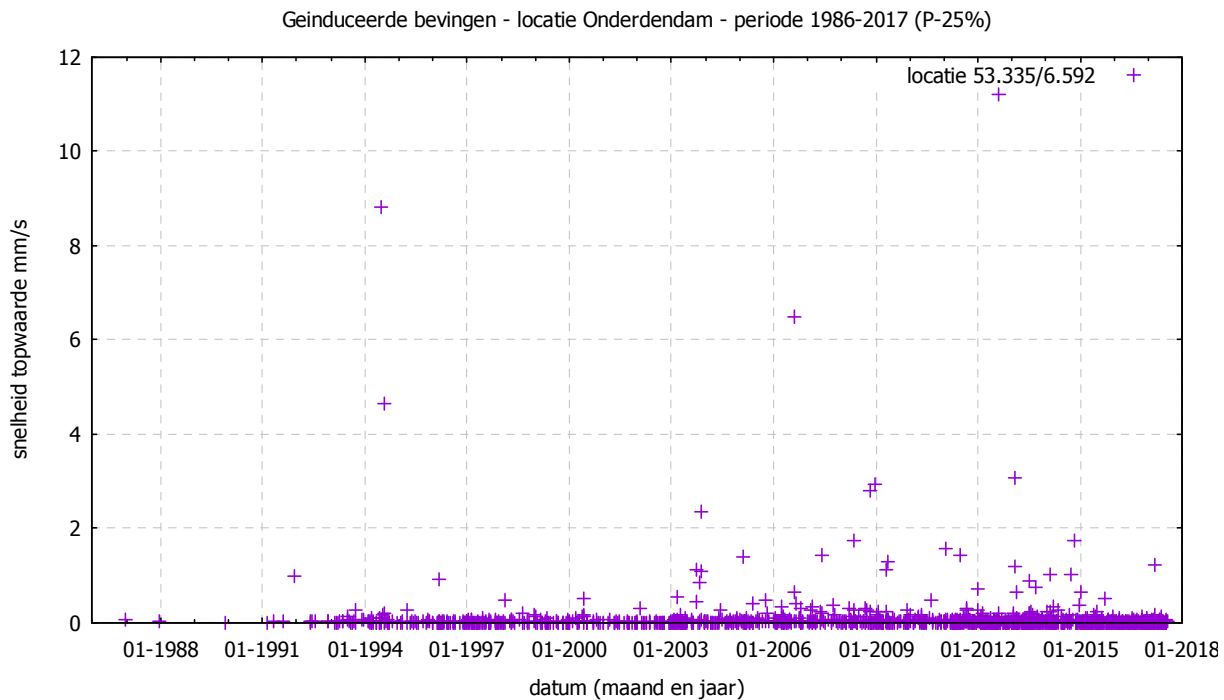


Ondiep grondonderzoek (handboringen)



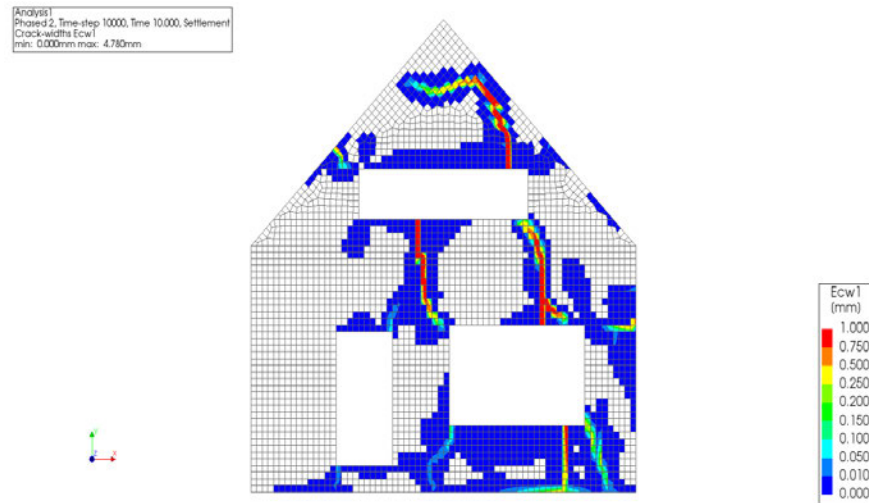
Funderingsinspecties

Geïnduceerde bevingen 1986-2017

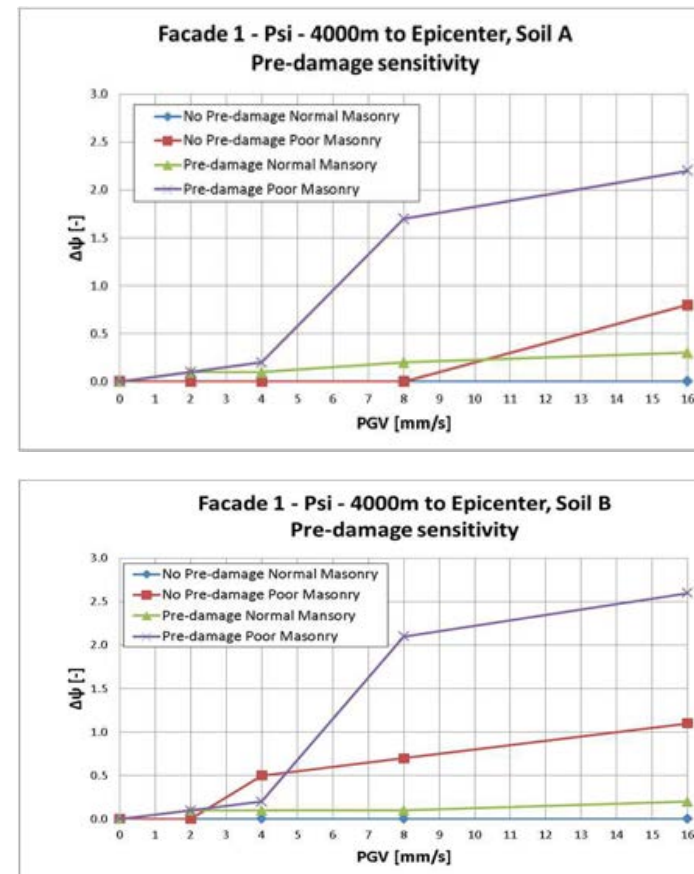


Trillingssterkte van alle historische bevingen afzonderlijk per locatie teruggerekend

Modelberekeningen



Triggerwerking is een belangrijk aspect bij bevingen – ontstaan van schade bij geringe trillingsnelheid in combinatie met een spanningsituatie met een andere oorzaak



Cases

- Bevatten ruim 2300 schades
- Schades afzonderlijk beoordeeld door deskundigenteam
- Per schade zijn steeds ca. 40 mogelijke schadeoorzaken (TNO methodiek) onderzocht met als doel: *verifiëren of falsificeren*
- Bepaling oorzakelijk verband op basis van '*best verklarende scenario's*' met één of meer oorzaken
- Schatting van de '*technische toerekenbaarheid*': aandeel van een oorzaak in het ontstaan van de schade

Resultaten – oorzakelijk verband



Meerderheid van oorzaken in scenario's:

- Gebouw gebonden oorzaken (onafhankelijk van locatie en fundering)
- Ongelijkmatige zettingen (fundering/bodem en bodemvervorming door gebouw)

Andere oorzaken in scenario's:

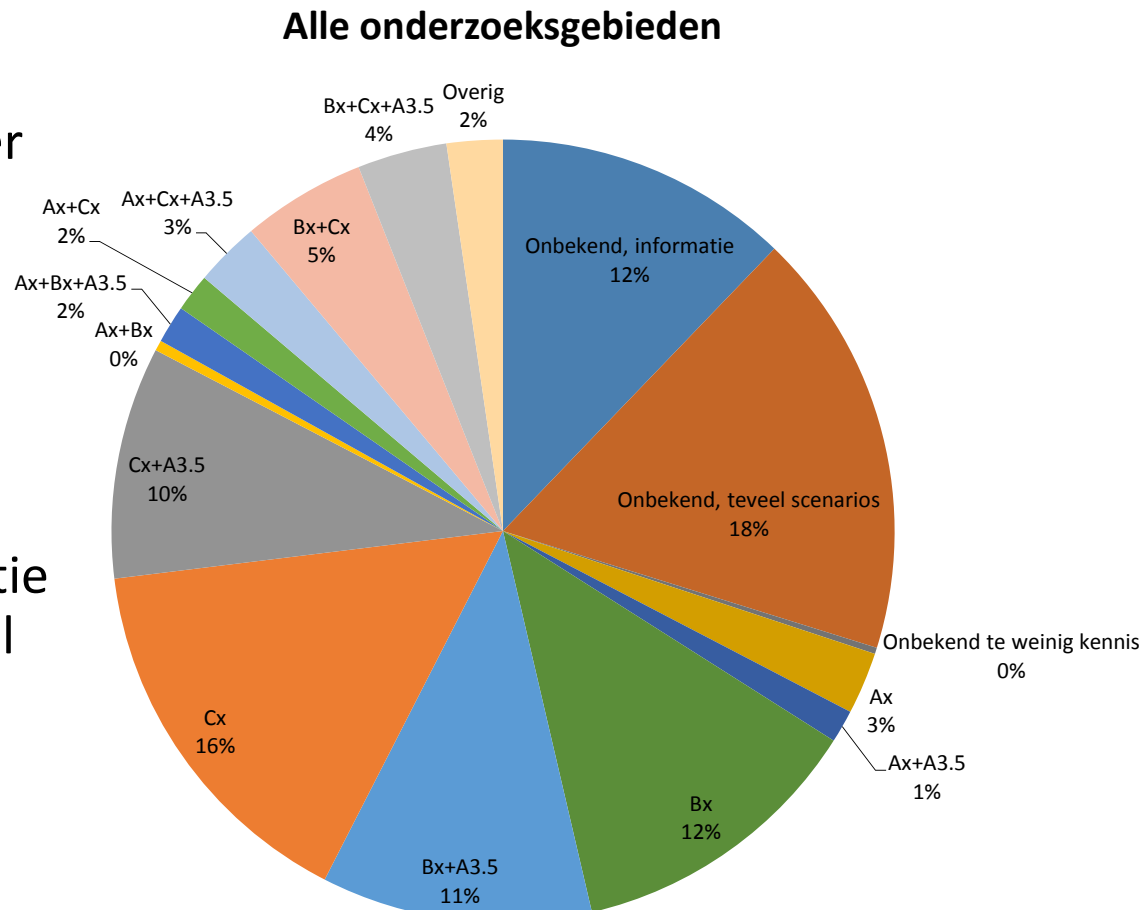
- Bevingen hebben voornamelijk rol als *trigger* bij ontstaan schade
 - Ook bij zeer lage trillingssnelheid mogelijk!
 - Andere onderliggende oorzaken zijn noodzakelijke voorwaarde
- *Directe* rol van bevingen is er alleen in specifieke situaties, m.n. binnen contour
- Zettingen door externe oorzaken (peilaanpassingen): in enkele specifieke situaties
- Diepe bodemdaling speelt geen rol in termen van vervorming van de bodem
- Stapeling van mijnbouwactiviteiten speelt in het algemeen geen rol

Resultaten – samenstelling scenario's

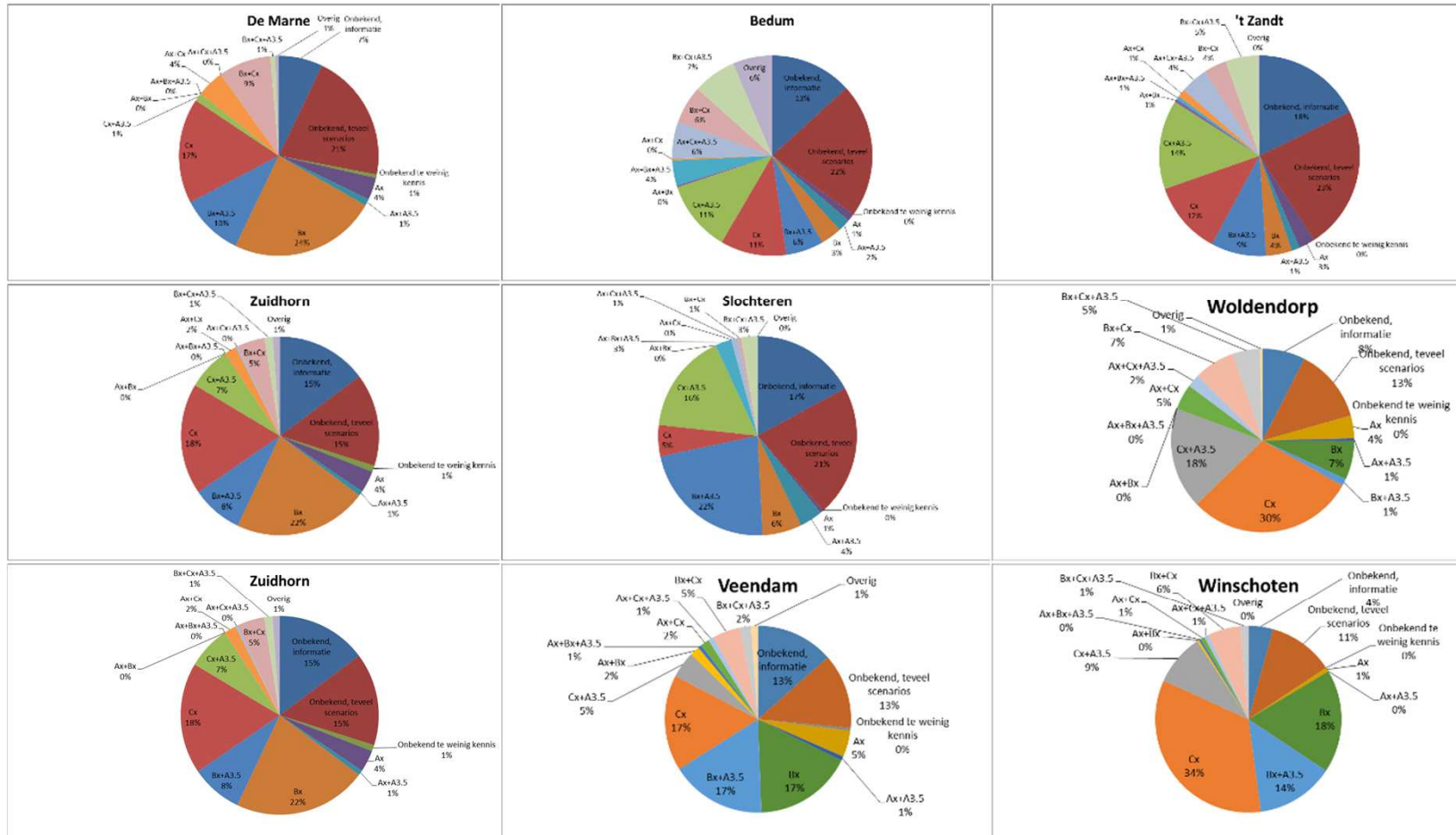
Best verklarende scenario's voor ongeveer 70 % van de schades vastgesteld.

In andere 30 %:

- te veel plausibele scenario's of
- onvoldoende informatie over de schade (vooral binnen contour)



Resultaten – samenstelling scenario's



Toerekenbaarheid – gebouwtype en bouwjaarklasse

	Kleine afstand tot epicentra			Grote afstand tot epicentra		
	Gebouw gebonden	Bevingen	Zetting	Gebouw gebonden	Bevingen	zettingen
B	middelmatig	Klein/middelmatig	middelmatig	middelmatig	(vrijwel) geen	middelmatig
V	middelmatig	Klein/middelmatig	middelmatig	middelmatig	zeer klein	middelmatig
T	middelmatig	Klein/middelmatig	klein	middelmatig	zeer klein	klein

	Kleine afstand tot epicentra			Grote afstand tot epicentra		
	Gebouw gebonden	Bevingen	Zetting	Gebouw gebonden	Bevingen	zettingen
<1900	middelmatig	Klein/middelmatig	middelmatig	middelmatig	(vrijwel) geen	middelmatig
1900-1940	middelmatig	Klein/middelmatig	middelmatig	middelmatig	(vrijwel) geen	middelmatig
1940-1970	middelmatig	Klein/middelmatig	klein	middelmatig	zeer klein	middelmatig
>1970	middelmatig	Klein/middelmatig	klein	groot	zeer klein	klein

Toerekenbaarheid – gebouwtype en bouwjaarklasse

	Kleine afstand tot epicentra			Grote afstand tot epicentra		
	Gebouw gebonden	Bevingen	Zetting	Gebouw gebonden	Bevingen	zettingen
B	middelmatig	klein/middelmatig	middelmatig	middelmatig	(vrijwel) geen	middelmatig
V	middelmatig	klein/middelmatig	middelmatig	middelmatig	zeer klein	middelmatig
T	middelmatig	klein/middelmatig	klein	middelmatig	zeer klein	klein

orde 33 %

orde 1% - 10 %

	Kleine afstand tot epicentra			Grote afstand tot epicentra		
	Gebouw gebonden	Bevingen	Zetting	Gebouw gebonden	Bevingen	zettingen
<1900	middelmatig	klein/middelmatig	middelmatig	middelmatig	(vrijwel) geen	middelmatig
1900-1940	middelmatig	klein/middelmatig	middelmatig	middelmatig	(vrijwel) geen	middelmatig
1940-1970	middelmatig	klein/middelmatig	klein	middelmatig	zeer klein	middelmatig
>1970	middelmatig	Klein/middelmatig	klein	groot	zeer klein	klein

orde 33 %

orde minder dan 1 %

Resultaten – bredere geldigheid

- Onderzoek geeft een realistisch beeld van schadeoorzaken en aandelen van oorzaken bij de onderzochte schadegevallen
- Conclusies over oorzaken van schade (in grote lijnen) in veel gevallen van toepassing op andere meldingen van schade in deze gebieden en onder vergelijkbare omstandigheden
- Beeld over de rol van gebouwgebonden oorzaken en ongelijkmatige zettingen bij schade in gebouwen heeft bredere geldigheid (provincie of zelfs breder)

Aanbevelingen

1. Leg bestaande schade aan panden beter vast.
2. Grottere rol voor lintvoegwaterpassingen bij beoordeling ongelijkmatige zettingen
3. Maak onzekerheden in de beoordeling van bouwkundige schades expliciet
4. Gebruik modelvorming om meer inzicht te krijgen in gevoeligheid voor bevingen
5. Breid bestaande monitoringprogramma's voor bodemdaling uit en maak meer gebruik van beschikbare nieuwe monitoringtechnologie.
6. Stel de sensornetwerken voor het meten van trillingen van TNO open voor breder gebruik
7. Verbeter het inzicht in actuele grondwaterstanden bij kwetsbare objecten aanzienlijk
8. Verbeter het inzicht in de complexe wisselwerking tussen grondwaterstanden en ondiepe en diepe bodemdaling en bevingen

Resultaten - toerekening

Toerekenbaarheid is alleen indicatief en kwalitatief aangegeven

Kwalificatie	Orde van grootte
(vrijwel) geen	minder dan 1 %
zeer klein	tussen 1 % en 10 %
klein	tussen 10 % en 33 %
middelmatig	tussen 33 % en 66 %
groot	tussen 66 % en 90 %
zeer groot	tussen 90 % en 99 %
(vrijwel) volledig	groter dan 99 %

Date 16/12/2020
 Internal reference TUD_MemoSubsidenceModelling_ConceptV1
 Authors Jan G. Rots, Paul Korswagen Eguren, Michele Longo
 E-mail J.G.Rots@tudelft.nl, P.A.KorswagenEguren@tudelft.nl
 Document name Computational modelling checks of masonry building
 damage due to deep subsidence
 Document type Memorandum



Management samenvatting

IMG heeft TNO en TU Delft gevraagd advies uit te brengen over criteria ter beoordeling van schade ten gevolge van diepe bodemdaling bij de gasopslag Norg en het Groningerveld. Componenten onder het advies zijn een studie naar de mate van verticale en horizontale bodemvervorming aan het maaiveld, een literatuurstudie naar bestaande kennis over de respons van gebouwen op zo'n bodemvervorming en de kans op schade, en deze modelstudie. De verwachting is dat de opgetreden of nog op te treden maaiveldvervormingen ten gevolge van diepe bodemdaling bij Norg en het Groningerveld ruim onder de grenswaarden liggen waarbij schade zou kunnen optreden. De beschikbare kennis uit literatuur, bijv. [1], hoofdstuk 12.4 uit [2], en [3,4], gaat uit van empirische modellen die een gebouw als een eenvoudige ligger schematiseren, in combinatie met een impliciet rek-criterium voor schade. Hoewel breed toegepast, kunnen nog steeds vragen bij deze methode worden geplaatst, bijvoorbeeld ten aanzien van de bepaling van rekken in het metselwerk en de objectiviteit van het begrip "kritische rek" als schademaat.

Om extra zekerheid in te bouwen is een aanvullende modelstudie uitgevoerd. Hierbij is een expliciet schade-criterium gehanteerd (de 'psi'-benadering [5] die rechtstreeks scheurwijdte, scheurlengte en scheuraantal in zich bergt en daarmee kan discrimineren binnen de laagste schadeklasse) in combinatie met conservatieve, worst-case model-aannames. Deze notitie doet verslag.

De aanpak is drie-laags, op basis van de eindige elementenmethode. Het begint met een groot model waarin een denkbeeldig gasveld wordt leeggetrokken of een denkbeeldige gasopslag wordt opgepompt. De vervormingen worden doorgegeven aan een kleiner model nabij de oppervlakte, en vervolgens aan een detailmodel van een metselwerkgevel. Het model blijkt krommingen en horizontale rekken aan het maaiveld goed te kunnen voorspellen. Het is gekalibreerd aan metingen bij Norg en analytische geo-mechanische studies van TNO. Het is vervolgens bruikbaar in gekoppelde, semi-gekoppelde of ontkoppelde berekeningen [6] van de gevel. De aannname van ontkoppelde berekeningen is de meest ongunstige. Hierbij wordt verondersteld dat alle grondvervorming (zowel verticaal als horizontaal) volledig wordt doorgegeven aan het gebouw. In werkelijkheid heeft het gebouw stijfheid en massa en zal daardoor aanmerkelijk minder vervormen dan de grond ter plaats van het maaiveld. Naast dit meest ongunstige scenario zijn variatiestudies uitgevoerd waarbij van niet 100% maar resp. 75, 50, 25 en 0% van de horizontale grondvervorming wordt overgedragen op het gebouw. Uit literatuur is bekend dat slechts een klein percentage horizontale overdracht reëel is, indicatie maximaal 30% [7]. Ook is de locatie van het gebouw op de meest ongunstigst denkbare plek in de dalingskom aangenomen, ter plaatse van de grootste kromming en horizontale rek, zowel voor neerbuiging (sagging) als opbuiging (hogging). Verschillende gevels zijn onderzocht, met aanname van zwakke metselwerkeigenschappen.

Het resultaat is dat de marge (reserve) tot het ontstaan van een eerste zichtbare scheur varieert van een factor 5,5 tot 110 voor de onderzochte casussen. De factor 5,5 correspondeert met de most worst case, 100% overdracht van de horizontale rekken, voor hogging en een lange gevel. Voor de casussen met 35% horizontale overdracht (vergelijkbaar met genoemde 30% uit [7]) is dit een factor 16.

De resultaten ondersteunen de algemene bevinding dat schade door directe diepe bodemdaling bij Norg en het Groningerveld extreem onwaarschijnlijk is.

Report (draft version, 16 december, 17h, literature list and some text to be updated)

In the recent years, gas extraction in Groningen region, in the Netherlands, is leading to man-induced earthquakes which are causing structural and aesthetical damage to masonry buildings. Together with earthquakes, gas extraction through fracking process could lead to subsidence of the subsoil.

This memo provides preliminary insights over possible damage on masonry façades generated by settlement profiles that could be typically associated to subsidence due to gas extraction.

Soil Model Description

For the evaluation of the subsidence, a 3-tiered approach method is employed. The settlement profile produced by the shrinkage/expansion of the underground soil, is simulated via a soil model that includes the location where such process takes place. Thus, a soil block 8x3 km (named as Deep Soil Model) is numerically modelled by the software DIANA FEA 10.4 [1]. The soil model is represented in 2D in plane strain condition (infinite length over the thickness) and it is divided in different horizontal layers over the height. Material properties and thickness of the soil layers are specified in Appendix A. An overview of the Deep Soil Model is depicted in Figure 1, while its mesh is shown in Figure 2. The model is subjected to gravity load (after initializing the soil stress condition) and to a prescribed strain applied to an area of 250x200 m located at the centre of the bottom edge of the model. The strain is applied in both horizontal (X) and vertical (Y) direction with an amplitude of 0.5%. Both shrinkage and expansion situations are analysed.

Quadratic 8-noded plane strain elements (CQ16E and CT12E) are used to model the soil. The timber beams at the roof level are modelled with Class-III beam element (CL18B). Curved composed line elements (CL3CM) are employed for the extrapolation of the force in the single elements. The model is restrained vertically at the base and horizontally at the two sides. The mesh ranges from 50x50 m to 5x5 m.

Contour plots of displacement and horizontal strain generated by the Deep Soil Model, are depicted in Figure 3, Figure 4 and Figure 5. Results at the surface of the model are plotted in Figure 6.



Figure 1. Deep Soil Model overview.



Figure 2. Deep Soil Model mesh overview.

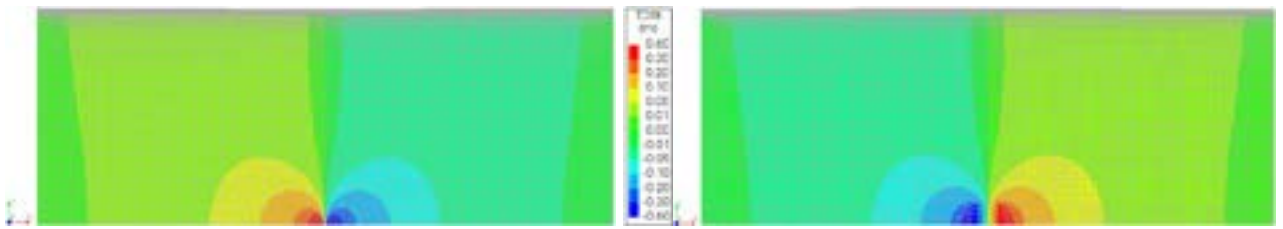


Figure 3. Horizontal displacement Deep Soil Model subjected to shrinkage (left) and expansion (right). Deformed mesh magnified x200.

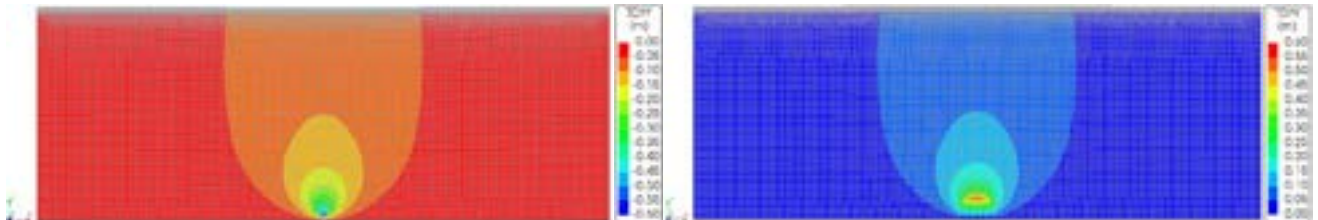


Figure 4. Vertical displacement Deep Soil Model subjected to shrinkage (left) and expansion (right). Deformed mesh magnified x200.

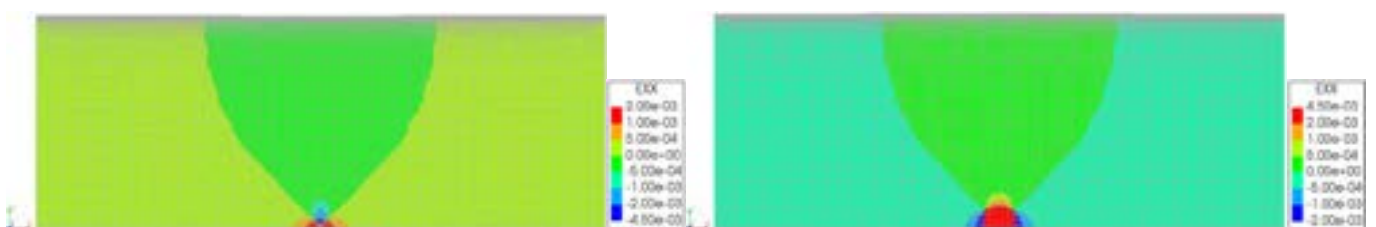


Figure 5. Horizontal strain Deep Soil Model subjected to shrinkage (left) and expansion (right). Deformed mesh magnified x200.

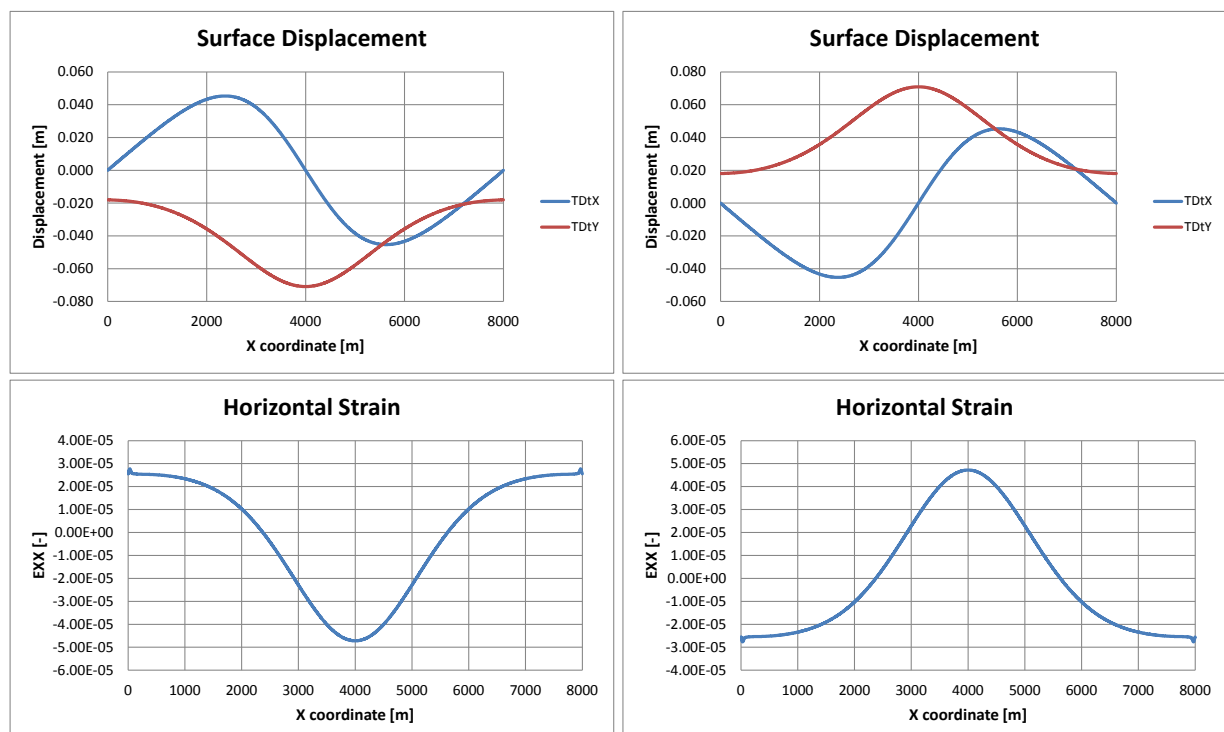


Figure 6. Displacements and horizontal strain of surface of Deep Soil Model subjected to shrinkage (left) and expansion (right).

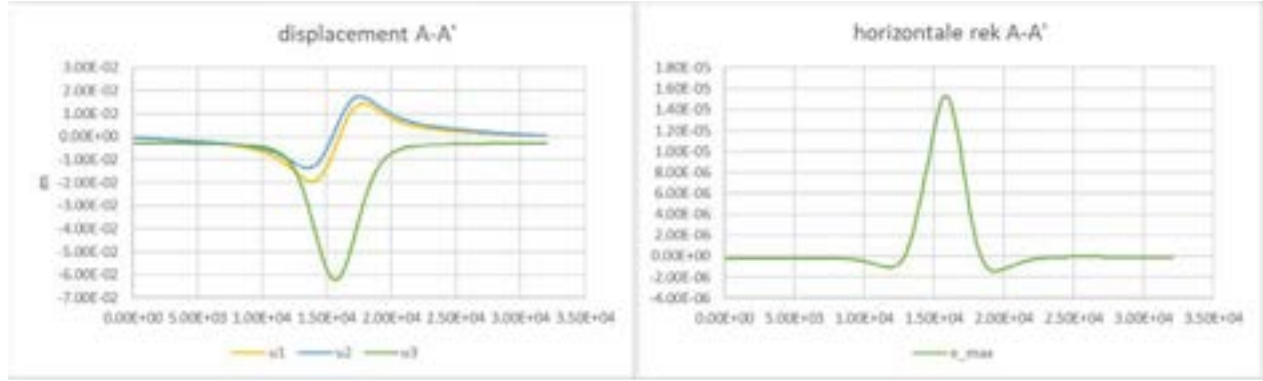


Figure 7. Displacements and strain obtained from analytical calculations at the location of Norg [2].

The Deep Soil Model results show a good agreement with the analytical results provided in [2]. In order to evaluate the effects of the horizontal strain to a set of façades, with an amplitude similar to what evaluated analytically in [2], the Deep Soil Model results are scaled to the analytical one for the location of Norg. Scaled results of displacement and strains are shown in Figure 8.

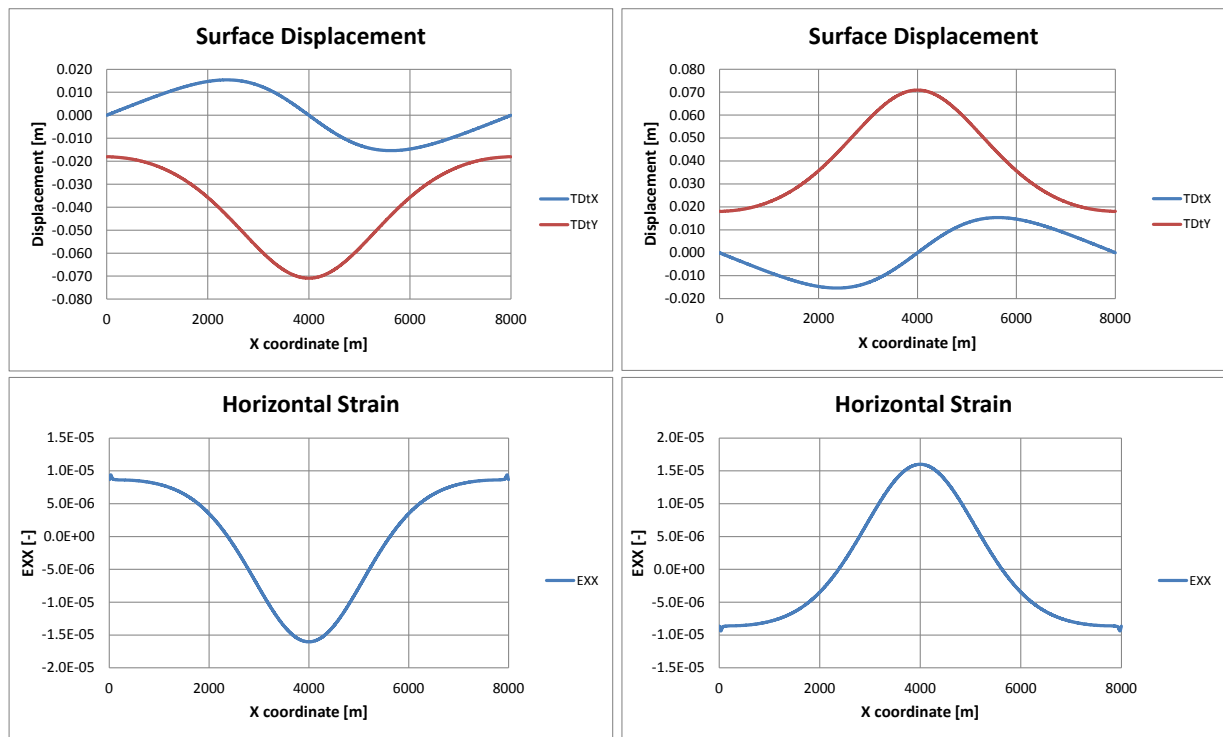


Figure 8. Displacements and horizontal strain of surface of Deep Soil Model scaled to analytical solution amplitude. Shrinkage (left) and expansion (right).

Since the mesh of Deep Soil Model is too coarse to be able to include directly the surface displacements to the bottom of a façade, they are “filtered” through a smaller soil block with finer mesh. The model is a portion of the Deep Soil Model, specifically the portion at the surface located in the middle of the model. It has a dimension of 300x30 m. The displacements at this location (Figure 9), are extrapolated from the Deep Soil Model and directly transferred to the Shallow Soil Model. The area in the middle of the model is chosen. Such location can be considered as the worse-case position (Figure 10). In fact, highest curvature and horizontal stress are found. Displacement at this location is thus included as input in the smaller soil model. The Shallow Soil Model has a finer mesh (1x1 m) in order to better capture the displacement at the surface. An overview of the model and its mesh are shown in Figure 11 and Figure 12. In a similar fashion as done between Deep and Shallow model, the displacements at the foundation in the Shallow model (Figure 13) are directly assigned as input in the plane stress façade models. The input for the façade models is plotted in Figure 14.

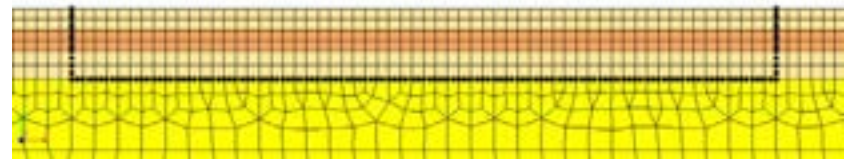


Figure 9. Location of output points in the Deep model used as input in the Shallow model.

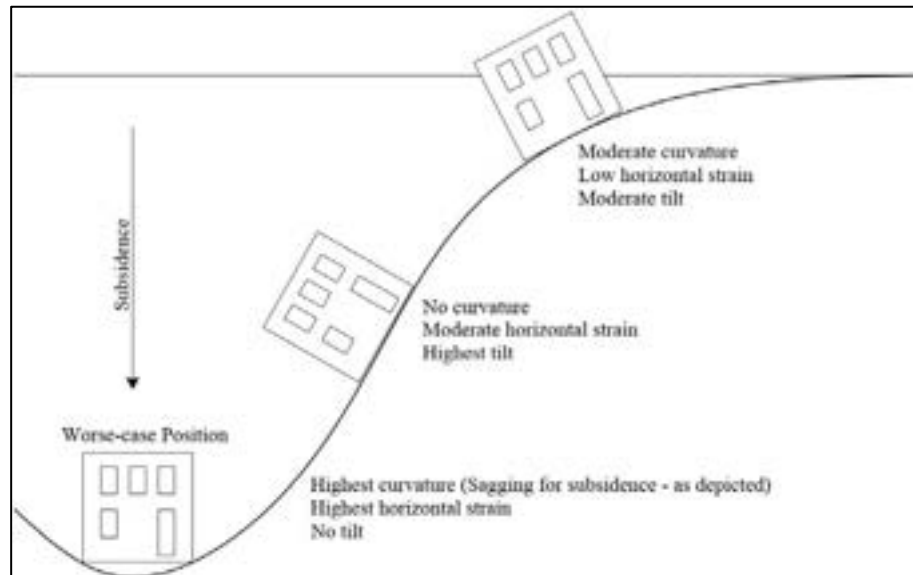


Figure 10. Comparison of a building placed at different locations close to the subsidence.

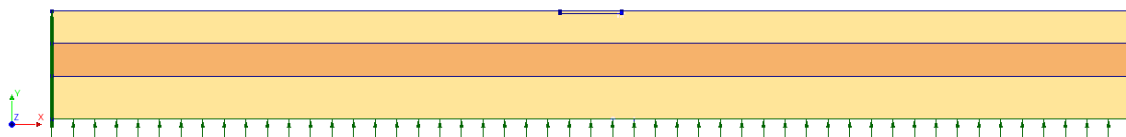


Figure 11. Shallow Soil Model overview.

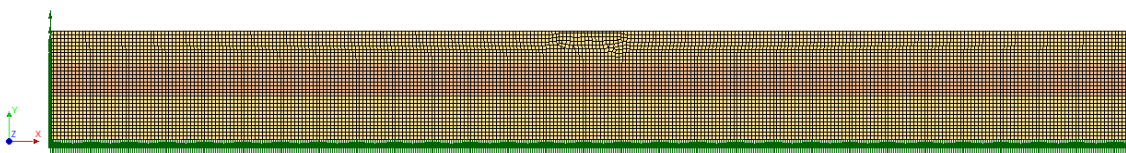


Figure 12. Shallow Soil Model mesh overview.

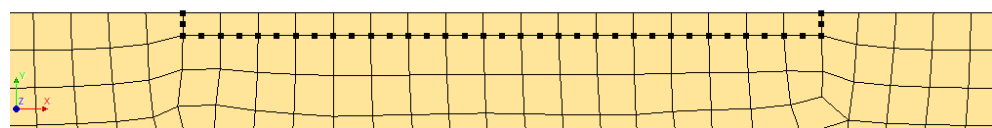


Figure 13. Location of output points in the Shallow model used as input in the Façade model.

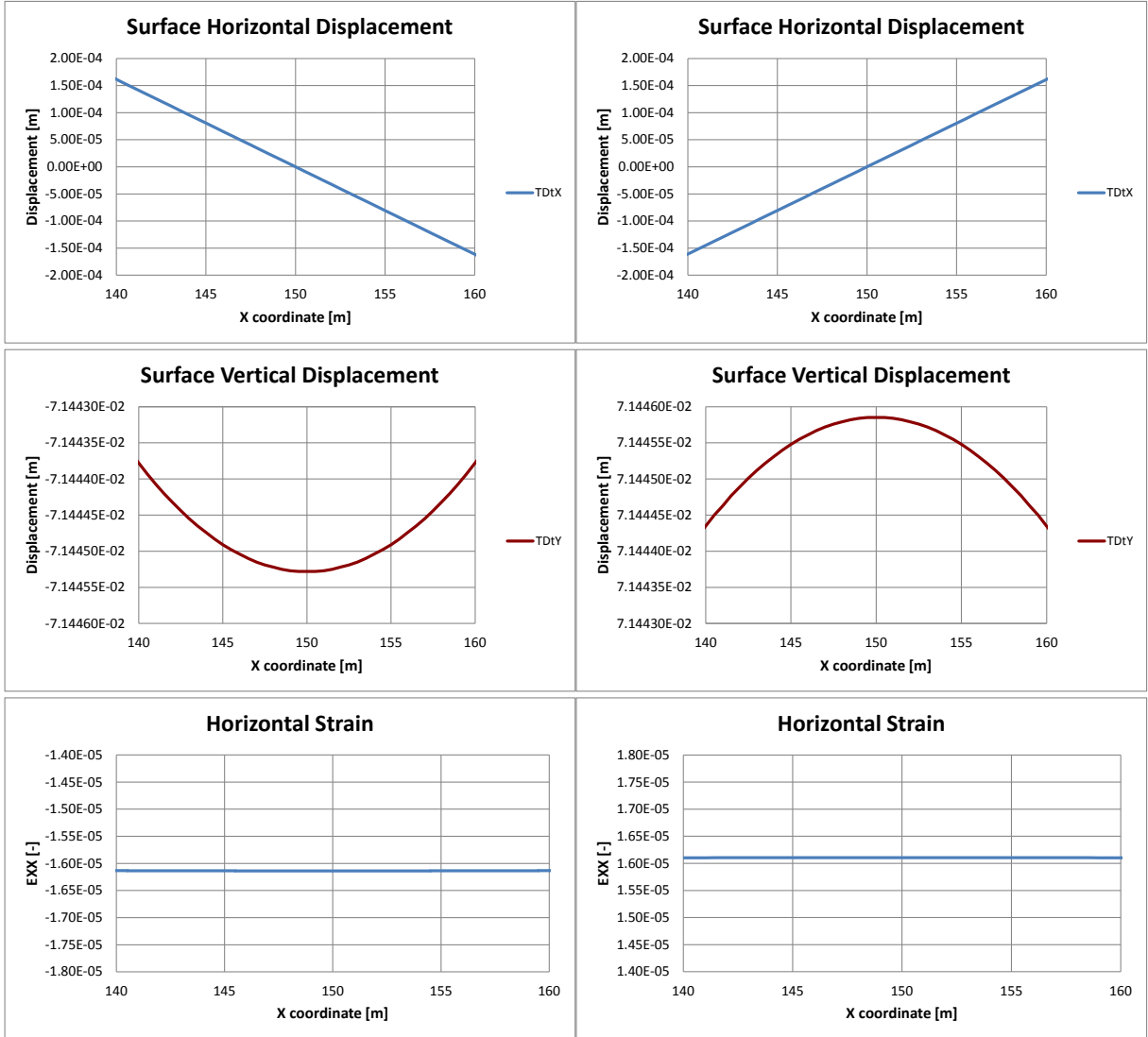


Figure 14. Horizontal, vertical displacement and horizontal strain of surface of Shallow Soil Model. Shrinkage (left) and expansion (right).

Façade Model Description

Façade A and B

The output taken from the Shallow Soil Model is directly applied as prescribed displacement at the foundation of the façade model. This follows the hypothesis that the horizontal strain from the soil is fully transmitted to the foundation of the masonry façade. The horizontal displacement is applied with an amplitude of 0.14 mm. For the sagging case, negative displacement are applied to the left side of the façade, while positive to the right side and vice versa for the hogging case. Vertical displacement has a maximum amplitude at the middle of the façade, with an amplitude of about 7.14 mm. Its relative displacement though, between middle and sides of the façade is about 0.001 mm. The horizontal strain amplitude is about 1.61E-05 with a maximum amplitude in the middle of the façade.

Two façade variations of a farm house are modelled and analysed. Both façades are 17 m long and 3.8 m high on the right side and 2.4 m high on the left side (representing the shed of a farm house) with a thickness of 210 mm. The foundation, 600 mm high, is modelled with a thickness of 610 mm. Class-III beam elements (CL9BE) are placed to the two lateral side of the façades to simulate the extra stiffness provided by the transversal walls. The beam elements have a stiffness equal to 1/3 of the masonry stiffness, with a cross section representing the dimension of a double-wythe wall. This follows the validation of numerical model as in [3]. Clay masonry properties are assigned to the wall. Overburden due to roof and floor weight are taken into account in the models and assigned as distributed force. As material model, the Engineering Masonry Model [4] is used. The material properties of the façades are listed in Appendix A.

Quadratic 8-noded plane stress elements (CQ16M and CT12M) are used to model foundation and façade. The model is assumed to be fixed base (no soil-structure interaction is considered), so that it is fully restrained at the bottom from translations. The elements are meshed with an average size of 200x200 mm. A representation of the models are depicted in Figure 15 and Figure 16.

The façades are subjected to three different type of loads. Gravity load, overburden and displacement due to subsidence are considered in the model. A non-linear calculation is performed. Gravity load is applied first in five equal steps, then overburden is applied in five steps and finally the displacement settlement in twenty load steps. The Secant BFGS (Quasi-Newton) method is adopted as iterative method. Displacement, force and energy norms must be all satisfied during the iterative procedure within a tolerance of 1% for displacement and force and 0.01% for energy. The Parallel Direct Sparse method is employed to solve the system of equations. The second order effects are considered via the Total Lagrange geometrical nonlinearity.

Shrinkage and expansion of the Deep (and thus Shallow) Soil Model leads respectively to sagging and hogging settlement of the façade. Contour plots of the two different façades when subjected to sagging and hogging are presented. The results show the contours of horizontal and vertical displacement, horizontal strain, horizontal and vertical stress, principal stress and principal stress tensors. Results are shown for the façade only, excluding the foundation.

Figure 17 and Figure 18 show the horizontal and vertical displacement of façade A and B when subjected to sagging settlement. The negative strain applied at the base (Figure 19) produces the horizontal shrink at the base of the façade. Positive horizontal stresses (Figure 20) are present at the lateral side and above the window openings. Positive vertical stress are shown at the top and bottom of window openings (Figure 21). Contour of principal stresses are depicted in Figure 22. Principal negative stress tensors are shown in Figure 23.

Displacements produced by hogging settlement for both façade A and B are depicted in Figure 24 Figure 25. The deformed mesh and horizontal strain plot (Figure 26) clearly show the expansion of the bottom side of the façades due to positive strain. On the contrary of the sagging settlement situation, the banks and spandrels of the façades are almost entirely subjected to positive horizontal stress, with highest values right at bottom and top of window openings (Figure 27). Figure 28 depicts vertical stresses, which are mostly negative. Positive values are found above and below window openings and at the bottom left corner of the façades mainly due to delamination mechanism. Principal stress contour and tensors plots are shown in Figure 29 and Figure 30. For all cases no damage is found. The stresses are in all cases below the masonry tensile strength.

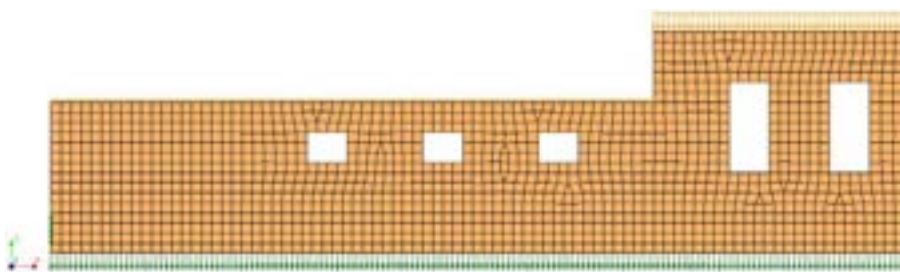


Figure 15. Plane Stress Façade Model A mesh overview.

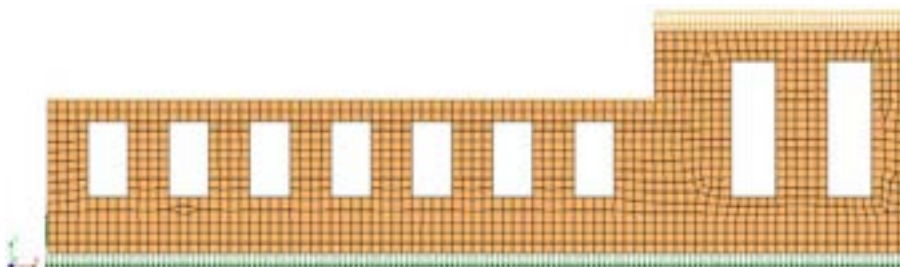


Figure 16. Plane Stress Façade Model B mesh overview.

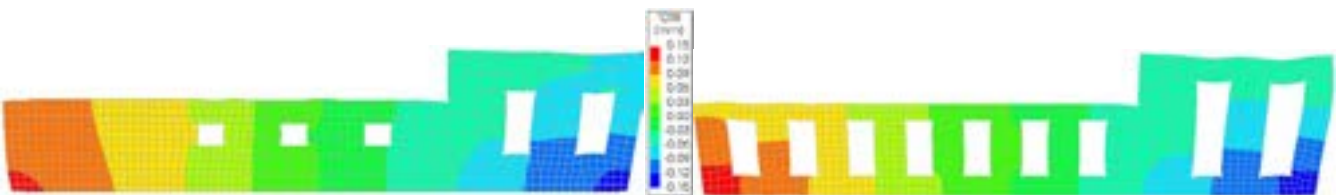


Figure 17. Horizontal displacement façades subjected to sagging. Façade A (left) and Façade B (right). Deformed mesh magnified x5000.

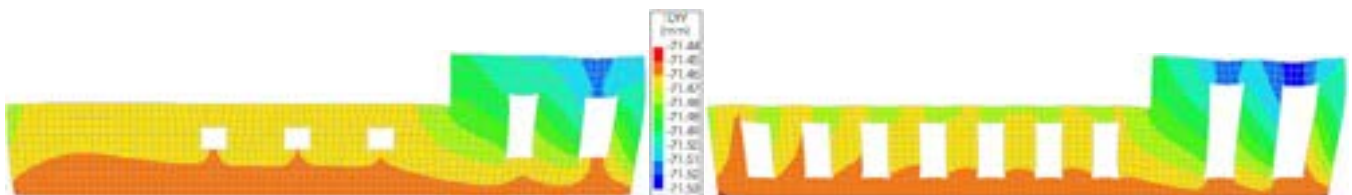


Figure 18. Vertical displacement façades subjected to sagging. Façade A (left) and Façade B (right). Deformed mesh magnified x5000.

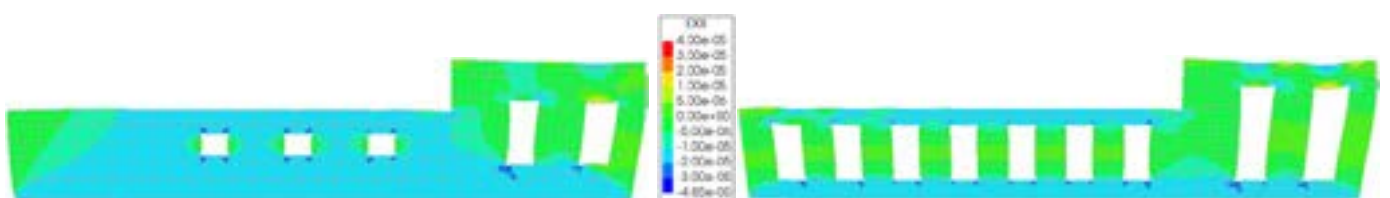


Figure 19. Horizontal strain façades subjected to sagging. Façade A (left) and Façade B (right). Deformed mesh magnified x5000.

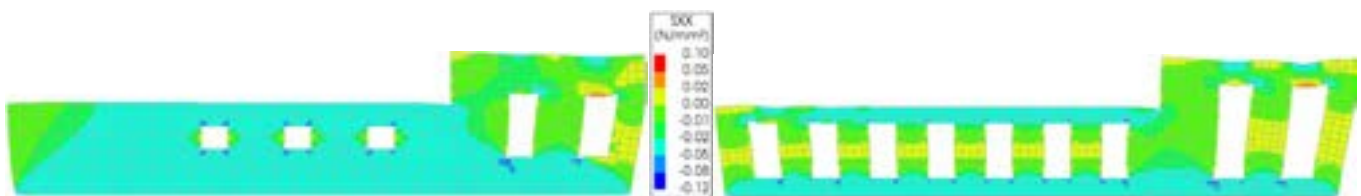


Figure 20. Horizontal stress façades subjected to sagging. Façade A (left) and Façade B (right). Deformed mesh magnified x5000.

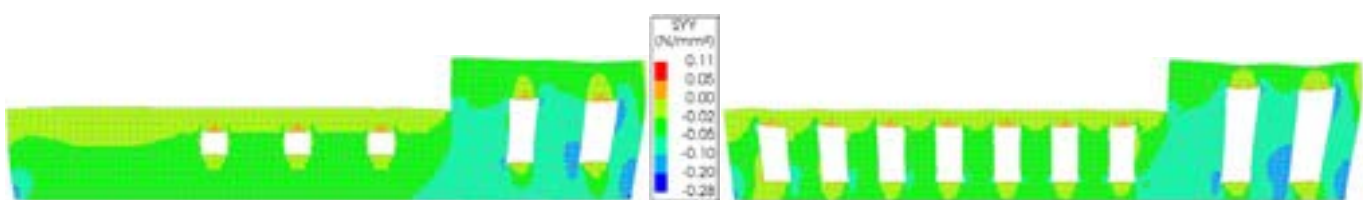


Figure 21. Vertical stress façades subjected to sagging. Façade A (left) and Façade B (right). Deformed mesh magnified x5000.

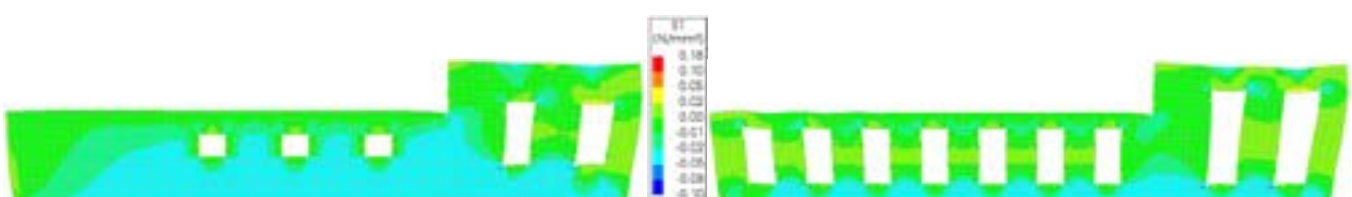


Figure 22. Principal stress façades subjected to sagging. Façade A (left) and Façade B (right). Deformed mesh magnified x5000.

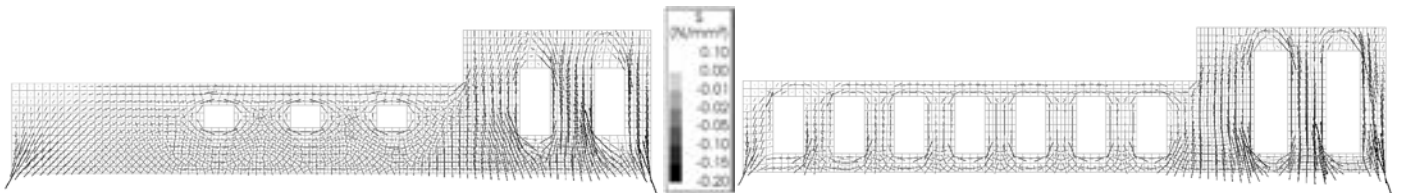


Figure 23. Principal stress compressive tensors façades subjected to sagging. Façade A (left) and Façade B (right). No deformed mesh.

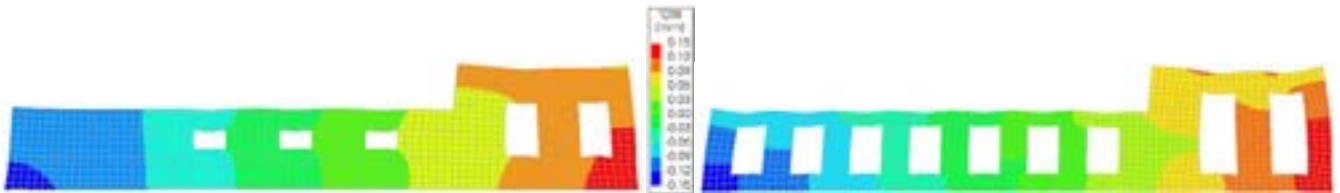


Figure 24. Horizontal displacement façades subjected to hogging. Façade A (left) and Façade B (right). Deformed mesh magnified x5000.

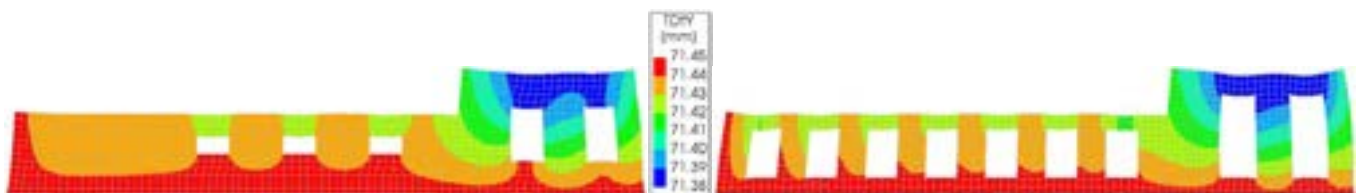


Figure 25. Vertical displacement façades subjected to hogging. Façade A (left) and Façade B (right). Deformed mesh magnified x5000.

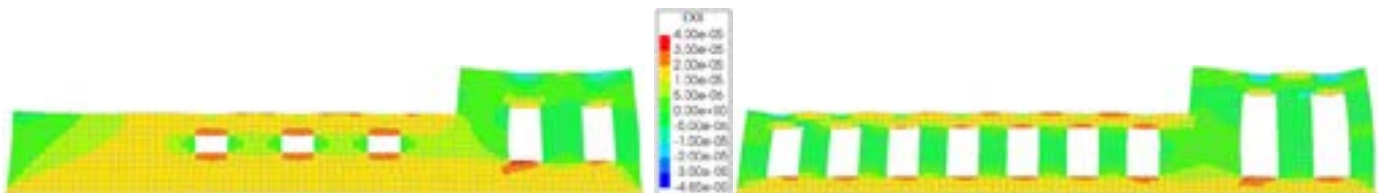


Figure 26. Horizontal strain façades subjected to hogging. Façade A (left) and Façade B (right). Deformed mesh magnified x5000.

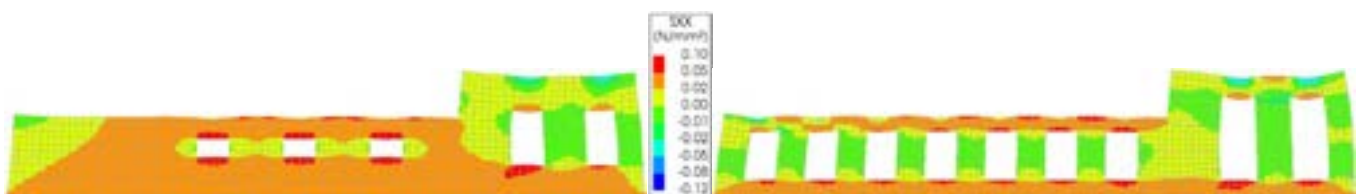


Figure 27. Horizontal stress façades subjected to hogging. Façade A (left) and Façade B (right). Deformed mesh magnified x5000.

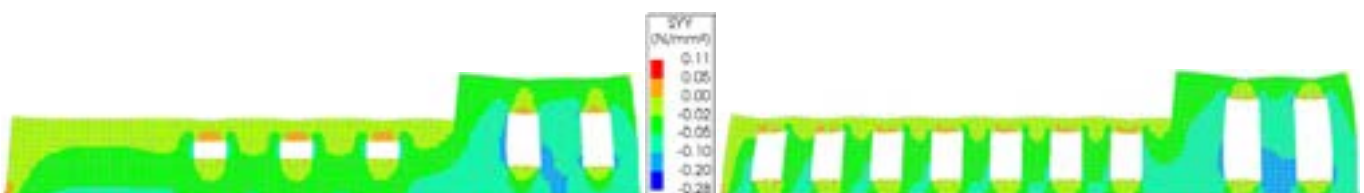


Figure 28. Vertical stress façades subjected to hogging. Façade A (left) and Façade B (right). Deformed mesh magnified x5000.

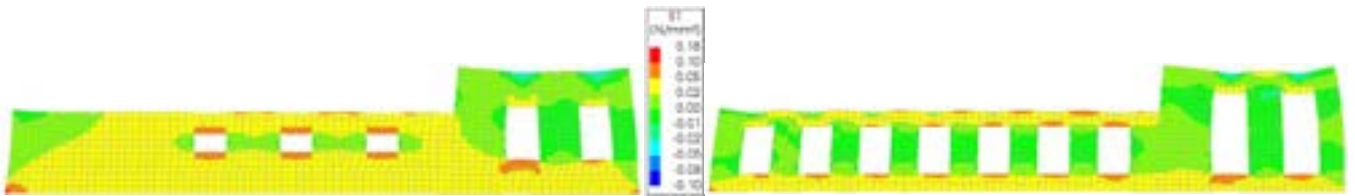


Figure 29. Principal stress façades subjected to hogging. Façade A (left) and Façade B (right). Deformed mesh magnified x5000.

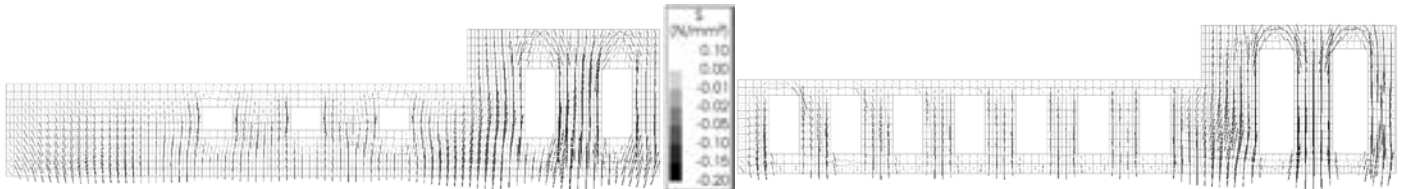


Figure 30. Principal stress compressive tensors façades subjected to hogging. Façade A (left) and Façade B (right). No deformed mesh.

The presented results can be considered as the worst case scenario, since the horizontal strain of the soil is considered as fully coupled with the façade's foundation. A sensitivity study is performed on the horizontal displacement amplitude applied at the base of the façades. Values equal to 75%, 50%, 25% and 0% of the original horizontal displacement are employed and analysed (Figure 31). The vertical displacement is also applied and kept constant and equal to the original (100%) value. As of the original (100%) displacement, all these cases do not show any damage in the masonry façade. In order to evaluate the point when visible cracking starts appearing on the façade, the different displacement cases are iteratively scaled up. The iteration results concluded when the façade reaches the “light” damage state. As defined in [5], a façade enters the “light” damage zone, when a crack, of about 0.1 mm in width and 100 mm in length, is identified. Summarizing the global façade damage with a scalar damage, this means that the façade has a Psi (damage parameter) equal to 1.0 [5].

Typical crack patterns detected in the two façades when subjected to displacement amplification, are depicted in Figure 32 and Figure 33. The figures shows the principal crack width for sagging and hogging settlement, when the horizontal displacement is 50% of the one employed in the first part. For sagging settlements, cracks are mainly localized at the window's corners. For hogging settlement, cracks due to delamination at the two base corners of the façade and below windows openings are present.

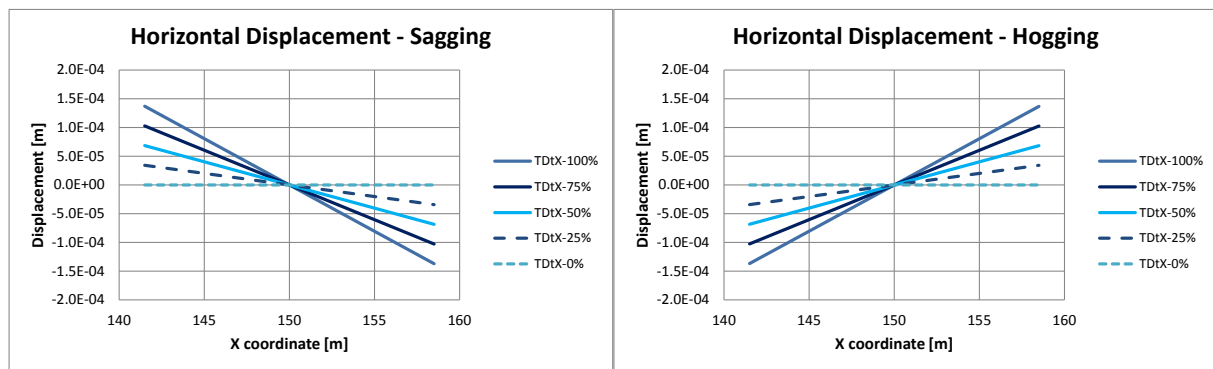


Figure 31. Horizontal displacement sensitivity for the masonry façades. Displacement applied at the foundation.

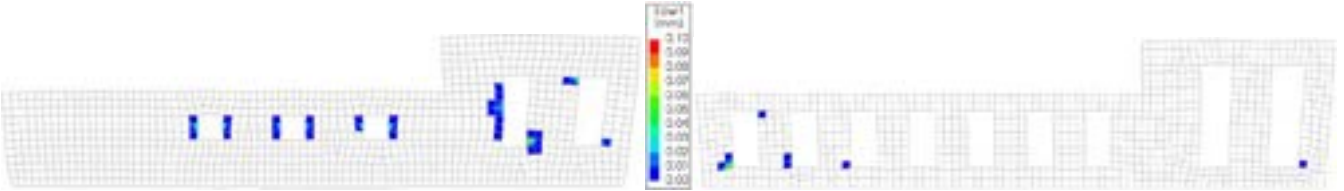


Figure 32. Principal crack width façades subjected to sagging. Maximum horizontal displacement applied equal to 50% of the original amplified 22.0 times (about 1.50 mm) for Façade A (left), and 12.5 times (about 0.93 mm) for Façade B (right). Deformed mesh magnified x500.

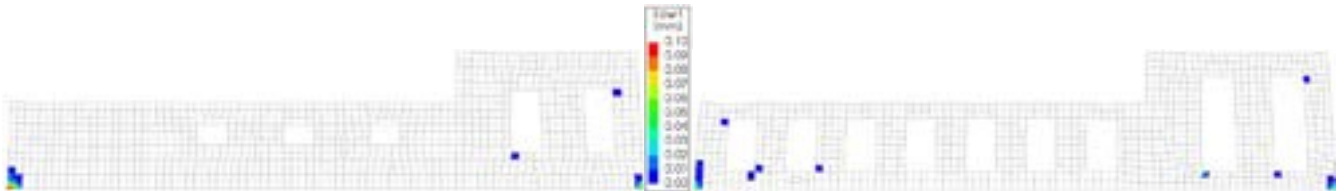


Figure 33. Principal crack width façades subjected to hogging. Horizontal displacement applied equal to 50% of the original amplified 10.5 times (about 0.75 mm) for Façade A (left), and 11.9 times (about 0.82 mm) for Façade B (right). Deformed mesh magnified x500.

Façade C

Together with façade A and B, another façade geometry is modelled. As well as for the previous case, the applied displacement is taken directly from the Shallow Soil Model and scaled to the analytical solution. The prescribed displacement applied at the foundation level are plotted in Figure 14. The horizontal displacement is applied with an amplitude of 0.06 mm. Vertical displacement has a maximum amplitude at the middle of the façade, with an amplitude of about 7.14 mm. Its relative displacement though, between middle and sides of the façade is about 0.001 mm. The horizontal strain amplitude is about 1.61E-05 with a maximum amplitude in the middle of the façade. The façade is 7 m long and 5.5 m high with a thickness of 210 mm. The foundation, 600 mm high, is modelled with a thickness of 610 mm. Reinforced beams are placed to the lateral side as for the previous cases. Clay masonry properties are assigned to the wall. As material model, the Engineering Masonry Model [4] is used. The material properties of the façade are listed in Appendix A. For the masonry lintel located above the door, is considered a rotated local axis, so that the bed-joint properties are aligned with the global vertical direction.

Quadratic 8-noded plane stress elements (CQ16M and CT12M) are used to model foundation and façade. The model is assumed to be fixed base (no soil-structure interaction is considered), so that it is fully restrained at the bottom from translations. The elements are meshed with an average size of 200x200 mm. A representation of the model is depicted in Figure 34.

The façades are subjected to two different type of loads. Gravity load and displacement due to subsidence are considered in the model. A non-liner calculation is performed. Gravity load is applied first in five equal steps, then the displacement settlement in twenty load steps. Same analysis procedure as described in the previous section is employed.

Contour plots of the façade when subjected to sagging and hogging are presented. The results shown the contours of horizontal and vertical displacement, horizontal strain, horizontal and vertical stress, principal stress and principal stress tensors. Results are shown for the façade only, excluding the foundation.

Figure 35 and Figure 36 show the horizontal and vertical displacement of façade C when subjected to sagging and hogging settlement. The negative strain applied at the base (Figure 37Figure 19) produces the horizontal shrink at the base of the façade. Positive horizontal strain and stresses (Figure 37 and Figure 38) are located at the base and at above window openings, mainly at the ground floor for both sagging and hogging case. Positive horizontal stress are shown for the hogging case at the two base corners, which indicate delamination mechanism. Lower positive stresses are found in the vertical component (Figure 39), located mainly at top of window openings. Principal stress contour and tensor of the principal compressive stress are shown in Figure 40 and Figure 41. For all cases no damage is found. The stresses are in all cases below the masonry tensile strength.

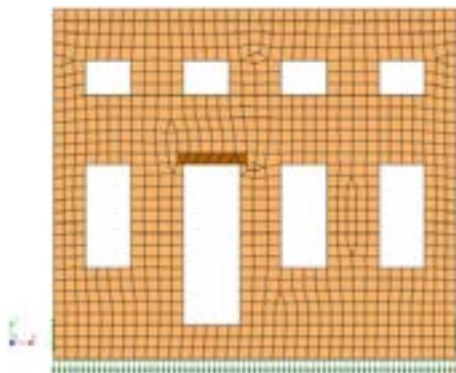


Figure 34. Plane Stress Façade Model C mesh overview.

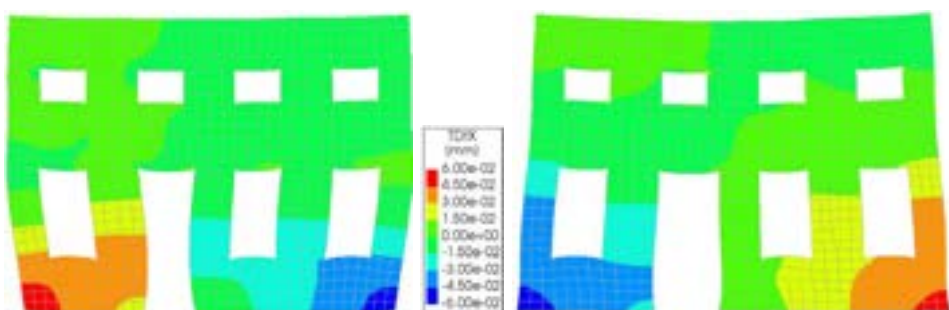


Figure 35. Horizontal displacement façade C when subjected to sagging (left) and hogging (right). Deformed mesh magnified x5000.

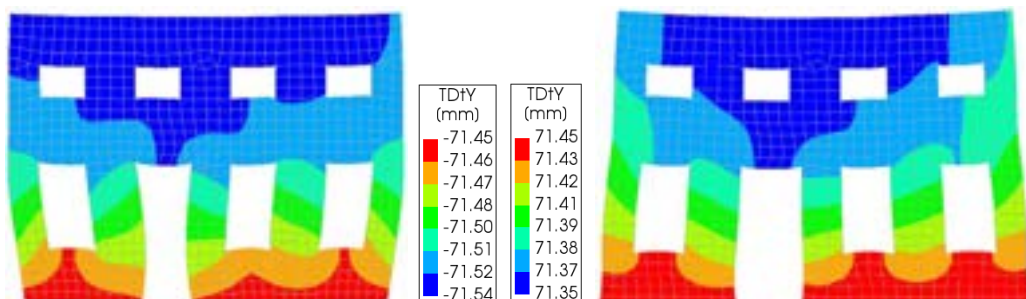


Figure 36. Vertical displacement façade C when subjected to sagging (left) and hogging (right). Deformed mesh magnified x5000.

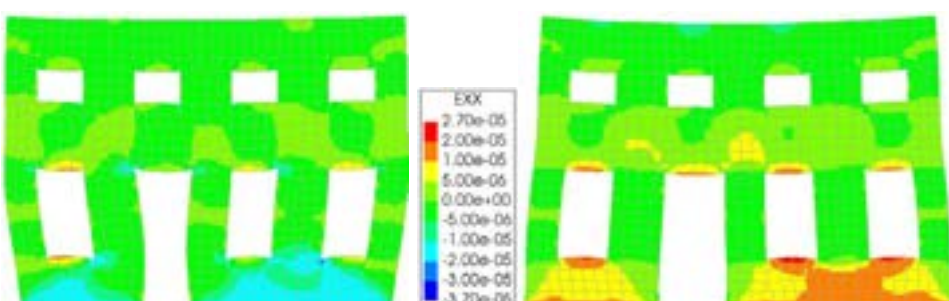


Figure 37. Horizontal strain façade C when subjected to sagging (left) and hogging (right). Deformed mesh magnified x5000.

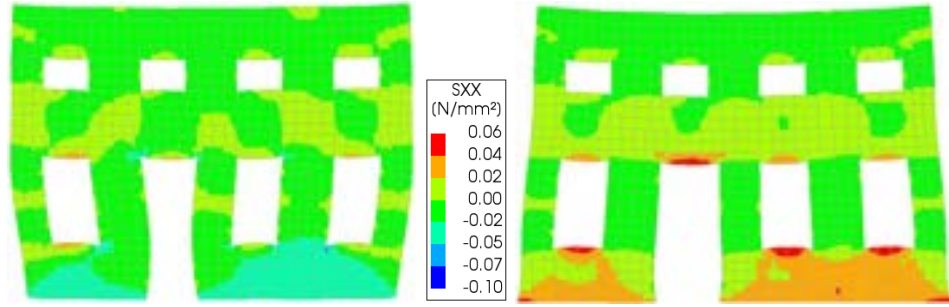


Figure 38. Horizontal stress façade C when subjected to sagging (left) and hogging (right). Deformed mesh magnified x5000.

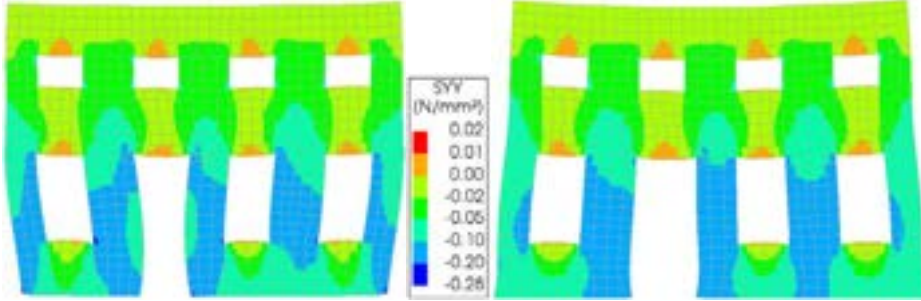


Figure 39. Vertical stress façade C when subjected to sagging (left) and hogging (right). Deformed mesh magnified x5000.

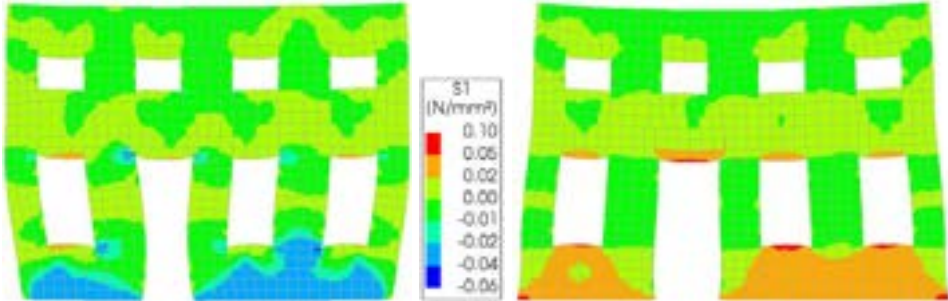


Figure 40. Principal stress façade C when subjected to sagging (left) and hogging (right). Deformed mesh magnified x5000.

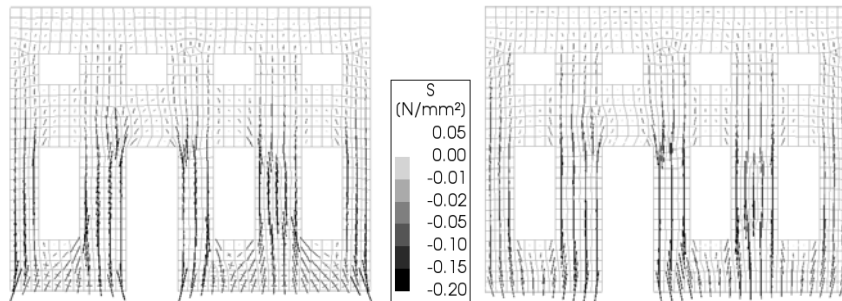


Figure 41. Principal stress compressive tensors façade C when subjected to sagging (left) and hogging (right). No deformed mesh.

As for the previous façades, a sensitivity study is performed on the horizontal displacement amplitude applied at the base of the façades. Values equal to 75%, 50%, 25% and 0% of the original horizontal displacement are employed and analysed (Figure 42). The vertical displacement is also applied and kept constant and equal to the original (100%) value. As of the original (100%) displacement, all these cases do not show any damage in the masonry façade. In order to evaluate the point when visible cracking starts appearing on the façade, the different displacement cases are iteratively scaled up. The iteration results concluded when the façade reaches the “light” damage state, or $\Psi_i = 1$ [5]. Typical crack patterns detected in the façade when subjected to displacement amplification, are depicted in Figure 43. The figures shows the principal crack width for sagging and hogging settlement. For sagging settlements, cracks are

mainly localized at the pier at the left side of the door. For hogging settlement, cracks due to delamination at the two base corners of the façade and in the lintel above the door are present.

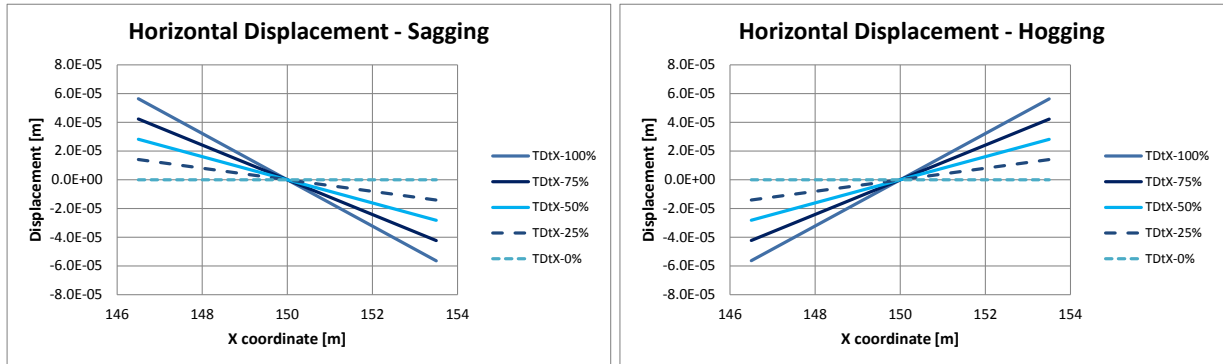


Figure 42. Horizontal displacement sensitivity for masonry façade C. Displacement applied at the foundation.

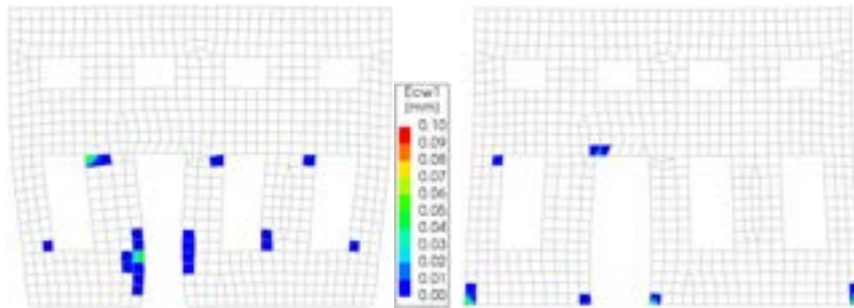


Figure 43. Principal crack width façade C. Maximum horizontal displacement applied equal to 100% of the original amplified 12.5 times (about 0.71 mm) for sagging (left), and 7.0 times (about 0.39 mm) for hogging (right). Deformed mesh magnified x500.

Summary of the Results

An overview of the amplification factors, applied to the horizontal displacement of the different façades for different settlement profiles is tabulated in Table 1**Error! Reference source not found.** and depicted with a plot in Figure 44**Error! Reference source not found.**. Figure 45 and Figure 46 show the direct comparison in terms of displacement amplification for different façade typology and settlement profiles. As can be seen, for façade A, the hogging settlement is almost twice as critical as the sagging one. The façade results much more vulnerable to this kind of displacement profile. “Light” damage is reached when the original horizontal displacement is amplified about 11 times for sagging and 5.5 times for hogging settlement, which results to a maximum displacement of about 1.50 mm (strain of 17.6E-05) for the first and 0.75 mm (strain of 8.85E-05) for the second type settlement. Façade C shows a similar trend, with amplification values close to façade A but slightly higher. The amplification for sagging is 12.5 against 10.85 and for hogging is 7.0 against 5.5 of façade A. When the opening’s number and size is increased (façade B), the vulnerability due to sagging settlement drastically increases. For this case, an amplification factor of 6.9 is necessary to reach a damage value of 1.0, which consists of an horizontal displacement of about 0.93 mm (strain of 10.9E-05). On the other hand, when subjected to hogging settlement, the extra flexibility gained by the extra openings, let façade B being slightly stronger than façade A (about 12% stronger). For all three façades, the hogging settlement remains the most vulnerable situation. Average values of horizontal displacement and horizontal strain which lead to “light” damage ($\Psi_i = 1$) are listed in Table 2.

Table 1. Amplification factors of the different façades for different settlement profiles and amplitudes required to reach $\Psi_i = 1$.

Displacement Percentage	Sagging Facade A	Hogging Facade A	Sagging Facade B	Hogging Facade B	Sagging Facade C	Hogging Facade C
100%	10.85	5.50	6.90	6.00	12.50	7.00
75%	14.80	7.30	9.00	8.00	16.00	8.50
50%	22.00	10.50	12.50	11.90	23.00	11.50
25%	39.00	16.00	21.20	19.00	36.00	17.50
0%	110.00	35.00	65.00	37.00	105.00	33.00

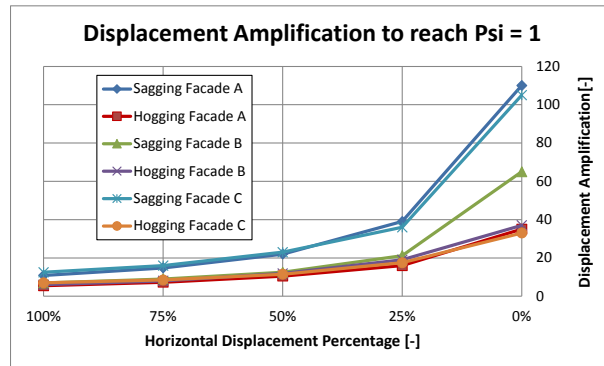


Figure 44. Horizontal displacement amplification for different settlement profiles and amplitudes required to reach $\Psi_i = 1$.

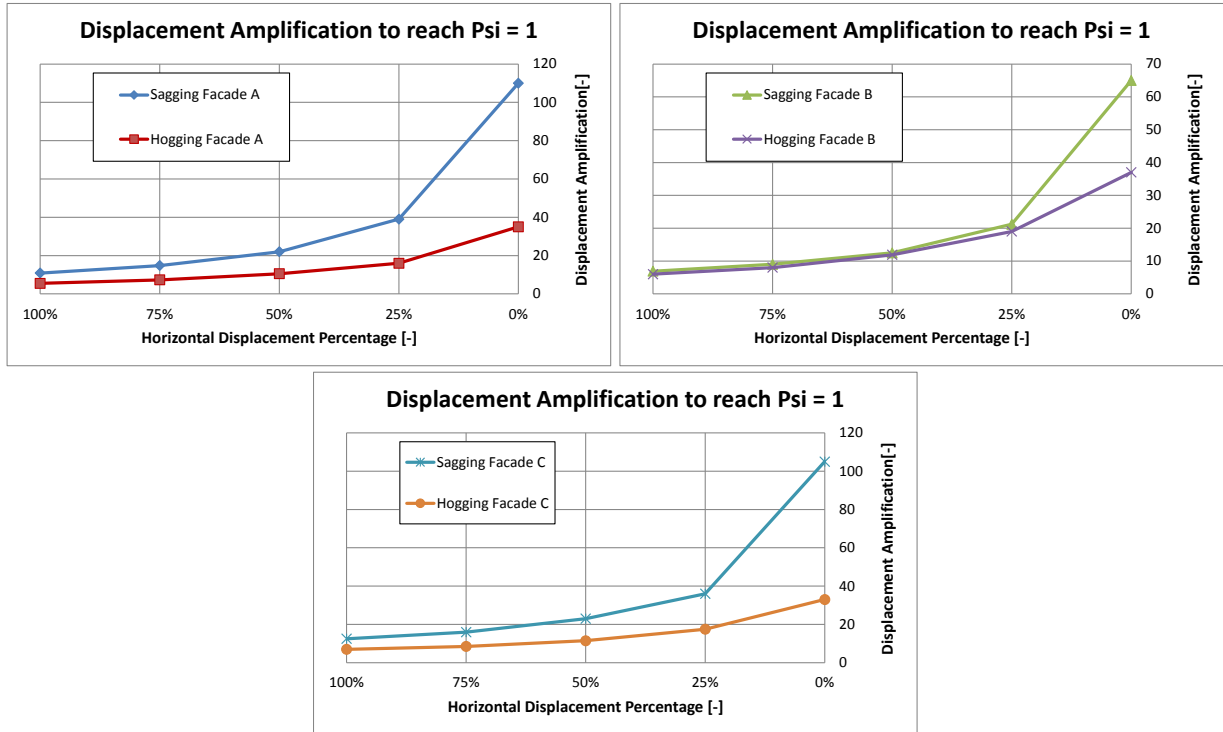


Figure 45. Horizontal displacement amplification for different settlement profiles and amplitudes required to reach $\Psi_i = 1$. Façade A (top left), façade B (top right) and façade C (bottom).

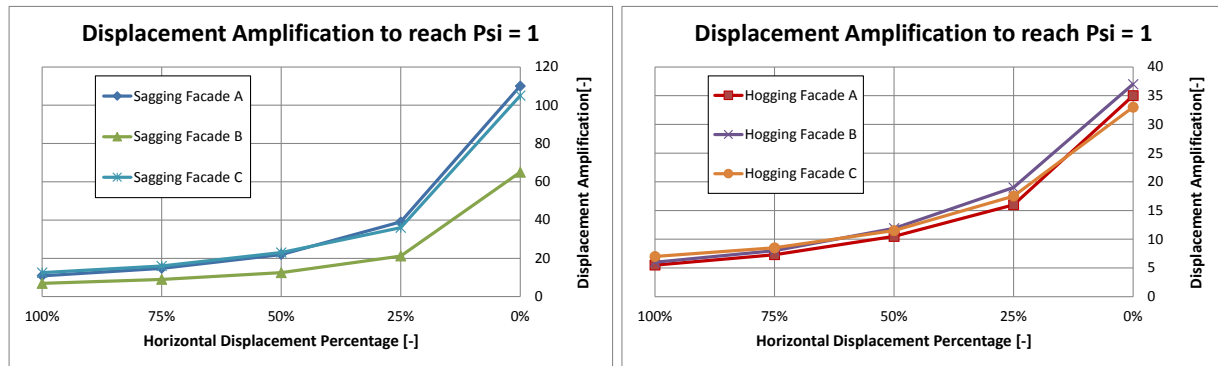


Figure 46. Horizontal displacement amplification for different façades and amplitudes required to reach $\Psi_i = 1$. Sagging (left) and hogging (right).

Table 2. Average horizontal displacement and strain of the different façades for different settlement profiles and amplitudes required to reach $\Psi_i = 1$.

	Applied	Sagging Facade A	Hogging Facade A	Sagging Facade B	Hogging Facade B	Sagging Facade C	Hogging Facade C
AVG Horizontal Displacement [mm]	0.14 FA-B 0.06 FC	1.50	0.75	0.93	0.82	0.70	0.40
AVG Horizontal Strain [-]	1.61E-05	17.6E-05	8.85E-05	10.9E-05	9.66E-05	19.5E-05	10.3E-05

Appendix A. Material Parameters

The material parameters used in the model are listed below:

- **SOIL LAYERS:** Soil layers properties of the first 30 m are taken from field data, while the rest of the properties is taken from literature. The soil is modelled as linear elastic. Diana automatically computes the initial stress when the gravity load is applied. The properties of the upper 30 m layers are employed also in the Shallow Soil Model.

Table 3. Soil layer material properties employed in the model

Layer	Soil Depth [m]	Mass Density [Kg/m ³]	Poisson's Ratio [-]	Young's Modulus Top-Bottom [MPa]	K0 [-]	Mesh size [mxm]
1 - Silty Sand	0-9	1700	0.30	44.2 - 143.2	0.50	5x5*
2 - Clay	9-18	1700	0.45	77.0 - 151.0	0.65	5x5*
3 - Silty Sand	18-30	2000	0.35	393.7	0.50	5x5*
4 - Sand	30-60	2200	0.30	700.7	0.50	10x10
5 - Sand	60-100	2200	0.30	1430.0	0.50	20x20
6 - Rock	100-500	2500	0.22	1525.0	0.00	40x40
6 - Rock	500-1000	2500	0.22	6100.0	0.00	50x50
6 - Rock	1000-1500	2500	0.22	13725.0.0	0.00	50x50
9 - Rock	1500-3000	2500	0.22	24400	0.00	50x50

* 1x1 m for Shallow Soil Model

- **MASONRY:** The Engineering Masonry Model [4] is used as material model for foundation and façade. Masonry façade is modelled with a thickness of 210 mm. Masonry foundation is modelled with a thickness of 610 mm. Local y axis is aligned to the global Y axis in order to define the bed joint orientation. Local x axis is aligned to the in-plane direction of the elements (global X).

Table 4. Masonry material properties employed in the model

Property	Unit	Value
Young's modulus vertical direction E _y	MPa	5000
Young's modulus vertical direction E _x	MPa	2500
Shear modulus G _{xy}	MPa	2000
Bed joint tensile strength f _{t,y}	MPa	0.15
Minimum head-joint strength f _{t,x}	MPa	0.45
Fracture energy in tension G _{t,I}	N/mm	0.01
Angle between stepped crack and bed-joint α	rad	0.5
Compressive strength f _c	MPa	8.5
Fracture energy in compression G _c	N/mm	20000
Factor to strain at compressive strength	-	3
Unloading factor	-	Secant
Friction angle ψ	rad	0.64
Cohesion c	MPa	0.30
Fracture energy in shear G _s	N/mm	0.1
OOP shear failure	-	No
Crack bandwidth specification	-	Rots

Mass Density	Kg/m ³	1980
--------------	-------------------	------

- MASONRY TRANSVERSAL WALLS: Linear elastic isotropic material is assigned to the beam elements representing the transversal wall. Note that no mass density is assigned to such elements. The stiffness is taken as three times lower than the one of the masonry. The cross-section of the transversal wall is taken as 210x210 mm for the façade and as 210x610 mm for the foundation. The use of such elements has been validated in [3].

Table 5. Masonry transversal wall material properties employed in the model

Property	Unit	Value
Young's modulus E	MPa	1666.67
Poisson's ratio ν	-	0.15
Mass Density	Kg/m ³	-

References

- [1] Diana User's Manual -- Release 10.4, 2020; <https://dianafea.com/manuals/d104/Diana.html>
- [2] Voortgangsoverleg IMG-TNO-TU Delft, 23 November 2020.
- [3] Korswagen et al. (2019) Experimental and Computational Study of the Influence of Pre-Damage Patterns in Unreinforced Masonry Crack Propagation Due to Induced, Repeated Earthquakes. 13th North American Masonry Conference, June 2019.
- [4] Schreppers et al. (2016) DIANA validation report for masonry modelling.
- [5] Korswagen et al. (2019) Light Crack Initiation and Propagation in Unreinforced Masonry Specimens Subjected to Repeated, in-Plane Loading. Bulletin of Earthquake Engineering, Springer 2019.

Memo: InSAR Analyses of surface vertical displacements - Norg

Author: P. Korswagen - TU Delft

Summary

InSAR satellite data measuring the elevation of the ground surface from the combination of four satellite datasets can be used to estimate the effect of (cyclic) deep soil actions caused by extraction and injection of gas in the field of Norg. The satellite data is post-processed to produce a time lapse of elevation contours lines; these, in turn, are used to determine the relative vertical displacements and surface curvatures over select cross-sections across the 6 km buffer-zone of the gas field. The post-processed data is compared against GPS measurements and analytical model results for gas reservoir depletion and storage, revealing no stark dissimilarities and good compatibility overall. Furthermore, in contrast to thresholds for building damage, the values of curvature and derived horizontal strains from the satellite elevation data, appear lower even when considering individual satellite datasets which present a higher variability and uncertainty. This analysis concludes therefore that analytical models can well represent ground surface deformations in the context of deep-soil effects and that observed soil deformations appear below set thresholds for building damage parameters.

Samenvatting

De InSAR satellietdata die de hoogte van het grondoppervlakte meet, en op basis van vier satellietdatasets, kan worden gebruikt om het effect van (cyclische) diepe bodemacties in te schatten welke worden veroorzaakt door gaswinning en opslag in het gasveld van Norg. De satellietgegevens worden nabewerkt om een tijdlijn van hoogtelijnen te produceren; deze worden dan gebruikt om de relatieve verticale verplaatsingen en oppervlaktekrommingen te bepalen over geselecteerde dwarsdoorsneden door de 6 km bufferzone van het gasveld. De bewerkte gegevens worden vergeleken met GPS-metingen en analytische modelresultaten voor winning en opslag van gas, waarbij geen grote verschillen te ontdekken zijn; over het algemeen zijn de metingen en modellen goed compatibel. Bovendien, in contrast met de drempelwaarden voor gebouwschade, zijn de waarden van kromming en afgeleide horizontale spanningen uit de hoogtegegevens van de satellieten lager, zelfs wanneer de vergelijking wordt uitgevoerd met individuele satellietdatasets, die een grotere variabiliteit en onzekerheid vertonen. De analyse concludeert daarom dat analytische modellen grondoppervlakvervormingen goed kunnen weergeven in de context van diepe bodemeffecten en dat waargenomen bodemvervormingen verschijnen onder vastgestelde kritische waarden voor parameters van gebouwschade.

1. Introduction

This memo reports the analysis of satellite measurements of vertical surface displacements for the area of Norg. The goal is to compare these measurements with the analytical model of the deep-soil effect of storage and extraction of gas in this field, with the purpose of further validating the analytical results and framing the thresholds for building-damage indicators with comparisons to real-world values. The case of Norg has been analysed first using the publicly-available data at bodemdalingskaart.nl, version 2.0. This data contains the vertical displacements of a large pool of measurement locations over the field, for various measurement instances over the period of 2015 to 2019. For orderliness, the referenced figures are presented separately at the end.

2. Methods

2.1. Extraction of soil surface displacement contours

The two satellites, Sentinel-1a and Sentinel-1b, each in a climbing and descending trajectory, produce four sets of satellite data. These cover the region encircled by the six kilometre buffer contour around the Norg gasfields, with approximately one million measurement points with a quality indicator greater than 0.65 and at 800 different measurement moments (about 200 per individual location); see Table 1 and Figure 1. The data presents the vertical displacement of each point, post-processed from satellite imagery [1, 3]. While the data of individual points is too noisy to reveal precise trends and the results are heavily dependent on the post-processing parameters of the raw satellite data, combining multiple points and the output of multiple satellites, leads to reliable deformation maps of the surface of the region, as will be shown here. Furthermore, the locations surveyed by the satellites are not evenly distributed over the region, but are concentrated in built areas and leave other spots uncovered. Figure 2 shows the density of points covered by the four satellites; the points have been gathered on grid cells of approximately 275x275 m; Figure 2.b shows that combining the various data sets leads to a greater coverage of the interest area. The measurements of the individual points were smoothed over a period of 5 to 10 weeks to remove the noise while maintaining seasonal variations; two examples of this approach are illustrated in Figure 3. Subsequently, the smoothed individual measurements were combined with all the other points in the grid cell considering the point quality as reported in the InSAR data; this weighted mean resulted in a single vertical displacement value for each surveyed grid cell for each measurement instance. Finally, a logical surface (LOWESS [2]) with polynomial sections was fitted through all the grid cells and spanning over the regions devoid of data. This produced a smooth surface for each measurement instance; an example is presented in Figure 4. The contour lines given by the surface reveal the seasonal trends of the soil, with clearly detectable movements associated with the seasonal injection and extraction of gas.

Table 1. Summary of the four data sets employed.

Description	Satellite 1	Satellite 2	Satellite 3	Satellite 4
	Oost 1	Oost 2	Midden 1	Midden 2
Number of Locations (within buffer zone)	185,388	262,467	283,859	290,815
Measurement instances (dates)	206	204	200	207
Date Interval	January 2015 October 2019	March 2015 October 2019	November 2015 October 2019	May 2015 October 2019

To further increase the reliability of the results, the output of the four satellites may be combined in space and time; this ensures that more regions are covered with measurement points, and measurement instances span smaller time intervals. Furthermore, the inherent variability of each data set is smoothed out to produce a more reliable output better representing the deep-soil effect. To guarantee compatibility in time, each individual satellite data is linearly interpolated to all measurement instances. The combination is achieved again via a weighted mean. The weighting function derived considers the number of points in each grid cell and the distance to the nearest points; this means that the satellite data more abundant and closest to a specific grid cell becomes more relevant when determining the displacement value of that cell.

Moreover, a common datum is obtained for the satellites: Since the interest of this analysis is to observe the relative displacements and derived surface curvatures, the absolute elevations provided by the InSAR data are not as relevant. Consequently, each data set is shifted up or down to better coincide with the mean of all satellites on the date when the data presented the smallest deviation. This common datum allows for the preservation of some extreme surface displacement values. Finally, a logical surface is fitted again to the combined data to produce smooth contour lines; see Figure 5. In Figure 5, the global subsidence trend of the region can be observed; this effect is ignored in these analyses since it affects the entire region equally and thus does not lead to deformations in the soil but to a uniform, sinking, vertical displacement. A summary of the entire processes is gathered in Figure 6.

As an alternative combination method, all the satellite data was pooled together on grid cells before drawing individual point trends. This did not lead to meaningful results and is thus not discussed further; yet, it validates the notion of first establishing individual points trends and then determining data sets trends before combining the information from multiple satellites.

2.2. Cross-sections

The displacement contours are analysed with six cross-sections, identical to those employed in the analytical models [4]. The vertical displacement troughs can be observed to swell up and sag down with the seasonal changes (see Figure 7); this leads to curvatures in the soil which can adversely affect buildings. Consequently, the cross sections are employed to determine the curvatures present in the region due to gas extraction and storage. The curvatures are calculated as the second derivative of the vertical soil deformations. Furthermore, the curvatures can be employed to estimate the horizontal strains at the soil surface by using a simplistic model of the soil on top of the gas reservoir as an Euler-Bernoulli beam. The InSAR data available does not include horizontal displacements, so the actual surface horizontal strains cannot be observed. With this simple and conservative assumption, the horizontal strains can be computed as per equation 1:

$$\epsilon_h = 1 - \frac{1}{\bar{\kappa} \cdot \left(\frac{1}{\bar{\kappa}} \pm \frac{D}{2} \right)} \quad \text{Equation 1}$$

Where ϵ_h is the estimated horizontal strain at the surface, D is the depth of the soil on top of the gas field ($D \approx 3000$ m), and $\bar{\kappa}$ is the mean curvature of the soil over a grid cell length. See also Appendix 1.

Moreover, the curvature values can also be used to calculate the angular distortion of a façade based on its foundation length. As is presented in [4], the angular distortion and curvature are related as:

$$\beta = \frac{1}{2} \cdot L_f \cdot \kappa \quad \text{Equation 2}$$

Where β is the angular distortion, κ is the curvature of the soil surface, and L_f is the foundation length which is assumed herein as 10 m [4].

3. Results and Discussion

The ‘loess’ surface fit to the mean satellite measurements observes the trends of the soil surface over a few hundred metres, thus removing the presence of local soil effects and individual point deformations in the data and directly presenting the consequences of deep-soil actions. Figure 8.a presents the vertical displacements and derived curvatures for November of 2017, right before the beginning of the winter season. All cross-sections (see Figure 1) display a swelling of the surface of the soil of up to 5 mm above the edges of the section line as would be expected when gas has been stored underground. This heave is linked to a curvature of approximately $5 \cdot 10^{-10}$ rad/m as shown in Figure 8.b. In comparison, the subsidence trough for the full gas reservoir, as calculated with the analytical model [4], is about 2 times larger in magnitude and its derived curvature is about 8 times larger. The results for the maximum of the entire data history are collected in Table 2. Nonetheless, the maximum values are not the only relevant comparison measure but also the shape of the soil surface and its curvature are of interest. In this context, the analytical model shows remarkable similarities with the InSAR data especially for lines 1 and 2, which are the lines cutting directly through the middle of the gas field. In Figure 8, where the analytical model is drawn for comparison albeit at a modified scale, these similarities can be observed.

In the InSAR data, the effect of settlement is not as clear as the upwards heaving of the surface. It is not known whether this is due to the fact that the gas reservoir was not fully emptied in the observed period, whether the satellites, under certain incident angles, have difficulty detecting local downwards troughs, or whether a shallow soil effect has limited this settlement. Furthermore, the four sets of satellite data present slightly varied results. Within this analysis, it cannot be determined whether these differences appear because of the post-processing method or are due to the aleatory uncertainty of the measurement techniques. A probabilistic approach with a confidence margin would allow more insight into this variability;

however, with millions of measurement points, such an approach is unreasonable within the scope of this study. Instead, Table 2 includes the highest values observed from any of the four original data sets and any of the potential set combinations; this is a conservative approach and can be viewed as the upper confidence bound. When comparing this maximum set against the heave estimations, the values are similar; the satellite data produces slightly larger curvatures, as would be expected due to the influence of shallow soil effects not present in the analytical models.

Yet, in comparison to the larger subsidence values, the soil deformations measured with the InSAR method in the period 2015-1029, are smaller. Moreover, the critical values to produce visible building light damage determined in [5], are at least one order of magnitude higher than those observed with the InSAR data for Norg. And furthermore, the maximum values of relative rotation and horizontal strain derived from the InSAR data, at any of the cross-sections on any given moment, are significantly lower than those reported in literature as discussed in [7].

*Table 2. Comparison of results between analytical model and InSAR post-processed data. *The horizontal strain is estimated from the curvature measurements; horizontal displacements are not available in the InSAR data.*

Description	Unit	Geo-Analytical Model [4]		InSAR Data Analysis	
		Subsidence	Heave	Combination four sets	Maximum from any satellite data set
Vertical extrema of trough	mm	44.4	14.8	6.4	13.0
Curvature	rad/m	1.7E-08	3.1E-09	6.6E-10	4.2E-09
Relative Rotation	rad	8.6E-08	1.6E-08	3.3E-09	2.1E-08
Horizontal Strain*	m/m	1.1E-05	2.2E-06	9.6E-07*	5.4E-06*

A further comparison can be made against GPS data. High-resolution GPS receivers are capable of determining position and elevation with a precision of about 1 millimetre. NAM measured the elevation of the Norg UGS facility over several years and registered its progress [6]. Here it was observed that the maximum amplitude of the seasonal variation in elevation was 21 mm in the period 2014-2018. Figure 9 presents the comparison with the InSAR data at this location and shows good agreement between GPS and InSAR data, especially considering that the InSAR data has been smoothed over a larger region to capture the deep-soil effects and the GPS measurement, in contrast, is limited to a single location and thus lacks context of its surrounding, and may include local (shallow-soil) effects. Figure 9 is based on satellite 2 because it offered the most points around the GPS location in a smaller grid of 50x50 m and over a longer timespan. The trends of the individual points are plotted and their mean is also drawn; the mean value compares really well with the GPS point, while the InSAR surface is slightly damped, again, because of the larger grid of 275x275 m and the smoothed surface fit. Nonetheless, both GPS and InSAR show a linearly descending general trend and a clear seasonal variation.

The comparison against the GPS data confirms that the larger subsidence predicted by the analytical models in case of full reservoir depletion has not taken place in the timeframe observed by the InSAR data; in this case, the comparison against heave (due to gas storage) seems more applicable and is so depicted in Figure 8.

4. Conclusions

The post-processed InSAR data for Norg does not reveal any stark dissimilarities when compared against the expected values of soil surface displacement and curvature from an geo-analytical model [4]. Furthermore, the observed values are well below those determined as critical for the light damage of masonry buildings [5]. In this light, the analysis of Groningen InSAR data seems unwarranted, seeing that the larger fields produce similar soil curvatures and the analytical model has proven to be insightful in determining strains and curvatures in general from deep-soil effects.

5. References

1. Bodemdalingskaart.nl, (2020). v2.0. Post-processed satellite InSAR data sets. <https://bodemdalingskaart.nl/nl/kennis-datacentrum/> Retrieved 15 of January of 2021. License: CC BY-SA 4.0
2. Cleveland, William S. (1981). "LOWESS: A program for smoothing scatterplots by robust locally weighted regression". *The American Statistician*. 35 (1): 54. doi:10.2307/2683591. JSTOR 2683591.
3. M Berger, J Moreno, JA Johannessen, PF Levelt, RF Hanssen (2012). ESA's sentinel missions in support of Earth system science. *Remote Sensing of Environment* 120, 84-90
4. TNO (2021). Effecten diepe bodemdaling en -stijging rondom de Norg gasopslag en het Groningen gasveld. TNO Report 2020 R12068
5. Rots, J.G., Korswagen, P.A., Longo, M. (2021). Computational modelling checks of masonry building damage due to deep subsidence. Delft University of Technology. Report number 01, Version 01, 1 February 2021.
6. Continue GPS hoogtemetingen NAM Norg (2018) - Rapportage december 2017 - <https://www.nlog.nl/noord-nederland-groningen-grijpskerk-norg>. Retrieved 1 February 2021.
7. TNO (2021). Literature Review: Effects of subsidence on buildings. TNO Report 2020 R12073

6. Figures

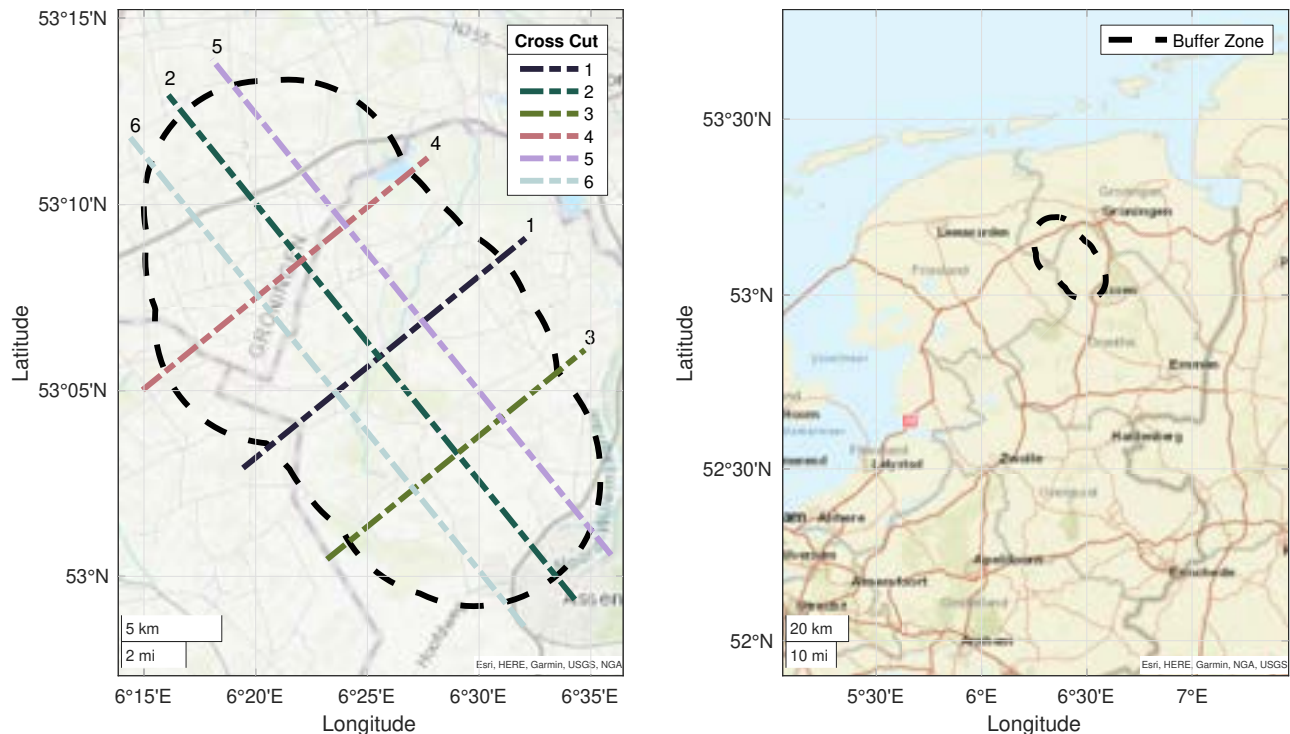


Figure 1. Location of the buffer zone of 6 kilometres around the gas fields of Norg. Six cross-sections are marked.

Density of Point Samples

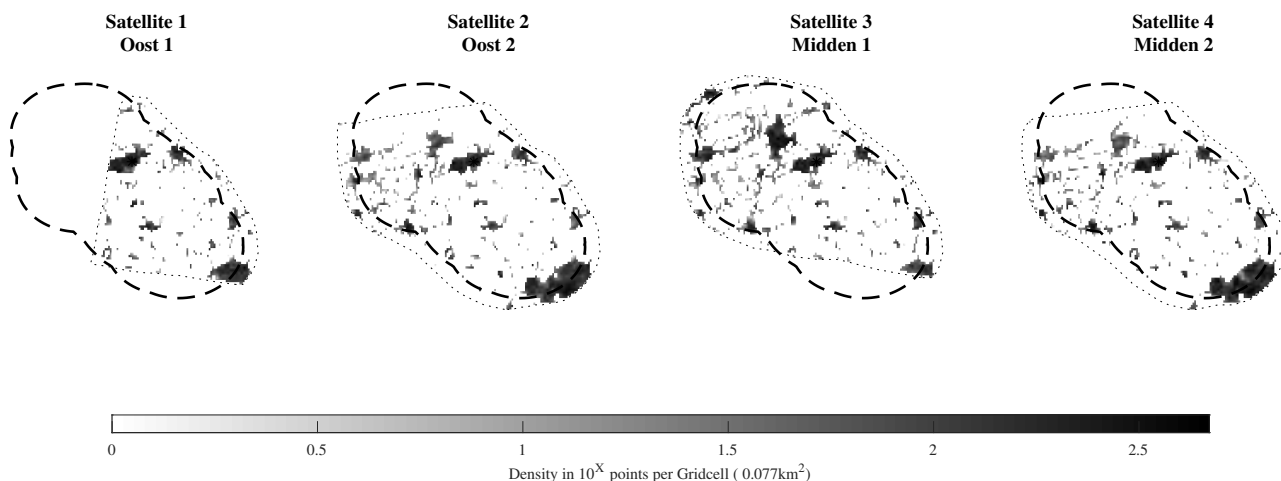


Figure 2.a. Distribution and density of points in relation to the buffer zone for the four satellite data sets. The area covered by each set is highlighted with a dotted perimeter.

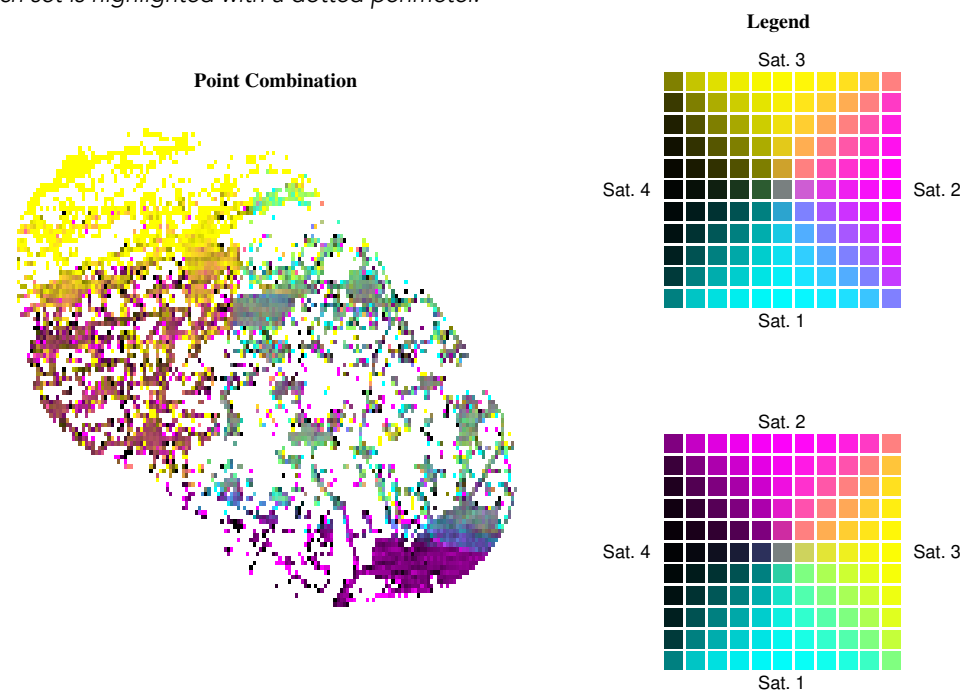


Figure 2.b. Combination of all four satellite sets. This figure must be viewed in full color: the color tone and darkness indicate which satellite dominates in each grid cell. Grid cells coloured in grey are equally covered by all four satellites, while for example, fully dark cells have data exclusively from satellite 4 and green cells are covered in equal ratio between satellites 1 and 3.

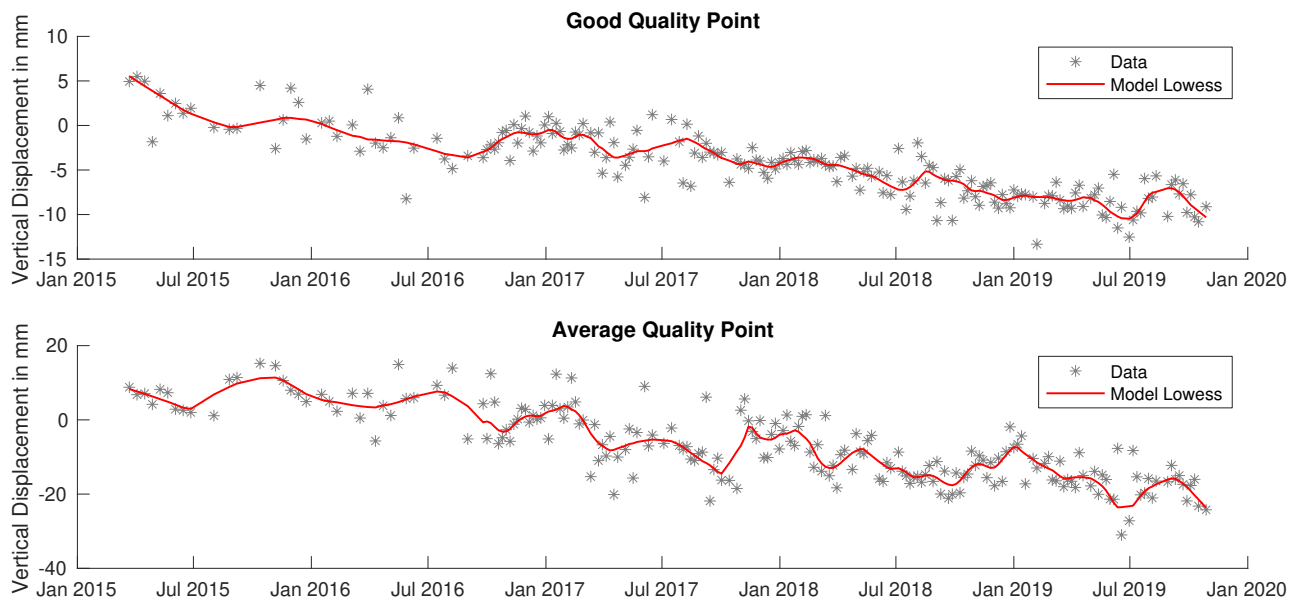


Figure 3. Individual trend and fitted line for two random points towards the centre of the buffer zone. Notice different vertical scales related to the noise in the data. The points are described with different 'quality indexes' in the tables provided by bodemdalingskaart.nl; these indexes refer to the noise present in the point data. Seasonal trends are somewhat observable with the applied filter (Model Lowess).

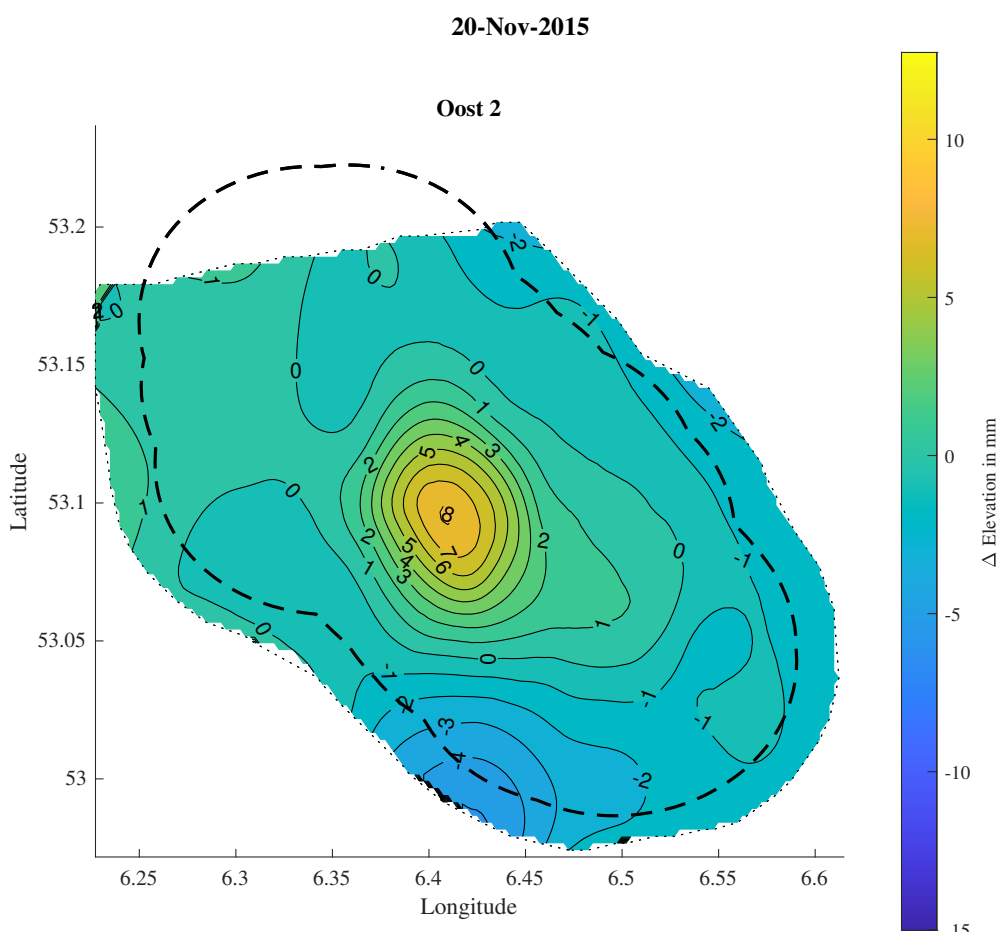


Figure 4. Example of fitted surface to the data set "Oost 2" for November of 2015. The heave of about 4 millimetres located towards the centre of the buffer zone is visible.

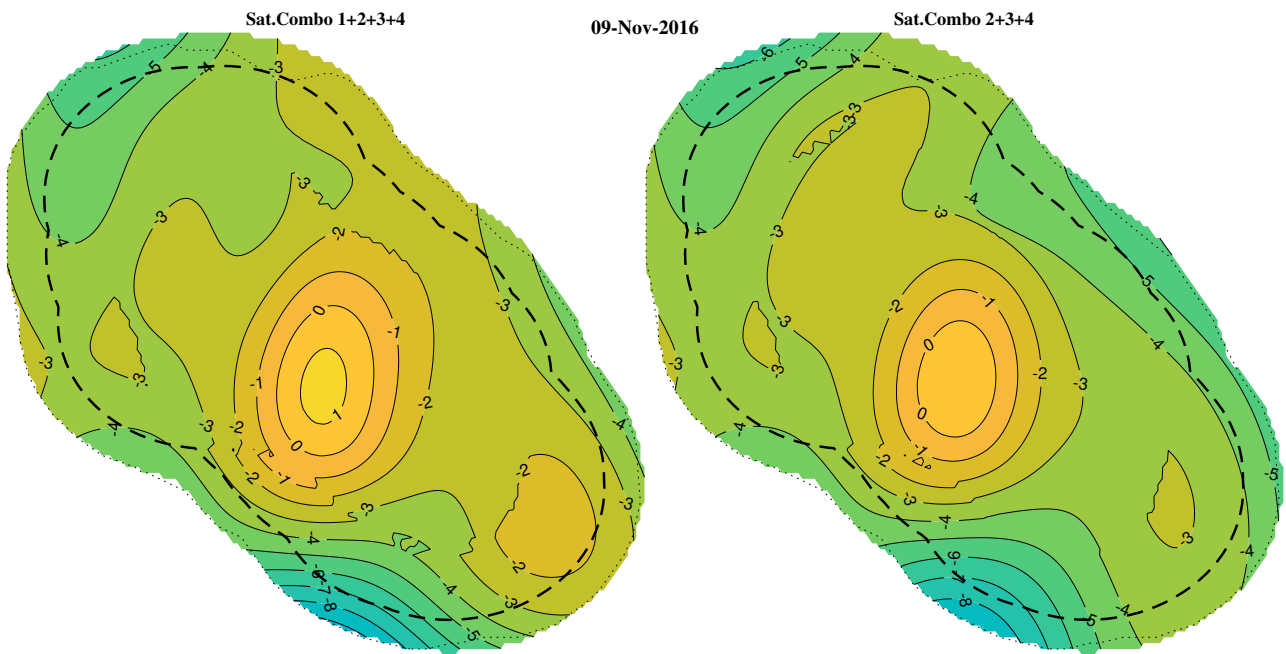


Figure 5. Example of soil surface displacement contours for the combination of all data sets (left) and the exclusion of satellite set 1. The inclusion of the partial cover of satellite 1 (see Figure 2) leads to discontinuities around the centre of the buffer zone; nonetheless, the contours remain almost identical between both combination sets.
This figure can also be viewed as an animation over the entire survey period. The animation can be downloaded from: <https://edu.nl/gam9a>

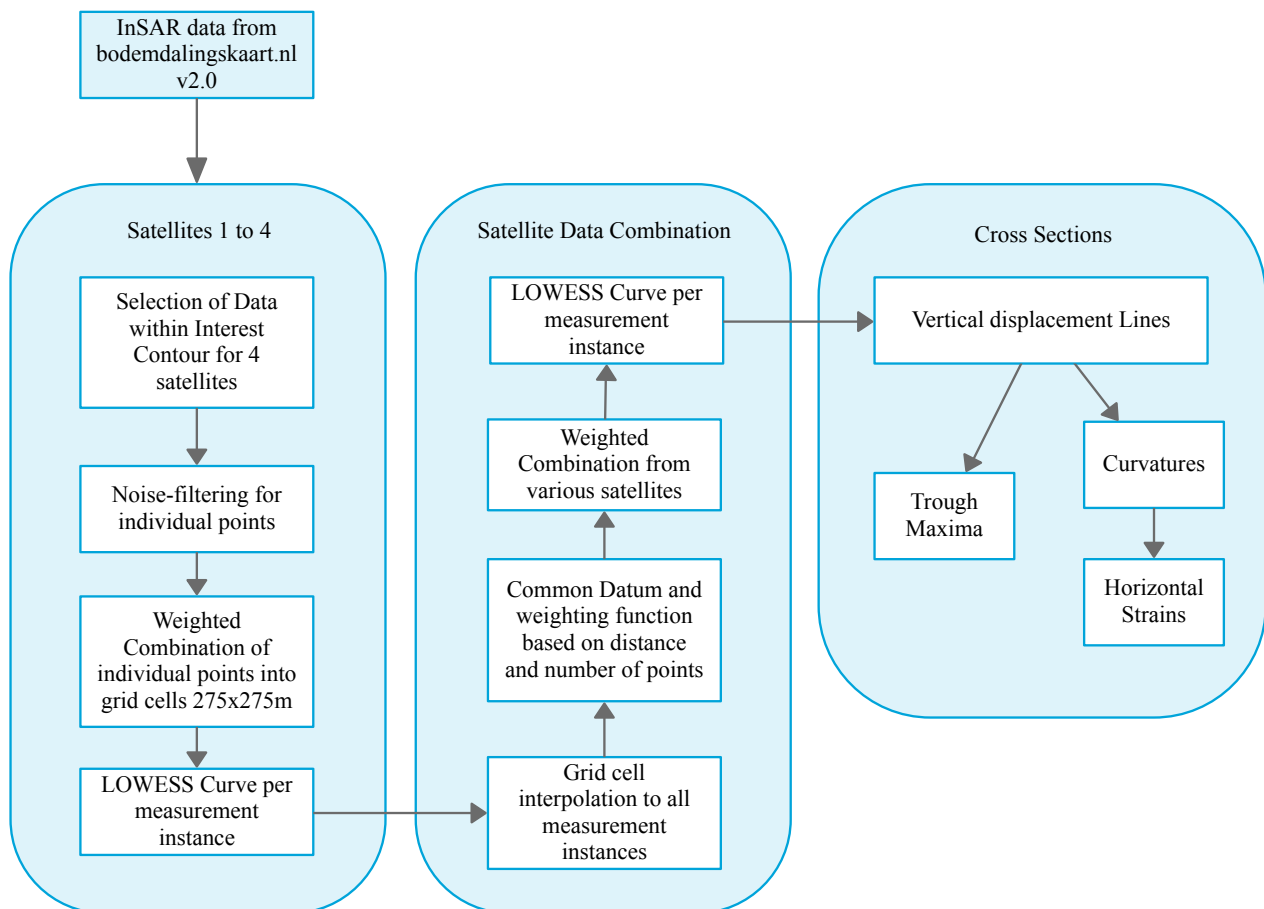


Figure 6. Flow chart for the post-processing of the data downloaded from individual points to surface curvatures.

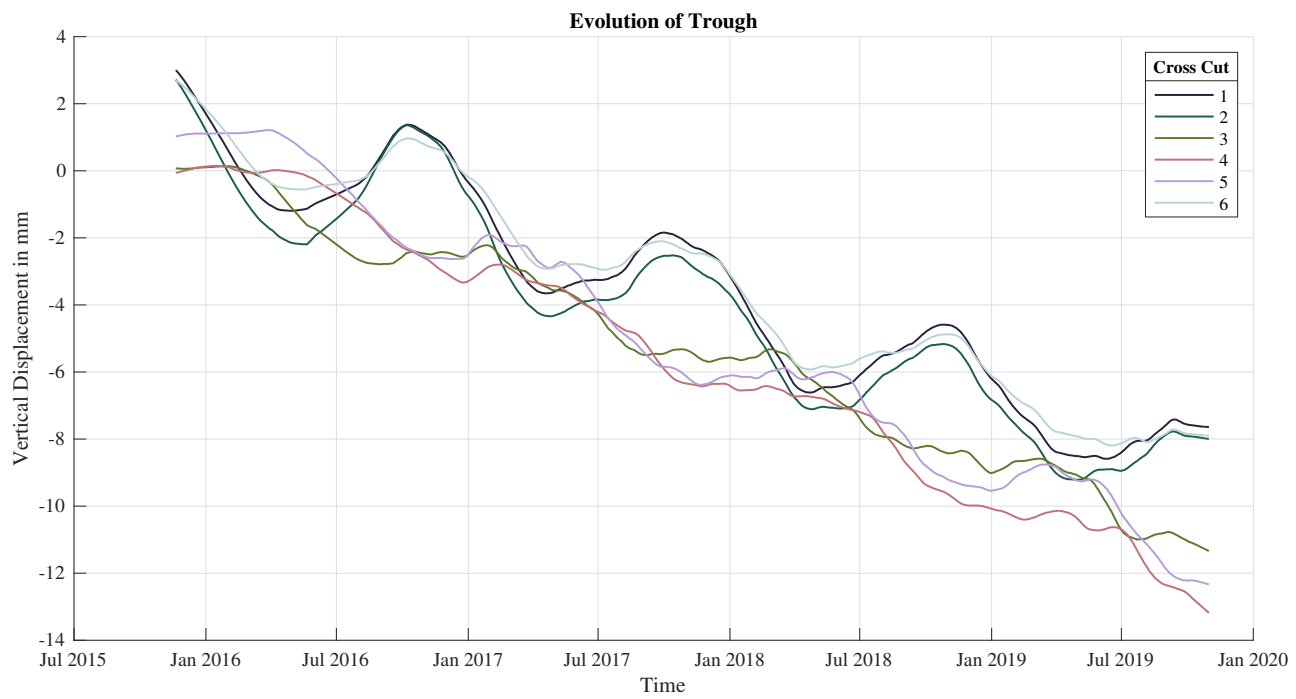


Figure 7. Trough extrema elevation over the surveyed period. A continuous subsiding trend, mixed with a seasonal variation, can be observed. This continuous, linear trend appears globally in the region and thus does not affect the local curvatures and strains.

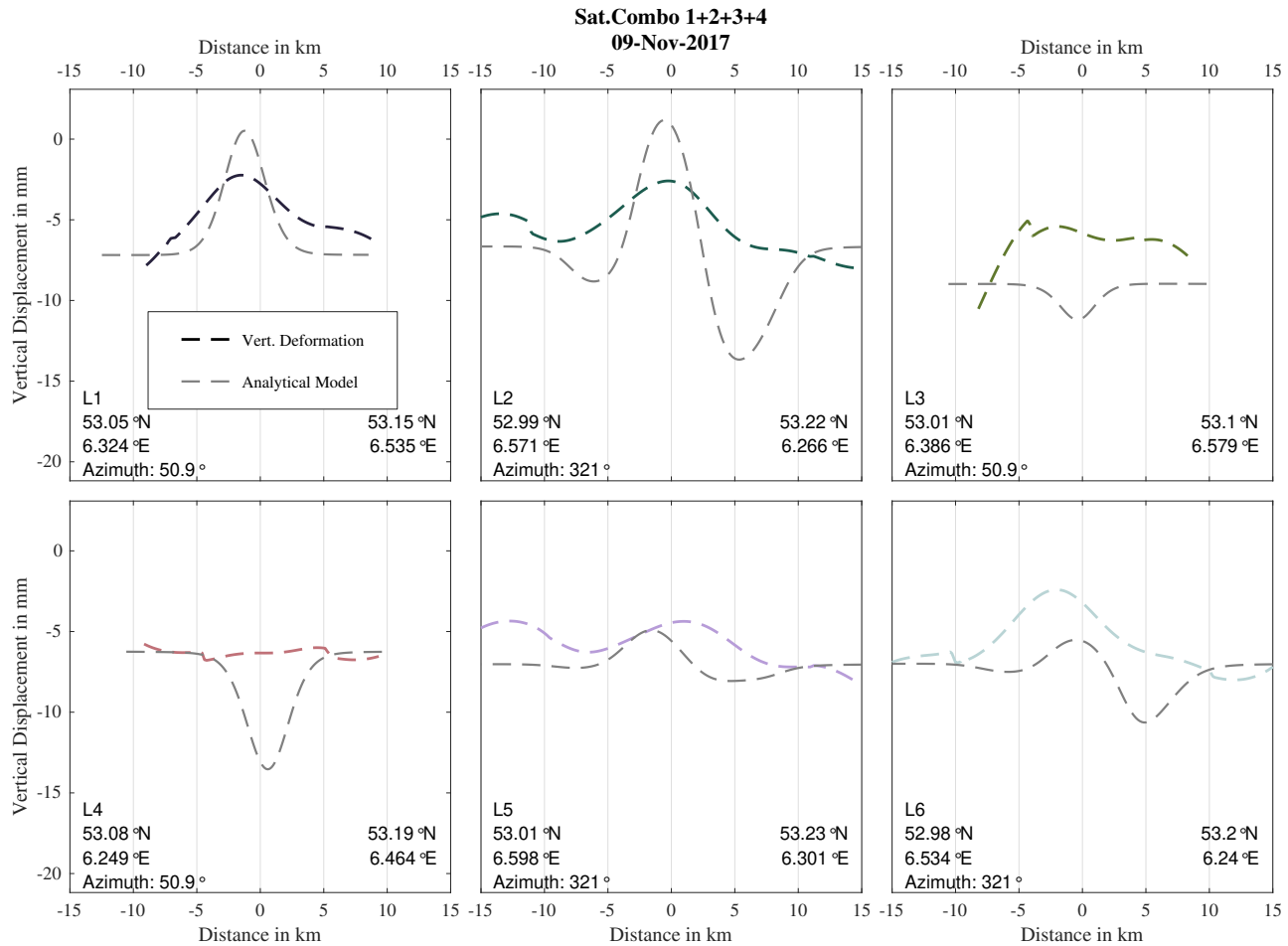


Figure 8a. Displacements over the six cross-sections for November of 2017, at the beginning of the winter season thus corresponding to maximum heave for that year. Comparison against the vertical displacement from the analytical model from TNO [4] for the full gas reservoir.

A version of this figure can also be viewed as an animation over the entire survey period. It can be downloaded from:
<https://edu.nl/euqj9>

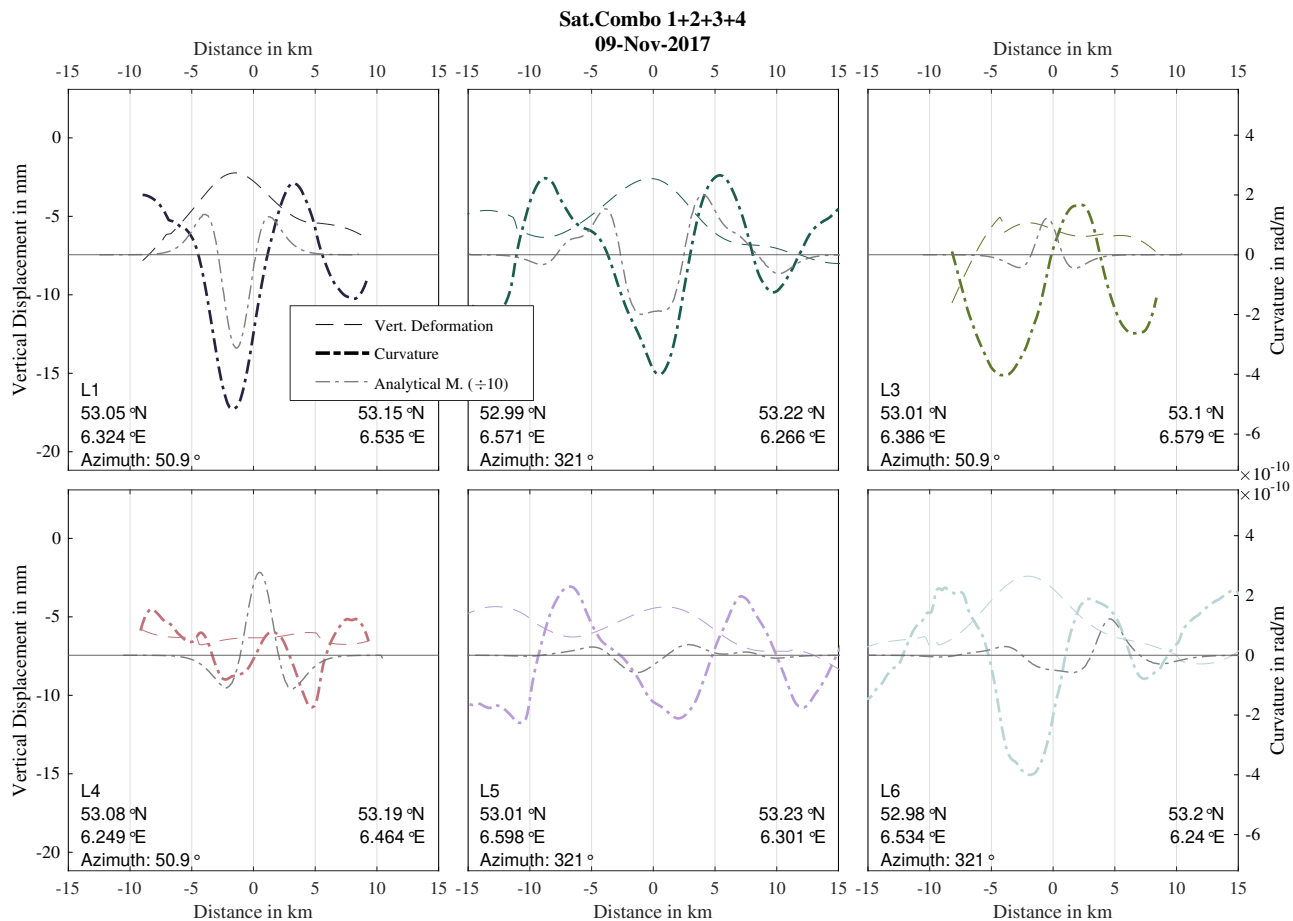


Figure 8.b. Curvatures over the six cross-sections for November of 2017, at the beginning of the winter season thus corresponding to maximum heave for that year. Comparison against the surface curvature from the analytical model from TNO [4] for the full gas reservoir. Additionally, the vertical displacement from the InSAR surface is provided as reference (see Figure 8.a.). Note also that the analytical model line has been scaled down by a factor of 10 for comparison purposes.

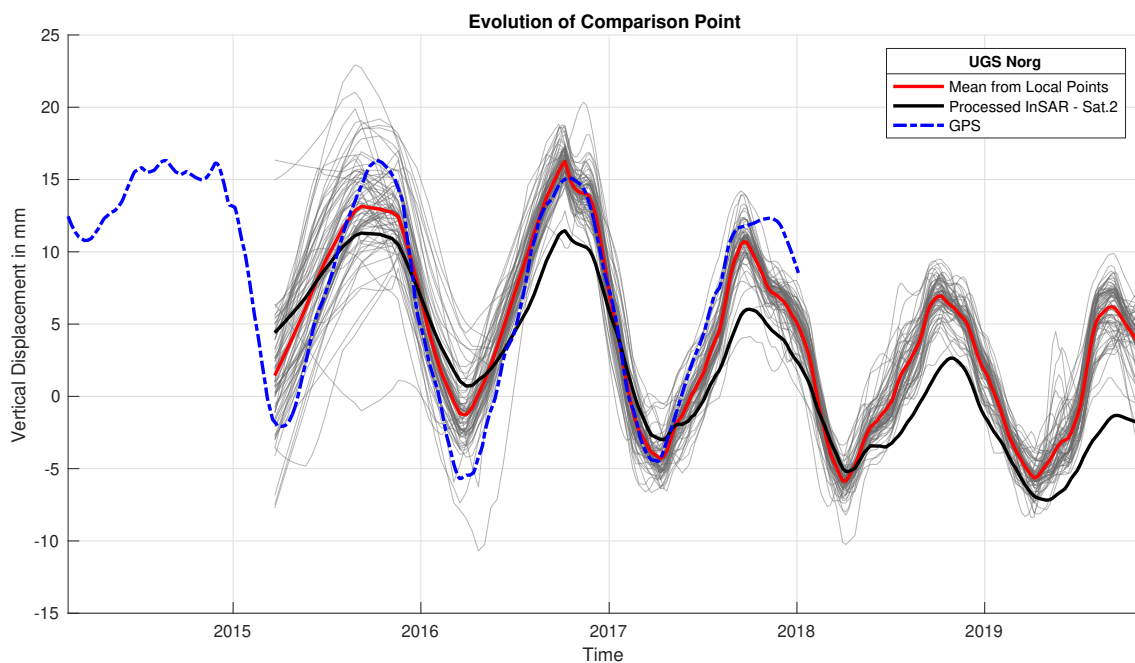


Figure 9. Comparison of InSAR processed data against a local measurement performed with GPS at the UGS Norg Facility. Within a radius of 50 m from the GPS coordinates, about 85 InSAR points are detected by satellite 2, the mean value of these point measurements is included in the comparison and further contrasted against the processed InSAR data which is devised on a 275m grid and includes effects of neighbouring grid cells.

Appendix 1 - Approximate Relationship Curvature-Strain

The curvatures can be employed to estimate the horizontal strains at the soil surface by using a simplistic model of the soil on top of the gas reservoir as an Euler-Bernoulli beam. The InSAR data available does not include horizontal displacements, so the actual surface horizontal strains cannot be observed. With this simple and conservative assumption, the horizontal strains can be computed as per equation 1:

$$\epsilon_h = 1 - \frac{1}{\bar{\kappa} \cdot \left(\frac{1}{\bar{\kappa}} \pm \frac{D}{2} \right)} \quad \text{Equation 1}$$

Where ϵ_h is the estimated horizontal strain at the surface, D is the depth of the soil on top of the gas field ($D \approx 3000$ m), and $\bar{\kappa}$ is the mean curvature of the soil over the length of a grid cell.

Figure A.1 illustrates the Euler-Bernoulli relationship between strain and curvature. In this case, because the curvature is measured at the surface half the soil thickness ($D/2$) needs to be considered in addition or subtraction. The illustration depicts a unitary length of soil which curves up and by doing so, the top fibre of soil stretches horizontally.

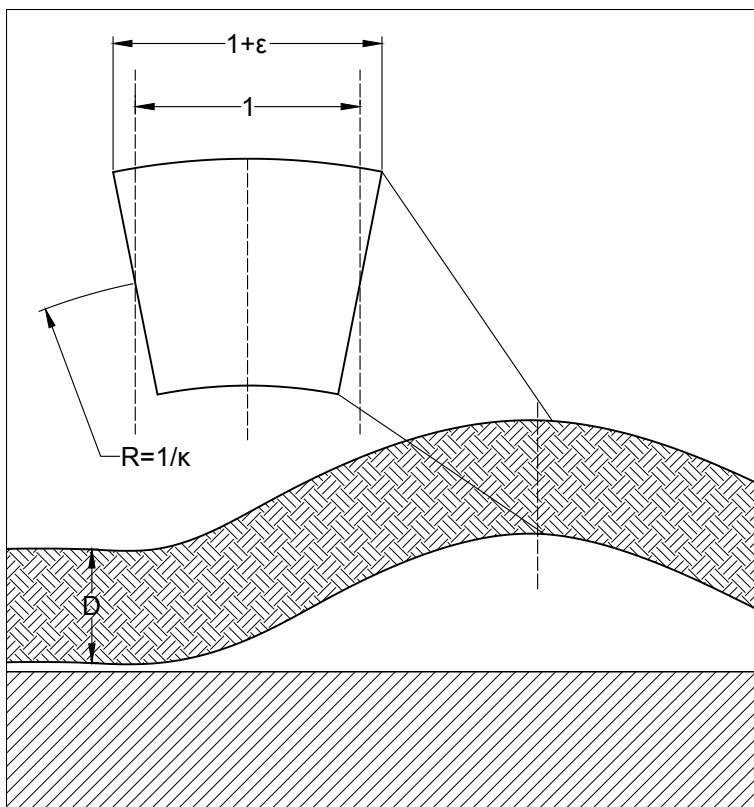


Figure A.1. Sketch of the soil layer of thickness D deformed due to gas storage and the relationship between curvature and horizontal strain. Note that deformations are greatly exaggerated for illustration purposes.

Project	Advies Schadebeoordeling IMG Onderbouwing kans op schade bij opgelegde zettingen door indirekte effecten van diepe bodemdaling
Report number	00
Internal Reference	
Date	October 3, 2022
Version	02
Status	Final

SUPPORTING ANALYSES TO DETERMINE PROBABILITY OF DAMAGE AND FRAGILITY CURVES DUE TO INDIRECT SUBSIDENCE EFFECTS

Client: IMG

Authors Paul A. Korswagen
 P.A.KorswagenEguren@tudelft.nl
 Michele Longo
 M.Longo@tudelft.nl
 Jan G. Rots
 J.G.Rots@tudelft.nl
 Alfonso Prosperi
 A.Prosperi@tudelft.nl

Address Delft University of Technology
 Faculty of Civil Engineering and Geosciences
 Stevinweg 1, 2628 CN, Delft

 <p>Faculty of Civil Engineering and Geosciences Stevinweg 1 2628 CN Delft PO 5048 2600 GA Delft www.citg.tudelft.nl</p>		Report
Title: Supporting analyses to determine probability of damage and fragility curves due to indirect subsidence effects		
Author(s): Paul Korswagen Michele Longo Jan G. Rots Alfonso Prosperi		
Date: Oct 3, 2022		
Client(s): IMG	Version: 02	Status: Final
Project number:	Project name: Advies Schadebeoordeling IMG Onderbouwing kans op schade bij opgelegde zettingen door indirecte effecten van diepe bodemdaling	File reference:
Cite as: P.A. Korswagen, M. Longo, J.G. Rots, A. Prosperi (2022). Supporting analyses to determine probability of damage and fragility curves due to indirect subsidence effects. Delft University of Technology. Report number 00, Final Version 2, October 3, 2022.		

Copyright statement

All rights reserved. No part of this publication may be reproduced, stored in a retrieval system of any nature, or transmitted, in any form or by any means, electronic, mechanical, photocopying, recording or otherwise, without the prior written permission of TU Delft.

Liability statement

TU Delft and those who have contributed to this publication did exercise the greatest care in putting together this publication. However, the possibility should not be excluded that it contains errors and imperfections. Any use of this publication and data from it is entirely on the own responsibility of the user. For everybody who has contributed to this publication, TU Delft disclaims any liability for damage that could result from the use of this publication and data from it, unless the damage results from malice or gross negligence on the part of TU Delft and/or those who have contributed to this publication.

I. Abstract

The extraction and storage of gas in the north of the Netherlands has led to soil subsidence. While its direct effect on buildings is negligible due to the subsidence's deep nature which leads to extremely small curvatures and strains at the ground surface, its indirect effects, via changes in the water table for example, which in turn affect the soil near the ground surface on a local scale, may well cause soil distortions that affect buildings. This study does not focus on what these distortions values may be, but on the response of masonry buildings when subjected to soil distortions in the form of differential settlement profiles, thus establishing safe thresholds based on the probability of exceeding light damage (with cracks wider than 2 mm) for these fired-clay and calcium-silicate brick buildings.

About three thousand finite-element-method numerical models are used herein to estimate the initiation of cracks on masonry façades when subjected to a settlement profile underneath their foundation. The intensity of the settlement deformation is characterised via the angular distortion, with distortions of 1/500 leading to a 20% probability of damage for clay-brick walls on unreinforced (masonry) foundations or 8% for calcium-silicate walls on reinforced (concrete) foundations. The models include geometrical variations, with various façades, opening percentages and opening sizes, and length/height (L/H) ratios characteristic of existing buildings. Material properties are varied based on earlier experimental campaigns and the shape of applied settlement profiles is derived (and varied) from bed joint level measurements from reports of real buildings. The models include a soil-structure interface designed to account for the contribution of the soil around the foundations, which may cushion wall deformation. Six soil-related situations are considered with stiffer or more flexible soil and its interaction with the building. These variations are weighted to match observed parameter distributions, such as the material strength following a normal probabilistic distribution. In this manner, fragility-like exceedance curves are constructed.

The insight gained with these in-plane 2D FEM models reveals that much of the deformation that originates in the soil is not transferred to the buildings. The relatively-stiff foundations and walls, in combination with the flexible soil, limit the amount of distortion reaching the building. Consequently, the distortions measured on damaged masonry walls are 5 to 10 times smaller than applied soil distortions and up to 100 times smaller on walls that attained no damage. In general, slender façades of stiff and strong material, with reinforced concrete foundations, supported on a layer of flexible soil, displayed the least damage, with applied distortions of up to 1/10 generating no damage in many cases; while, long façades on unreinforced foundations (with a L/H ratio larger than 2.5) had an almost 50% probability of exceeding light damage at an applied soil distortion of 1/500.

II. Highlights

- This report describes a FEM modelling study where a settlement displacement is applied to the bottom side of an interface opposite to a 2D masonry geometry, modelled with the continuum Engineering Masonry Model.
- Variations in the masonry properties and geometry, and interface properties mimicking the soil, are used to investigate the probability of cracking in the masonry model.
- Two of the parameters varied have a large influence in determining whether masonry facades will develop damage when subjected to soil distortions: the type of foundation and the length/height ratio of the geometry of the wall.
- Masonry walls on unreinforced foundations are vulnerable. When free-field settlement profiles would show angular distortions of 1/500, the probability of fired-clay brick walls to exceed light damage has been computed at 20%.
- On the other hand, masonry walls, typically calcium-silicate brick walls, on reinforced concrete foundations are significantly less vulnerable, with many models not exceeding light damage even at high values of applied ground distortion; at 1/500, the probability is estimated at 8%.
- Longer facades are more vulnerable; those with a length/height ratio around 4, exhibited about 50% more damage than the average. Conversely, facades shorter than 5 metres or slender than the average ($L/H < 1$) show almost no damage.
- A key observation is that the applied soil distortion must be transferred to the façades for these to deform and crack. Stiffer, shorter, slender, and stronger façades on more flexible soil, will resist this transfer and are thus less vulnerable; while their counterparts will follow the applied distortion more easily and become damaged. This transfer factor varies between 5 to 10 but can go up to 100 for the stiffer façades on flexible soil.

Table of Contents

<i>I. Abstract.....</i>	3
<i>II. Highlights.....</i>	4
<i>III. Management Samenvatting.....</i>	6
<i>IV. Executive Summary.....</i>	15
<i>V. Report.....</i>	23
1. Introduction.....	23
Reader.....	23
Approach.....	23
2. FEM Model – Modelling Approach.....	23
Selected Façades.....	25
Scenarios.....	29
3. Results FEM Model.....	37
Façade 1.....	41
Façade 2.....	47
Façade 3.....	49
Façade 4.....	51
Summary – Unreinforced foundation (Façades 1-2-3-4).....	53
Summary – Reinforced foundation (Façades 5-6-7-8).....	56
4. Probabilistic Results – Fragility Curves.....	61
Exceedance Count.....	61
Weighing for Fragility Curves.....	63
Log-normal distribution Fit.....	65
5. Discussion & Conclusions.....	67
Discussion.....	67
Conclusive Discussion.....	71
Conclusions.....	73
<i>VI. References.....</i>	74

III. Management Samenvatting

Achtergrond

In opdracht van IMG hebben TNO en TU Delft begin 2021 onderbouwd dat diepe bodemdaling bij gasopslag Norg en het Groningerveld in directe zin geen schade aan gebouwen veroorzaakt. Wat betreft de indirekte effecten, bijv. ten gevolge van peilaanpassingen, is onderzoek nog gaande. Deltares heeft geconcludeerd dat de kans op schade bij indirekte effecten niet kan worden uitgesloten. Bij IMG wordt vervolgens een werkinstructie voorbereid hoe hiermee om te gaan.

Op 12 oktober 2021 heeft een overleg plaatsgevonden tussen IMG, Deltares, TNO en TU Delft. Daar is geconstateerd dat er behoefte is aan het onderbouwen van de aannname betreffende de kans op schade aan gebouwen indien zettingen optreden ten gevolge van indirekte effecten. Nader overleg heeft plaats gevonden en aansluitend heeft IMG met externe deskundigen de stand van zaken samengevat waar drie vervolgacties zijn gedefinieerd. Dit rapport betreft de derde voorgestelde vervolgactie: een onderzoek of in kort tijdbestek, op basis van betrekkelijk eenvoudige numerieke modellen, een betere duiding of een eerste inzicht kan worden gekregen over de gehanteerde kans op schade aan gebouwen door ongelijkmatige zettingen.

Gaswinning leidt tot bodemdaling

De gaswinning en gasopslag in de regio Groningen heeft de afgelopen jaren geleid tot diepe bodemdaling en aardbevingen. De vervormingen die door gaswinning en -injectie worden veroorzaakt, kunnen leiden tot scheeftrekkingen, hellingen, krommingen en horizontale rekken van het grondoppervlak, die schadelijk kunnen zijn voor gebouwen. Deze directe effecten van diepe bodemdaling zijn onderzocht door TNO en TU Delft [20, 10, [21]. De conclusie uit het onderzoek sluit het directe effect van gaswinning in het Groningengebied als oorzaak van schade aan gebouwen uit, aangezien de vervormingen van de bodem over grote afstanden optreden en dus leiden tot zeer kleine vervormingen op gebouwniveau die ruim beneden drempelwaarden blijven.

Bodemdaling veroorzaakt indirekte lokale effecten

Maar naast directe effecten kan diepe bodemdaling ook andere bodemverschijnselen veroorzaken die op hun beurt gebouwen aantasten; dit zijn de indirekte effecten. In feite kan de bodemkrimp-/uitzetting door gaswinning/-injectie leiden tot een langzame verandering van de relatieve grondwaterstand (ten opzichte van het maaiveld) [22]. Volgens Deltares [24] kunnen deze veranderingen in de relatieve grondwaterstand (met name de verlaging van dat peil) leiden tot ongelijkmatige zettingen van gebouwen door consolidatie van de ondiepe ondergrond onder de fundering, uitdroging van veen onder de fundering (veenoxidatie), of krimp/zwelling van kleilagen onder de fundering. De beoordeling van de kans op schade door ongelijkmatige zettingen wordt momenteel analytisch geschat op basis van een aantal beschouwingen uit literatuur en metingen [22, 23]. Er is behoefte aan een betere onderbouwing van de kans op schade. Het in dit rapport gepresenteerde onderzoek richt zich daar op. Het richt zich niet zozeer op het bepalen van de verwachte zettingen en bodemvervormingen zelf, maar op de reactie van gebouwen op bepaalde bodemvervormingen.

Geen nieuwe ontwikkelingen afgelopen decennia

Bij het raadplegen van bestaande literatuur over bodemvervorming en gebouwschade, verwijzen de meeste studies terug naar enkele belangrijke publicaties uit de jaren '80 [23] of afgeleiden daarvan; weinig nieuwe gegevens of inzichten zijn opgedaan. Aan de ene kant is dit te wijten aan de moeilijkheid om empirische gegevens te verkrijgen die schade aan gebouwen relateren aan grondvervorming, hetzij vrije-veld grondvervorming of grondvervorming na interactie met het

gebouw; en, aan de andere kant, de noodzakelijke complexiteit van numerieke modellen, die erop gericht zijn voldoende variabiliteit in gebouwen en grond op te nemen om de relatie tussen vervorming en schade nauwkeurig weer te geven, wat zelfs met de huidige rekenkracht nog steeds lastig blijkt. De beschikbare literatuur is daarnaast veelal beperkt tot uitgravingen van tunnels of bouwputten, waar langs de route van de tunnel of rondom de bouwput gerichte monitoringsgegevens kunnen worden verzameld en vergeleken. Dergelijke gegevens van zettingen en schade bij uitgravingen kunnen slechts gedeeltelijk worden vergeleken met de situatie van bodemverstoringen veroorzaakt door de indirecte effecten van mijnbouw-geïnduceerde diepe bodemdaling.

In dit licht presenteert de huidige studie een verdiepende methode, met nieuwe analyses, voortbouwend op bestaande kennis maar op onderscheidende wijze nieuwe resultaten opleverend. De nieuwe elementen, zoals een interface voor de statische interactie tussen bodem en structuur, een materiaalmodel dat in staat en gekalibreerd is om schade in metselwerk te repliceren, een objectieve schadebeoordelingsschaal en een probabilistische benadering met duizenden variaties in gebouwgeometrie, materiaaleigenschappen, etc., stellen deze studie in staat om zijn nieuwe inzicht te verschaffen. Tegelijkertijd moet terughoudendheid worden betracht omdat verschillende aannames zijn gedaan die beperkingen met zich mee brengen. Een aantal aspecten beperken de toepasbaarheid van de conclusies, zoals de 2D-geometrieën en of hun vormen representatief zijn voor kwetsbare metselwerkgebouwen, gebruik van semi-gekoppelde berekeningen (volledig gekoppelde berekeningen waarin zowel de grond als het gebouw worden gemodelleerd waren in het korte tijdsbestek en gezien de scope die zich richtte op een eerste inzicht, niet mogelijk) beperking tot alleen in-het-vlak acties en het niet expliciet meenemen van langetermijneffecten. Deze beperkingen worden verderop besproken.

De intensiteit van zettingsprofielen wordt gekarakteriseerd aan de hand van hun vervorming

Er zijn verschillende parameters die kunnen worden gebruikt om de ernst of mate van vervorming van een zettingsprofiel te bepalen, zoals de rotatie of helling (tilt), de maximale verticale verplaatsing, de relatieve rotatie of de relatieve hoekvervorming. De relatieve hoekvervorming lijkt de schade beter weer te geven [Appendix G] en is ook gebruikt om de kans op schade uit te drukken in kernpublicatie [23]; bijgevolg wordt deze mate van vervorming, uitgedrukt als een kleine hoek of helling, hier gebruikt om de zettingsprofielen te karakteriseren en wordt deze aangeduid met β (bèta).

Vervormingsdrempels voor schade

De criteria voor schade door ongelijkmatige zettingen zijn afgeleid van de relatie tussen schade en de mate van hoekvervorming, zoals gehanteerd in de literatuur. Een eerste hypothese, op basis van literatuuronderzoek naar verschillende criteria, heeft aangegeven dat een hoekvervorming van $\beta = 1/2500$ schade kan uitsluiten. Daarnaast veronderstelt de hypothese dat de kans op schade bij een gehanteerd testcriterium $\beta = 1/500$ gelijk is aan 10%. Deze criteria zijn van toepassing op gebouwen van de naoorlogse generatie, gebouwd met gemetselde bakstenen en mortelvoegen.

Er is echter aanvullend onderzoek nodig om deze waarden te ondersteunen; want verschillende soorten gemetselde gevels/gebouwen zullen zich namelijk verschillend gedragen op basis van verschillende geometrische eigenschappen (zoals lengte, hoogte, lengte/hoogte verhouding), verschillend materiaal, type ‘onderliggend’ zettingsprofiel, bodemgesteldheid, voorschade, enz.

Toegepaste vs. gemeten (opgelegde vs. resulterende) vervormingswaarden

In dit document worden de termen “toegepast” en “gemeten” vaak gebruikt om onderscheid te maken tussen het zettingsprofiel dat op het gebouw wordt toegepast (opgelegd, aan onderzijde fundering) en het zettingsprofiel dat op het gebouw zelf wordt gemeten (resulterend, in de muren van het gebouw). Dit is een belangrijk onderscheid. De eerste staat voor de vervorming van de

bodem als gevolg van bodemverschijnselen zoals bodemverdichting of diepe bodemdaling. Als er geen gebouw aanwezig zou zijn, zou dit profiel aan het oppervlak van de grond worden waargenomen. In deze studie wordt dit vrije-veld vervormde bodemprofiel toegepast op (opgelegd aan) de fundering van het gebouw. Als het gebouw perfect flexibel zou zijn, zou deze het toegepaste profiel volgen en rechtstreeks doorgeven aan de muren van het gebouw. Het gebouw en de fundering zijn echter meestal stijver dan de grond, en dus zullen de vervormingen die op het gebouw worden gemeten, verschillen van de vervormingen die zouden optreden aan het maaiveld voor het geval zonder aanwezigheid van gebouwen. De aanwezigheid van een gebouw zal vanwege haar stijfheid en massa de vervorming van de bodem veranderen en veelal verkleinen ten opzichte van vrije-veld situatie zonder het gebouw. Dit probleem van gekoppelde interactie is moeilijk in kort tijdbestek op te lossen, vooral gezien de talloze variaties in grond en gebouwen. Deze studie gaat daarom uit van een conservatieve benadering die de grote vervorming van de grond fixeert en toepast (oplegt) onder de fundering van het gebouw via een interface die rekening houdt met de flexibiliteit van de grond rond de fundering van het gebouw; dit is een semi-gekoppelde benadering. Ten gevolge van dit toegepaste zettingsprofiel zullen verschillende gebouwen verschillende vervormingsprofielen vertonen. Met andere woorden, het toegepaste profiel kan worden beschouwd als de belasting die op gebouwen inwerkt en die kan worden bepaald door de bodemvervormingsverschijnselen waar te nemen, terwijl de gemeten vervormingsprofielen op de gebouwen overeenkomen met hun reactie bij blootstelling aan het toegepaste profiel.

Dit geeft een soort conceptuele patstelling: enerzijds kan het toegepaste zettingsprofiel waaraan een gebouw wordt blootgesteld worden bepaald en ingevoerd, maar is het lastig te valideren omdat het niet kan worden gemeten; anderzijds is de vervorming op het gebouw wel meetbaar maar lastig te voorspellen of te relateren aan de bodemvervorming. Dit heeft te maken met het sterk niet-lineaire gedrag van het systeem met voortschrijdende scheurvorming in het gebouw bij toenemende zetting. Dienovereenkomstig streeft dit onderzoek ernaar om twee vragen te beantwoorden: Ten eerste, hoeveel schade kan worden verwacht wanneer een gemeten vervorming aanwezig is in gemetselde gebouwen? En ten tweede, welke gemeten vervorming is te verwachten op gebouwen wanneer een bepaalde bodemvervorming wordt toegepast? Dit maakt het mogelijk om schade aan gebouwen te voorspellen wanneer bodemverschijnselen redelijkerwijs worden begrepen. De studie is op deze wijze ingericht, de schade is beschreven met een nieuw geïntroduceerde scalaire schadeparameter, een verzameling van modellen met variaties is doorgerekend en vervolgens zijn de bevindingen samengevat.

Gemetselde wanden op betonnen strookfunderingen vertonen zeer beperkte schade

Bij een bétawaarde van 1/500 voorspelt de verzameling van modellen die hier zijn geëvalueerd een kans van 25% op lichte of cosmetische schade in baksteenmuren op traditionele gemetselde funderingen. Modellen van kalkzandsteenmetselwerk op gewapend betonnen strookfunderingen vertoonden daarentegen geen of slechts voor het menselijk oog onzichtbare schade bij eenzelfde mate van opgelegde bodemvervorming. Een gewapend betonnen strookfundering zorgt er kennelijk voor dat de bodemvervorming niet of nauwelijks wordt overgedragen naar de muren, terwijl een ongewapende metselwerkfundering die overdracht niet kan voorkomen zodat de wanden vervormen en worden onderworpen aan spanningen die tot zichtbare scheuren leiden.

Deze conclusie is een aanwijzing voor IMG om bij de uitwerking van de regeling voor indirekte effecten te overwegen een onderscheid te maken tussen relatief oude gebouwen op gemetselde funderingen en nieuwe gebouwen op betonnen strookfunderingen.

Schade wordt gemeten met een integrale schadeparameter voor zichtbare scheuren

De meeste gebouwschade, als gevolg van indirekte effecten van bodemdaling, zal van lichte of cosmetische aard zijn, aangezien de bodemvervormingen ook klein zijn. Licht beschadigde gemetselde gebouwen vertonen scheuren die zichtbaar worden vanaf een breedte van ongeveer 0,1

millimeter. Flinkere scheuren met een wijde groter dan 2 mm zijn gemakkelijker te detecteren, moeilijker te repareren en kunnen overeenkomen met constructieve schade. Het begin van scheuren is dus geen academische kwestie, omdat het overeenkomt met het begin van lichte schade. In dit onderzoek is de kans op het bereiken of overschrijden van deze lichte schade gekwantificeerd. Een schadeparameter, Ψ , die de breedte, lengte en het aantal scheuren in een muur in één getal samenvat, onder de veronderstelling dat grotere of een groter aantal scheuren ook beter detecteerbaar en duurder te repareren zijn, wordt gebruikt voor de drempel voor lichte schade. De drempel van 2 mm voor het definiëren van lichte schade is relatief streng in vergelijking met andere onderzoeken; dit zorgt ervoor dat de verkregen waarden voor de vervorming die schade veroorzaakt conservatief zijn.

Verzameling eindige-elementenmodellen om schade aan gebouwen die onderhevig zijn aan bodemvervorming te evalueren

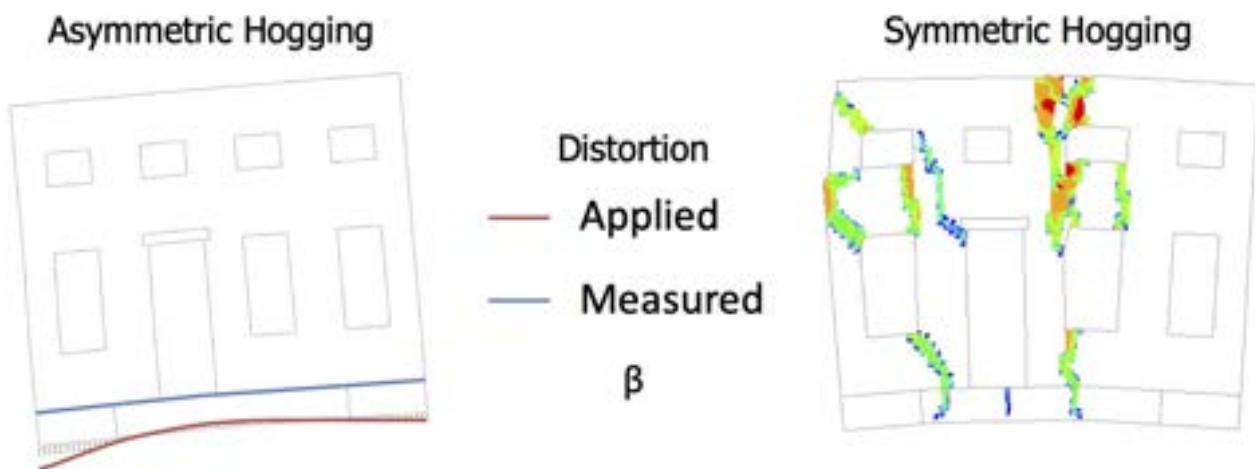
Om de relatie tussen bodemvervorming en bouwschade, en meer specifiek de kans op bouwschade, te beoordelen, wordt in deze studie een groot aantal eindige-elementenmethode-modellen gegenereerd, doorgerekend en geanalyseerd. Deze rekenmodellen dienen ter ondersteuning van literatuur en empirische gegevens over het indirekte effect van de diepe bodemdaling, met als einddoel het kwantificeren van de kans op schade aan metselwerkgevels bij specifieke hoekvervormingen. Om dit te bereiken, worden verschillende gemetselde gevels geselecteerd en numeriek gemodelleerd in 2D. De verschillende gevels beschrijven gebouwen van specifieke bouwperiodes, met verschillende geometrieën, dus variërend in lengte, hoogte en openingsconfiguraties (openingspercentages). Het indirekte effect van de diepe bodemdaling gerelateerd aan een verandering van het waterpeil is in het model opgenomen als toegepaste (opgelegde) zettingsvervorming. Er worden verschillende vervormingsprofielen geanalyseerd. Daarnaast worden materiaaleigenschappen, grondsoort onder de gevel en bodem-gebouw interactie-eigenschappen meegenomen in de modellen. Ongeveer honderd modellen met metselwerk van kalkzandsteen op gewapend betonfunderingen en bijna drieduizend modellen van het meer gevoelige baksteenmetselwerk op ongewapende metselwerkfunderingen zijn geëvalueerd in meer dan zesduizend uur computertijd. De grote hoeveelheid verzamelde gegevens maakt het mogelijk om de resultaten op een probabilistische manier te verwerken.

Zwak metselwerk is het meest gevoelig

Er werden twee materialen en twee funderingstypes onderzocht: kalkzandsteenmetselwerk, gefundeerd op gewapende betonnen strokenfunderingen (al dan niet op palen), kenmerkend voor nieuwere gebouwen en baksteenmetselwerk op ongewapende gemetselde funderingen, kenmerkend voor oudere constructies, en ook enkele variaties voor baksteenmetselwerk op gewapend betonnen stroken funderingen. Materiaaleigenschappen zoals sterkte en elasticiteitsmodulus werden gevarieerd in drie sets die overeenkomen met een zwak, standaard en sterk metselwerk. Voor metselwerk van baksteen op gemetselde funderingen, dat het meest gevoelig was voor de bodemvervormingen, werden twee aanvullende materiaalsets onderzocht voor redelijk-zwak en redelijk-sterk. Deze variatiesets, gebaseerd op uitgebreide metselwerkcharakterisering uitgevoerd aan de TU Delft, dienden om een goed beeld te krijgen van de invloed van het materiaal op de kans op schade door bodemverstoringen. Het zwakkste metselwerk, ongeveer vier keer zwakkere in trek dan de gemiddelde waarde in de NPR voor bestaand metselwerk, liep ook het grootste risico op het ontwikkelen van scheuren. Terwijl de op de gebouwen gemeten vervorming tussen de verschillende materialen vergelijkbaar was, volgde het zwakkere en ook flexibele materiaal de aangebrachte zettingsvervorming gemakkelijker en raakte zo beschadigd bij ongeveer de helft van de vervormingswaarden die het gemiddelde materiaal kon weerstaan.

Vier Façade-varianten om de meest kwetsbare gevallen vast te leggen

De EEM-modellen die in DIANA zijn uitgewerkt, maken gebruik van het Engineering Masonry Model met parameters die zijn gekalibreerd tegen experimenten op metselwerkmuur van baksteen die specifiek zijn uitgevoerd om het ontstaan en de voortplanting van scheuren te onderzoeken. Dit niet-lineaire materiaalmodel, dat dus in staat is om te reproduceren hoe scheuren verschijnen en groeien in metselwerk, wordt gebruikt om vier verschillende gevelgeometrieën te analyseren, elk met verschillende variaties. In totaal zijn ongeveer 40 geometrieveranderingen doorgevoerd met verschillende gevallenlengtes, hoogtes, openingspercentages en openingstypen met veel kleine openingen voor ramen, of grotere openingen. De lengte/hoogte verhouding varieerde van 1 (een vierkante gevel) tot 4 (een lange gevel). De langere gevallen waren gevoeliger voor zettingsschade, waarbij de relatief flexibele gevallen de aangebrachte vervorming beter volgden en scheuren aan de bovenkant van de gevel sneller en bij lagere vervormingswaarden begonnen.



Figuur 1. Illustratie van de twee onderzochte zettingsprofielen. Links, asymmetrische hoging met differentiële zetting aan de linkerkant, het verschil tussen het aangebrachte profiel onder de fundering en het gemeten vervormingsprofiel op het gebouw. Rechts, een voorbeeld van symmetrische hoging met de locatie van de resulterende scheuren in de gemetselde gevel.

Asymmetrische hoging-zettingsprofielen zijn het meest schadelijk

De modellen bevatten ook variaties in de vorm van de onder de gebouwen aangebrachte zettingsprofielen. Voorlopige modellen toonden aan dat hoging-gevallen, waarbij het bodemprofiel een convexe vorm heeft en beide of slechts één uiteinde van het gebouw naar beneden beweegt, schadelijker waren dan de sagging-gevallen, met een concave kromming waarbij het midden van het gebouw naar beneden beweegt. Dienovereenkomstig werden hoging-gevallen, zowel symmetrisch (beide uiteinden bewegen naar beneden) als asymmetrisch (alleen het linker uiteinde vervormt) nader onderzocht, elk met twee typen waarbij een kleiner of groter deel van de fundering naar beneden werd vervormd. De symmetrische gevallen waarbij een groter deel van de fundering verticaal verplaatste, vertoonden eerder schade bij strengere vervormingswaarden.

Variaties in de bodem werden ook bestudeerd

De stijfheid van de grond en hoe deze samenwerkt met de constructie erboven speelt ook een rol. De grond rond een gebouw kan dienen als kussen voor de grondvervormingen op grotere diepte. Om hoeveel grond het gaat, hangt af van de afmetingen van de fundering, de eigenschappen van het gebouw en de eigenschappen van de grond. Equivalenten veren worden gemodelleerd op het grensvlak tussen de onderkant van de fundering en het toegepaste zettingsprofiel; deze veren bootsen het effect van de grond rondom het gebouw na en zijn gedefinieerd op basis van eerdere kalibraties en internationale geaccepteerde formuleringen. Om de potentiële verschillen in bodemprofielen te evalueren, zijn een zandbodem en een veenbodem opgenomen, beide met extra variaties in grensvlakstijfheid (laag, standaard en hoog) voor in totaal zes bodemgerelateerde

variaties. Zoals verwacht, absorbeert de zachtere veengrond de aangebrachte bodemvervormingen waardoor de gebouwen de mogelijkheid hebben om te roteren maar niet vervormen, waardoor er minder vervorming in het metselwerk en dus minder schade ontstaat. Onder gebouwen op zachte grond moet gemiddeld een twee keer zo grote vervorming worden aangebracht om dezelfde schade te veroorzaken als gebouwen op de stugger zandgrond.

Er verschijnen scheuren rond ramen

De modellen laten zien hoe in de meeste gevallen scheuren ontstaan rond de openingen voor de ramen. De scheuren beginnen bij de hoeken en planten zich diagonaal of horizontaal voort, of beginnen in het midden van de omtrek rond de openingen en planten zich verticaal voort. De scheuren groeien in de breedte en in de lengte totdat ze de bovenkant van de muur of een andere opening bereiken; dan groeien scheuren aanzienlijk als de muur zich in meerdere blokken splitst na de aangebrachte bodemvervorming. Op dit punt heeft het metselwerk de lichte schade ruimschoots overschreden. De aanvankelijke scheuren, hoewel lichte schade, wijzen op een mogelijk later faalmechanisme met betrekking tot de veiligheid of de uiterste grenstoestand van de constructie. Dit suggereert dat de staat van lichte schade potentieel ook van invloed kan zijn op de latere veiligheid van de constructie; dit effect is echter niet onderzocht in deze studie.

In deze studie werd alleen gekeken naar 'lichte schade'-scheuren in het vlak

Lichte schade is het meest voorkomende type schade in constructies, aangezien zeer lage vervormingen al kleine scheuren in metselwerkmuur kunnen veroorzaken. Om deze reden heeft dit onderzoek zich gericht op deze initiële schadetoestand. Om dit te doen, is het gedrag van de muren in het vlak geanalyseerd, waarbij scheuren in detail zijn geobserveerd; schade is echter niet beperkt tot scheuren: effecten uit het vlak, zoals naar voren of naar achteren kantelen, of uitpuilen of uitbuiken van de wanden kunnen niet worden waargenomen met de in deze studie gebruikte 2D-modellen. Desalniettemin wordt verwacht dat deze vervormingen uit het vlak geassocieerd zijn met een hogere mate van constructieve schade dan lichte schade. Verder is er rekening gehouden met 3D-effecten aan de begrenzingen van de muren, maar complexe 3D-interacties met andere bouwcomponenten zoals vloeren of zadeldaken kunnen eenvoudigweg niet worden meegenomen in de 2D-gevelmodellen. Evenzo bevatten de zettingsprofielen alleen verticale verplaatsingen; horizontale rekken of verplaatsingen zijn verwaarloosd vanwege hun aanzienlijk kleinere omvang in vergelijking met de verticale en ook omdat de opgenomen interface tussen grond en gebouw slip toelaat, wat de potentiële invloed van horizontale verplaatsingen verder zou verminderen. Bijkomende beperkingen van de modellen hebben betrekking op hun weergave van de geometrieën van de gebouwen; deze zijn geselecteerd om kwetsbare Nederlandse gemetselde gebouwen en hun variaties nauwkeurig weer te geven, maar niet alle unieke of extreme gevallen zullen zijn afgedekt.

Een relatie tussen vervorming (β) en lichte schade met behulp van een gewogen benadering

Van de bijna drieduizend gevelmodellen die voor het geval van bakstenenmuren op gevoelige funderingen zijn gebruikt, overschreed ongeveer 18% van hen de lichte schade wanneer de toegepaste vervorming 1/500 bereikte en vertoonde ze een meetbare vervorming op de muren die ongeveer zeven keer kleiner was (~1/3500). Bij een toegepaste bèta van slechts 1/1000 overschreed ongeveer 8% van de modellen lichte schade. Het tellen van het aantal modellen dat drempels overschrijdt, is echter niet helemaal correct, aangezien het zeer zwakke of zeer sterke materiaal minder voorkomt in echte gebouwen dan bijvoorbeeld het standaard of gemiddelde materiaal. Daarom wordt een gewogen benadering gebruikt om de geanalyseerde modellen beter te laten lijken op de verdelingen van de verschillende parameters zoals aanwezig in echte gebouwen op de getroffen locatie. De gewichten wijzigen de telling van de modellen zodat het de probabilistische verdelingen nabootst die in echte gebouwen worden waargenomen. Onder dit uitgangspunt zijn de materiaalparameters ingesteld om een normale verdeling te volgen met een bekende

standaarddeviatie; de zachte grond komt minder vaak voor; asymmetrische profielen zijn waarschijnlijker; interface stijfheden zijn gecorreleerd met grondsoorten; en zettingsvormen zijn gecorreleerd aan de lengte van gevels. De gewogen resultaten verschillen enigszins van de ongewogen resultaten; toch vergroot deze benadering het vertrouwen in de geproduceerde ‘fragility curves’.

Gemeten vervormingswaarden zijn 5 tot 10 keer kleiner dan de bodemvervorming onder de fundering

Deze studie heeft een schril contrast aangetoond tussen de vervorming die wordt aangebracht onder de fundering, die de vervorming van de bodem nabootst door verdichting, uitdroging, diepe bodemdaling of andere geotechnische verschijnselen, en de vervorming die optreedt op de muren of gevels van de gebouwen. Gebouwen gefundeerd op strokenfunderingen van gewapend beton (voornamelijk gebouwen van kalkzandsteen) werden goed ondersteund door hun funderingen, zodat bodemvervormingen niet werden overgedragen en dus niet meetbaar waren in de gebouwen. Aan de andere kant konden gevoeligere, ongewapende funderingen, zoals gemetselde funderingen, niet voorkomen dat de grondbewegingen werden overgedragen naar de muren. Desalniettemin werd de hoeveelheid overgedragen vervorming verminderd door de stijfheid van het gebouw en de interactie met de grond. Flexibele gebouwen volgden de bodemvervormingen nauwkeuriger, maar vertoonden nog steeds slechts ongeveer 1/5 van de toegepaste vervorming, terwijl stijvere gebouwen slechts 1/10 of zelfs minder van de toegepaste vervorming vertoonden voor waarden van grondvervorming rond 1/500. Ook langere gevels volgden beter het bodemprofiel. Naarmate het metselwerk beschadigd raakt, worden de gevels flexibeler en wordt het verschil tussen de aangebrachte en gemeten vervorming kleiner; een gevel opgesplitst in meerdere blokken, voorbij lichte schade, zou het bodemprofiel bijna 1:1 volgen.

Empirische vergelijkingsgegevens laten minder schade zien

De resultaten van dit modelleringsonderzoek zijn vergeleken met empirische gegevens uit de analyse van gebouwschaderapporten [Appendix G]. In de vergelijkende studie werd gekeken naar de schade die werd gerapporteerd in ongeveer 390 gevallen van gemetselde gebouwen die ook werden onderzocht door de vervormingen van de voegen van het metselwerk te meten (waterpas lintvoegmetingen). De horizontale voegen van het metselwerk worden verondersteld waterpas te zijn gebouwd en door hun posities nauwkeurig te volgen, kunnen de vervormingen van de gebouwen in de loop van de tijd worden gereproduceerd. Met andere woorden, de empirische studie relateert de gemeten gebouwvervorming aan de intensiteit van de schade. Wanneer naast de uitkomst van dit modelleringsonderzoek de door de vergelijkingsstudie vastgestelde grens voor lichte schade (DL1) wordt getrokken, komt de kans op schade voor waarden van de toegepaste (opgelegde) vervorming vanuit de bodem goed overeen. In de vergelijkende studie wordt echter gekeken naar de gemeten vervorming van gebouwen waarvan is vastgesteld dat deze ongeveer 7 keer kleiner is dan de toegepaste vervorming. Dit betekent dat óf de resultaten van dit modelleringsonderzoek te strikt conservatief zijn, óf dat de empirische curven te optimistisch zijn.

Binnen het bestek van deze studie is het niet mogelijk geweest om dit verschil te verzoenen, maar er zijn verschillende hypothesen geformuleerd. Ten eerste zijn de definities van lichte schade in beide onderzoeken niet identiek. In deze modelstudie is een drempel van ca. 2 mm voor de scheurwijdte (overeenkomend met een waarde van de schadeparameter $\Psi=2,5$) gesteld, terwijl het vergelijkende onderzoek is gebaseerd op de beoordeling van foto's van de schade die wordt beïnvloed door de waarneming van schade, aangezien scheuren langs mortelvoegen aan het zicht kunnen worden onttrokken. Ten tweede kan het meten van de vervorming van echte muren leiden tot hogere β 's, omdat punten op vaste, beperkte intervallen worden verzameld, wat suggereert dat schade optreedt bij hogere vervormingswaarden dan wat er feitelijk aanwezig zou kunnen zijn. Evenzo kan de

locatie of hoogte op de muren waar de metingen worden uitgevoerd, van invloed zijn op de uitvoer van bêtawaarden. Ten derde kan de empirische dataset vertekend zijn omdat de inspecties zijn uitgevoerd op gebouwen die schade vertoonden, maar andere gebouwen, die bijvoorbeeld hoge vervormingswaarden vertonen maar geen schade vertonen, zijn mogelijk niet onderzocht. De dataset vertegenwoordigt een gemakssteekproef en niet een willekeurige.

Ten vierde kunnen vervormingen die in de loop van jaren langzaam plaatsvinden, door het metselwerk worden opgevangen zonder scheuren te vertonen. Dit kruipeffect kan zelfs worden versterkt door autogene genezing van het cement of de kalk in de mortel, die kleine scheurtjes kan opvullen [20]. Er werden enkele modelvariaties uitgevoerd die rekening hielden met het kruipeffect, maar er bleef een verschil van 3 tot 5 over tussen de toegepaste en gemeten vervormingen. Ten vijfde zijn de materiaaleigenschappen niet gekalibreerd tegen grote en oude metselwerkmonsters die een flexibeler algemeen gedrag zouden kunnen vertonen dan wat is gemodelleerd op basis van proeven op kleine monsters. Hierdoor zou ook de gemeten vervorming dichter bij de toegepaste bodemvervormingen komen te liggen.

Samengevat, schadecurven van empirische resultaten liggen dicht bij die geproduceerd door te kijken naar de toegepaste vervormingswaarden, wat suggereert dat gemeten vervormingswaarden op metselwerkgevels minder strikt zouden moeten zijn en nauwer de toegepaste bodemvervormingen zouden moeten volgen.

Funderingstype en muurlengte/hoogte meest invloedrijke parameters

Bij het onderzoeken van de relatie tussen schade en de verschillende onderzochte parameters zijn twee parameters verreweg het meest invloedrijk. Ten eerste het funderingstype, of de fundering nu gewapend beton of ongewapend metselwerk van beton is. De sterkere en stijvere fundering beperkt de bodemvervorming die wordt overgedragen op de gebouwen. Gemetselde muren op de gewapende funderingen zijn bestand tegen bodemvervormingen die een orde van grootte hoger zijn dan die op ongewapend funderingen. Ten tweede bepaalt de wandgeometrie, uitgedrukt in de verhouding lengte tot hoogte, ook sterk of gemetselde muren zullen worden aangetast door bodemvervormingen. De langere muren, met verhoudingen van ongeveer 3 tot 4, lopen twee keer zoveel schade op bij gelijke bodemvervorming als hun vierkante tegenhangers (verhouding 1).

Conclusie: lichte schade waarschijnlijk voor gevoelige funderingen

Extreem hoge waarden van bodemvervorming (1/100) waren nodig om scheuren van 0,1 mm te veroorzaken in gebouwen met gewapend betonnen funderingen, die vanaf 1970 gebruikelijk zijn onder metselwerkconstructies en typisch gebouwd zijn van kalkzandsteen; de eindige-elementenmodellen overtroffen de lichte schade niet bij welke realistische waarde van bodemvervorming dan ook. Andere constructies, met ongewapende (metselwerk)funderingen en meestal met baksteenmetselwerkgevels waren echter significant kwetsbaarder met een kans van 25% op lichte schade (scheuren wijder dan 2 mm) bij aangebrachte vervormingen (relatieve rotatie) in de orde van 1/500. Bij een bodemvervorming van 1/4000 wordt de kans op overschrijding van lichte schade voor de gebouwen op kwetsbare funderingen geschat op 10%.

Verergering/toename van schade

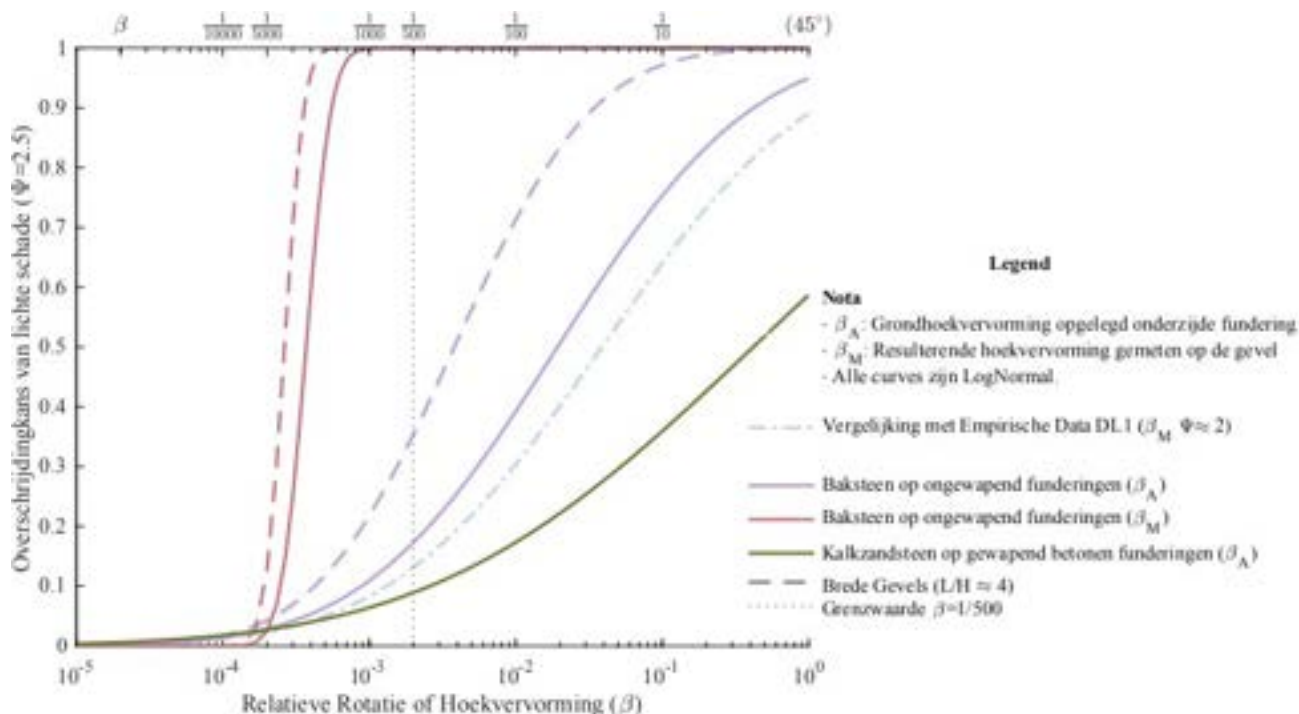
Verder is het mogelijk dat schade veroorzaakt door andere acties zoals thermische uitzetting, krimp of differentiële zettingen door autogene oorzaken, en die al aanwezig kan zijn in het metselwerk, wordt vergroot of verergerd door de indirekte effecten van diepe bodemdaling. Het gescheurde metselwerk gedraagt zich flexibeler en volgt daardoor beter de vorm van het toegepaste zettingsprofiel. Bovendien hoeven bestaande scheuren slechts iets groter te worden om zichtbaar te worden of lichte schade te overschrijden. De modelresultaten werden geanalyseerd en een toename van vervorming werd gerelateerd aan een toename van schade ($\Delta\beta \rightarrow \Delta\Psi$). Als een gemeten bêta van minimaal 1/10.000 wordt waargenomen of voorspeld en er is sprake van bestaande, nauwelijks

zichtbare gebouwschade, dan schatten de analyses dat de kans op overschrijding van lichte schade groter is dan 10% voor gebouwen zowel op onversterkte als versterkte funderingen. Merk op dat de gebouwen op versterkte funderingen minder snel deze meetbare vervorming vertonen.

Er is de vraag of deze verergering van de schade economisch verlies vertegenwoordigt, aangezien de reparatiekosten vergelijkbaar, en soms identiek, voor de bestaande of de verergerde schade zijn.

Kwetsbaarheidscurven geven de kans op lichte schade als gevolg van zettingen weer voor verschillende soorten gebouwen

Voor verschillende geotechnische fenomenen zoals veranderingen in de grondwaterspiegel, oxidatie van veen, verdichting van klei of andere diepliggende oorzaken kunnen maaiveld- of vrije bodemvervormingen worden bepaald. Deze bodemvervormingen kunnen, wanneer toegepast op gebouwen, vervormingen veroorzaken op de stijve gemetselde gevels die op hun beurt scheuren en schade kunnen veroorzaken. De in dit rapport gepresenteerde kwetsbaarheidscurven geven het type en de waarschijnlijkheid van lichte schade aan die kan worden verwacht voor deze bodemvervormingen, gemeten als relatieve rotatie (vervorming) van de zettingsprofielen voor verschillende soorten metselwerkgebouwen.



Figuur 2. Vervorming tegen de kans op overschrijding lichte schade, zowel voor de door de bodem aangebrachte vervorming als de vervorming gemeten op de gemetselde gevels. Ongeveer 70% van de gebouwen op funderingen van gewapend beton (RC) vertoonden helemaal geen lichte schade, terwijl de gebouwen op ongewapende (UR) funderingen aanzienlijk meer schade vertoonden. Lange gevels zijn gevoeliger.

IV. Executive Summary

Gas extraction led to Soil subsidence

In recent years, gas extraction and gas storage in the Groningen region has led to deep subsidence and earthquakes. The deformations caused by gas extraction and injection produce skews, slopes, curvatures and elongations of the ground surface, which can be harmful to buildings. These direct effects of deep subsidence have been investigated by TNO and TU Delft [10, 20, 21]. The conclusion from the research excludes the direct effect of gas extraction in the Groningen Area as a cause of damage to buildings since the deformations of the soil occur over large distances and so lead to negligible distortions at the building level.

Soil subsidence caused indirect local effects

Besides direct effects however, deep subsidence can also have trigger other soil phenomena that in turn affect buildings; these are the indirect effects. In fact, the soil shrinkage/expansion due to gas extraction/injection can lead to a slow change in the relative groundwater level (relative to the ground level) [22]. According to Deltares [24] these changes in the relative groundwater table (in particular the lowering of said level) can lead to uneven settlements of buildings due to consolidation of the shallow subsoil underneath the foundation, dryness of peat under the foundation (peat oxidation), or shrinkage/swelling of clay layers under the foundation. The assessment of damage due to uneven settlements is determined analytically on the basis of a number of considerations taken from literature and field measurements [22, 23]. However, the determination of the expected settlements and soil deformations are not the topic of the study presented herein; instead, the response of buildings towards certain deformations is explored.

No new developments in past decades

When consulting existing literature relating ground distortion to building damage, most studies refer back to a few key publications in the 1980s [23] or derivations therefrom; little new data or insight has been gained. On the one hand, this is due to the difficulty in obtaining empirical data that compares building damage and free-field ground distortion where buildings are present; and, on the other hand, the necessary complexity of numerical models, that aim to include sufficient building and soil variability to accurately portray the distortion-damage relationship, which makes them expensive even with today's computational power. The available literature is thus confined to tunnelling situations, where, along the tunnel's route, data over varying cases can be collected and contrasted. Yet, tunnelling-induced distortions can only partially be compared to the situation of ground distortions caused by the indirect effects of deep ground subsidence.

In this light, the current study presents a new method, with new analyses, building upon existing knowledge but distinctively producing new results and new insights. Accordingly, these first findings must be critically judged and their limitations kept present. While the new elements such as an interface for the static soil-structure interaction, a material model capable and calibrated to replicate damage in masonry, an objective damage assessment scale, and a probabilistic approach with thousands of variations in building geometry, material properties, soil properties, etc., allow this study to provide its new insight, several aspects also limit the applicability of its conclusions, such as the 2D geometries and whether their shapes are representative of vulnerable masonry buildings, restriction to only in-plane actions, and neglect of long-term effects. These limitations are discussed further on.

The intensity of settlement profiles is characterised using their distortion

There are several parameters that can be used to determine the severity or degree of deformation of a settlement profile such as its rotation or tilt, its maximum vertical displacement, or its relative rotation or distortion. The distortion seems to better represent damage [Appendix G] and has also been used to express the probability of damage [23]; consequently, the degree of distortion, expressed as a small angle or slope, is used herein to characterise the settlement profiles and is denoted β (beta).

Set distortion thresholds for damage

The criteria for damage due to uneven settlements are derived from the relationship between damage and the degree of angular deformation, as employed in literature. Based on a literature study into various criteria, a first hypothesis has indicated that an angular distortion of $\beta_x = 1/2500$ could exclude damage due to soil deformation. The chance of damage with the applied test criterion $\beta_x = 1/500$ is 10%. These criteria apply to post-war generation buildings, built with masonry bricks and mortar joints.

However, additional research is required to support these values; as, in fact, different types of masonry façades/buildings will behave differently based on various geometrical properties (such as length, height, length/height ratio, etc), material, imposed settlement profile, soil condition, pre-damage, etc.

Applied vs. Measured Distortion Values

In this document, the terms applied and measured are used often to distinguish between the settlement profile that is applied to the building and that which appears on the building itself. This is an important distinction. The former represents the deformation of the soil as a consequence of ground phenomena such as soil compaction or deep subsidence. If a building were not present, this profile would be observed at the surface of the ground. In this study, this innate, deformed soil profile is applied at the foundation of the building. If the building were perfectly flexible, it would follow the applied profile and this would be mimicked on the walls of the building. However, the building and its foundation are usually stiffer than the soil, and so the deformations measured on the building will differ from those that would appear at the ground surface free of buildings. Furthermore, the presence of a building will also alter the deformation of the soil. This coupled interaction problem is difficult to solve, especially considering the myriad of soil and building variations. This study has conservatively fixated the large deformation of the soil and applied it below the foundation of the building via an interface that considers the flexibility of the soil surrounding the foundation of the building; this is a semi-coupled approach. Under this applied settlement profile, different buildings will exhibit distinct deformation profiles. In other words, the applied profile can be considered as the load acting on buildings and which can be determined by observing the soil deformation phenomena, while the measured deformation profiles on the buildings correspond to their response when subjected to the applied profile.

This presents the following dichotomy: on the one hand, the applied settlement profile to which a building will be exposed can be calculated, but is difficult to validate since it cannot be measured. On the other hand, the deformation on the building can be measured but is difficult to predict or relate to the soil deformation. Accordingly, this study strives to answer two questions: First, how much damage can be expected when a measured deformation is present in masonry buildings? And second, what measured deformation can be expected on buildings when a certain soil deformation is applied? This will allow predictions of building damage when soil phenomena are reasonably understood.

Masonry walls on concrete strip foundations show limited damage

At a beta value of 1/500, the collection of models evaluated herein predict a 25% probability of exceeding light or cosmetic damage in bare, clay-brick masonry walls. However, other models of

calcium-silicate brick masonry, founded on reinforced concrete strip foundations, showed no or invisible damage at similar soil distortions. The clay-brick walls, with conservative brick or unreinforced foundations, could not prevent the soil deformation from being transferred to the buildings. Therefore, the walls also become distorted and subjected to stresses in tension which lead to visible cracks. These results are further elaborated in the following paragraphs.

Cosmetic damage is measured with the width of visible cracks

Most building damage, consequence of the indirect effects of subsidence, will be of a light or cosmetic nature as the soil deformations are also small. Lightly damaged masonry buildings exhibit cracks which become visible at around 0.1 millimetres in width and can reach up to 2 mm. Wider cracks are easier to detect, more difficult to repair, and may correspond to more serious structural damage. The onset of cracking is thus not an academic issue, as it corresponds to the beginning of light damage. In this study, the probability of reaching or exceeding this light damage has been quantified. A damage parameter, Ψ , which summarises in one number the width, length and number of cracks in a wall, under the premise that longer or a larger number of cracks are also more detectable and costlier to repair, is used to measure and set the threshold for light damage. Note that the threshold of 2 mm for defining light damage is relatively strict in comparison with other studies; this ensures that the values obtained for the distortion that causes damage are conservative.

Finite-element models to evaluate building damage subjected to soil deformation

To assess the relationship between the soil distortion and building damage, but more specifically, the probability of building damage, a large number of finite-element-method models are analysed herein. These computational models are to support literature and empirical data on the indirect effect of the deep subsidence, with the final objective being the quantification of the probability of damage of masonry façades at specific angular distortions. To achieve this, several masonry façades are selected and numerically modelled in two dimensions. The different façades describe buildings of specific construction periods, having different geometries, thus varying in length, height and opening configurations (opening percentages). The indirect effect of the deep subsidence related to a change of the water level is included in the model as applied settlement deformation. Various deformation profiles are analysed. In addition, material properties, soil type underneath the façade, and soil-structure interaction properties are included in the models. About one hundred models with calcium-silicate brick masonry on RC foundations and almost three thousand models of the more sensitive clay-brick masonry on masonry foundations have been evaluated in over six thousand hours of computational analysis time. The large amount of data acquired allows handling of the results in a probabilistic manner.

Weak masonry is most sensitive

Two materials and two foundation types were investigated: calcium-silicate brick masonry, more typical in newer buildings founded on (piled) reinforced concrete strip foundations, and fired-clay brick masonry on concrete strip but also masonry strip foundations and characteristic of older structures. Material properties such as strength and elastic moduli were varied in three sets corresponding to a weak, standard and strong masonry. For clay-brick masonry founded on masonry footings, which was most sensitive to the soil distortions, two additional material sets were investigated for slightly weak and slightly strong. These variation sets, based on extensive masonry characterisation conducted at the TU Delft, served to provide a good picture of the material's influence on the probability of damage against soil distortions. The weakest masonry, about four times weaker in tension than the mean value given by the NPR to characterise existing masonry, was also the most at risk of developing cracks. While the distortion measured on the buildings was similar between the various materials, the weaker and also more flexible material followed the

applied settlement distortion more easily and thus became damaged at about half the distortion values that the average material could withstand.

Four Façade variations to capture most vulnerable cases

The FEM models elaborated in DIANA employ the Engineering Masonry Model with parameters calibrated against experiments on clay-brick masonry walls specifically conducted to investigate the initiation and propagation of cracks. This non-linear material model, thus capable of reproducing how cracks appear and grow in masonry, is used to analyse four different façade geometries, each with several variations. In total, about 40 geometry variations were implemented with various façade lengths, heights, opening percentages and opening types with many small openings for windows, or larger openings. With length/height ratios varying from 1 (a square façade) to 4 (a long façade). The longer façades were more susceptible to settlement damage, with the comparatively more flexible façades following the applied distortion more closely and cracks initiating at the top of the façade quicker and at lower distortion values.

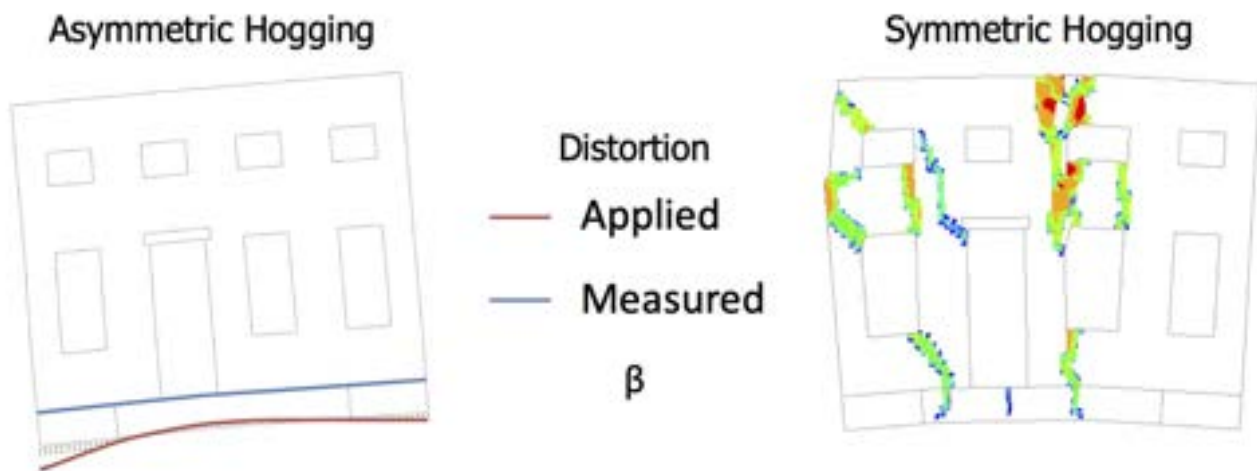


Figure 1. Illustration of the two settlement profiles investigated. On the left, asymmetric hogging with differential settlement on the left, showing the difference between the applied profile underneath the foundation and the measured distortion profile on the building. On the right, an example of symmetric hogging displaying the location of the resulting cracks on the masonry façade.

Asymmetric settlement profiles are most damaging

The models also included variations in the shape of the settlement profiles applied underneath the buildings. Preliminary models showed that hogging cases, where the soil profile has a convex shape and both or only one end of the building moves downwards, were more damaging than the sagging cases, with a concave curvature where the centre of the building moves downwards. Accordingly, hogging cases, both symmetric (both ends move downwards) as asymmetric (only the left end deforms) were further investigated each with two types where a smaller or larger portion of the foundation was deformed downwards. The symmetric cases where a larger portion of the foundation was allowed to settle vertically, exhibited damage earlier at stricter values of distortion.

Variations in the soil were also studied

The stiffness of the soil and how it interacts with the structure above it also plays a role. The soil around a building can act as a cushion for deeper deformations. How much of the soil is involved depends on the dimensions of the foundations, the properties of the building and the properties of the soil. Equivalent springs are modelled at the interface between the bottom of the foundation and the applied settlement profile; these springs mimic the effect of the soil surrounding the building and are defined based on earlier calibrations and internationally-accepted formulations. To evaluate the potential differences in soil profiles, a sandy soil and a peat soil are included, both with

additional variations in interface stiffness (low, standard, and high) for a total of six soil-related variations. As expected, the softer peat soil absorb the applied soil deformations allowing the buildings to rotate but not deform thus generating a lower distortion in the masonry and less damage. On average, a distortion twice as large needed to be applied under buildings on soft soil to generate the same damage as buildings on the stiffer sandy soil.

Cracks appear around windows

The models show how in most cases, cracks initiate around the openings for the windows. The cracks start at the corners and propagate diagonally or horizontally, or start at the middle of openings and propagate vertically. The cracks grow in width and in length until they reach the top of the wall or another opening; then, cracks grow substantially as the wall splits in multiple blocks following the applied soil deformation. At this point, the masonry has greatly exceeded light damage. The initial cracks, while light damage, already indicate the later failure mechanism related to the safety or ultimate limit state of the structure. This suggests that the light damage condition also influences the later safety of the structure; however, this effect has not been explored in this study.

This study only looked at ‘light damage’ cracks in-plane

Light damage is the most prevalent type of damage in structures as very low distortions can already trigger small cracks in masonry walls. For this reason, this study has focused on this initial damage state. To do so, the in-plane behaviour of the walls has been analysed observing cracking in detail; however, damage is not limited to cracks: out-of-plane effects like tilting forwards or backwards, or bulging of the walls cannot be observed with the 2D models employed herein. Nevertheless, these out-of-plane deformations are expected to be associated with higher degrees of structural damage beyond light damage. Furthermore, 3D effects at the boundaries of the walls have been considered, but complex 3D interactions with other building components such as floors or gable roofs can simply not be included in the 2D façade models. Similarly, the settlement profiles include only vertical displacements; horizontal strains or displacements have been neglected due to their significantly smaller magnitude in comparison to the vertical ones and because the included building-soil interface also allows slip which would further decrease the potential influence of horizontal displacements. Additional limitations of the models concern their representation of the buildings’ geometries; these have been selected to accurately depict vulnerable Dutch masonry buildings and their variations, but unique cases are bound to be excluded.

A relationship between distortion (β) and light damage using weights

From the almost three thousand façade models run for the case of clay-brick masonry walls on sensitive foundations, about 18% of them exceeded light damage when the applied distortion reached 1/500 and displayed a measurable distortion on the walls about seven times smaller (~1/3500). At an applied beta of only 1/1000, about 8% of the models exceeded light damage. However, counting the number of models to exceed certain thresholds is not entirely correct as the very weak or very strong material are less likely to appear in real buildings than the standard or average material, for example. Consequently, a weighted approach is used to make the analysed models better resemble the distributions of the varied parameters as present in real buildings in the affected location. The weights modify the count of the models so that it mimics probabilistic distributions observed in real buildings. Under this premise, the material parameters are set to follow a normal distribution with a known standard deviation; the soft soil is less common; asymmetric profiles are more likely; interface stiffness are correlated to soil types; and, settlement shapes are correlated to the length of façades. The weighted results differ slightly from the unweighted ones; yet, this approach increases the confidence in the result curves produced.

Measured distortion values are 5 to 10 times smaller than the soil deformation under the foundations

This study has evidenced a stark contrast between the distortion that is applied underneath the foundation, which mimics the deformation of the soil due to compaction, drying, deep subsidence or other geotechnic phenomena, and the distortion that appears on the walls or façades of the buildings. Buildings founded on reinforced concrete strip footings (predominantly calcium-silicate buildings) were well supported by their foundations and so, soil distortions did not transfer and were thus not measurable in the buildings. On the other hand, more sensitive, unreinforced foundations such as masonry footings, could not prevent the soil movements from being transferred to the buildings. Nevertheless, the amount of distortion transferred was reduced due to the stiffness of the building and its interaction with the soil. Flexible buildings followed the soil deformations more closely but still displayed only about 1/5 of the applied distortion, while stiffer buildings showed only 1/10 or even less of the applied distortion for values of distortion around 1/500. Longer façades also followed the soil profile more closely. As masonry became damaged, the façades become more flexible and the difference between the applied and measured distortion decreases; a façade split into multiple blocks, beyond light damage, would follow the soil profile almost 1:1.

Empirical comparison data shows less damage

The results of this modelling study were compared to empirical data from the analysis of building damage reports [Appendix G]. The comparison study looked at the damage reported in approximately 390 cases of masonry buildings which were also surveyed by measuring the deformations of the masonry bed joints. The horizontal masonry joints are presumed to have been built level and so, accurately tracking their horizontal positions allows to reproduce the buildings' deformations over time. In other words, the empirical study relates the measured building distortion to the intensity of damage. When the threshold for light damage (DL1) set by the comparison study is drawn next to the outcome of this modelling investigation, the probability of damage for values of the applied distortion by the soil deformation are in good agreement. However, the comparison study looks at measured building distortion which has been determined to be around 7 times smaller than the applied distortion. This means that the results of this modelling study are too strict or conservative, or that the empirical curves are too optimistic.

Within the scope of this study, it has not been possible to reconcile this difference yet several hypotheses have been formulated. Firstly, the definitions of light damage are not identical in both studies. Herein, a threshold of approx. 2 mm for the crack width ($\psi=2.5$) has been set, whereas the comparison study is based on the assessment of photographs of the damage which are affected by the perception of damage as cracks along mortar joints may be hidden from view. Secondly, measuring the distortion from real walls may lead to higher betas since points are gathered at fixed, limited intervals, thus suggesting that damage appears at higher values of distortion than what could actually be present. Similarly, the location or height on the walls where the measurements are taken could influence the beta values output. Thirdly, the empirical dataset may be biased since the inspections have been carried out on buildings that displayed damage, but other buildings, exhibiting high distortion values but no damage for example, may not have been surveyed. The data set represents a convenience sample and not a random one.

Fourthly, deformations taking place slowly over the span of years may be accommodated by the masonry without displaying cracks. This creep effect could even be enhanced by autogenous healing of the cement or lime in the mortar, which are capable of filling small cracks [20]. A few models considering the creep effect were run but a difference of 3 to 5 still remained between the applied and measured distortions. Fifthly, material properties have not been calibrated against large

and old masonry samples which could exhibit a more flexible overall behaviour than what has been modelled. This would also shift the measured distortion closer to the applied soil distortions. In sum, damage curves from empirical results are close to those produced by looking at the applied distortion values thus suggesting that measured distortion values on masonry façades should be less strict and follow more closely the applied soil deformations.

Foundation type and wall length/height most influential parameters

When examining the relationship between damage and the different parameters that have been investigated, two parameters are by far the most influential. Firstly, the foundation type, whether the foundation is reinforced concrete or unreinforced masonry or concrete. The stronger and stiffer foundation limits the soil deformation that is transferred to the buildings. Masonry walls on the reinforced foundations, are able to withstand soil deformations one order of magnitude higher than those on unreinforced foundations. Secondly, the wall geometry, expressed in its length over height ratio, also heavily determines whether masonry walls will be affected by soil distortions. The longer walls, with ratios around 3 to 4, sustain twice as much damage at equal soil distortion, as their square counterparts (ratio 1).

Conclusion: light damage likely for sensitive foundations

Extremely large values of soil distortion (1/100) were necessary to cause cracks of 0.1 mm in buildings with reinforced concrete foundations, common under masonry structures from 1970 onwards and typically built of calcium-silicate brick; the finite-element models did not exceed light damage at any realistic value of soil deformation. Other structures, with unreinforced (masonry) foundations and mostly of fired-clay brick masonry façades however, were significantly more vulnerable with a probability of 25% of exceeding light damage (cracks larger than 2 mm wide) at applied distortions (relative rotation) in the order of 1/500. At a soil deformation of 1/4000, the probability of exceeding light damage for the buildings on vulnerable foundations is estimated at 10%.

The models are revealed that if a settlement deformation is measurable in practice, then a masonry façade is determinately cracked.

Aggravation/Increase of damage

Furthermore, it is also possible that damage caused by other actions such as thermal expansion, shrinkage, or differential settlements due to autogenous causes, and which may already be present in the masonry, is increased or aggravated due to the indirect effects of deep subsidence. The cracked masonry behaves more flexibly and so follows the shape of the applied settlement profile more easily. Moreover, existing cracks need only to widen slightly to become visible or exceed light damage. The model results were analysed and an increase in distortion was related to an increase in damage ($\Delta\beta \rightarrow \Delta\Psi$). If a measured beta of at least 1/10.000 is observed or predicted and existing, barely-visible building damage is present, then, the analyses estimate that the probability of exceeding light damage is larger than 10% for buildings both on unreinforced and reinforced foundations. Note that the buildings on reinforced foundations are less likely to exhibit this measurable distortion.

Whether this damage aggravation represents economic loss is disputable since repair costs are similar, and sometimes identical, for the existing or the aggravated damage.

Curves present the probability of light damage due to settlements for various building types

Green- or free-field soil deformations can be determined for various geotechnic phenomena such as changes in the water table, oxidation of peat, compaction of clay, or other deep-sourced causes. These soil deformations, when applied to buildings, may cause distortions on the stiff masonry façades that will in turn trigger cracks and damage. The curves presented herein indicate the type

and probability of light damage that can be expected for these soil deformations measured as relative rotation (distortion) of the settlement profiles for various types of masonry buildings.

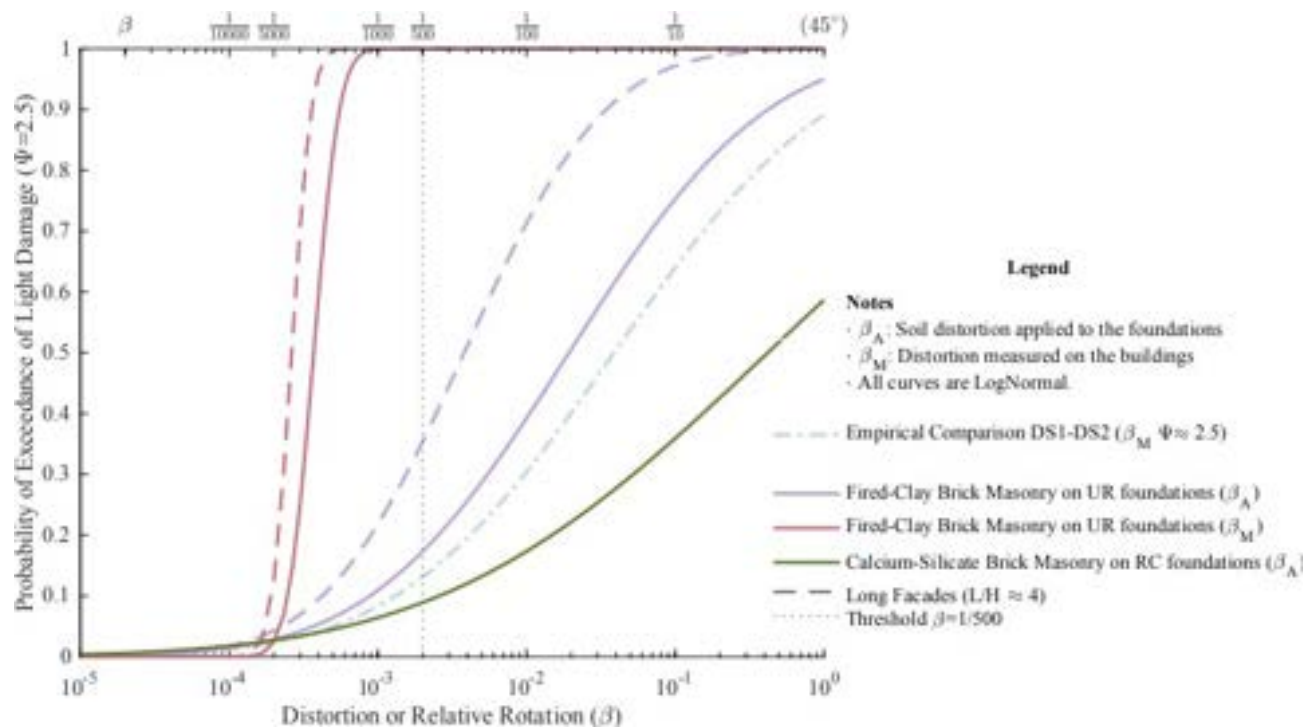


Figure 2. Distortion against the probability of exceeding light damage, both for the distortion applied by the soil and the distortion measured on the masonry façades. About 70% of the buildings on reinforced concrete (RC) foundations did not exceed light damage at all, while the buildings on unreinforced (UR) foundations displayed significantly more damage. Long façades were more susceptible to damage.

V. Report

1. Introduction

This study aims to provide insight into the sensitivity of masonry structures subjected to soil deformations like those caused by soil compaction, peat oxidation or deep subsidence. To date, several studies provide thresholds to limit the appearance of damage but there is no data about the probability of damage at these thresholds. Moreover, the building types to which these values refer to, are unclear or do not correspond to Dutch building typologies. Furthermore, damage is qualitatively defined which raises doubts about the type of damage to which the limit thresholds refer to. Consequently, this modelling study will employ an objective and clear damage metric based on the width of the expected cracks in masonry walls, and will introduce sufficient variations typical of sensitive Dutch masonry buildings to estimate the probability of damage at different intensities of soil deformation.

Reader

This report is divided into three main sections: an extended summary, which contains the main details, observations, and conclusions of this study redacted in an approachable manner; the main body of the report, which organises the various topics and elements of the study with increasing detail; and, a series of appendixes, which are stand-alone, thorough subtopics of the study and are related to the main research via the body of the report.

Approach

This modelling study consists mainly of three steps: first, masonry façade geometries and modelling strategies are collected from previous studies; second, a large pool of finite-element-models is used to explore the relationship of building damage to soil deformations, the main topic of the study; and third, the results are interpreted to obtain the probability of light damage for increasing soil distortion.

2. FEM Model - Modelling Approach

Numerical 2D finite element models of different masonry façades [16] subjected to settlement actions are investigated and interpreted. The attention of this study is focused on the relation between angular distortion and damage of the different façades computed with numerical plane stress models. Moreover, the ratio between the angular distortion measured at façade level and the one measured from the input displacement is also analysed. Non-linear behaviour of the façades, 3D effect, foundation and the soil-structure interaction are taken into account.

A total of 8 façades are numerically modelled with the software Diana FEA version 10.5 with 2D plane stress element. The façades are modelled with 8-noded quadratic elements (CQ16M). A Gauss 3x3 integration scheme is used with a mesh size of 100 mm. A non-linear masonry foundation is modelled below the façades to simulate the shallow foundation of typical old masonry building (see Appendix D). The foundation has a total height of 600 mm and a thickness 400mm wider than the wall thickness. For buildings of late '70, a variation study on the foundation is investigated to take into account the modern reinforced concrete strip foundation (Appendix D). The strip foundation is modelled as non-linear, employing the Total Strain Rotating Crack Model. A concrete C25 (according to fib 2010 normative) is used. Rebar are modelled as elastic-plastic material by making use of the Von Mises plasticity model. An equivalent diameter is used to take into account number and bar diameter in the thickness of the foundation. 3D effects are also included in the model. Transversal walls at the two lateral edges are modelled as vertical linear elastic beam elements, with

a fictitious cross-section of one brick,. These elements have a third of the elastic modulus of the masonry (perpendicular to bed-joints) and a Poisson's ratio of 0.16. No density is assigned to these elements. A detailed model of the lintel is also taken into account. Three different modelling options are selected according to the size of the opening. For window/door openings with a length smaller than one meter, no lintel is used. Above the opening, the material is kept the same as the masonry façade. For openings between one and one and a half metres the lintel is in general made by vertical masonry bricks as the one depicted in Figure 2.1. For larger openings, possible employed solutions are a steel or concrete beam placed above the window/door. A picture of this type of lintel is shown in Figure 2.1. Since both steel or concrete have an elastic behaviour much different than masonry, the connection between steel (or concrete) and the surrounded masonry is modelled using a non-linear interface with Coulomb-friction behaviour. The interface stiffnesses are calculated according to [27] considering a mortar joint thickness between steel (or concrete) and masonry of 10 mm. Cohesion and tensile strength of the interface have half of the analogous properties of the masonry. A friction angle of 0.3 rad is used while the dilatancy angle is set to 0 rad. Brittle failure is chosen after cracking. A similar interface is also placed between the reinforced concrete foundation (façades part of the terraced house) and the masonry. In concrete lintel, the steel rebar is also modelled following the same approach already employed for modelling the reinforcement in the foundation.

Possible additional vertical loads from floor, roof are included in the model via distributed force. The presence of a potential concrete floor between ground and first floor of a façade is also modelled with an equivalent stiffness to include the additional stiffness of this element.

A set of springs is placed underneath the foundation to simulate the effect of the soil on the structure. The calibration of the stiffness properties is carried out following the Gazetas's equations suggested in [26] and [16]. A non-linear behaviour is employed for the interface. The discrete cracking law is used to account for tensile and shear failure. Tensile strength of the interface is set to zero and its softening branch is considered brittle so that the façade is not pulled down during the application of the settlement loading. Once opening is detected in the connection, no shear forces are transferred. An example of mesh of a façade is depicted in Figure 2.2.



Figure 2.1. Type of lintels. Masonry lintel (left) and steel lintel (right).

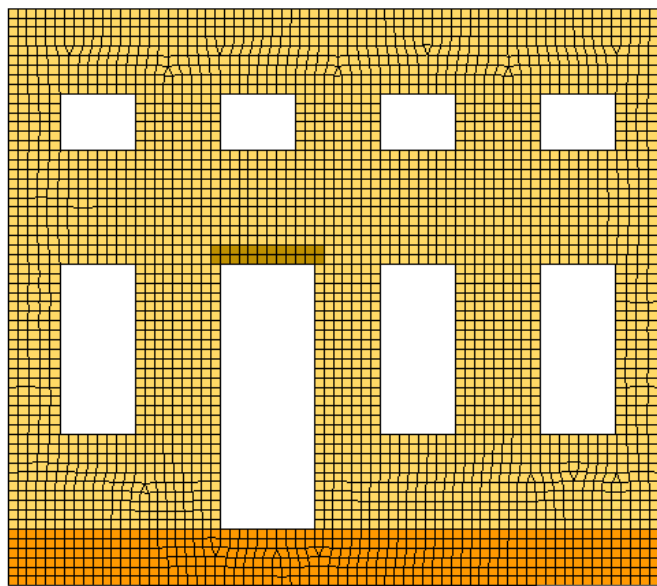


Figure 2.2. Example of FEM mesh of a masonry façade.

Masonry material is modelled as non-linear with the Engineering Masonry Model (EMM). The model accounts for material orthotropy and different failure mechanisms for tensile, compression and shear behaviour typical of masonry ([14], [15]).

The list of the material properties can be found in Appendix A.

Non-linear analyses are performed. In the first phase, the gravity load is applied in ten equal steps. Potential vertical load from floor-roof weight is applied in ten equal steps. Then, the displacement are reset to zero and the settlement actions are applied as prescribed deformation at the bottom of the interface. A variable load step is employed for the settlement. The first 100 steps a rate of 0.1 mm/step is used. Then the load step is increased to 0.2 mm/step for the following 450 steps. The remaining steps are conducted with a rate of 0.5 mm/step until the settlement reaches a maximum angular distortion of 1/10.

The Secant BFGS (Quasi-Newton) method is adopted as iterative method. Energy norm with a tolerance of 0.01% is employed. The Parallel Direct Sparse method is used to solve the system of equations. The second order effects are considered via the Total Lagrange geometrical nonlinearity.

The material model is calibrated against a test of a scaled façade subjected to settlement actions ([6]). More information of the calibration is given in Appendix B.

Selected Façades

Four different masonry structures are modelled and analysed: a farm-house and a detached house pre-1945, made of baked-clay bricks and two typical terraced houses of the '70s where a typical cavity wall system (calcium silicate bricks plus clay brick veneer) is used. For each structure, two façades are extrapolated, a front and a side façade. Additionally, variations of these façades in terms of length, height, opening percentage and opening typology are also investigated to account for the building variability. An extra long façade made with cavity wall system is analysed. Six of the nine façades have a flat upper side and could be present in buildings with flat roofs or on the sides of buildings with gables; and, the remaining three façades have a gable for a twin-slope roof. This distribution is consistent with a statistical study on geometric characteristics of existing buildings; see Appendix K.

The nine façades are here described and classified:

- Façade 1: front façade of a farmhouse built in 1883 with a dimension of 7.0x5.5 m. The façade is non load-bearing and is double wythe (thickness of 210 mm). Four openings with a dimension of 0.8x0.6 m are located at the upper floor. The ground floor is characterised by three openings of 0.8x1.8 m and a door opening with a size of 1.0x2.8 m. A masonry lintel is modelled above this opening. The same material model of the masonry is used for the lintel, but with rotated local axes of 90° to account for the construction detail (as shown in Figure 2.1). A view of the façade is depicted in Figure 2.3. The front façade 1 is non load-bearing, hence it is not subjected to any vertical loading except for the gravity loading. The transversal walls are modelled up to the floor height of 3.8 m. The façade has an opening percentage equal to 23.5%.
- Façade 2: side façade of a farmhouse built in 1883. The façade is composed of two main parts: the side part of the house (right part of the façade in Figure 2.4 having a dimension of 5.0x3.8 m and the shed part (left part of the façade in Figure 2.4) which is 12 metres long and 2.4 m high. The total length is thus 17 m. The thickness of the façade is 0.21 m. Three window openings of 0.8x0.6 m are located in the middle part of the shed. Two bigger openings of 0.8x1.8 m are placed to the right side of the façade. Both timber floors and timber roof bear along the top right edge of the façade for a total overburden of 21 kPa. The shed part is subjected only to roof compression instead. The overburden is equal to 3 kPa. The façade has an opening percentage equal to 9%.

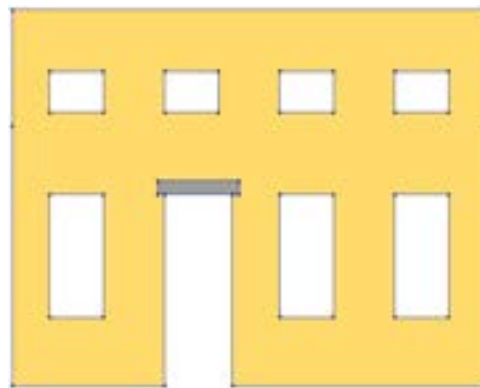


Figure 2.3. Model of façade 1.

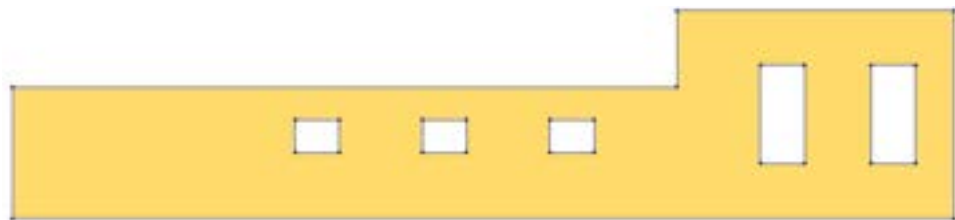


Figure 2.4. Model of façade 2.

- Façade 3: front façade of a detached house built in 1930. Such a house typology is composed by a cavity wall system with both leaves of baked-clay bricks. Each leaf has a thickness of 100 mm and their connection is provided in general by steel ties. Usually, ties are mainly working in the out-of-plane direction of the wall. For old structures, the in-plane resistance produced by the ties is negligible. For this reason, in the models, the in-plane behaviour of the two leaves is supposed to be decoupled. Only the inner leaf is considered. The façade has a dimension of 6.8x7.1 m. It contains a top window opening of 3.0x0.75 m located in the middle of the gable. At the ground floor the façade has a window of 2.4x1.5 m to the right side and a door opening to the left side of 1x2 m. The façade has an opening percentage equal to 21.4%. A masonry lintel is modelled above the door opening. The top part of the two large window openings is modelled with a linear elastic steel lintel.

An IPE200 is selected as cross-section. In order to avoid mesh distortions and achieve the full contact along the thickness between steel and masonry, the lintel is modelled with a rectangular cross-section of 100x200 mm. An equivalent Young's modulus is calculated in order to obtain the same flexural rigidity (EI) of an IPE200 section. The view of the model is depicted in Figure 2.5. Façade 3 bears a small portion of the roof structure. A vertical loading of about 18 kPa is applied as line load to the roof edges.

- Façade 4: it represents the side façade of the detached house. It is 12 m long and 3 m high; it has 4 openings. Starting from the left side, an opening of 1.4x0.5 m is located at 2 m from the ground; then, a large opening of 2.4x1.5 m is located in the middle of the façade. To its right side, a small 0.4x1.0 m opening is modelled 0.4 high from the ground. Lastly, an inverted L-shape opening is located close to the right edge. The length of the larger edge is equal to 1.5 m while the height is 1.5 m. The façade has an opening percentage equal to 17.4%. Both right and middle window openings are modelled with a steel lintel on top as specified for Façade 3. The left window is modelled with a masonry lintel. Timber roof and timber floor bear along the top edge of the façade for a total overburden of almost 60 kPa; it is applied as line load in the model. The model is depicted in Figure 2.6.

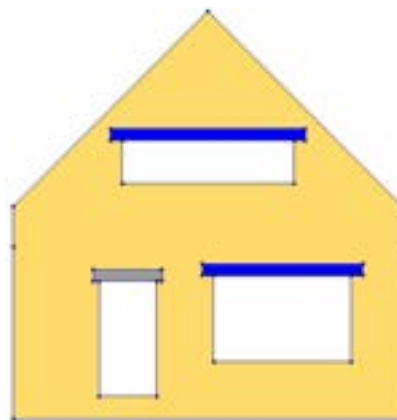


Figure 2.5. Model of façade 3.

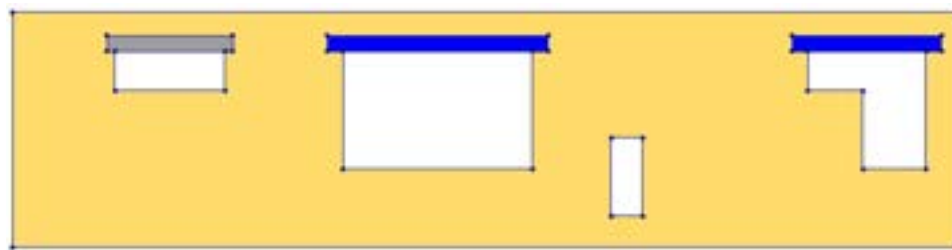


Figure 2.6. Model of façade 4.

- Façade 5: the front façade of a typical terraced house of the '70s. This type is usually built with cavity walls, where calcium silicate (CS) bricks are used for the load bearing inner leaf and clay brick for the outer leaf. The façade is 6.75 meter long and 5.4 m tall. As for façade 3 and 4, only the 100 mm of the inner leaf is modelled. The façade is characterized by three large openings, two at the ground floor and one at the first floor for a total opening percentage of 39%. The façade does not bear any load from either floor and roof. The timber gutter beam above the opening at the first floor is also modelled as beam element. Differently from the first four façades, these building type are often founded on reinforced concrete strip foundations. The strip foundation has a T-shape with a total height of 0.5 meter (flange height equal to 0.15 m) and a base thickness of 0.6 meter (0.27 m for the web). A view of the façade is given in Figure 2.7.

- Façade 6: it represents the side inner façade of a terraced house. It's characterized by a length of 8.4 m and a height of 8.3 m. The opening percentage is well lower than Façade 5 and it is equal to 9%. The façade bears a NeHoBo floor at the first storey, the timber floor at the second storey and the roof. The NeHoBo floor strip is explicitly modelled to take into account the extra stiffness at the first level. The weight of the floor is applied in the model as line load of 53 kPa. The load of the attic floor and the roof is included as distributed load of 27 kPa and 22 kPa respectively. Load bearing transversal walls of this type of houses have usually strip foundation with a larger base. To take into account this detail, the strip foundation has total height of 0.5 meter (flange height equal to 0.15 m) and a base thickness of 1.6 meter (0.27 m for the web). A view of the façade is given in Figure 2.8.

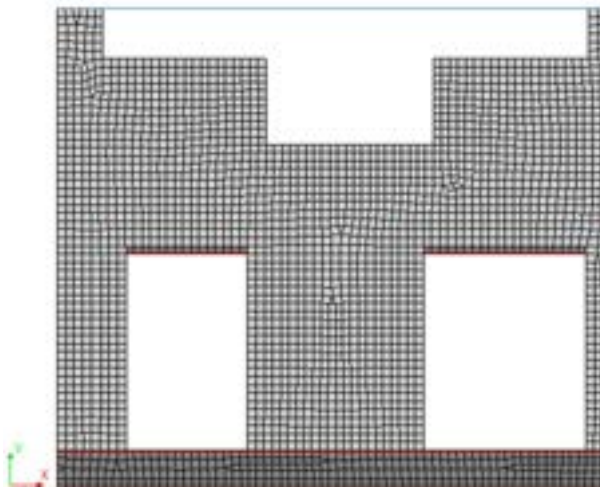


Figure 2.7. Model of façade 5.

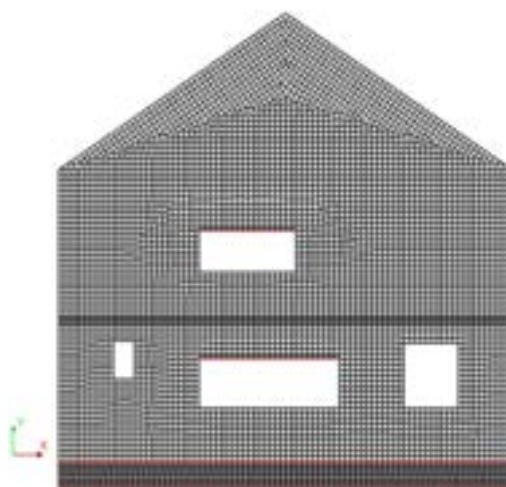


Figure 2.8. Model of façade 6.

- Façade 7: it represents the front façade of the laboratory test EUC-BUILD-2. The test replicates a typical Dutch terraced house of the late '70s and, as for Façade 5 and 6, is built with cavity walls. The façade has a dimension of 5.76x5.51 m. The façade is characterized by large openings at the first floor. The total opening percentage is equal to 44.5%. The concrete floor at the first floor spans on both front and side façade. This is modelled as a strip with a thickness of 1 meter, to take into account the stiffness. The weight of the concrete floor bearing on the façade is included in the model as line load of about 47 kPa. Rebar with equivalent diameter are also modelled. Reinforced

strip foundation is modelled in the same fashion of Façade 5. A view of the façade is given in Figure 2.9.

- Façade 8: the side façade of EUC-BUILD-2 is a load bearing solid façade. There are no openings either at the ground floor nor at the first floor. The façade has a dimension of 5.22x7.83 m. The weight of the concrete floor at first level, the timber attic and roof are included in the model as line load. Values of 52 kPa, 18 kPa and 20 kPa are assigned at the first level, attic level and roof. Same foundation typology of Façade 6 is modelled. A view of the façade is given in Figure 2.10.

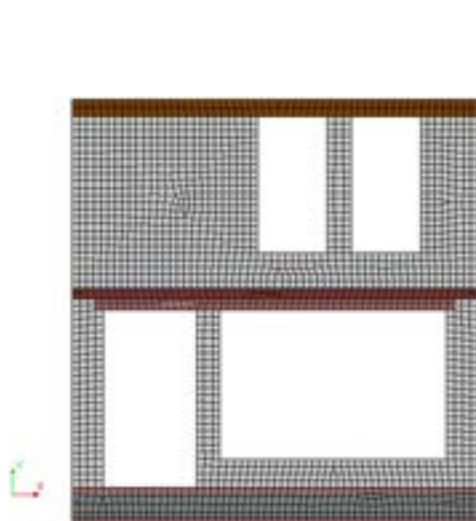


Figure 2.9. Model of façade 7.

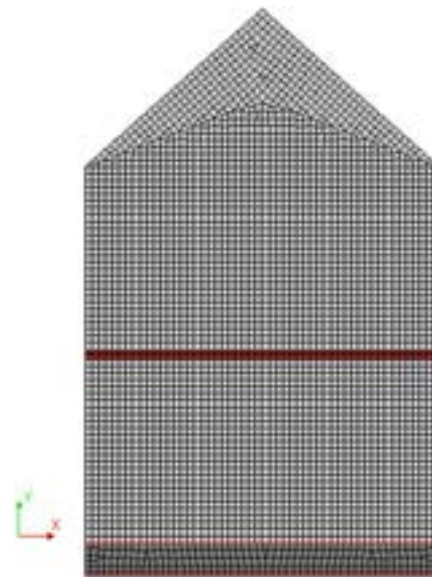


Figure 2.10. Model of façade 8.

- Façade 9: the façade follows a similar geometry of Façade 4. It represents the side façade of a detached house. The single load-bearing inner calcium silicate leaf is modelled. It is 9 m long and 3 m high; it has 3 openings. Starting from the left side, an opening of 1.6x1.2 m is located at 1 m from the ground; to its right side, a small 0.4x1.0 m opening is modelled 0.4 m high from the ground. Lastly, an inverted L-shape opening is located close to the right edge. The length of the larger edge is equal to 1.3 m while the height is 1.3 m. The façade has an opening percentage equal to 13.4%. Both right and middle window openings are modelled with a steel lintel on top as specified for Façades 3 and 4. Timber roof and timber floor bear along the top edge of the façade for a total overburden of almost 60 kPa; it is applied as line load in the model. The model is depicted in Figure 2.11.

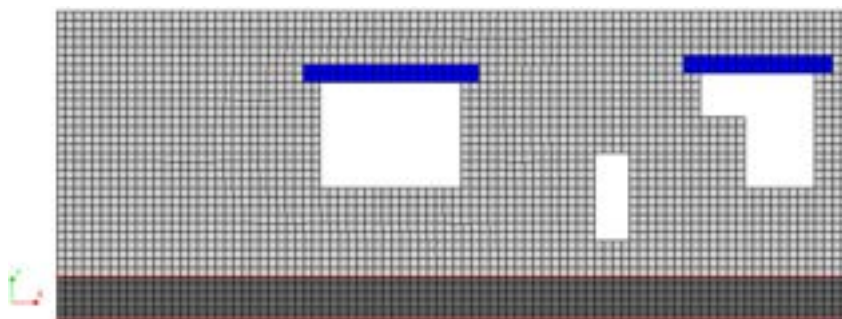


Figure 2.11. Model of façade 9.

Scenarios

In order to investigate the parameters that could influence the behaviour of the different models subjected to settlement actions, various model variations are built and analysed. In addition, the inclusion of variability allows to process the data in a probabilistic manner as it is described in the following chapters. The choice of the variations tries to cover a wide aspect of uncertainties present in the physical problem and which could lead to different outcomes. The aspects that are varied in the models are here listed:

- **Settlement profiles:** this parameter affects the amplitude and the convexity of the prescribed displacement at the base of the masonry building. It represents the way how the ground settles and displaces underneath the foundation. The settlement applied in the model represents the displacement resulting from natural (e.g. peat oxidation, shrinkage) or anthropogenic (e.g., excavation, groundwater lowering) drivers or a combination of both. In total, four different settlement profiles are selected. The profiles replicate hogging deformation since they load, for this type of façade, to more conservative results with respect to sagging profiles (Appendix H). Two symmetric (SH) and two asymmetric (LH) profiles are selected. For each type of settlement, two different ‘knick’ points are employed. These points are a measure for the length of the slope of the profile; see later point B in Figure 3.1. For the symmetric hogging, the knick points are located at $0.5L$ ($\frac{1}{2}$ of the length of the façade) and $0.25L$ (a quarter of the façade length). The acronyms of the two cases are SH2 and SH4 respectively. For the asymmetric hogging profile, the selected knick points are placed at $1/3L$ (LH3) and $1/5L$ (LH5). The highest displacement is applied at the left side of the building. The settlement profiles are fit to the façade length. An overview of the four total settlement profiles are shown in Figure 2.12. The maximum settlement amplitude is directly computed from the input profile with a fixed angular distortion (β) of $1/10$. This means that, at constant angular distortion, larger the façade will require a higher settlement amplitude. This is shown in Table 2.1 as an example for different façades.

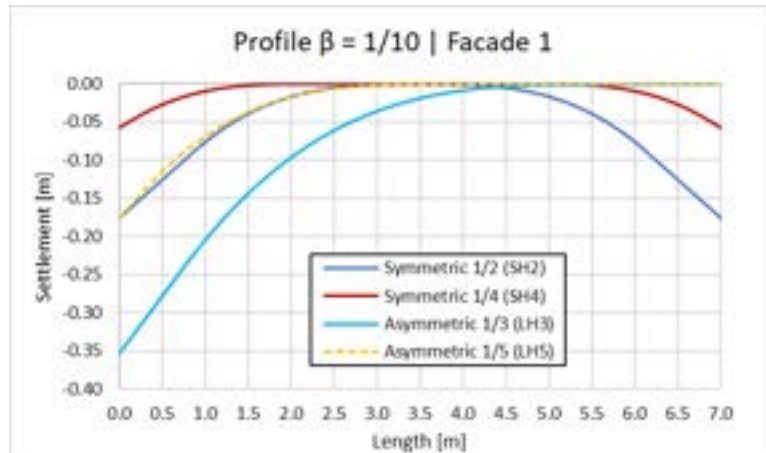


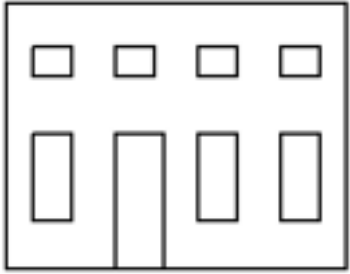
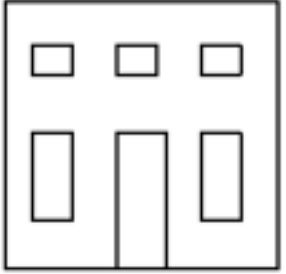
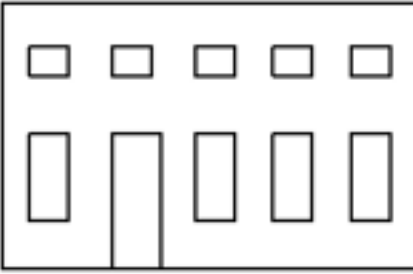
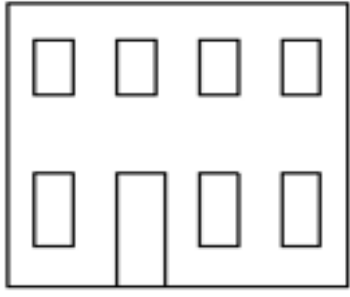
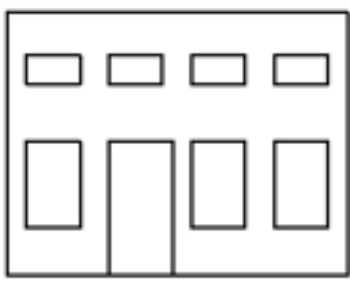
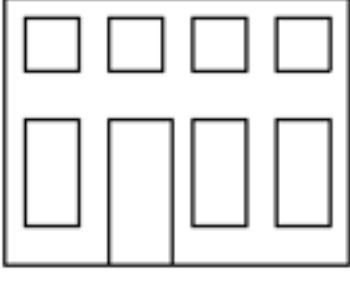
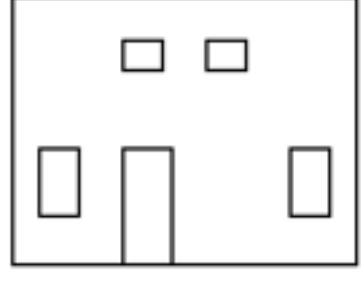
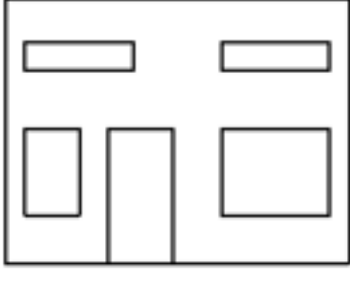
Figure 2.12. Different settlement profiles applied to Façade 1. All profiles have an angular distortion β of $1/10$.

Table 2.1. Settlement amplitude of different settlement profiles for different façades. All profiles have an angular distortion β of 1/10.

Façade	Length [m]	SH2 [mm]	SH4 [mm]	LH3 [mm]	LH5 [mm]
Façade 1	7.00	175.9	58.4	353.6	176.1
Façade 2	17.00	427.1	141.9	858.6	427.7
Façade 3	6.80	170.8	56.8	343.5	171.0
Façade 4	12.00	301.5	100.2	606.1	301.9
Façade 5	6.75	169.6	56.3	340.9	169.8
Façade 6	8.40	211.1	70.1	424.3	211.3
Façade 7	5.76	144.7	48.1	290.9	144.9
Façade 8	5.22	131.1	43.6	263.7	131.3
Façade 9	9.00	226.1	75.1	454.6	226.4

- **Material properties:** The ‘Standard’ set of material properties is mainly defined starting from the conservative values provided by table F.2 of NPR 9998. Part of the values are then calibrated (based on the Giardina’s model, Appendix B) or selected according to the matured experience on such types of analyses. In addition to the ‘Standard’ material, four sets of properties are investigated, two weaker and two stronger than the ‘Standard’. For these sets, the elastic and strength material properties are reduced (or increased) by 25% and 50% with respect to the ‘Standard’. The material properties are fully listed in Appendix A. The different material sets take into account the variability of the masonry properties in the field. In this way various flexibility of masonry and strengths are included in the variations. Additional sensitivity on the elastic properties of the masonry can be found in Appendix E.
- **Soil profile:** the soil of the Groningen area has pretty different superficial stratigraphy (Appendix C) where sand, clay and peat can be found. Two soil variations are included in the model. A sandy (‘Soil A’) and a clayey (‘Soil B’) soil are considered. The properties of the soil, such as shear modulus and Poisson’s ratio are included in the interface formulation to define a proper soil-structure interaction. More information about the material properties of the soil are described in Appendix A.
- **Soil-structure interface:** The non-linear interface modelled underneath the foundation represents the interaction between the façade and the soil. Its stiffness properties influence how stresses and displacement are transmitted to the façade. To investigate this variability, three different sets of stiffness parameters are assigned to the interface. Beside the ‘Original’ stiffness defined by Gazetas in [26], the computed normal stiffness is then divided (‘Low’) and multiplied (‘High’) by a factor 10. The shear stiffness has minor impact on the results of the analyses as described in Appendix E. The formulation to compute the ‘Original’ interface stiffness is reported in Appendix A.
- **Geometry variations:** The behaviour of a façade subjected to settlement actions, mainly depends on its shape (i.e. length and height) and also presence, percentage and location of openings. In order to investigate the effects provided by these parameters, several geometry variations are investigated. Extra geometry variations are modelled for Façade 1, 3 and 4. In addition to length, height and opening percentage, also the opening typology is investigated. Especially, the length of the windows is analysed and two categories are created. The two

categories divide ‘Short’ openings with length lower than 1.5 m and ‘Large’ openings with a length greater than 1.5 m. For this last category, a steel lintel beam is modelled above the opening as indicated in the previous section. The overview of the ten variations of Façade 1, and seven variations of Façade 3 and 4 are shown in Figure 2.13, Figure 2.15 and Figure 2.16 respectively. The long Façade 2 and the CS façades, Façade 5, 6 and 7 are only modelled in their single geometry variation. They are represented in Figure 2.14, Figure 2.17 and Figure 2.18. Two variations are modelled for Façade 8 and Façade 9 to evaluate the effect of the façade length and opening percentage on the results for the CS façades. The variations are shown in Figure 2.19 and 2.20. Façade 9-B is characterized by timber floors at both first and roof level. A pre-compression load of 27 kPa and 22 kPa is applied respectively at the two levels.

		
Façade 1 – A 7.00 x 5.50 m L/H = 1.27 Opening % = 23.5%	Façade 1 – B 5.50 x 5.50 m L/H = 1.00 Opening % = 23.5%	Façade 1 – C 8.48 x 5.50 m L/H = 1.54 Opening % = 23.5%
		
Façade 1 – D 7.00 x 7.00 m L/H = 1.00 Opening % = 23.5%	Façade 1 – E 7.00 x 3.80 m L/H = 1.84 Opening % = 23.5%	Façade 1 – F 7.00 x 5.50 m L/H = 1.27 Opening % = 31.7%
		
Façade 1 – G 7.00 x 5.50 m L/H = 1.27 Opening % = 41.6%	Façade 1 – H 7.00 x 5.50 m L/H = 1.27 Opening % = 14.5%	Façade 1 – I 7.00 x 5.50 m L/H = 1.27 Opening % = 31.7% (Large)

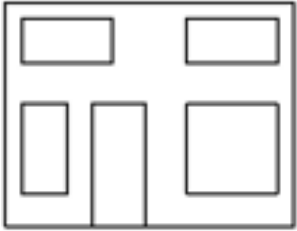
		
Façade 1 – J 7.00 x 5.50 m L/H = 1.27 Opening % = 41.6% (Large)		

Figure 2.13. Ten geometry variations of Façade 1.

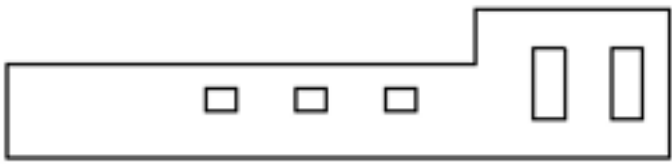
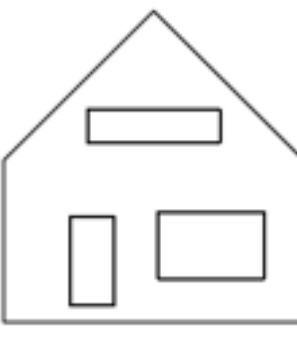
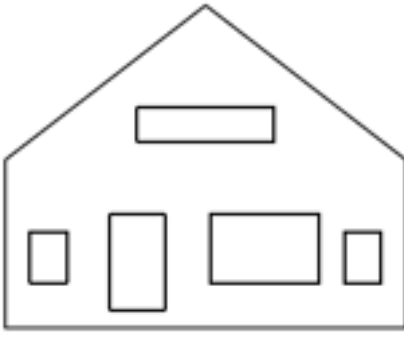

Façade 2 – A 12.00 x 2.40 m + 5.00 x 3.60 m L/H = 5.00 Opening % = 9.0%

Figure 2.14. Single geometry variation of Façade 2.

		
Façade 3 – A 6.80 x 7.10 m L/H = 0.96	Façade 3 – B 4.80 x 7.10 m L/H = 0.68	Façade 3 – C 8.80 x 7.10 m L/H = 1.24

Opening % = 21.4% (Large)	Opening % = 21.4% (Large)	Opening % = 21.4% (Large)
Façade 3 – D 6.80 x 10.0 m L/H = 0.68 Opening % = 21.4% (Large)	Façade 3 – E 6.80 x 4.20 m L/H = 1.62 Opening % = 21.4% (Large)	Façade 3 – F 6.80 x 7.10 m L/H = 0.96 Opening % = 13.0%
Façade 3 – G 6.80 x 7.10 m L/H = 0.96 Opening % = 30.4% (Large)		

Figure 2.15. Seven geometry variations of Façade 3.

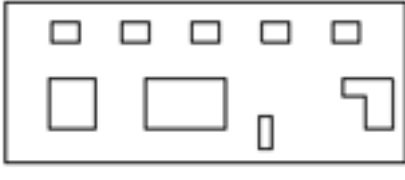
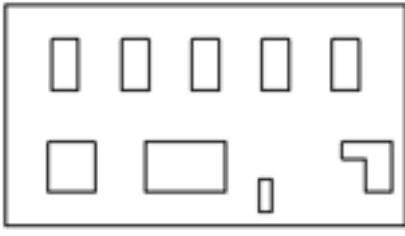
		
Façade 4 – A 12.00 x 3.00 m L/H = 4.00 Opening % = 17.4% (Large)	Façade 4 – B 6.00 x 3.00 m L/H = 2.00 Opening % = 17.4% (Large)	Façade 4 – C 9.00 x 3.00 m L/H = 3.00 Opening % = 17.4% (Large)
		
Façade 4 – D 12.00 x 4.80 m L/H = 2.50 Opening % = 17.4% (Large)	Façade 4 – E 12.00 x 6.60 m L/H = 1.82 Opening % = 17.4% (Large)	Façade 4 – F 12.00 x 3.00 m L/H = 4.00 Opening % = 10.0% (Large)
		
Façade 4 – G 12.00 x 3.00 m L/H = 4.00 Opening % = 32.8% (Large)		

Figure 2.16. Seven geometry variations of Façade 4.

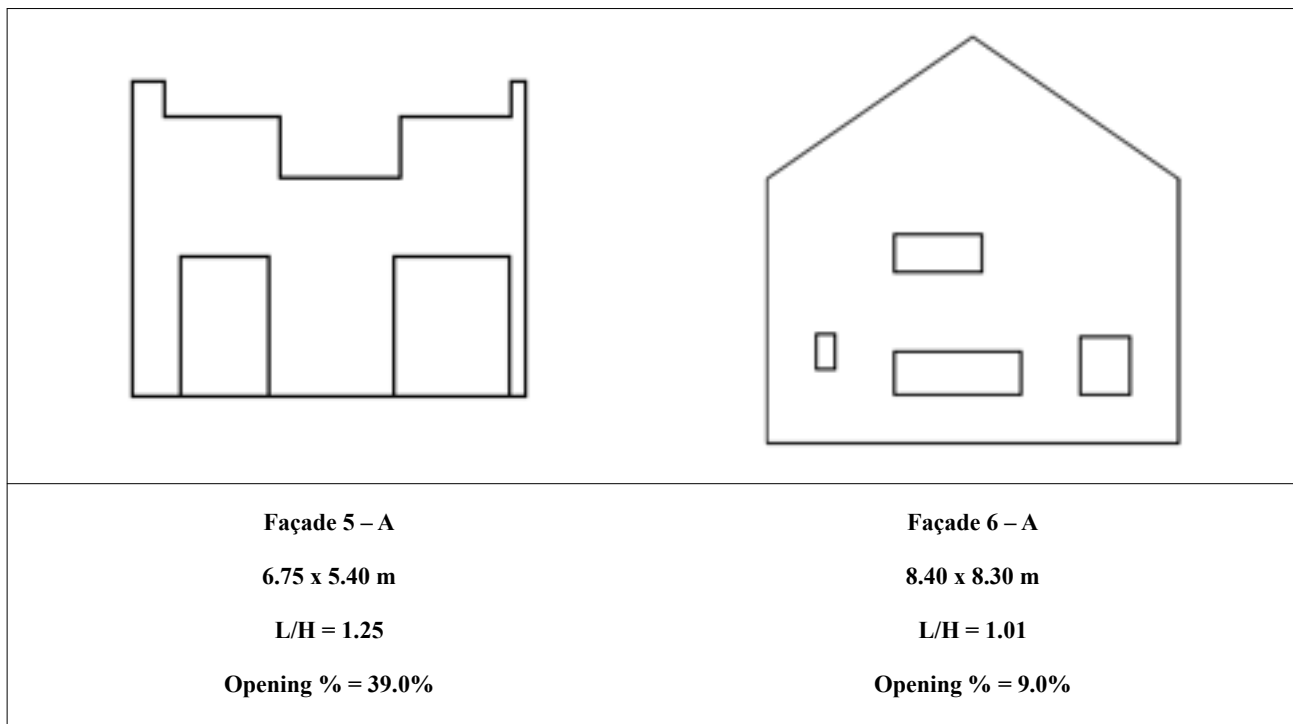


Figure 2.17. Single geometry variation of Façade 5 and 6.

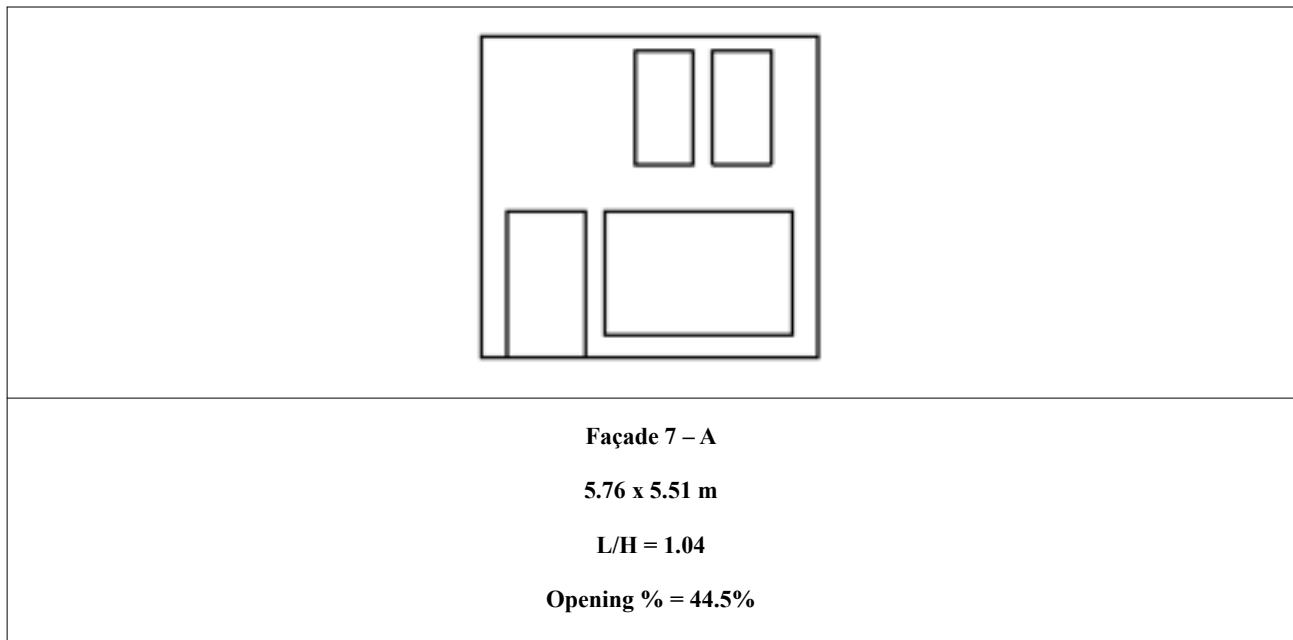


Figure 2.18. Single geometry variation of Façade 7.



Figure 2.19. Two geometry variations of Façade 8.

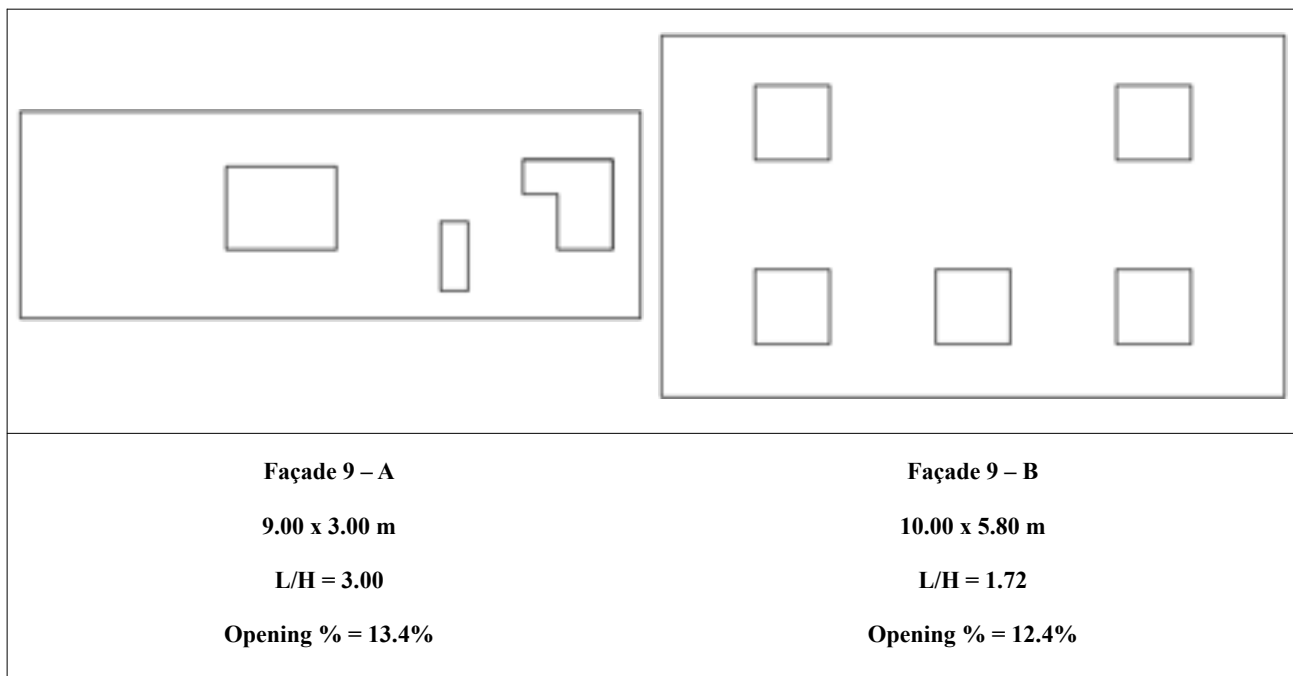


Figure 2.20. Two geometry variations of Façade 9.

3. Results FEM Model

The results of the finite element models are presented and discussed. From the numerical calculations different outputs are extrapolated and analysed. First of all, the vertical deformation of all nodes at the base of the façade (top edge of the foundation) is recorded during the entire settlement loading. For each step, the main deformation parameters produced by the hogging settlement are computed. An overview of the different parameters is shown in Figure 3.1. Although all parameters are able to describe the severity of the settlement deformation, the results in the following sections are going to be presented mainly in terms of angular distortion β . This parameter is also often used in literature and in codes to define damage limits of structures [6]. Beside the computation of the angular distortion at the base of the façade (here called as “measured β ”), the imposed deformation at interface level is also computed and analysed. This is the applied deformation at the base of the model (here called “applied β ”). The “applied β ” represents the deformation that the soil would exhibit without the presence of the building. The “measured” deformation represents the displacements that would be measurable with levelling techniques along the brickwork courses of the real façade. The difference between the applied and measured deformation depends on the soil-structure interaction, which depends on the dimension of the structure and the subsoil on which it rests. A picture showing the difference between the measured and applied β is shown in Figure 3.2.

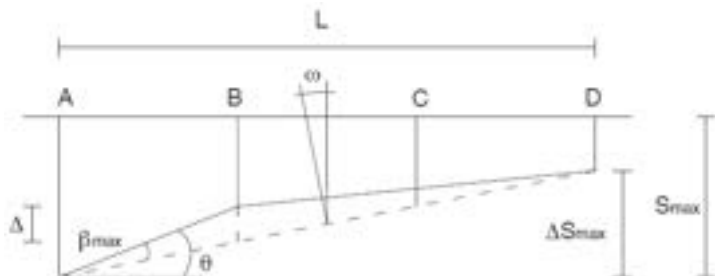


Figure 3.1. Deformation parameters, settlement S , differential settlement ΔS , relative deflection Δ , deflection ratio Δ/L , rotation ω , angular distortion (or relative rotation) β and tilt ω [6].

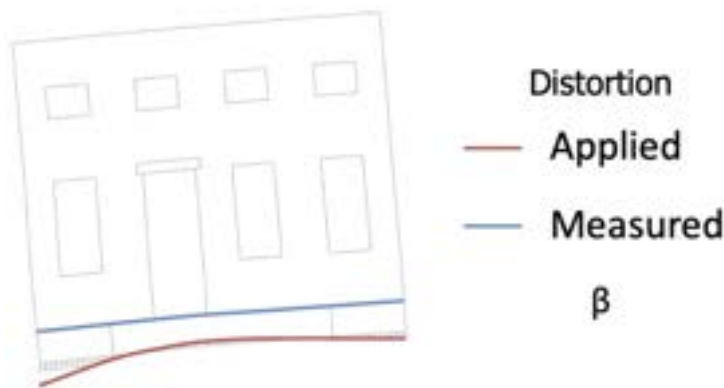


Figure 3.2. Applied and measured angular distortion β .

In addition to the deformations at base of the façade and interface, the evolution of the damage of the façade is also computed. For each loading step, the principal crack width data is recorded for the masonry façade. Then, the damage of the structure is computed in terms of Ψ (Psi parameter). This parameter provides an objective damage level based on number of cracks, crack width and length, and most importantly, is evaluated automatically to provide a single value of damage at every one of the hundreds of load steps in each of the thousands of models. A more detailed description and

application of this parameter can be found in [7]. Table 3.1 reports a classification of the damage parameter Ψ according to its value and the correspondent damage state. The Ψ value for its transition from DS1 to DS2 (from visible to exceeding light settlement damage) can be found at about $\Psi=2.5$ [9].

The damage parameter Ψ is automatically computed for each loading step with a script and then processed and plotted in combination with “applied” and “measured” values of angular distortion β . An example of the results from the script is depicted in Figure 3.3. The evolution of the damage with the increase in angular distortion is described with different interpolation functions that are automatically generated according to the available data (Appendix J). This functions allow to obtain smoother β - Ψ data respect to the one obtained in the numerical model and to evaluate data for specific models that do not reach a specific damage level.

Crack pattern produced by the different settlement actions is also checked and classified according to literature data [25]. Possible damage patterns that can be found in masonry façades subjected to uneven settlement are summarized in Table 3.2.

Table 3.1. Damage scale based on damage parameter ψ [9].

Values of Ψ	Description	Representative Crack Width	Damage State
$\Psi = 0$	No damage	N.A.	
$\Psi \approx 0.5$	Invisible damage	< 0.1 mm	DS0
$\Psi \geq 1.0$	Visible light damage	> 0.1 mm	
$\Psi \geq 2.0$	Easily-observable light damage	> 1 mm	DS1
$\Psi \geq 2.5$	Severe light damage	> 2 mm	DS1 or DS2
$\Psi \geq 3.0$	No longer light damage, usage of a different damage measure is required.	> 4 mm	DS2 or higher

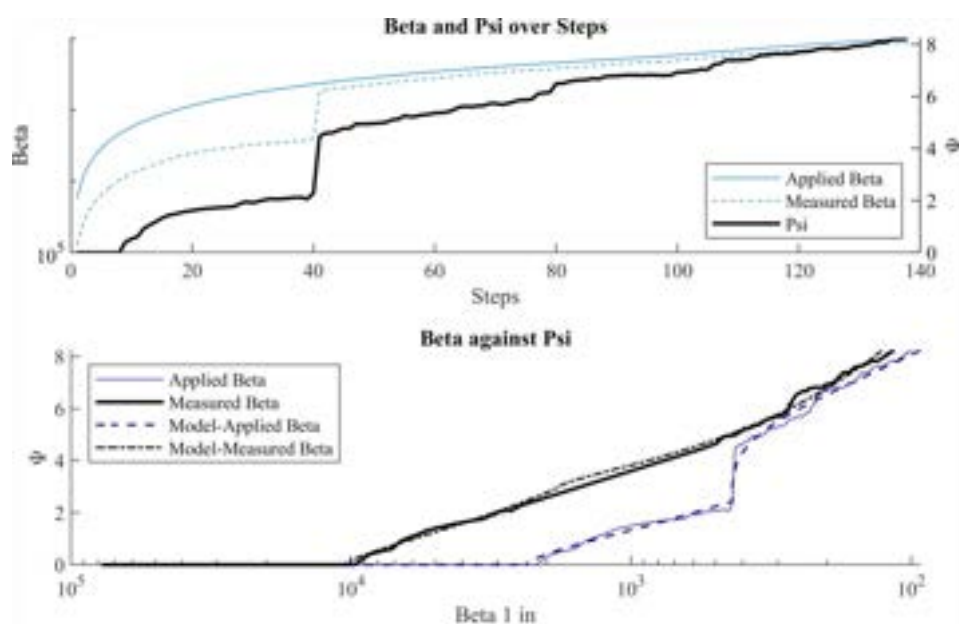
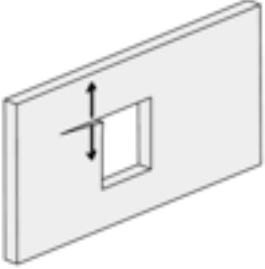
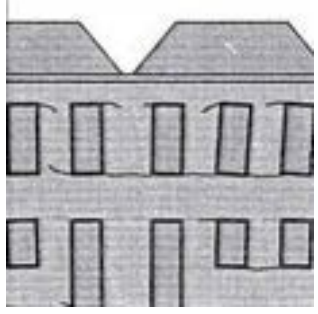
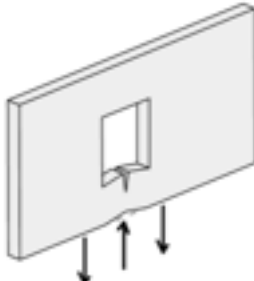
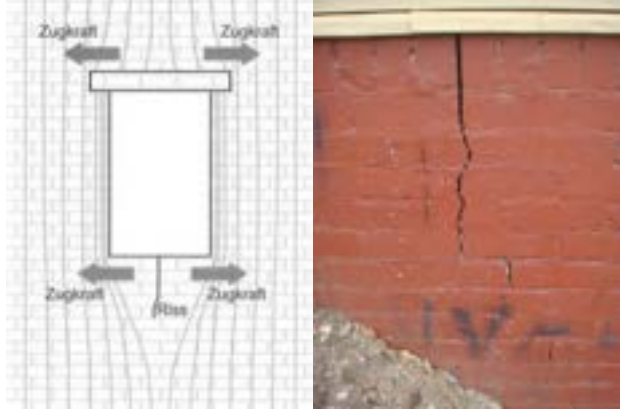
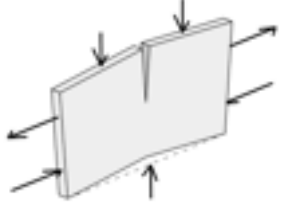
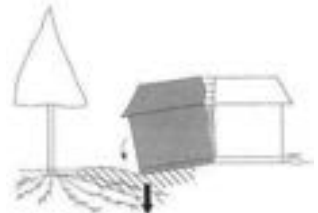
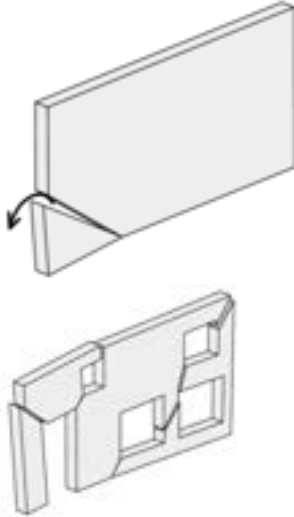
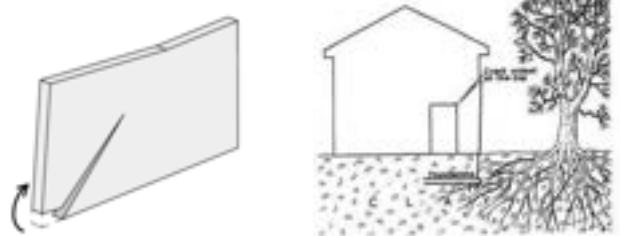


Figure 3.3. Post-processing of FEM analysis results. Angular distortion and damage over step (above) and angular distortion against damage (bottom). Facade 1-A, soil A, ‘Original Interface’, SH2, weak material.

The results are first split and analysed for each specific façade. A comparison between the different variations of each single façade is also discussed. Then, the behaviour of the different façades is analysed. The results are presented in terms of β - Ψ for both “measured” and “applied” angular distortion. The two curves include both actual models that reach a specific damage level and the interpolated function for models that only reach lower damage levels. The value of β refers to the average of different groups of models. The models that, for an applied angular distortion of 1/10 (applied during the last step of the loading protocol) do not reach the minimum damage level, set as $\Psi = 0.5$, are removed from the average count. In the plots, the $\beta = 1/500$ limit mentioned in the current IMG advice is also introduced.

Table 3.2. Common damage patterns for hogging settlement [25].

Type of cracks	Damage Pattern	
1 – Horizontal crack near opening		
2 – Vertical crack below opening		
3 – Vertical cracks top of the building		
4 – Diagonal cracks		

Façade 1

The average values of angular distortion β against the damage parameter Ψ for the 1200 variation models is depicted in Figure 3.4 and tabulated in Table 3.3. The amount of models that are able to reach a specific damage level after applying a settlement with an angular distortion of 1/10 are reported in Figure 3.4. Severe light damage ($\Psi \geq 2.5$) is attained by 60% of the models. Visible light damage ($\Psi = 1.0$) is reached for a measured β of 1/5880 and applied β of 1/505. Severe light damage ($\Psi \geq 2.5$) is attained for a measured β of about 1/2400 and applied β of 1/170. The damage mechanism is characterized by horizontal cracks at the window corners of the ground floor (Figure 3.5). While increasing the settlement amplitude, the cracks grow in length and width (Figure 3.5). Additional cracks are detected also at the first floor at the start of the severe light damage. The ratio between measured and applied β of Façade 1 ranges from 9 to 14 and increases with the compared damage level.

When analysing the soil-structure interaction (SSI), which is modelled via line interface elements resembling the stiffness of the subsoil, it can be seen that the softer soil (soil B) provides less vulnerable results in terms of both measured and applied β . This effect is even more evident from the variation with a reduced normal stiffness (low k_n), in Figure 3.6. In fact, the reduced stiffness properties of the interface allows a better redistribution of the stress coming from the applied deformation. The model presents a less reactive façade, with a larger ration between measured and applied β . Nonetheless, the ratio increases from 8 to 76 (when referring to $\Psi = 2.5$). In addition to the lower vulnerability in terms of β , also the amount of models that reach failure are sensibly less. Only 43% of models reach severe light damage when a low value of k_n is employed, with respect to the original value where 65% of the models reach the same damage level (Figure 3.6). The models with sandy soil (Soil A) and interface stiffness amplified by 10 times (High k_n) are the most vulnerable models with measured β in the order of 1/2500-1/2800 and applied beta 1/206-1/340 (at $\Psi = 2.5$). A summary of the β values for each damage level is provided in Table 3.4. The damage pattern is not affected by the SSI variations and it results similar to what is depicted in Figure 3.5.

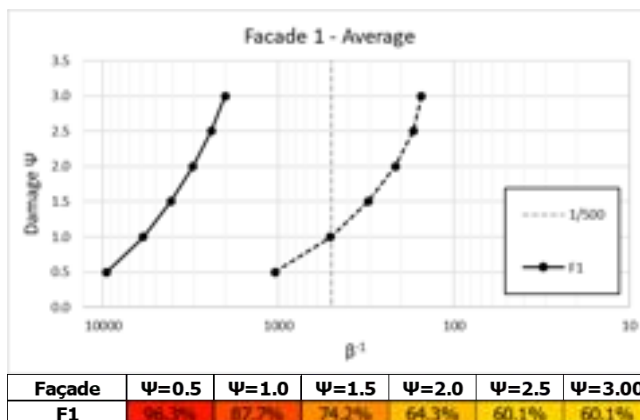


Figure 3.4. Angular distortion (β^{-1}) against damage and percentage of models that reach a specific damage level of Façade 1. Average results. Dashed lines refers to applied β .

Table 3.3. Measured (left) and applied (right) β^{-1} values of Façade 1.

Façade	$\Psi=0.5$	$\Psi=1.0$	$\Psi=1.5$	$\Psi=2.0$	$\Psi=2.5$	$\Psi=3.00$	Façade	$\Psi=0.5$	$\Psi=1.0$	$\Psi=1.5$	$\Psi=2.0$	$\Psi=2.5$	$\Psi=3.00$
F1	9526	5880	4107	3076	2415	2007	F1	1048	505	308	215	171	153

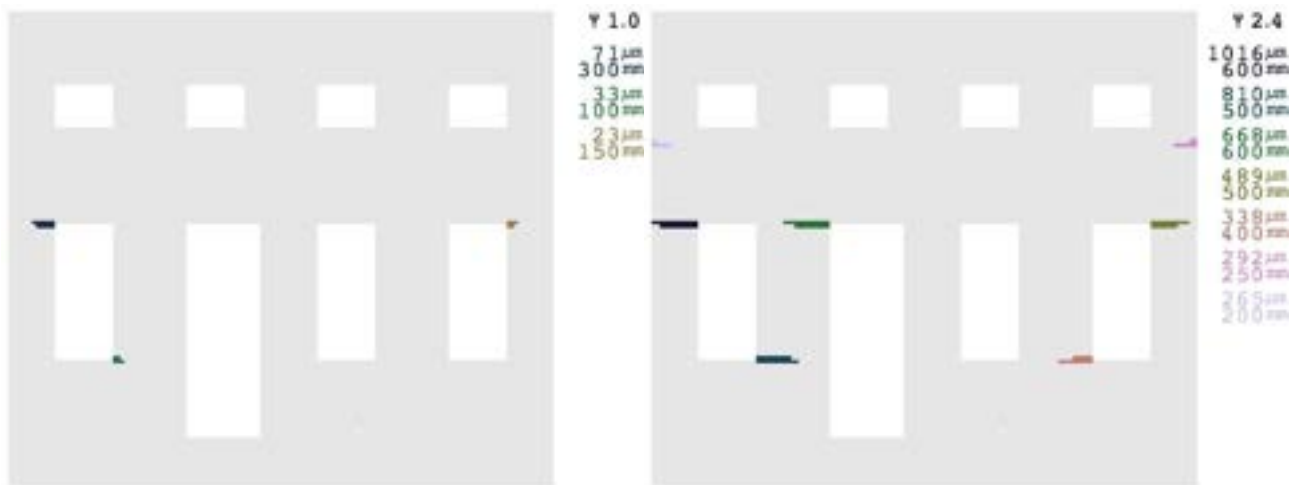


Figure 3.5. Crack pattern of Façade 1, geometry A, standard material, soil A, original interface and asymmetric settlement, knick point=L/3. Cracks at DS1 (left) and DS2 (right).

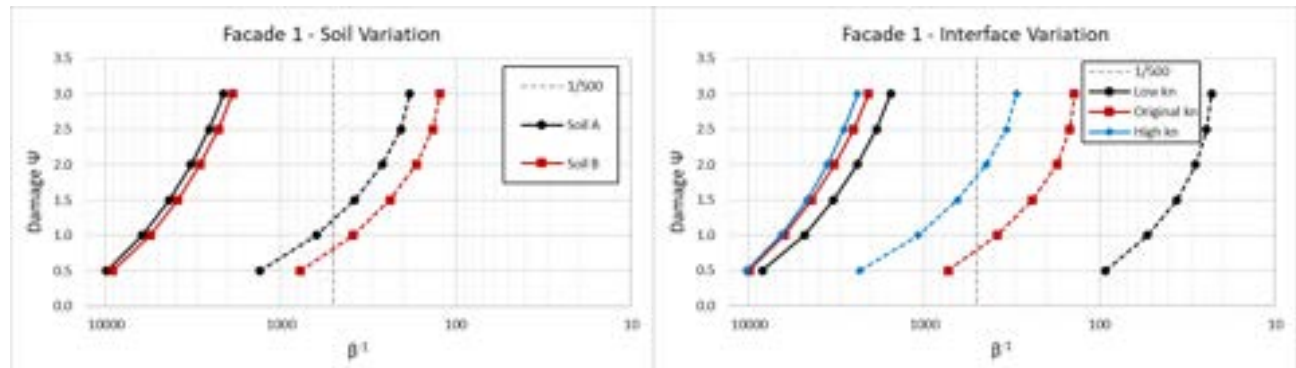


Figure 3.6. Angular distortion (β^{-1}) against damage and percentage of models that reach a specific damage level of Façade 1. Soil and interface variation. Dashed lines refers to applied β^{-1} .

Table 3.4. Measured (left) and applied (right) β^{-1} values of Façade 1. Soil and interface variation.

Soil	Ψ=0.5	Ψ=1.0	Ψ=1.5	Ψ=2.0	Ψ=2.5	Ψ=3.00	Soil	Ψ=0.5	Ψ=1.0	Ψ=1.5	Ψ=2.0	Ψ=2.5	Ψ=3.00
Soil A	9901	6185	4341	3261	2566	2125	Soil A	1322	626	379	263	206	183
Soil B	9151	5576	3874	2890	2265	1889	Soil B	776	385	238	168	136	123
Interface	Ψ=0.5	Ψ=1.0	Ψ=1.5	Ψ=2.0	Ψ=2.5	Ψ=3.00	Interface	Ψ=0.5	Ψ=1.0	Ψ=1.5	Ψ=2.0	Ψ=2.5	Ψ=3.00
Low kn	8359	4829	3283	2412	1864	1551	Low kn	93	53	36	28	25	23
Original kn	9930	6279	4379	3249	2522	2076	Original kn	729	384	241	175	148	139
High kn	10290	6534	4660	3566	2860	2393	High kn	111	1079	647	443	339	298

The material properties show a high sensitivity to the amount of models that reach a specific damage level once a settlement of $\beta = 1/10$ is applied. The weaker the masonry material, the larger the amount of models that reach a specific damage level. For example, 90% of the models with weak material get damaged up to $\Psi = 2.5$ while only the 25% reach the same damage level when the strong material is employed (Figure 3.7). When looking at values of measured β , the larger stiffness of the stronger material leads to an earlier cracking initiation ($\Psi = 0.5$) besides the bigger strength properties. This effect scales down for a higher level of damage, making the sensitivity of the material properties basically negligible in terms of measured β . In fact, for $\Psi = 2.5$, the

measured β ranges between 1/2100 and 1/2600 (Table 3.5). This effect is not observed in the applied β (and β ratio). Here, a stronger material has a visible impact on the point of damage. The stronger the material, the larger the settlement amplitude that should be applied to attain the same damage level. The β ratio between measured and applied also increases when material stiffness and strength increases, from 6 to 60 for severe light damage. Crack pattern is not affected by material variations. The different settlement actions applied at the base of the model are also compared. Figure 3.8 reports the β - Ψ plots comparison between symmetric and asymmetric hogging settlement. In addition, the effects of the different knick points of the deformation profiles are also confronted. The plots show that the symmetric hogging with a knick point at L/2 results the most vulnerable, but it results quite sensitive to the variation of the knick point. In fact, when the knick point shifts to L/4 the measured β to achieve the same damage increases almost by 30%. The applied angular distortion increases even further. Moreover, the amount of models of symmetric settlement L/2 that reach severe light damage is almost 3 times higher than the one with lower knick point. Façade 1 with asymmetric settlement profiles is more prone to damage than the symmetric one (71% against 49% for severe light damage). The difference can be found mainly in the large chance of damage of the case with lower knick point (L/5). The applied β of the asymmetric case is lower than the symmetric one. Values of measured and applied β are reported in Table 3.6. The lower knick points are also associated with a smaller portion of the façades being subjected to vertical displacements which explains why these are also less vulnerable than the higher knick points involving a profile that affects most of the length of the façades.

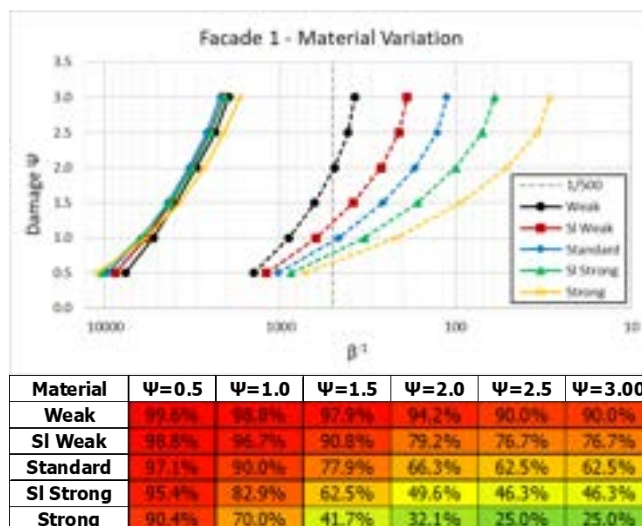


Figure 3.7. Angular distortion (β^{-1}) against damage and percentage of models that reach a specific damage level of Façade 1. Material variation. Dashed lines refers to applied β^{-1} .

Table 3.5. Measured (left) and applied (right) β^{-1} values of Façade 1. Material variation.

Material	$\Psi=0.5$	$\Psi=1.0$	$\Psi=1.5$	$\Psi=2.0$	$\Psi=2.5$	$\Psi=3.00$	Material	$\Psi=0.5$	$\Psi=1.0$	$\Psi=1.5$	$\Psi=2.0$	$\Psi=2.5$	$\Psi=3.00$
Weak	7656	5290	3952	3018	2356	1963	Weak	1418	890	637	490	411	376
SI Weak	8741	5834	4195	3179	2511	2105	SI Weak	1196	625	383	266	211	189
Standard	9671	6198	4386	3314	2630	2200	Standard	1034	465	261	171	127	112
SI Strong	10478	6246	4252	3161	2489	2068	SI Strong	871	329	165	100	71	60
Strong	11084	5835	3752	2705	2091	1698	Strong	725	218	94	51	34	29

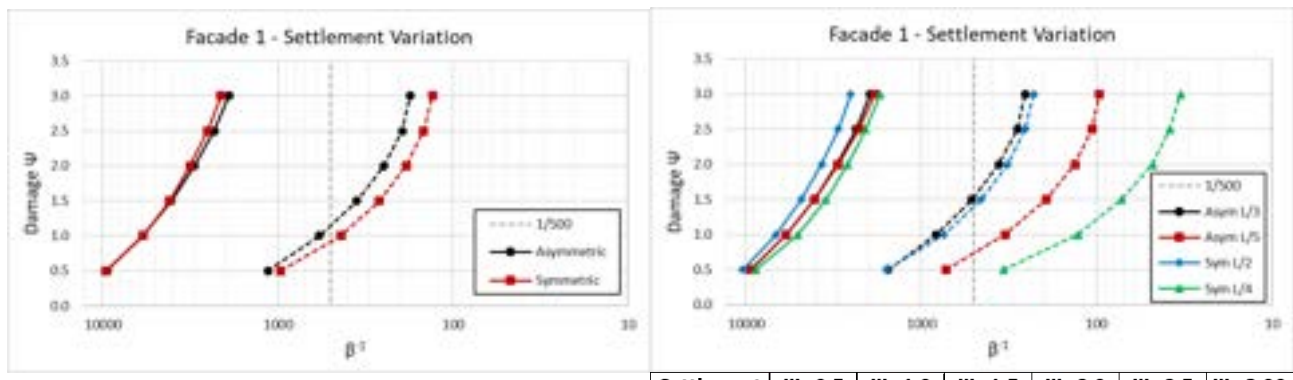


Figure 3.8. Angular distortion (β^{-1}) against damage and percentage of models that reach a specific damage level of Façade 1. Settlement variation. Dashed lines refers to applied β^{-1} .

Table 3.6. Measured (left) and applied (right) β^{-1} values of Façade 1. Settlement variation.

Settlement	$\Psi=0.5$	$\Psi=1.0$	$\Psi=1.5$	$\Psi=2.0$	$\Psi=2.5$	$\Psi=3.00$	Settlement	$\Psi=0.5$	$\Psi=1.0$	$\Psi=1.5$	$\Psi=2.0$	$\Psi=2.5$	$\Psi=3.00$	
Asymmetric	9449	5895	4061	2990	2310	1900	Asymmetric	1137	576	353	247	194	176	
Symmetric	9603	5866	4154	3161	2521	2114	Symmetric	961	435	263	185	147	131	
Settlement	$\Psi=0.5$	$\Psi=1.0$	$\Psi=1.5$	$\Psi=2.0$	$\Psi=2.5$	$\Psi=3.00$	Settlement	$\Psi=0.5$	$\Psi=1.0$	$\Psi=1.5$	$\Psi=2.0$	$\Psi=2.5$	$\Psi=3.00$	
Asym L/3	9418	5892	4069	3016	2349	1959	Asym L/3	1137	576	353	247	194	176	
Asym L/5	9480	5898	4053	2964	2271	1841	Asym L/5	1137	576	353	247	194	176	
Sym L/2	10429	6709	4828	3703	2969	2521	Sym L/2	1137	576	353	247	194	176	
Sym L/4	8806	5040	3491	2629	2080	1712	Sym L/4	1137	576	353	247	194	176	
Settlement	$\Psi=0.5$	$\Psi=1.0$	$\Psi=1.5$	$\Psi=2.0$	$\Psi=2.5$	$\Psi=3.00$	Settlement	$\Psi=0.5$	$\Psi=1.0$	$\Psi=1.5$	$\Psi=2.0$	$\Psi=2.5$	$\Psi=3.00$	
Asym L/3	1549	820	513	360	283	255	Asym L/3	1549	820	513	360	283	255	
Asym L/5	724	332	193	133	106	96	Asym L/5	724	332	193	133	106	96	
Sym L/2	1581	741	454	321	255	228	Sym L/2	1581	741	454	321	255	228	
Sym L/4	339	128	72	48	38	33	Sym L/4	339	128	72	48	38	33	

The different geometric variations of Façade 1 are characterized by various L/H ratios. Figure 3.9 compares the angular distortion to reach a certain damage level for the different variations. It can be seen that the higher the L/H ratio, the more vulnerable the façade and the more models reach failure. On the contrary, the ratio between measure and applied β reduces when increasing the L/H ratio. In fact, the increased length allows the façade to better follow the applied deformation. The small difference between the two highest ratios (i.e. 1.54 and 1.84) comes from the different length (and mass) of the models. In fact, the model with L/H=1.54 is longer and heavier than the one with L/H=1.84. The effects of these two parameters are better compared later in the section and in Appendix E. Severe light damage ($\Psi = 2.5$) is reached between measured $\beta = 1/1800$ (L/H = 1) and $\beta = 1/3150$ (L/H = 1.84). The applied β is equal to 1/50 and 1/180 respectively for L/H ratio of 1 and 1.84. All values are summarized in Table 3.7.

The models with L/H ratio equal to one include two geometry variations, namely variation B and D. Although they both have the same L/H ratio, the size of the façade is different. The two square cases, with L=H=5.5 m and L=H=7.0 m are compared in Figure 3.10 and Table 3.8. It is clear from the graph how the larger size has a negative impact on both angular distortion measured and applied to reach a specific damage and on the amount of models that reach that level (70% more models for $\Psi = 2.5$) even when the L/H are identical.

Opening percentage and type of openings (standard width against large opening) is analysed in Figure 3.11 and Table 3.9. For what regards the initiation of cracking ($\Psi = 0.5$), the effect on the measured β is similar of what is already seen for the material variation. The model with the lowest opening percentage cracks earlier than the others, but the amount of models that initiate cracks is the lowest between the four variations. On the contrary, the façade with the highest opening percentage, gets initiation of cracking at a measured β 20% higher than the one with lower

percentage. In addition all models reach $\Psi = 0.5$. The applied β required to reach a certain damage level increases when reducing the opening percentage. The comparison is somewhat similar to the material variation. Large openings do not influence the measured β to reach certain damage levels. The models with large openings appear more vulnerable in terms of applied settlement than the ones with lower opening width. The amount of models that reach failure when large openings are present is about 10% higher than the variation without.

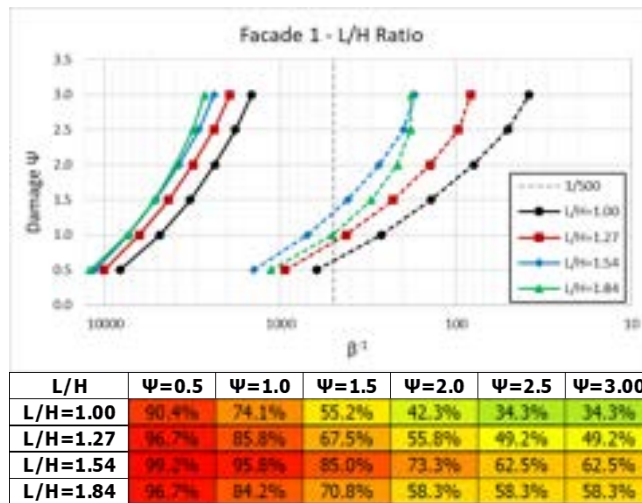


Figure 3.9. Angular distortion (${}^{\wedge}1$) against damage and percentage of models that reach a specific damage level of Façade 1. L/H ratio variations. Dashed lines refers to applied β^{-1} .

Table 3.7. Measured (left) and applied (right) β^{-1} values of Façade 1. L/H ratio variations.

L/H	$\Psi=0.5$	$\Psi=1.0$	$\Psi=1.5$	$\Psi=2.0$	$\Psi=2.5$	$\Psi=3.00$	L/H	$\Psi=0.5$	$\Psi=1.0$	$\Psi=1.5$	$\Psi=2.0$	$\Psi=2.5$	$\Psi=3.00$
L/H=1.00	8210	4846	3263	2367	1802	1459	L/H=1.00	623	266	139	79	51	38
L/H=1.27	10138	6361	4334	3143	2390	1941	L/H=1.27	940	421	228	141	97	82
L/H=1.54	11441	7351	5122	3774	2913	2389	L/H=1.54	1417	701	413	274	199	171
L/H=1.84	12196	7427	5201	3944	3154	2706	L/H=1.84	1137	504	303	215	181	178

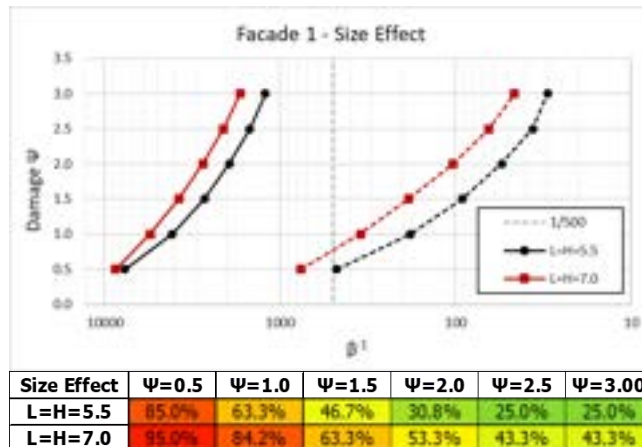


Figure 3.10. Angular distortion (${}^{\wedge}1$) against damage and percentage of models that reach a specific damage level of Façade 1. Size effect variations. Dashed lines refers to applied β^{-1} .

Table 3.8. Measured (left) and applied (right) β^{-1} values of Façade 1. Size effect variations.

Size Effect	$\Psi=0.5$	$\Psi=1.0$	$\Psi=1.5$	$\Psi=2.0$	$\Psi=2.5$	$\Psi=3.00$	Size Effect	$\Psi=0.5$	$\Psi=1.0$	$\Psi=1.5$	$\Psi=2.0$	$\Psi=2.5$	$\Psi=3.00$
L=H=5.5	7681	4125	2705	1950	1487	1215	L=H=5.5	477	180	92	55	36	30
L=H=7.0	8670	5527	3794	2764	2102	1690	L=H=7.0	765	348	185	103	64	46

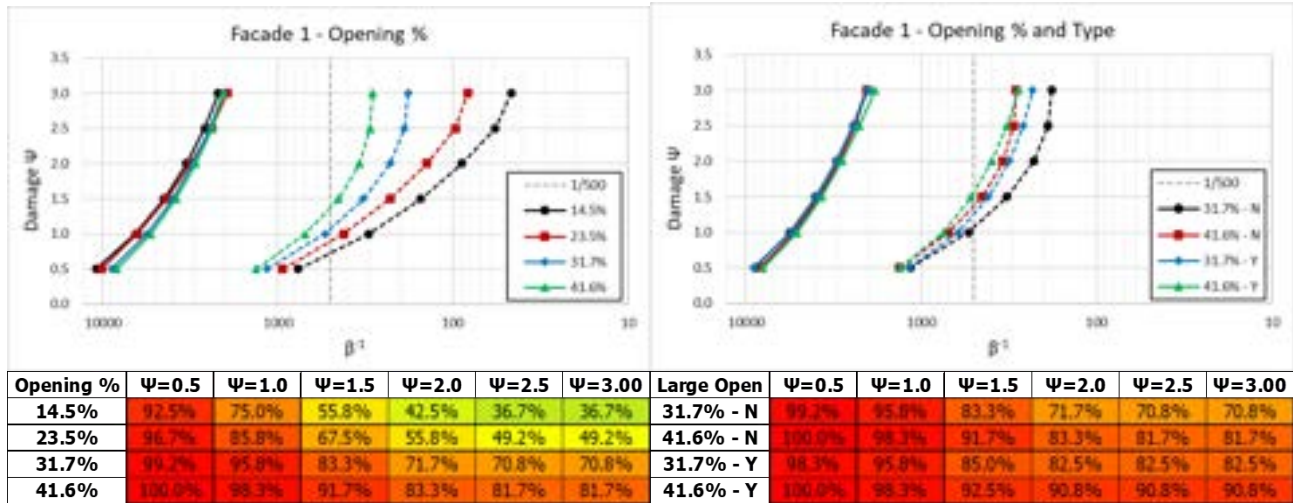


Figure 3.11. Angular distortion (β^{-1}) against damage and percentage of models that reach a specific damage level of Façade 1. Opening % and type variations. Dashed lines refers to applied β^{-1} .

Table 3.9. Measured (left) and applied (right) β^{-1} values of Façade 1. Opening % and type variations.

Opening %	$\Psi=0.5$	$\Psi=1.0$	$\Psi=1.5$	$\Psi=2.0$	$\Psi=2.5$	$\Psi=3.0$	Opening %	$\Psi=0.5$	$\Psi=1.0$	$\Psi=1.5$	$\Psi=2.0$	$\Psi=2.5$	$\Psi=3.0$
14.5%	10685	6486	4462	3320	2612	2187	14.5%	765	302	152	89	57	46
23.5%	10138	6361	4334	3143	2390	1941	23.5%	940	421	228	141	97	82
31.7%	8904	5598	3996	3052	2436	2044	31.7%	1155	538	324	228	189	181
41.6%	8320	5313	3811	2933	2375	2049	41.6%	1328	699	451	341	297	287
Large Open	$\Psi=0.5$	$\Psi=1.0$	$\Psi=1.5$	$\Psi=2.0$	$\Psi=2.5$	$\Psi=3.0$	Large Open	$\Psi=0.5$	$\Psi=1.0$	$\Psi=1.5$	$\Psi=2.0$	$\Psi=2.5$	$\Psi=3.0$
31.7% - N	8904	5598	3996	3052	2436	2044	31.7% - N	1155	538	324	228	189	181
41.6% - N	8320	5313	3811	2933	2375	2049	41.6% - N	1128	699	451	341	297	287
31.7% - Y	9069	5519	3958	3041	2432	2009	31.7% - Y	1178	615	415	314	262	231
41.6% - Y	7987	5098	3691	2833	2251	1839	41.6% - Y	1322	744	518	395	325	279

Façade 2

Façade 2, with its length of 17 m, results in a pretty vulnerable façade when subjected to settlement actions. Twelve variations are investigated for this farm house. The average values of β of all models at a specific damage level are plotted in Figure 3.12 and summarised in Table 3.10. All twelve models reach DS2. The measured β does not result so different from the values found in other shorter façades (i.e. Façade 1). The value is close to 1/2600. This suggests that β_m is similar between façades and is rather an expression of the vulnerability of the masonry, thus, a response of the structure.

The ratio between measured and applied β , however, is around a value of 2 remarking the high flexibility of the farm house façade to follow the applied settlement. The failure mechanism involves vertical cracking which develops close to window openings (asymmetric hogging, Figure 3.13) or at the connection between the shed and the living space (symmetric hogging, Figure 3.14). Additionally, as cracking develops the stiffness of the building may decrease significantly, allowing the façade to conform more closely to the ground movement [33, 34].

In general, the measured angular distortion at a specific damage level of Façade 2 is barely influenced by any parameter (material, soil, settlement, etc). But the different variations have a larger influence on the ratio between the measured and the applied β .

Additional plots and sensitivity according to the different parameters can be found in Appendix D.

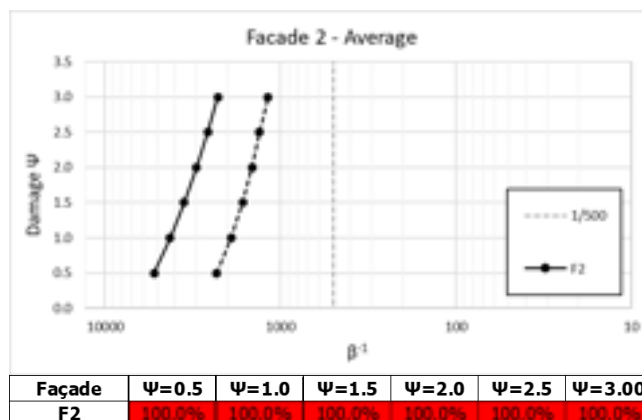


Figure 3.12. Angular distortion (\wedge^{-1}) against damage and percentage of models that reach a specific damage level of Façade 2. Average values. Dashed lines refers to applied β^{-1} .

Table 3.10. Measured (left) and applied (right) β^{-1} values of Façade 2.

Façade	$\Psi=0.5$	$\Psi=1.0$	$\Psi=1.5$	$\Psi=2.0$	$\Psi=2.5$	$\Psi=3.00$	Façade	$\Psi=0.5$	$\Psi=1.0$	$\Psi=1.5$	$\Psi=2.0$	$\Psi=2.5$	$\Psi=3.00$
F2	2306	1908	1636	1450	1317	1177	F2	5245	4255	3543	3003	2590	2271

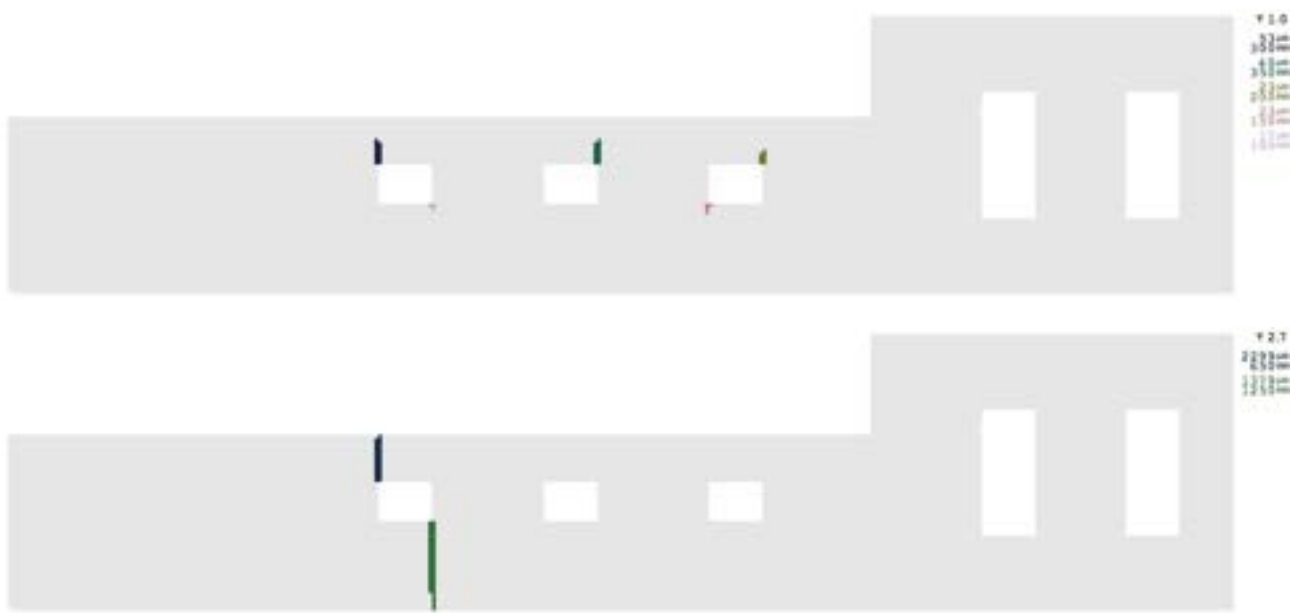


Figure 3.13 Crack pattern of Façade 2, geometry A, standard material, soil A, original interface and asymmetric settlement, knick point= $L/3$. Cracks at DS1 (top) and DS2 (bottom).



Figure 3.14. Crack pattern of Façade 2, geometry A, standard material, soil A, original interface and symmetric settlement, knick point= $L/2$. Cracks at DS1 (top) and DS2 (bottom).

Façade 3

Differing from the previous models, some of the models for Façade 3 (especially the ones with weak material properties) present damage after the application of gravity and vertical load application. These models (more or less 10% of the total) are not included in the plots below, where only results of non-predamaged models are shown. The average results in terms of $\beta\cdot\Psi$ of all variations of Façade 3 are shown in Figure 3.15 and Table 3.11. About 55% of the models reach severe light damage ($\Psi = 2.5$). An angular distortion of 1/2150 is required to the façade to reach such damage level. The applied β is about 16 times higher, equal to 1/130. The crack pattern of the geometry variation A at two damage states (1 and 2) is shown in Figure 3.16. Cracking initiates at the window corner of the ground floor. The two large window openings lead to vertical crack opening below the windows.

Figure 3.17 and Table 3.12 show the sensitivity of the L/H ratio. Similar to Façade 1, also in this case, the higher ratios are more vulnerable. Damage is reached for lower measured and applied β in respect to the smaller L/H ratios. The case with L/H=1.24, although it does not have the highest L/H ratio, shows the most vulnerable results in terms of β and amount of models that get damaged. In respect to the other models, this specific one has a bigger length which for this façade results in a dominant factor. Measured β values range from 1/1670 (L/H=0.68) to 1/3280 (L/H=1.24).

Another sensitivity parameter for Façade 3 is the opening percentage. Figure 3.18 and Table 3.13 summarize the $\beta\cdot\Psi$ behaviour of the variations. The models with 30% of (large) openings result in the most vulnerable. Almost 92% of the cases exceed light damage and reach DS2. The cases with 13% of openings, reach DS2 only in 15% of the models. Measured β at DS2 of the latter is about 1/1570 against 1/3400 for the case with the highest opening percentage. The large flexibility imposed by the window openings reduces the β ratio from 70 to 6 when the opening percentage increases from 13% to 30%; this is a significant decrease.

Additional plots and sensitivity according to the different parameters can be found in Appendix D.

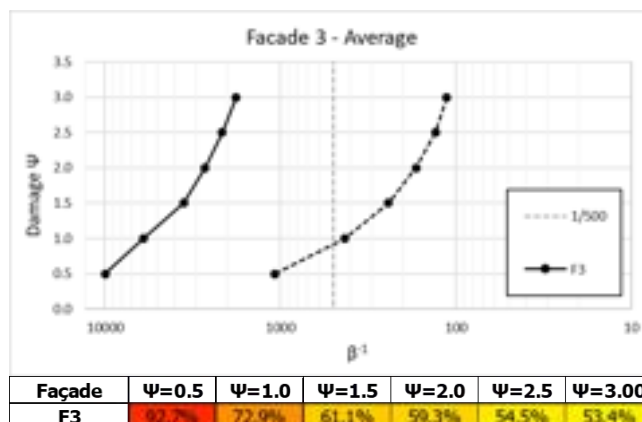


Figure 3.15. Angular distortion (β^{-1}) against damage and percentage of models that reach a specific damage level of Façade 3. Average values. Dashed lines refers to applied β^{-1} .

Table 3.11. Measured (left) and applied (right) β^{-1} values of Façade 3. Average values.

Façade	$\Psi=0.5$	$\Psi=1.0$	$\Psi=1.5$	$\Psi=2.0$	$\Psi=2.5$	$\Psi=3.00$	Façade	$\Psi=0.5$	$\Psi=1.0$	$\Psi=1.5$	$\Psi=2.0$	$\Psi=2.5$	$\Psi=3.00$
F3	9966	6035	3564	2692	2147	1789	F3	1072	430	242	168	131	113



Figure 3.16. Crack pattern of Façade 4, geometry A, standard material, soil A, original interface and asymmetric settlement, knick point=L/3. Cracks at DS1 (left) and DS2 (right). Notice how new cracks allow other cracks to close.

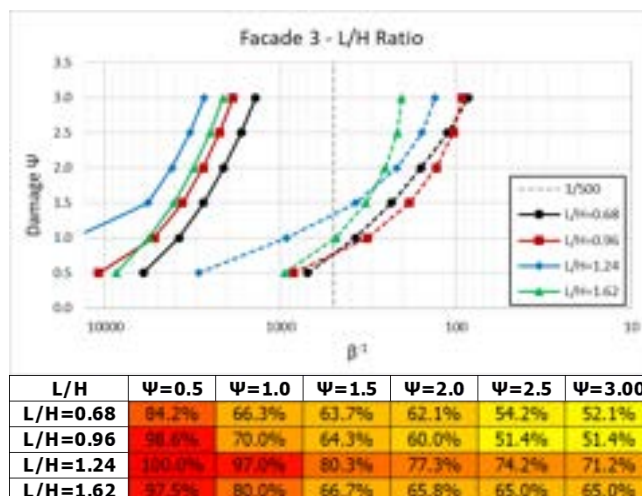


Figure 3.17. Angular distortion (β^{-1}) against damage and percentage of models that reach a specific damage level of Façade 3. L/H ratio variations. Dashed lines refers to applied β^{-1} .

Table 3.12. Measured (left) and applied (right) β^{-1} values of Façade 3. L/H ratio variations.

L/H	$\Psi=0.5$	$\Psi=1.0$	$\Psi=1.5$	$\Psi=2.0$	$\Psi=2.5$	$\Psi=3.00$	L/H	$\Psi=0.5$	$\Psi=1.0$	$\Psi=1.5$	$\Psi=2.0$	$\Psi=2.5$	$\Psi=3.00$
L/H=0.68	6055	3777	2740	2108	1671	1384	L/H=0.68	699	374	232	158	111	85
L/H=0.96	10885	5249	3609	2752	2222	1864	L/H=0.96	845	319	184	129	103	92
L/H=1.24	39923	15092	5694	4137	3276	2717	L/H=1.24	2933	920	372	217	157	131
L/H=1.62	8623	5616	4038	3113	2514	2118	L/H=1.62	943	481	326	252	215	204

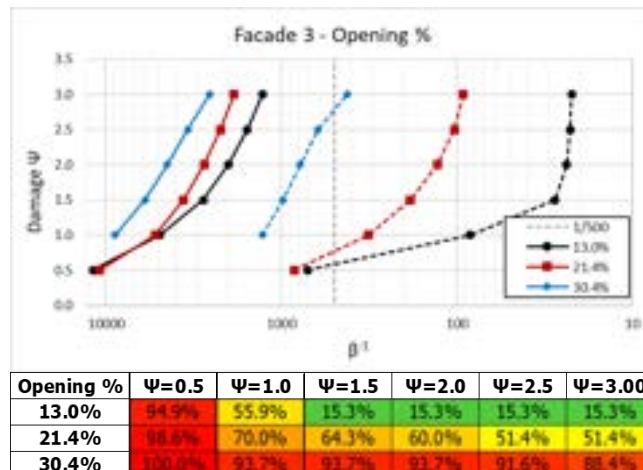


Figure 3.18. Angular distortion (β^{-1}) against damage and percentage of models that reach a specific damage level of Façade 3. Opening % variations. Dashed lines refers to applied β^{-1} .

Table 3.13. Measured (left) and applied (right) β^{-1} values of Façade 3. Opening % variation.

Opening %	$\Psi=0.5$	$\Psi=1.0$	$\Psi=1.5$	$\Psi=2.0$	$\Psi=2.5$	$\Psi=3.00$	Opening %	$\Psi=0.5$	$\Psi=1.0$	$\Psi=1.5$	$\Psi=2.0$	$\Psi=2.5$	$\Psi=3.00$
13.0%	11853	4926	2791	2009	1569	1285	13.0%	712	84	28	24	23	22
21.4%	10885	5249	3609	2752	2222	1864	21.4%	845	319	184	129	103	92
30.4%		8878	5993	4480	3422	2561	30.4%		1286	979	783	617	422

Façade 4

The transversal façade of the detached house, 12x3 meters, results the most vulnerable between the four analysed façades with unreinforced masonry foundation. More than 90% of the (virgin) models of Façade 4 reach DS2 ($\Psi = 2.5$), as shown in Figure 3.19. The measured and applied β at the onset of DS2 are 1/3600 and 1/800 respectively, with a ratio of about 4 (Table 3.14). The façade is characterized by reduced height of the spandrels. Cracking starts thus mainly at the top of the façade and progresses downward while the settlement actions grow in amplitude. A typical damage pattern for the geometry variation A for asymmetric and symmetric hogging settlement is depicted in Figure 3.20. Initial cracks (or pre-damage) initiate above the left window and according to the type of settlement extends below the window opening or, alternatively, a new vertical crack forms from the top edge above the window in the middle.

The changes in the L/H ratio is described by Figure 3.21 and Table 3.15. The model with larger ratio shows higher vulnerability and chance of damage than the ones with lower ratio. The sensitivity is even more evident for the applied angular distortion. Must be noted that the case with L/H=2 has also a reduced length with respect to the rest of the variations.

Additional plots and sensitivity according to the different parameters can be found in Appendix D.

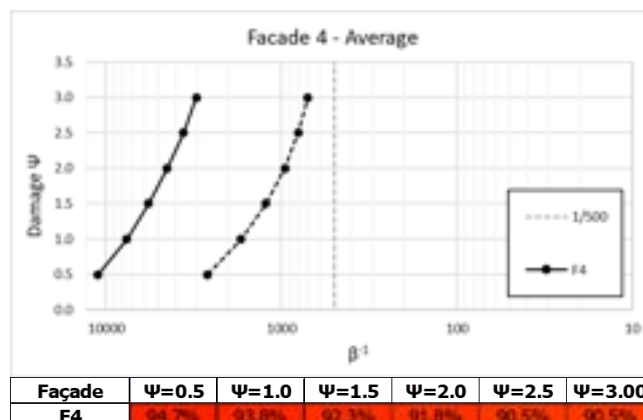


Figure 3.19. Angular distortion (β^{-1}) against damage and percentage of models that reach a specific damage level of Façade 4. Average values. Dashed lines refers to applied β^{-1} .

Table 3.14. Measured (left) and applied (right) β^{-1} values of Façade 4. Average values.

Façade	$\Psi=0.5$	$\Psi=1.0$	$\Psi=1.5$	$\Psi=2.0$	$\Psi=2.5$	$\Psi=3.00$	Façade	$\Psi=0.5$	$\Psi=1.0$	$\Psi=1.5$	$\Psi=2.0$	$\Psi=2.5$	$\Psi=3.00$
F4	11068	7604	5708	4470	3612	3047	F4	2638	1694	1225	956	803	706

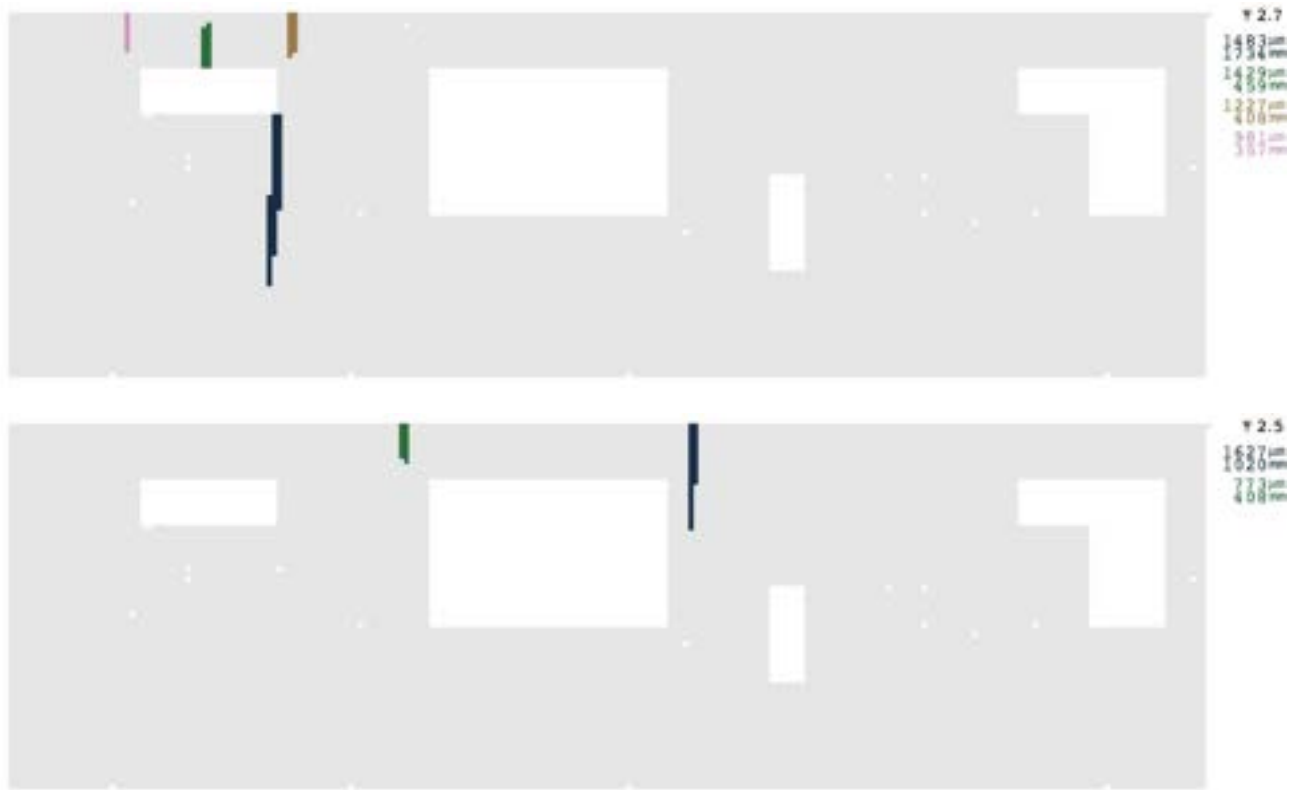
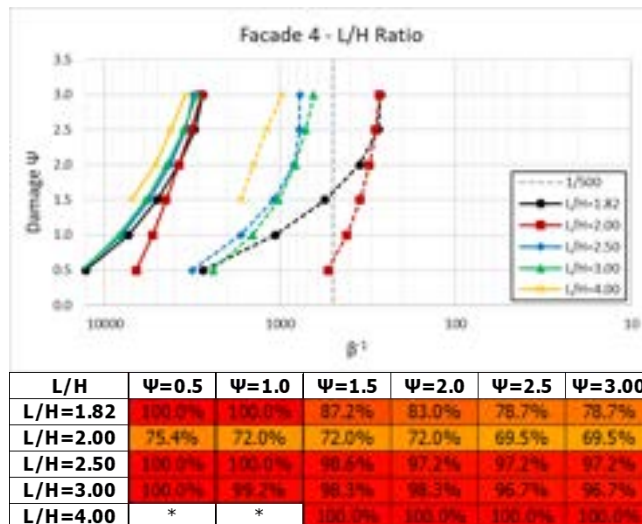


Figure 3.20. Crack pattern of Façade 4, geometry A, standard material, soil A, original interface at DS2. Asymmetric settlement, knick point L/3 (top) and symmetric settlement, knick point L/2 (bottom).

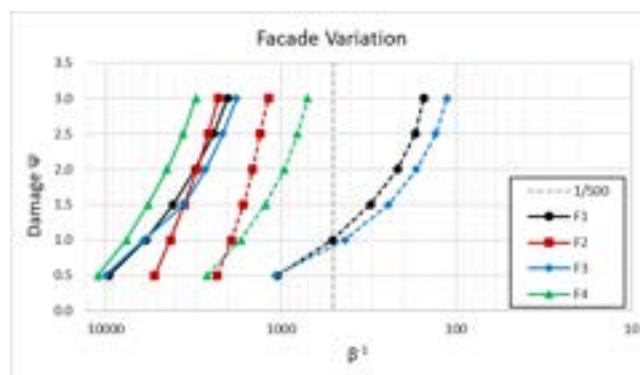
Figure 3.21. Angular distortion (^-1) against damage and percentage of models that reach a specific damage level of Façade 4. L/H ratio variations. Dashed lines refers to applied β^{-1} .Table 3.15. Measured (left) and applied (right) β^{-1} values of Façade 3. L/H ratio variations.

L/H	$\Psi=0.5$	$\Psi=1.0$	$\Psi=1.5$	$\Psi=2.0$	$\Psi=2.5$	$\Psi=3.00$	L/H	$\Psi=0.5$	$\Psi=1.0$	$\Psi=1.5$	$\Psi=2.0$	$\Psi=2.5$	$\Psi=3.00$
L/H=1.82	12839	7304	5030	3811	3067	2763	L/H=1.82	2750	1062	554	352	276	268
L/H=2.00	6622	5313	4471	3777	3211	2806	L/H=2.00	535	416	351	309	286	271
L/H=2.50	13430	8025	5609	4266	3476	3111	L/H=2.50	3183	1671	1092	832	776	772
L/H=3.00	13388	8280	5829	4427	3547	2995	L/H=3.00	2415	1438	1021	820	715	646
L/H=4.00	*	*	7040	5125	4203	3451	L/H=4.00	*	*	1675	1425	1195	979

Summary - Unreinforced foundation (Façades 1-2-3-4)

The results of all façades with unreinforced foundations are summarized and compared. In Figure 3.22 the amount of models that reach a specific damage level are shown together with the $\beta\text{-}\Psi$ curve. For the former, there is a clear distinction between the “long” (F2 and F4) and “short” façades (F1 and F3). In fact, almost all “long” façade models reach DS2 while the percentage of “short” models that reach $\Psi = 2.5$ is 30 to 40% smaller. A large difference is also detected in the applied settlement required to reach a certain damage level. For Façades 1 and 3 the value of the applied β is above 1/200, while for the two long transversal façades the value is lower than 1/800. This is related to the large flexibility and the capability of these façades to better follow the applied deformation at interface level. When comparing the measured value of β for the four different façades, it can be seen from Figure 3.22 and Table 3.16 that the maximum difference at the onset of DS2 is about 40%. The most vulnerable façade at this stage is Façade 4 (β_m 1/3600) and the least vulnerable is Façade 3 (β_m 1/2150).

When splitting all models in a continuous range of L/H ratios, trend-lines describing the probability of exceeding specific damage limits can be built in order to observe smooth trends; parabolic functions are used to describe these. Figure 3.23 shows the tabulated and the plotted values of different L/H ratios. It can be seen that the higher the L/H ratio of the façade, the higher the chance of reaching a certain damage level when a settlement up to a β of 1/10 is applied. The trend-line shows that for L/H ratios lower than 1 the chance of DS2 damage is about 40%. This increases to 51% for L/H=1, 76% for a ratio of 2 and 92% for L/H=3. Similar trend-lines are built for both average measured and average applied β . The curves are shown in Figure 3.24. The measured angular distortion presents curves that decrease at the increase of the L/H ratio. The last point, referring to L/H=5, tends to have a slightly higher value, but it might be led by the reduced geometric variation of this type of façade. The measured β for DS2 ranges from 1/1800 (L/H<1) to about 1/3600 for L/H=4. The applied settlement to reach a pre-defined damage level is much more sensitive to the L/H ratio than the measured one. The parabolic trend is similar to the measured one, but much more pronounced. In this case, the values range from 1/70 at L/H=1 to 1/1300 at L/H=5 for the onset of DS2. The summary of $\beta\text{-}\Psi$ for the different L/H cases is reported in Table 3.17.



Façade	$\Psi=0.5$	$\Psi=1.0$	$\Psi=1.5$	$\Psi=2.0$	$\Psi=2.5$	$\Psi=3.0$
F1	96.3%	87.7%	74.2%	64.3%	60.1%	60.1%
F2	100.0%	100.0%	100.0%	100.0%	100.0%	100.0%
F3	92.7%	72.9%	61.1%	59.3%	54.5%	53.4%
F4	94.7%	93.8%	92.3%	91.8%	90.5%	90.5%

Figure 3.22. Angular distortion (\wedge -1) against damage and percentage of models that reach a specific damage level. Façade variations. Dashed lines refers to applied β^{-1} .

Table 3.16. Measured (left) and applied (right) β^{-1} values. Façade variations.

Façade	$\Psi=0.5$	$\Psi=1.0$	$\Psi=1.5$	$\Psi=2.0$	$\Psi=2.5$	$\Psi=3.0$	Façade	$\Psi=0.5$	$\Psi=1.0$	$\Psi=1.5$	$\Psi=2.0$	$\Psi=2.5$	$\Psi=3.0$
F1	9526	5880	4107	3076	2415	2007	F1	1048	505	308	215	171	153
F2	5245	4255	3543	3003	2590	2271	F2	2306	1908	1636	1450	1317	1177
F3	9966	6035	3564	2692	2147	1789	F3	1072	430	242	168	131	113
F4	11068	7604	5708	4470	3612	3047	F4	2638	1694	1225	956	803	706

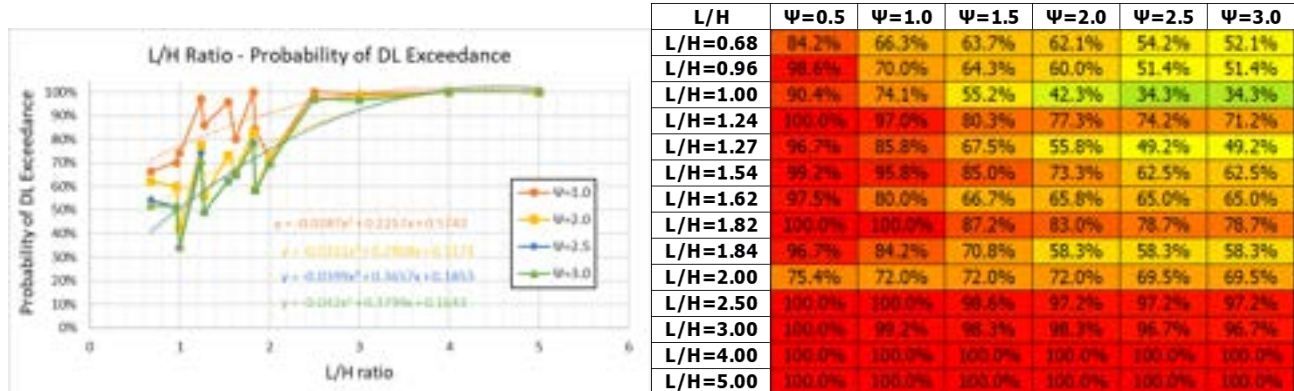


Figure 3.23. Amount of models subjected to a settlement of $\beta=1/10$ that reach a specific damage level. L/H ratio variation.

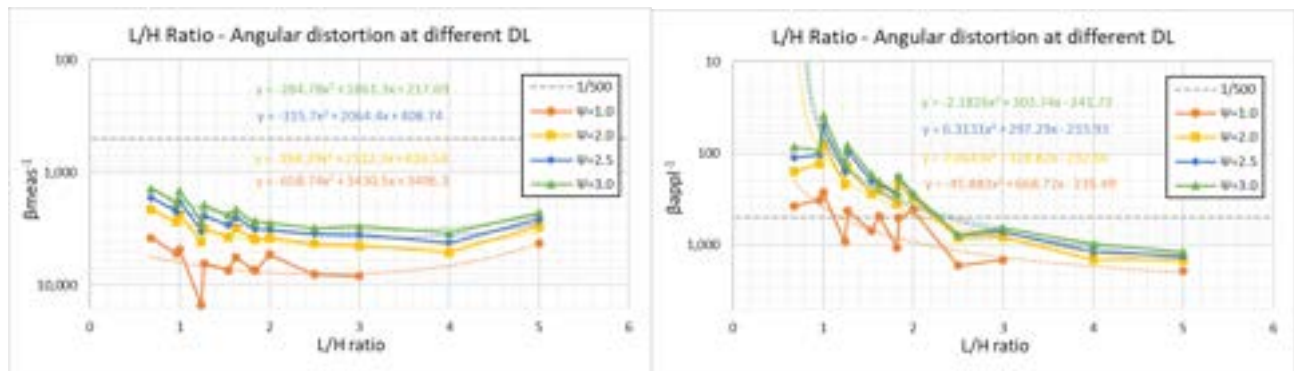


Figure 3.24. Measured (left) and applied (right) angular distortion (\wedge^{-1}) at different damage level. L/H ratio variation.

Table 3.17. Measured (left) and applied (right) value of β^{-1} . L/H ratio variation.

L/H	$\Psi=0.5$	$\Psi=1.0$	$\Psi=1.5$	$\Psi=2.0$	$\Psi=2.5$	$\Psi=3.0$	L/H	$\Psi=0.5$	$\Psi=1.0$	$\Psi=1.5$	$\Psi=2.0$	$\Psi=2.5$	$\Psi=3.0$
L/H=0.68	6055	3777	2740	2108	1671	1384	L/H=0.68	699	374	232	158	111	85
L/H=0.96	10885	5249	3609	2752	2222	1864	L/H=0.96	845	319	184	129	103	92
L/H=1.00	8210	4846	3263	2367	1802	1459	L/H=1.00	623	266	139	79	51	38
L/H=1.24	6923	15092	5694	4137	3276	2717	L/H=1.24	2933	920	372	217	157	131
L/H=1.27	10138	6361	4334	3143	2390	1941	L/H=1.27	940	421	228	141	97	82
L/H=1.54	11441	7351	5122	3774	2913	2389	L/H=1.54	1417	701	413	274	199	171
L/H=1.62	8623	5616	4038	3113	2514	2118	L/H=1.62	943	481	326	252	215	204
L/H=1.82	12839	7304	5030	3811	3067	2763	L/H=1.82	2750	1062	554	352	276	268
L/H=1.84	12166	7427	5201	3944	3154	2706	L/H=1.84	1137	504	303	215	181	178
L/H=2.00	6622	5313	4471	3777	3211	2806	L/H=2.00	535	416	351	309	286	271
L/H=2.50	13630	8025	5609	4266	3476	3111	L/H=2.50	3183	1671	1092	832	776	772
L/H=3.00	13288	8280	5829	4427	3547	2995	L/H=3.00	2415	1438	1021	820	715	646
L/H=4.00	*	*	7040	5125	4203	3451	L/H=4.00	*	*	1675	1425	1195	979
L/H=5.00	5245	4255	3543	3003	2590	2271	L/H=5.00	2306	1908	1636	1450	1317	1177

Additionally, the length of the façade is analysed separately. Figure 3.25 reports the chance of attaining a specific damage level for façades with different length when a hogging settlement is applied up to an angular distortion of 1/10. From the table and the trend-lines, it can be seen that the probability of damage becomes higher for longer length. The trend-line for the onset of DS2 looks almost linear. The data points to a drastic increase in possibility of severe light damage (from 74%

to 97%) for length equal or higher than 9 meters. The vulnerability of long façades is also confirmed when plotting the façade length against measured and applied β . The curves are shown in Figure 3.26. The data is summarized in Table 3.18. The measured angular distortion for different levels of damage show decreasing values for high length, with trend-lines that tend to a plateau. This plateau is found for a length between 8 and 9 meters. Contrary to the measured β , the applied β does not show a plateau in the trend, but follows more a parabolic function. The trend-line for onset of DS2 (at $\Psi = 2.5$) shows that the angular distortion that should be applied to cause severe light damage is higher than 1/500 for façades between 8 and 9 meters. Above this length, the settlement amplitude that should be applied to reach DS2 is lower, below 1/900. Consequently, the ratio between measured and applied angular distortion becomes lower.

No clear trends are evaluated when investigating the height of the façades. The results are led mainly by the correlated length. It is recommended to look at this parameter in combination with the length of the façade (L/H ratio). It must be noted that all presented results are only analysed in a deterministic way without including any probabilistic insight.

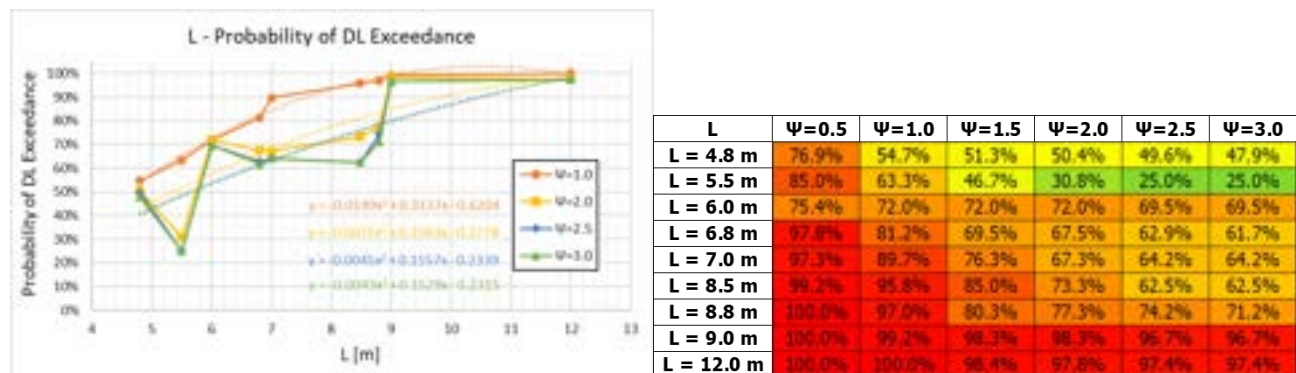


Figure 3.25. Amount of models subjected to a settlement of $\beta=1/10$ that reach a specific damage level. Length variation.

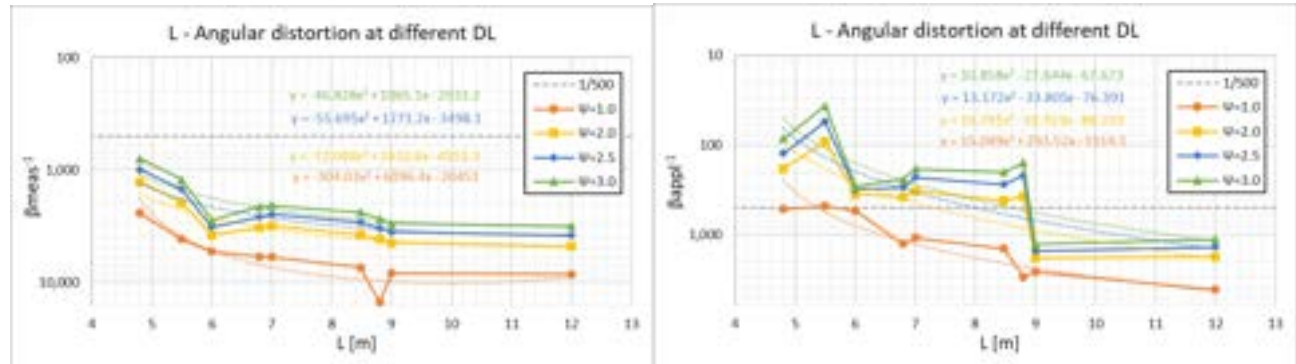


Figure 3.26. Measured (left) and applied (right) angular distortion (β^{-1}) at different damage level. Length variation.

Table 3.18. Measured (left) and applied (right) value of β^{-1} . Length variation.

L	$\Psi=0.5$	$\Psi=1.0$	$\Psi=1.5$	$\Psi=2.0$	$\Psi=2.5$	$\Psi=3.0$	L	$\Psi=0.5$	$\Psi=1.0$	$\Psi=1.5$	$\Psi=2.0$	$\Psi=2.5$	$\Psi=3.0$
L = 4.8 m	3973	2414	1715	1280	992	794	L = 4.8 m	514	287	182	124	84	63
L = 5.5 m	7681	4125	2705	1950	1487	1215	L = 5.5 m	477	180	92	55	36	30
L = 6.0 m	6622	5313	4471	3777	3211	2806	L = 6.0 m	535	416	351	309	286	271
L = 6.8 m	11940	5906	4184	3251	2610	2115	L = 6.8 m	1253	553	377	294	240	199
L = 7.0 m	9517	5916	4156	3129	2469	2058	L = 7.0 m	1074	521	322	228	184	166
L = 8.5 m	11441	7351	5122	3774	2913	2389	L = 8.5 m	1417	701	413	274	199	171
L = 8.8 m	10923	15092	5694	4137	3276	2717	L = 8.8 m	2933	920	372	217	157	131
L = 9.0 m	13288	8280	5829	4427	3547	2995	L = 9.0 m	2582	2157	1802	1503	1264	1069
L = 12.0 m	14934	8497	6146	4754	3812	3169	L = 12.0 m	4957	2408	1745	1358	1120	957

Summary - Reinforced foundation (Façades 5-6-7-8)

Seven façade variations with reinforced concrete (RC) foundations are analysed under settlement deformation. The façades represent buildings of the '70s which are characterized by cavity wall systems, RC foundations, and predominantly calcium-silicate (brick) walls.

Façade 5 and 6, representing the two inner calcium silicate (CaSi) leaves of a terraced house, are characterized by large openings and lengths of 6.75 and 8.4 meters. The crack patterns at onset of DS1 and DS2 are shown in Figure 3.27 and Figure 3.28. Façade 5 shows initiation of cracks at window corners of both ground and first floors. Once the settlement deformation increases, the crack pattern changes. A crack runs vertically underneath the window opening of the first floor. The large openings of Façade 6, also lead to a similar damage mechanism, with cracks that extend underneath the large opening at the ground floor due to bending of the window bank. Façade 7 shows pre-damage (before settlement loading) for almost all variations. An horizontal crack appears at the top right pier due to bending at floor level. The settlement actions only causes the development of a small vertical crack below the large window at the ground floor. The crack patterns are depicted in Figure 3.29. Façade 8-A, due to lack of openings and low L/H ratio does not show any damage for any modelled variation. Façade 8-B shows a small crack underneath the window opening at the ground floor (Figure 3.30). Façade 9, both variation A and B due to their long façade, undergoes vertical cracking starting from the top edge (Figure 3.31).

The β - Ψ curves of the different CaSi models on reinforced foundations are shown in Figure 3.32. Both Façades 5 and 6 are revealed as the most vulnerable in terms of measured β , applied β and amount of models that reach DS2. Damage state 1 (from $\Psi \geq 1$) is attained in almost all models: 80% for Façade 5 and 100% for Façade 6, at a measured β of 1/4600 and 1/7600, respectively. The amount of models that pass $\Psi = 3$, when an applied settlement of $\beta=1/10$ is applied, is much lower, 30% and 50% for Façades 5 and 6 respectively. The full β - Ψ data can be found in Table 3.19.

Vertical loading produces a pre-damage between $\Psi_0 = 1.0$ and $\Psi_0 = 1.8$ in Façade 7, according to the different variations. Because of the pre-damage and of the (resulting) large flexibility of the façade, it is able to withstand settlement actions, showing limited increase in damage. In fact, only 33% of the models reach a damage of $\Psi = 2$; while 25% of the models show an increment of the damage parameter of 0.5 and none of the models reach an increment of 1.0 in Ψ (Figure 3.33). The pre-damage and the increment of damage in terms of Ψ is computed for all variations of Façade 7 and reported in Figure 3.34. The average pre-damage of all models is equal to $\Psi_0=1.43$ and the average $\Delta\Psi=0.44$. Soil type has a minor influence on the initial and to the evolution of the damage. The asymmetric settlement shows a higher increment in damage respect to the symmetric one ($\Delta\Psi=0.52$ against $\Delta\Psi=0.38$). An interesting response to pre-damage and evolution of damage is found in the material properties. The weak material leads to higher initial damage with respect to the stronger materials. Though, the increment of damage is inversely proportional to the stiffness and strength of the material. The $\Delta\Psi$ is equal to 0.30, 0.38 and 0.65 for weak, standard and strong material respectively. The final damage attained maintains its proportionality to the material stiffness-strength, showing higher values for the weakest material. The average values of measured β to reach DS2 are equal to 1/220. Façade 8-A, with 0% openings, is impervious to settlement-induced damage; it rigidly tilts without showing any cracks. The addition of two openings (Façade 8-B), enhance a small vertical crack below the window at the ground floor (Figure 3.30). Such damage stabilizes at a maximum Ψ of 1.5 and does not grow any further, meaning that the low L/H ratio (below 1) affect positively the façade. The long Façades 9 (A and B) are mainly characterized by vertical cracking, which reduces their resistance to settlement action. The crack pattern is depicted in Figure 3.33. The value of applied angular distortion to obtain severe light damage is close to 1/500 (Table 3.20).

The selected façades with RC foundation and CaSi masonry, characterized by relatively large length and big openings, appear resistant to settlement actions. This is also valid for pre-damaged façades.

The cases that present damage are mainly characterized by vertical cracking below window openings. Average measured and applied β to reach DS2 are also higher with respect to the façades with unreinforced masonry. Also for the RC foundation façades, a larger L/H ratio results in a more vulnerable façade, while L/H below 1 shows high damage resistance with respect to settlement actions (Figure 3.35, Table 3.20).

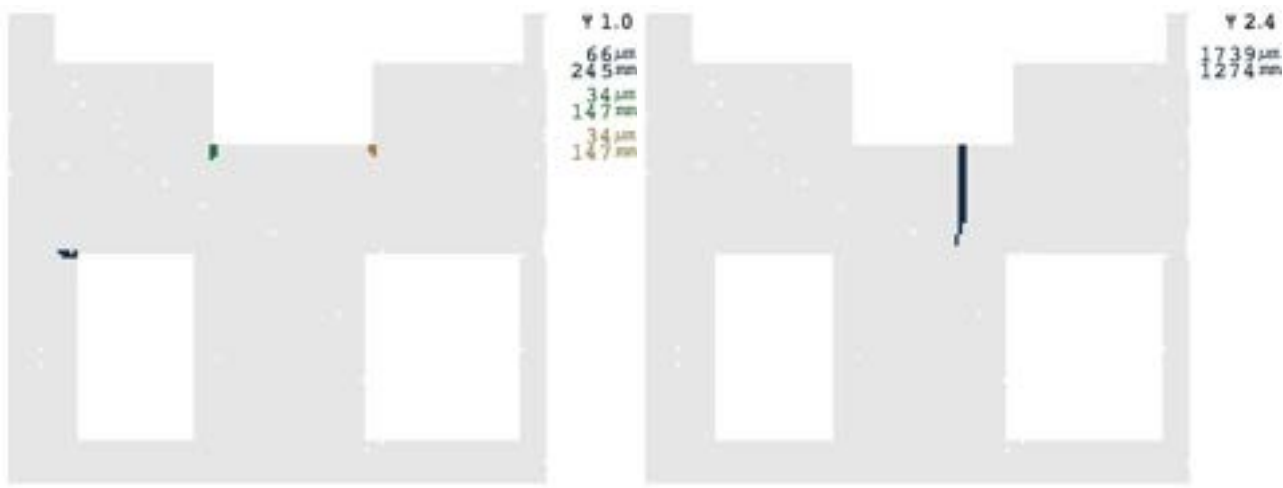


Figure 3.27. Crack pattern of Façade 5, geometry A, standard material, soil A, original interface and asymmetric settlement, knick point=L/3. Cracks at DS1 (left) and DS2 (right).



Figure 3.28. Crack pattern of Façade 6, geometry A, standard material, soil A, original interface and asymmetric settlement, knick point=L/3. Cracks at DS1 (left) and DS2 (right).

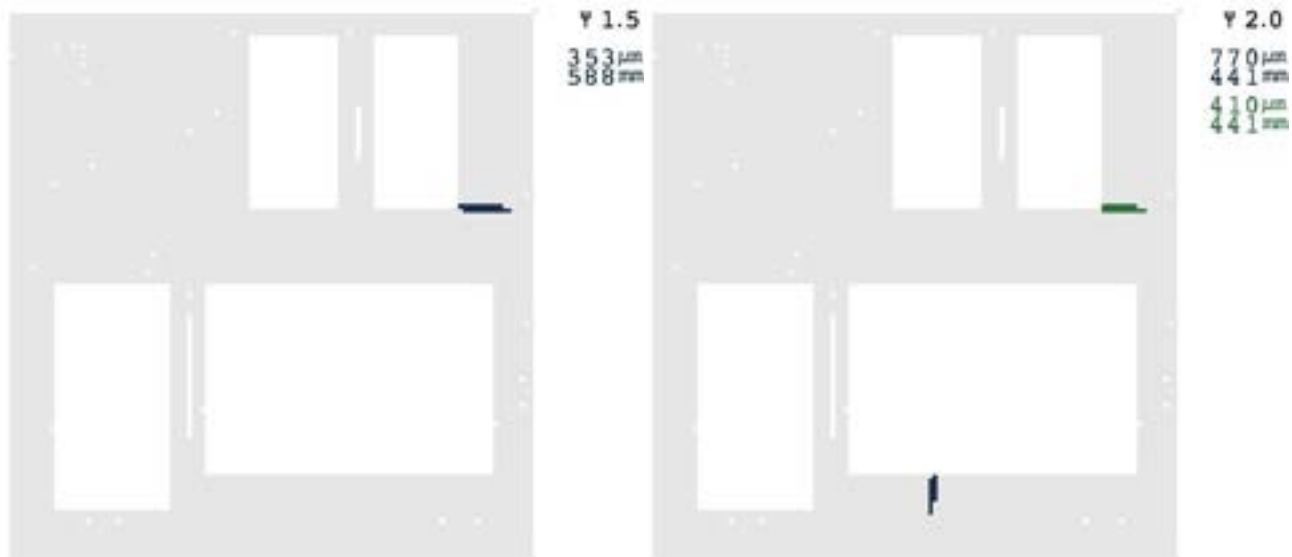


Figure 3.29. Crack pattern of Façade 7, geometry A, standard material, soil A, original interface and asymmetric settlement, knick point=L/3. Cracks after vertical loading (left) and applied beta at $\Psi=2$ (right).

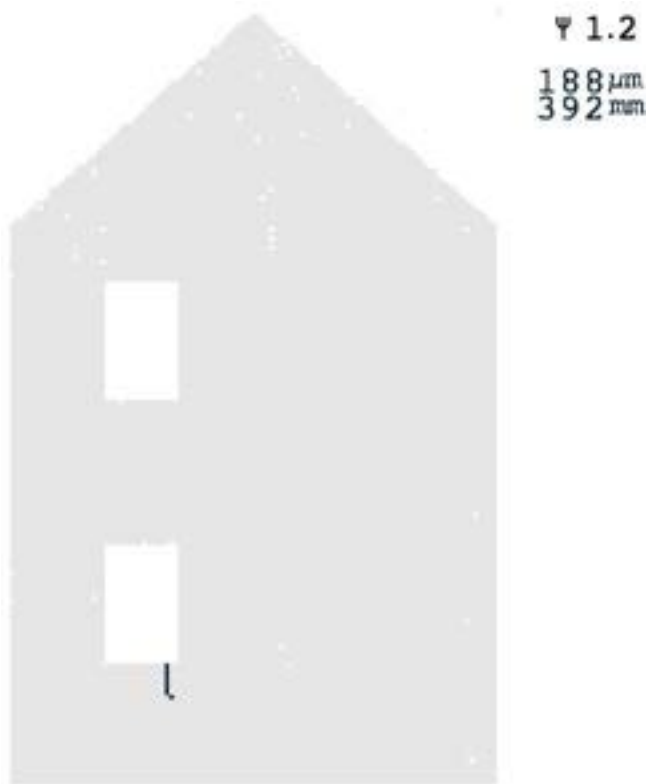


Figure 3.30. Crack pattern of Façade 8-B, geometry A, standard material, soil A, original interface and asymmetric settlement, knick point=L/3. Cracks at $\Psi=1.2$.

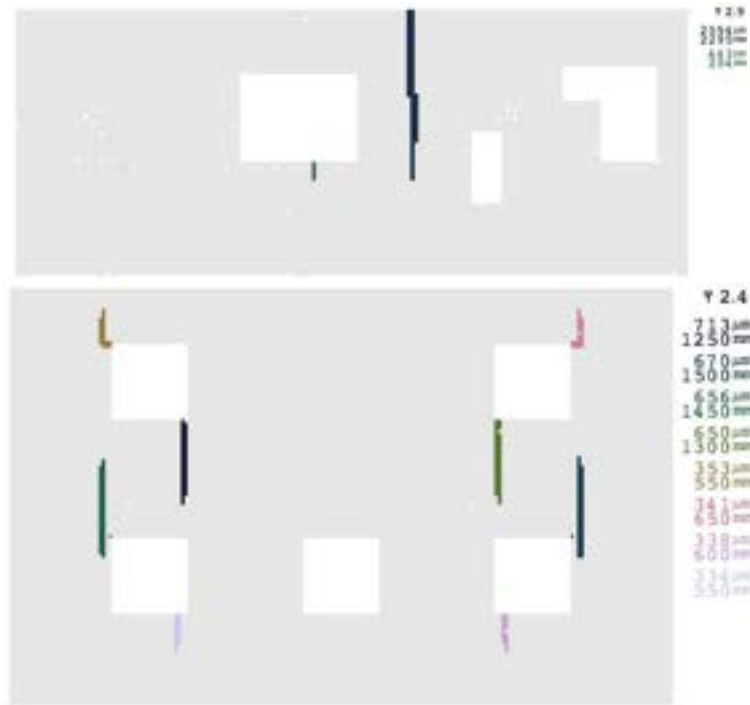
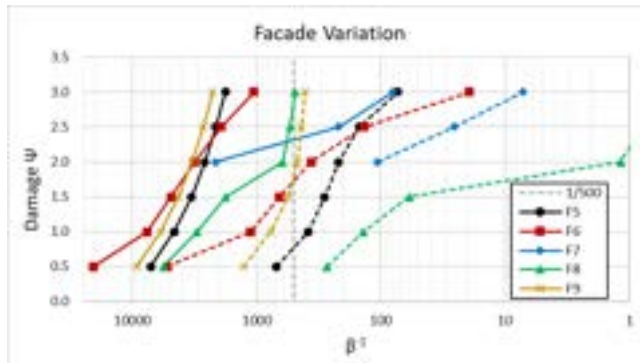


Figure 3.31. Crack pattern of Façade 9, geometry A (top) and B (bottom), weak material, soil A, original interface and asymmetric settlement, knick point=L/3. Cracks at $\Psi \geq 2$.



Façade	$\Psi=0.5$	$\Psi=1.0$	$\Psi=1.5$	$\Psi=2.0$	$\Psi=2.5$	$\Psi=3.0$
F5	95.8%	79.2%	58.3%	58.3%	37.5%	29.3%
F6	100.0%	100.0%	100.0%	91.7%	79.2%	50.0%
F7	*	*	*	33.3%	0.0%	0.0%
F8	39.6%	29.2%	16.7%	0.0%	0.0%	0.0%
F9	100.0%	87.9%	91.7%	85.4%	79.2%	79.2%

Figure 3.32. Angular distortion (β^{-1}) against damage and percentage of models that reach a specific damage level. Façade variations. Dashed lines refers to applied β^{-1} . * damage level already reached after gravity loading.

Façade	$\Delta\Psi=0.5$	$\Delta\Psi=1.0$	$\Delta\Psi=1.5$	$\Delta\Psi=2.0$	$\Delta\Psi=2.5$	$\Delta\Psi=3.0$
F7	75.0%	0.0%	0.0%	0.0%	0.0%	0.0%

Figure 3.33. Percentage of pre-damaged models that reach a specific increase in damage level. Façade 7.

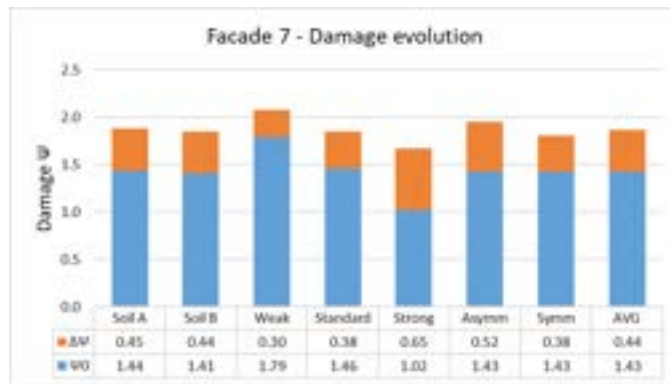
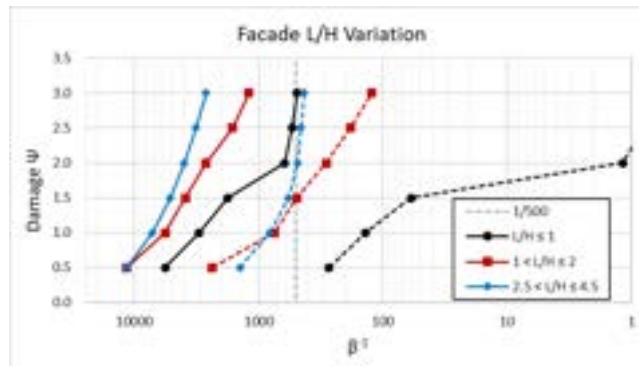


Figure 3.34. Initial pre-damage and increment of damage of different variations of Façade 7.

Table 3.19. Measured (left) and applied (right) β^{-1} values. Façade variations.

Façade	$\Psi=0.5$	$\Psi=1.0$	$\Psi=1.5$	$\Psi=2.0$	$\Psi=2.5$	$\Psi=3.0$	Façade	$\Psi=0.5$	$\Psi=1.0$	$\Psi=1.5$	$\Psi=2.0$	$\Psi=2.5$	$\Psi=3.0$
F5	7080	4612	3328	2613	2124	1782	F5	690	383	283	218	149	73
F6	7066	7604	4868	3135	1928	1054	F6	595	1111	654	364	135	19
F7	*	*	*	2152	219	80	F7	*	*	*	106	26	7
F8	5633	3022	1770	616	538	488	F8	270	138	59	1	1	1
F9	9223	5910	4268	3308	2688	2261	F9	1263	771	559	467	435	410



L/H	$\Psi=0.5$	$\Psi=1.0$	$\Psi=1.5$	$\Psi=2.0$	$\Psi=2.5$	$\Psi=3.0$
$L/H \leq 1$	39.6%	19.2%	16.7%	0.0%	0.0%	0.0%
$1 < L/H \leq 2$	99.8%	93.1%	83.3%	76.4%	61.1%	48.6%
$2.5 < L/H \leq 4.5$	100.0%	95.8%	91.7%	91.7%	91.7%	91.7%

Figure 3.35. Angular distortion (β^{-1}) against damage and percentage of models that reach a specific damage level. L/H variations. Dashed lines refers to applied β^{-1} . * damage level already reached after gravity loading.Table 3.20. Measured (left) and applied (right) β^{-1} values. L/H variations.

L/H	$\Psi=0.5$	$\Psi=1.0$	$\Psi=1.5$	$\Psi=2.0$	$\Psi=2.5$	$\Psi=3.0$	L/H	$\Psi=0.5$	$\Psi=1.0$	$\Psi=1.5$	$\Psi=2.0$	$\Psi=2.5$	$\Psi=3.0$
$L/H \leq 1$	5633	3022	1770	616	538	488	$L/H \leq 1$	270	138	59	1	1	1
$1 < L/H \leq 2$	11510	5619	3864	2642	1615	1196	$1 < L/H \leq 2$	2357	742	494	284	182	122
$2.5 < L/H \leq 4.5$	11502	7180	5142	3951	3186	2653	$2.5 < L/H \leq 4.5$	1410	809	572	484	454	430

4. Probabilistic Results - Fragility Curves

Exceedance Count

The large number of results can already be used to determine a probability of failure. For example, for an applied distortion value of 1/500, about 20% of the three thousand models have exceeded a damage level corresponding to $\Psi = 2.5$. Given the limited number of models, this approach loses confidence at very low values of probability where only one or two models have crossed the threshold. This can be reasonably compensated by applying a log-normal distribution fit to the results. Furthermore, not all models should be considered equally. Houses built with masonry that closely matches the average material properties are more likely to appear in the region than houses that correspond to the ‘very strong’ set of material parameters. This spread in material parameters can be captured with a probabilistic distribution; characterisation experiments in the lab have shown that the tensile strength follows a normal distribution with a 30% variance, for example. Similarly, the distributions of the other parameters that have been varied, such as the soil type, the settlement profile shape, etc. can be determined. Then, the models can be weighted so as to reproduce the likelihood of their combination of parameters appearing in buildings in the region; in this manner, the probability of failure for a more realistic combination of situations can be estimated. Appendix F contains a full list of the applied weights and the correlations between the various parameters such as weaker soil-structure interfaces being more likely on the softer soil, for instance. A structure with a material far from average, on bad soil but with a stiff soil-structure interface, subjected to a symmetric soil settlement profile that only deforms the ends of a short foundation, would receive the lowest weight possible of 0.06; while, a structure of average material, on the stiff soil and also a stiff soil-structure interface that transfers an asymmetric settlement distortion to a long foundation, would receive the highest weight of 4.5. These examples exclude weights assigned due to the geometry of the walls. It must be said, that this weighing approach can only be used if the various model variations cover the range of typical parameters found in real cases; this is discussed further ahead.

Figure 4.1 below depicts the curves as a result of counting the number of models that exceed a certain threshold of damage (Ψ). The region between $\Psi=1$ and $\Psi=2.5$ can be considered light damage with cracks between 0.1 mm (just visible to the naked eye) and 2 mm. The curves also show the degree of extrapolation required to complete the picture of probability above 50%. In several cases, the finite element models did not reach high values of Psi because the model was not reliable with too many cracks or because the required distortion was larger than what was applied. In these cases, a curve prediction was fit to the existing points and the relationship between distortion and Psi was extrapolated. The extrapolation is shown in grey and indicates the expected trajectory of the cumulative density curves. A log-normal distribution, typical for this type of phenomenon, was also fitted to the final curves including the individual extrapolations; see later Figure 5.3.

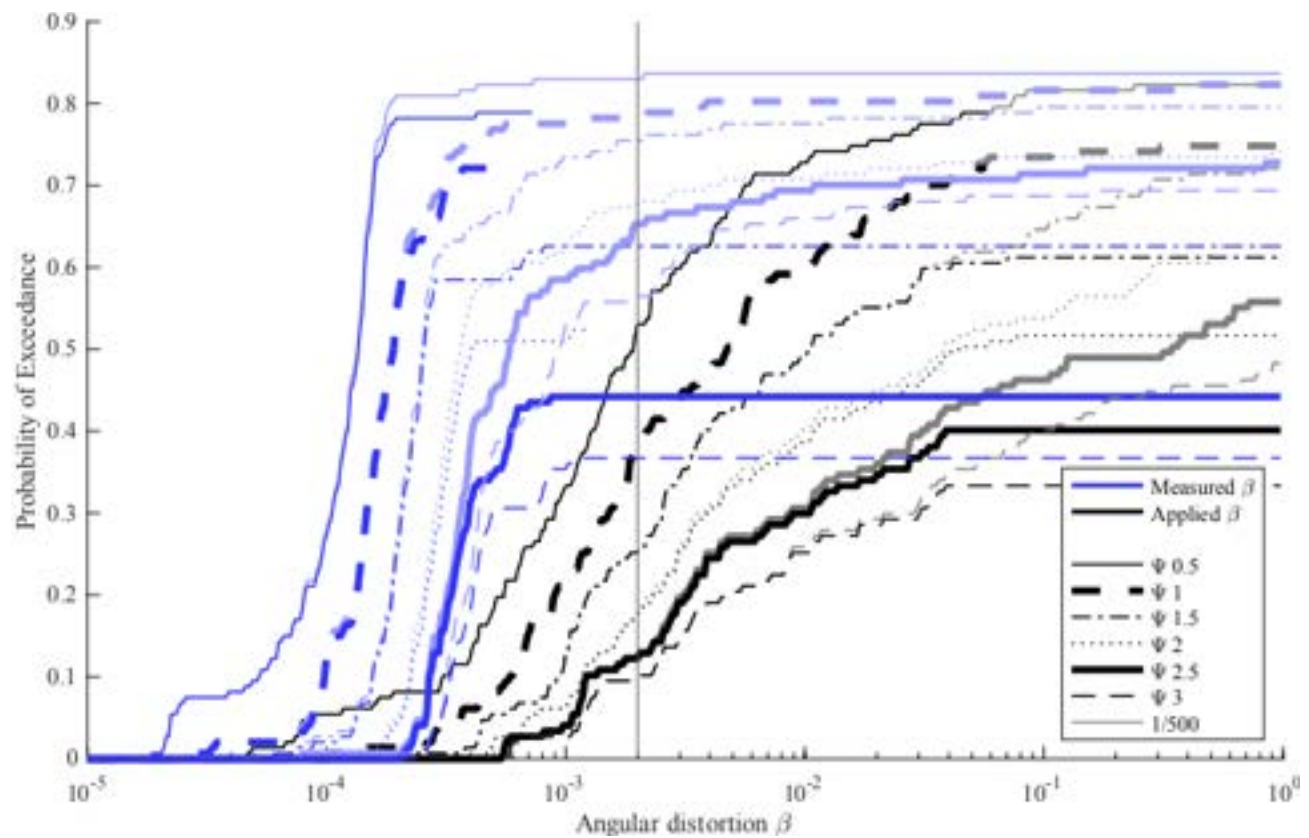


Figure 4.1. Curve for the exceedance count, ‘deterministic fragility curves’, of various damage thresholds for both measured and applied distortion. The lines with extrapolations continue in a dim colour, while the capped curves show the percentage of models that actually reached the indicated damage values (Ψ).

Weighing for Fragility Curves

These exceedance curves are then modified with weights as previously described; see also Appendix F. The weights include the likelihood of certain wall lengths and length/height ratios determined from a statistical study into real wall geometries; see Appendix K.

Figure 4.2 shows that the influence of these weights is not large; yet, the reduction in variability due to more common parameter combinations being more important, is visible. For example, because the material is normally distributed, models with weak and strong properties are less relevant and thus the variability reduces. Similarly, long façades ($L/H > 3$) are less common (App. K) and shorter facades are less vulnerable (Section 3), so the inclusion of geometry weights leads to a reduction in damage probability. In sum, the inclusion of the weights and their limited influence implies that the results are not too sensitive. However, from the three fired-clay brick façades on unreinforced foundations analysed, façade four, the longer façade, does show a larger influence, as evidenced in Figure 4.3. Additionally, it can be seen that this façade is also more vulnerable with lower values of distortion leading to a higher probability of damage than the other façades.

It is also important to note that the weights have little influence in the curves that relate the measured distortion (β_m) to damage. This suggests two observations: first, that the parameters that play a role in the relation between the applied beta and damage, such as the soil-structure interface, the flexibility of the structure, and the soil parameters, are more relevant than those that exclusively affect the relation between measured distortion and damage, such as the tensile strength of the masonry; and second, that the measured distortion is better characterised as a response of the structure than an imposed deformation.

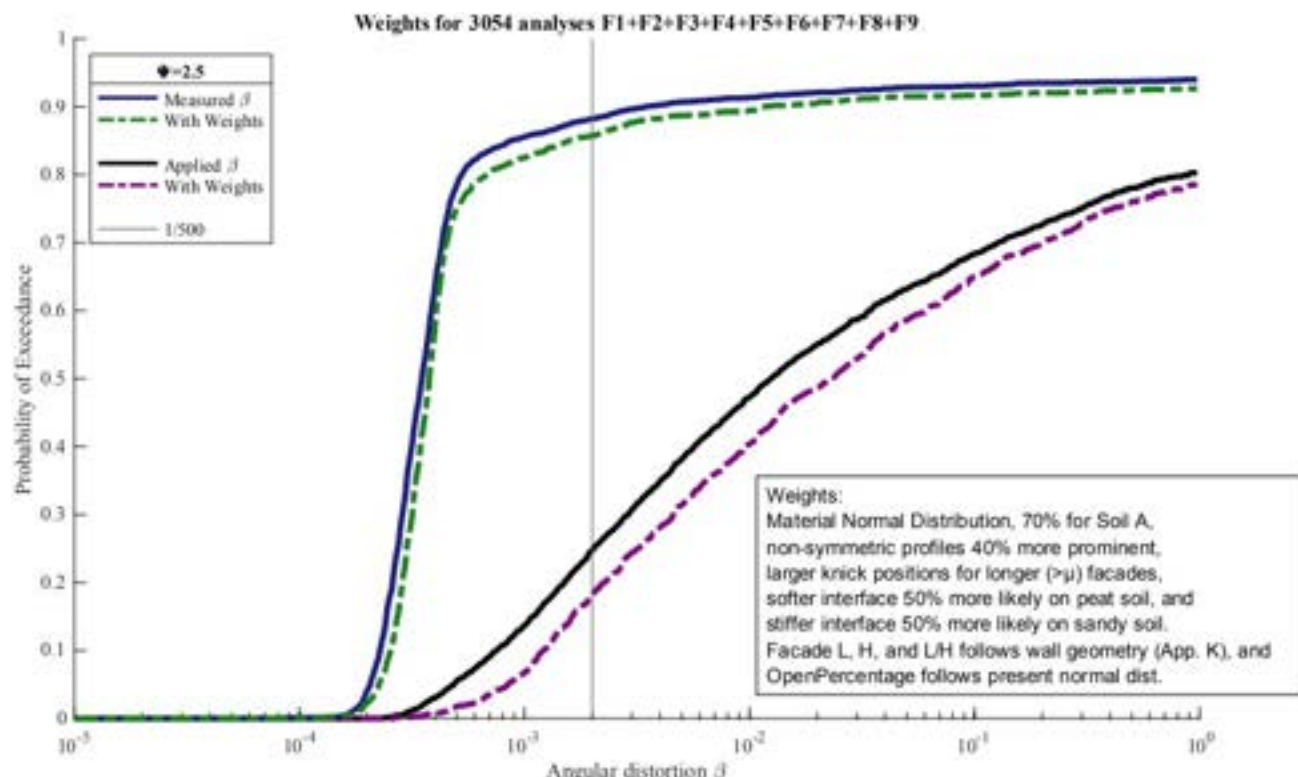


Figure 4.2. Exceedance curve with and without weights for both the applied and the measured distortion.

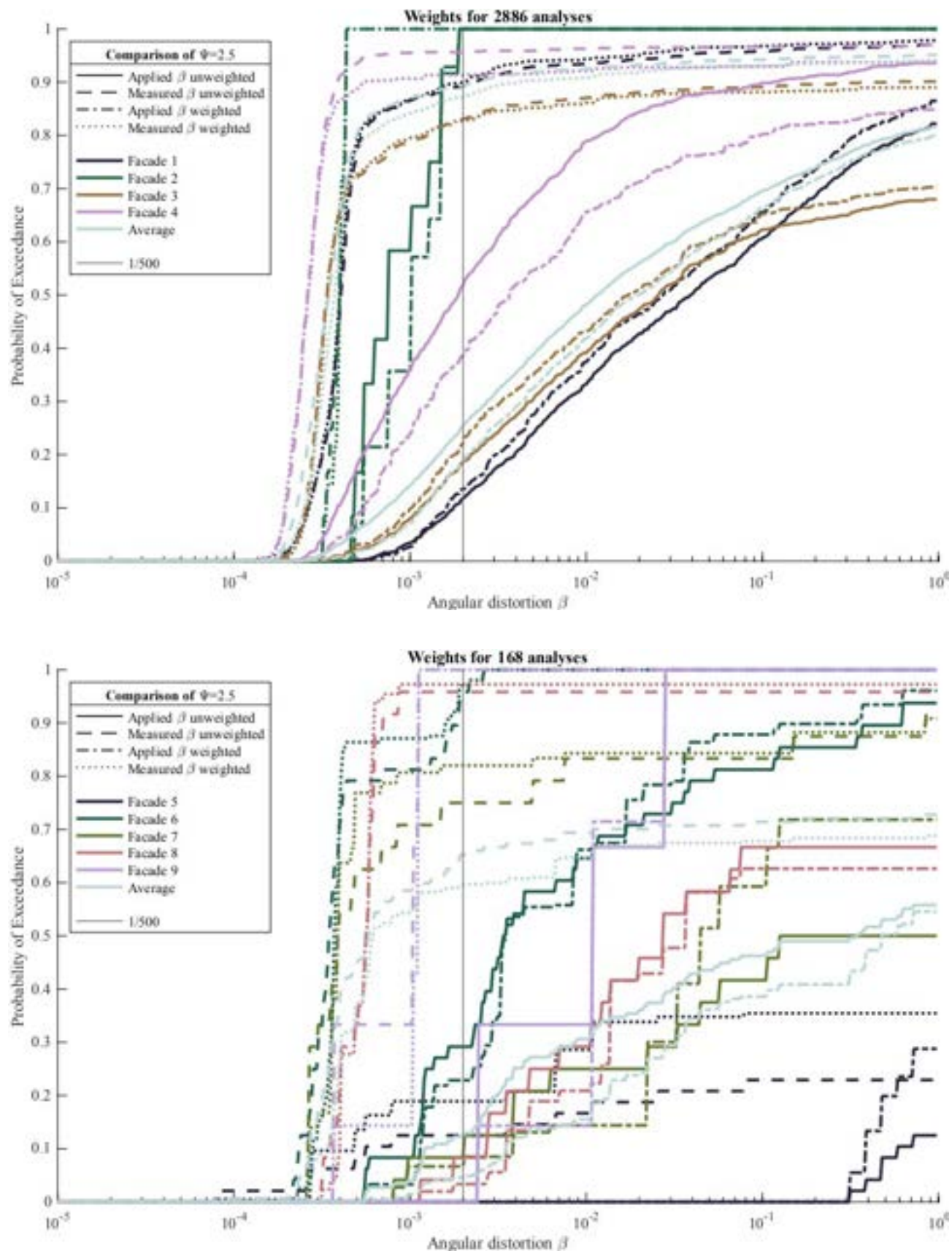


Figure 4.3. Weighted exceedance curves segregated per façade; top, for fired-clay brick on UR foundations; bottom, for Calcium-silicate facades on RC foundations. The longer façade 4 is most vulnerable and also most affected by the weighting scheme.

Log-normal distribution Fit

The exceedance curves (or cumulative density curves), in their weighted or unweighted form, are based on a limited number of models. Relatively large probability values, around 20 to 50%, can confidently be employed, but smaller values of probability cannot reasonably be considered accurate. It is common practice, in the field of fragility curves, to fit an S-curve, Gauss, or log-normal distribution to the limited data, under the assumption that a more complete sample of the population would be better represented hereby. Since the fit is based on the entirety of the sample size, smaller values of probability are also supported by the rest of the data which increases the confidence. The exceedance curves elaborated herein are thus fit to a lognormal distribution; however, because a significant number of models never reached high values of damage, the large probability values in the exceedance curves, correspond to extrapolations and therefore, the log-normal fit is restricted to the interval of probability of 0 to 60% ($0 < \text{prob}(\beta) \leq 0.6$), since most models do include data in this interval. The fit to the lognormal distribution allows the representation of these curves with two parameters such that they can be easily reproduced outside of this report.

The lognormal distribution slightly increases the apparent probability at small values; this can be observed later in Figure 4.4. or the summary Figure 2. Yet, this increase indicates that, had more data points be available, the curve for probability would also had been smoother.

Moreover, the weighted exceedance curves can be further segregated by length/height ratio and foundation type since these parameters have a large influence on the relationship between the applied distortion and the exceedance of light damage. Figure 4.4 shows clearly that longer walls and unreinforced foundations are more vulnerable. The graph needs to be interpreted carefully however, especially when looking at the (calcium-silicate brick) walls on reinforced foundations. This is because of two main reasons: Firstly, the number of variations on RC foundations is limited, about 160 against the 2800 on unreinforced foundations, which means that the results might not be entirely representative, in particular for $L/H < 1$ for which only two façades have been inspected. Secondly, several calcium-silicate walls already developed cracks when subjected to the gravity loads before the settlement profile was applied; this increases the apparent damage probability since only a $\Delta\Psi$ is needed to exceed light damage. Additional façades on unreinforced foundations would have to be explored to gain confidence in their corresponding curves; however, statistical insight has shown that longer façades are less common and, the FEM models, when observed directly, show little damage for the buildings on RC foundations with many models never reaching $\Psi=2.5$. Therefore, the three exceedance curves for RC foundations in Figure 4.4 are conservative and should be taken as depicting a worse-case scenario.

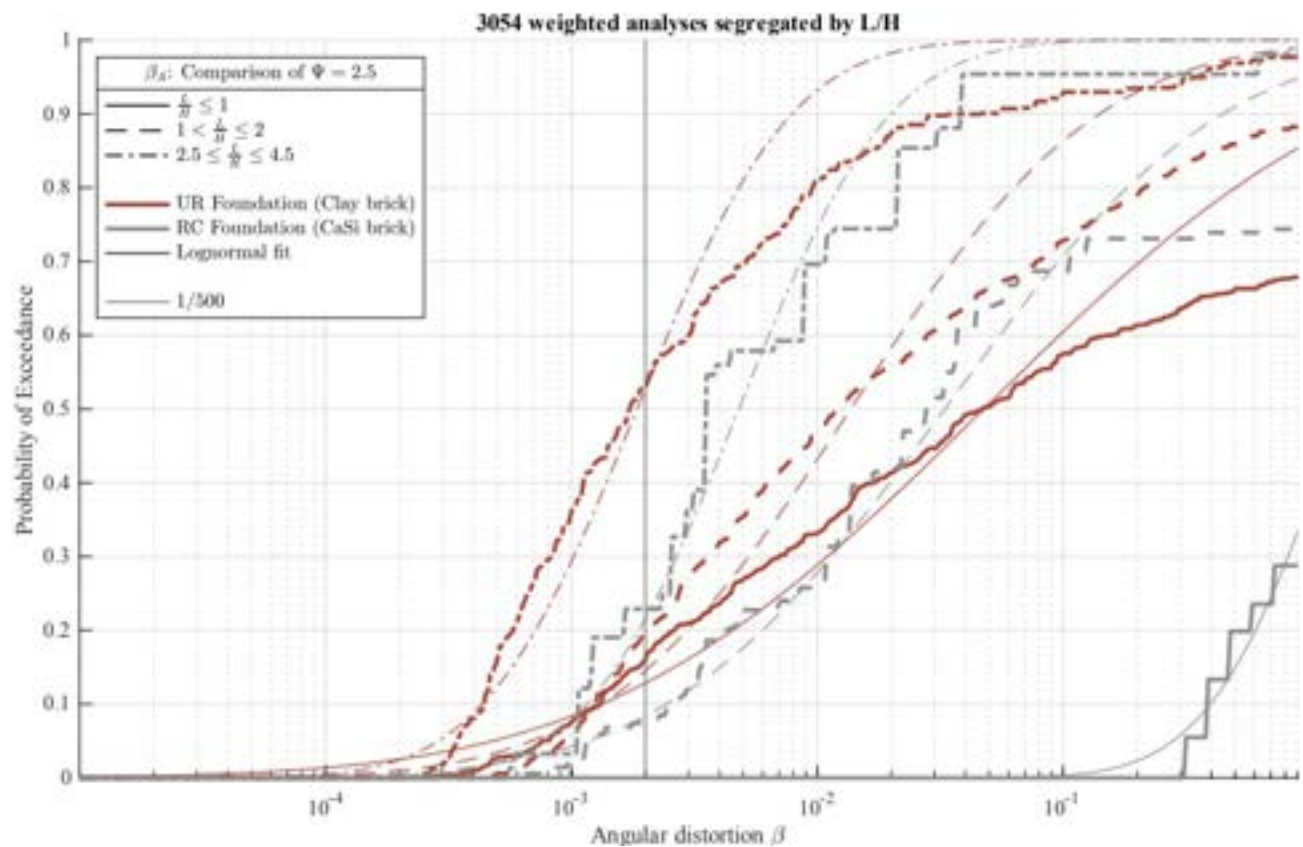


Figure 4.4. Exceedance curves for applied angular distortion against damage probability separated by length/height ratio and foundation type with the corresponding lognormal fit which more adequately represents low (and high) values of probability.

5. Discussion & Conclusions

Discussion

Data available from a parallel study, see Appendix G, can be compared against the fragility curves drawn with the weighted results of the finite element models. The comparison study looked at the measurable distortion of masonry walls via bed-joint level measurements and compared this to the reported damage via photographs. The curves, approximately translated to a damage scale based on cracks, show that damage occurs at much larger values of distortion (5 to 8 times larger), suggesting that the investigated buildings can tolerate higher distortion than what the models estimate. However, neither the comparison curves, based only on a few selected buildings, nor the models, formulated especially to look at vulnerable façades, should be regarded as portraying reality best.

Firstly, the definitions of light damage are not identical in both studies. Herein, a threshold of approx. 2 mm for the crack width ($\psi=2.5$) has been set, whereas the comparison study is based on the assessment of photographs of the damage which are affected by the perception of damage as cracks along mortar joints may be hidden from view, for instance. Secondly, measuring the distortion from real walls may lead to higher betas since points are gathered at fixed, limited intervals, thus suggesting that damage appears at higher values of distortion than what could actually be present. Similarly, the location or height on the walls where the measurements are taken could influence the beta values output. Thirdly, the empirical dataset may be biased since the inspections have been carried out on buildings that displayed damage, but other buildings, exhibiting high distortion values but no damage, for example, may not have been surveyed.

Fourthly, deformations taking place slowly over the span of years may be accommodated by the masonry without displaying cracks. This creep effect could even be enhanced by autogenous healing of the cement or lime in the mortar, which are capable of filling small cracks [20]. A few models considering the creep effect were run but a difference of 3 to 5 still remained between the applied and measured distortions. Fifthly, material properties have not been calibrated against large and old masonry samples which could exhibit a more flexible overall behaviour than what has been modelled. This would also shift the measured distortion closer to the applied soil distortions.

Moreover, the models, as any models, only depict a limited portion of real buildings, attempting to capture the effects that are most relevant and influential to the studied phenomenon. One effect that has been purposely neglected is that of the horizontal displacements or horizontal strains. Vertical soil deformations are usually accompanied by horizontal displacements. Depending on the scale of the phenomenon causing settlements, the relationship between vertical and horizontal displacements will change. For deep subsidence, vertical displacements occur over a large area and thus produce little distortion at the building scale, while horizontal strains may be more damaging; conversely, for local soil compaction, vertically-induced distortions will be more damaging than the comparatively small horizontal strains. Furthermore, opposite to the vertical situation where gravity attempts to force the building to follow vertical distortions, horizontal strains are not enforced on the foundations and may just be released as slip between soil and foundation; literature estimates that only about 30% of horizontal strains could be transferred to a building. For these reasons, the horizontal effect has been excluded from the models.

Additionally, the semi-coupled approach for soil-building interaction adopted herein, corresponds necessarily to a simplification of the fully-coupled approach, albeit in a conservative fashion. Whereas the semi-coupled method in this study corresponds to an interface that mimics the behaviour of the soil around the foundation and its interaction with the foundation of the building, a fully-coupled approach would include the soil itself in the model, which, among other benefits, would allow for a more complete formulation of the bedding heterogeneity, or local soil variability. However, this fully-coupled approach is, for probabilistic efforts, not only computationally

prohibitive but, the reproduction of the non-linear or plastic behaviour of the soil elements, and the inclusion of the loading action by means of imposed strains or deformations on the soil elements themselves, are studies of their own. Moreover, a fully-coupled approach would only be meaningful with a 3D geometry, which further complicates its execution.

It has been observed that the measured distortion should be considered a property of a masonry wall in the same way that a pushover curve characterises the lateral behaviour of a building. Figure 3.23 in Section 3 shows that the required distortion to reach a specific Ψ_i value has little variability between L/H ratios. This would mean that the analogy of a wall behaving as a beam subjected to a certain distortion or curvature and where damage of the beam is proportional to its tensile strength, will hold on a basic level. The various walls differ in the required distortion that needs to be applied to achieve the damaging measured distortion values.

In the models examined in this study, a maximum distortion (or angular deformation) of 1/10 has been applied; this corresponds to an angle or knick of about six degrees between two almost-horizontal lines underneath the foundation. Most walls on unreinforced foundations could not but follow this distortion and became damaged; yet several cases on reinforced foundations were able to withstand said distortion with little measurable distortion on the wall itself. It cannot be said at what value of distortion these walls would have failed completely, but, in the study of light damage, it is inconceivable that higher distortions would arise on the free soil surface. Presumably, a different soil failure mechanism would have to be modelled, one that could not be represented with the soil-structure interfaces employed herein, in order to generate substantial deformations on the reinforced foundations such that they, in combination with the superstructure, enter the highly non-linear regime. Do note that all foundations in this study have been modelled non-linearly with conservative assumptions about the embedded rebar. It was outside of the scope of this study to consider scenarios where the rebar in the foundations was in poor condition; nevertheless, it is sensible to conclude that buildings with affected reinforced foundations, where such damage can be verified, are more likely to behave like their vulnerable counterparts on unreinforced foundations.

The observation that the more flexible soil leads to lower damage on the façades may seem counter-intuitive since stiffer soils, and uncracked rock, are usually preferred as building substrata. This is true in the sense that a stiffer and more homogeneous bedding leads to smaller foundations and a lower chance of uneven autogenous settlements, which translates into cheaper buildings and lower construction risks. However, when the soil deformations appear from underneath, such as the direct or indirect effect of deep subsidence, the stiffness relationship between soil and building determines where the deformations will take place. A more flexible soil will cushion a stiffer building. Moreover, and while this was not investigated herein, buildings founded on softer soils usually present a stronger foundation and are thus already better equipped to deal with induced settlements.

The case of piled foundations has not been treated in this study. Firstly, because the indirect effects, as a result of changes in the water table, are assumed to occur above the support area of the piles, meaning that pile foundations are unaffected. Secondly, in the cases where the piles are relatively short, the water table relatively deep, or the soil such, that the piles heavily rely on skin friction, the approach with an interface that captures the behaviour of the soil around the foundation, such as employed in this study, would be inadequate. This would require an entirely different modelling approach that includes the complex interactions between soil, piles, foundation, and applied soil deformation. Such a strategy is a study on its own and would require yet-to-be-investigated simplifications or prohibitively-computationally-expensive models with non-linear soil elements and pile-soil interfaces. Thirdly, because the changes in the water table that could directly affect timber piles, such as biological wood degradation, lead to completely different loading of the structure and are again, a study of their own. And fourthly, because unreinforced foundations have

been observed to be more vulnerable and these are not associated with piles, yet whether reinforced foundations on piles would behave differently cannot be said. In sum, piled foundations have been neglected in this study, and while these are expected to be less vulnerable to soil distortions than the shallow foundations, the conclusions drawn herein, should still only be applied to masonry buildings on shallow foundations.

Some models already exhibit cracks before the soil distortion is applied. This is because of the gravity load which leads to some stresses in the masonry that due to its low tensile strength, quickly displays some cracks; at this stage, the flexibility of the soil also plays a role since it allows the masonry to deform under the gravity loads. In particular, façade 7 reaches relatively high initial values of Ψ_i when subjected to the gravity loads. It is difficult to say whether a staged analysis would render different results as the construction process loads the masonry progressively. Nonetheless, this initial damage is then aggravated by the applied soil distortion which makes façade 7 the most vulnerable of the walls on reinforced foundations. That pre-damage, which can be a result of shrinkage, previous settlement deformations, thermal expansion, or, as in this case, gravity loads, makes walls more vulnerable was also observed in this study. Here, some of the applied distortion, leading to a certain damage, can be considered as existing damage and so, the difference between a higher distortion and the final damage can be seen as a damage aggravation. From this perspective, Figure 5.1 has been produced. It shows that the probability of reaching $\Psi = 2.5$ when starting at $\Psi_0 = 1.0$ is much higher than when no initial damage is present; or, that the distortion required to reach the final Ψ is much lower.

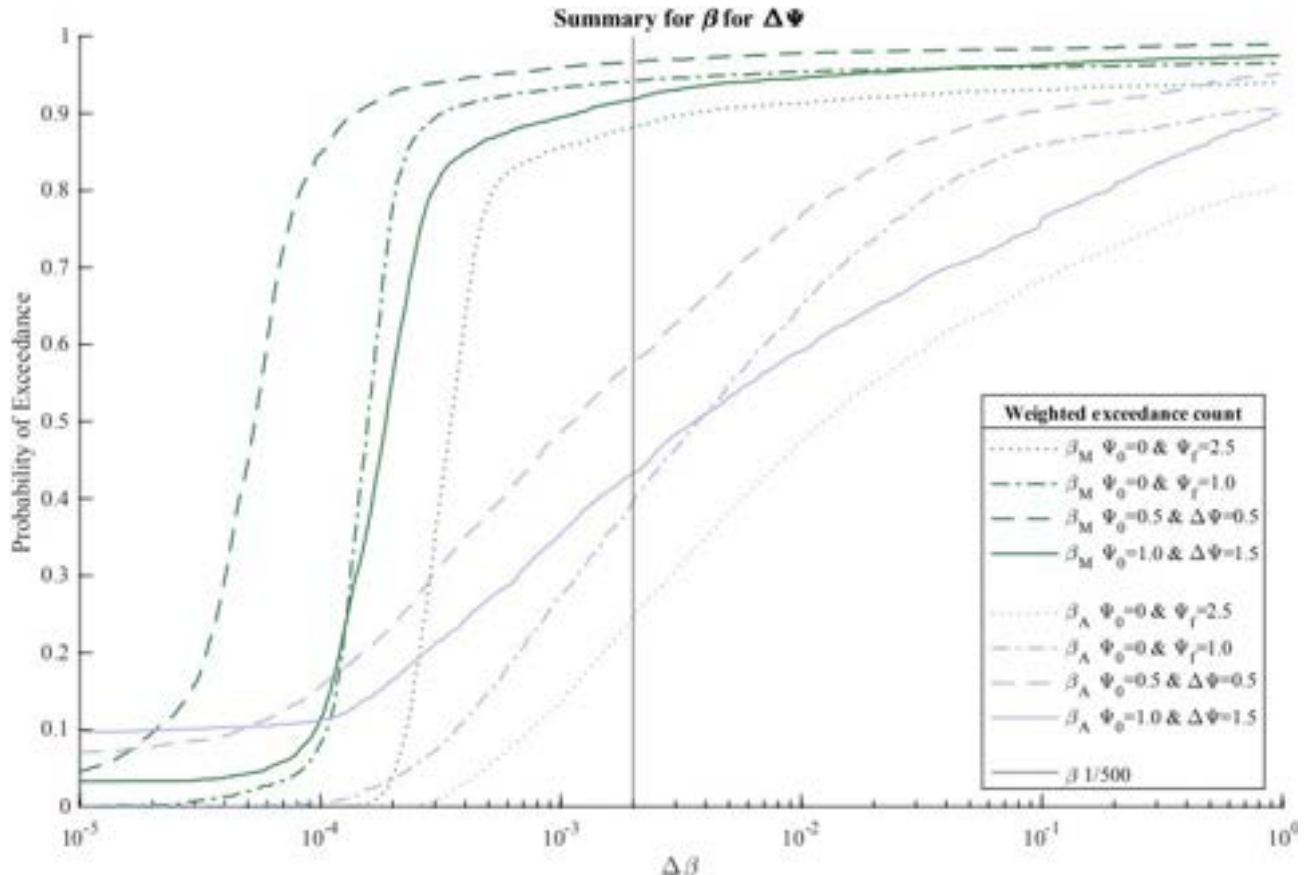


Figure 5.1. Delta Psi and delta beta.

A final point of discussion are the geometries employed for the modelling campaign. A careful selection of representative but also interesting wall geometries, from a structural perspective, was conducted when determining the façade shapes employed in this study. These are based on

experimental tests both at the TU Delft and elsewhere, past or parallel computational studies (with 3D geometries), and representative reports from real cases. The criteria were aimed at achieving a certain degree of representativeness while capturing the features that make masonry facades vulnerable. A study of a database with geometry information about buildings in the Netherlands, see Appendix K, was also conducted to determine which wall shapes and geometrical properties are present in the building stock. Figure 5.2 compares the geometries selected in the façade variations from this study with the distribution obtained from the database. When looking at the varied length/height ratios, the most relevant ratios appear well represented, with the variations of this study, from 0.65 to 4.5, covering more than 85% of the distribution's probability, and, if the very low L/H are disregarded since they belong to very slender walls which are unaffected by applied distortion, the variation represent most of the L/H values observed in practice. This means that the models are looking at the relevant cases and that the conclusions drawn from the models will be applicable. In terms of length, the models look at relatively longer walls, compared to the statistical average. However, as has been shown, the shorter walls are less vulnerable to soil distortion, and within a 3D building, probably belong to the shorter side walls of typical house expansions or recesses. If only wall lengths longer or of 3 metres are considered, the range of the variations, from 4.8m to 17m, fulfils about 60% of the present wall lengths. Finally, in terms of wall height, the models can represent walls of 3 metres and taller, albeit the most common wall height in the statistical data is that of one storey at 2.8 metres. Walls of two storeys are well covered with many variations in this height range. Regarding wall shape (rectangular, gable, etc.), the selected eight facades are also a good representation of real wall shapes with the majority of walls being rectangular (see Appendix K).

In sum, the variations performed with the FEM models in combination with the weights applied to the exceedance curves, are well capable of representing the distributions in wall length and height found in real walls. Whether the openings for windows also match existing layouts is unknown yet and may have to be explored once the 3D BAG database reaches the level of detail (LoD 3) that includes windows.

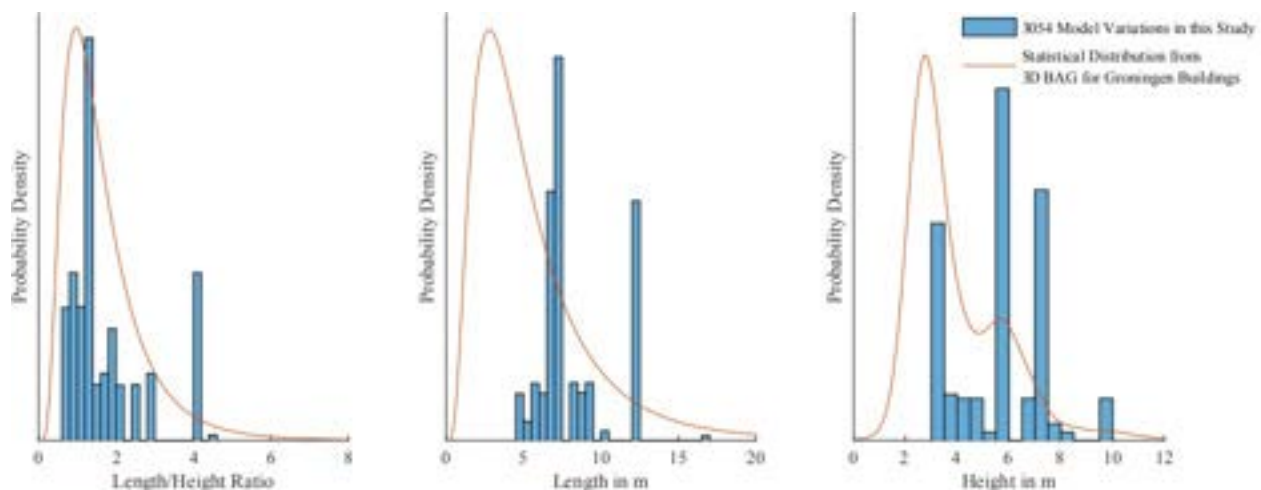


Figure 5.2. Comparison of the length, height, and length/height ratios employed in this study and the statistical distribution observed from an analysis of real buildings' wall geometries.

Conclusive Discussion

The curves corresponding to the applied distortion show a larger spread or variability than those for the measured distortion, as seen in Figure 5.3. This is reasonable since there are more parameters, such as the variability of the soil, the interface, and the settlement profile shape, between the applied distortion and damage than between the building distortion and damage. When fitted to a log-normal distribution, this increased variability also results in the longer tail of the curve. Therefore, both applied and measured distortion curves indicate that at a distortion of 1/5000, the probability of exceeding light damage is about 4%. At 1/500 (or a relative rotation of 2 %), the applied distortion curves indicate a probability of 20% while, if such a distortion is measured in a masonry wall, the probability of there being cracks larger than 2 mm wide is almost 100%. This value is not totally unexpected; the light damage study looked at lateral drift values causing damage in various masonry walls tested in the laboratory. Calcium-silicate walls displayed light damage for drifts between 0.15 and 0.65%, while fired-clay walls could withstand up to 1.1% before exceeding light damage [28]. A distortion of 1/1000 translates to a ‘vertical drift’ or relative settlement of 0.5% for a settlement shape with the highest curvature at 1/3 of the length, and to even 1% when the ‘knick’ point of the settlement profile is located at the middle of the façade. While horizontal and vertical deformations have different effects in an orthotropic material such as masonry, the magnitude of the distortions is comparable.

Figure 5.3 also evidences the differences between the clay and calcium-silicate brick façades. While the initiation of light damage (at $\Psi=1$) shows curves that are closer to each other, exceeding light damage requires greater distortions for the calcium-silicate walls and is therefore revealed by distinctively shallower curves. Among the curves for the applied distortion, the comparison empirical curves appear well represented even though these refer to the measured distortion.

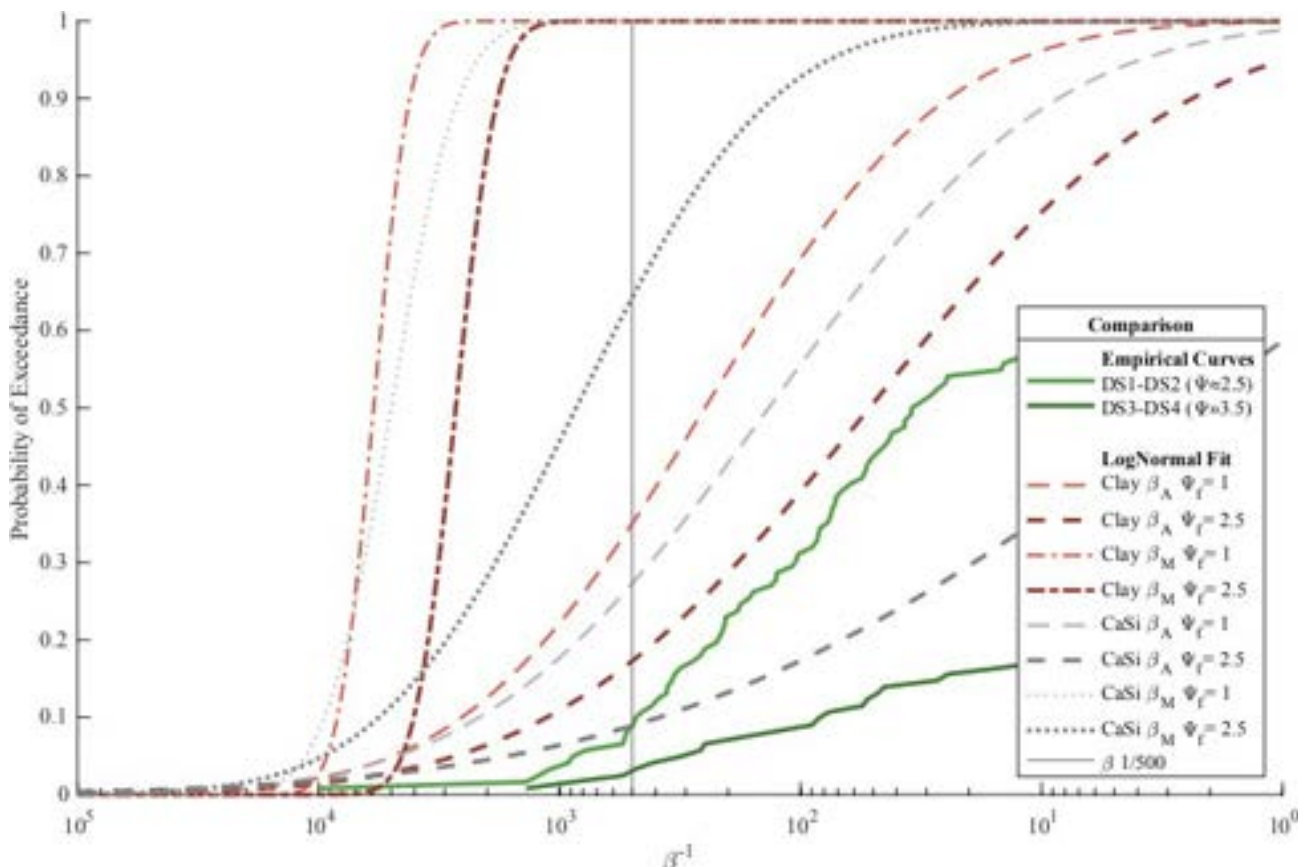


Figure 5.3. Comparison of fragility curves against empirical curves developed from field data.

For experts attempting to predict building damage, damage curves expressed on the basis of the measured distortion are of little use since the deformation of the building is not known a-priori. Instead, damage predictions rely on the calculation of the deformation of the soil and relating it to the damage on buildings. For this purpose, the curves based on the applied soil distortion can be used. These connect directly the calculated soil distortion to the likelihood of building light damage. Additionally, this study has obtained a relationship between the soil distortion that would appear on the free ground surface (greenfield) and the distortions that would be observable on the damaged building. Figure 5.4 displays the ratio between the measured and the applied distortion for the three thousand models on an unreinforced foundation. On average, the measured distortion is about seven times smaller than the applied distortion (or for the inverted relationship: 1/3500 for 1/500); however, how much the buildings distort, also depends on how much damage it has sustained. For high values of measured distortion, corresponding to damaged and cracked masonry walls, both measures are closer since the more flexible building follows the applied soil deformation better. In general, it can be said that about 15% of the applied distortion is transferred to the building before it exceeds light damage. This value is expected to be lower for buildings on reinforced concrete foundation, but no clear factors are given due to the limited number of models that have been evaluated for these cases.

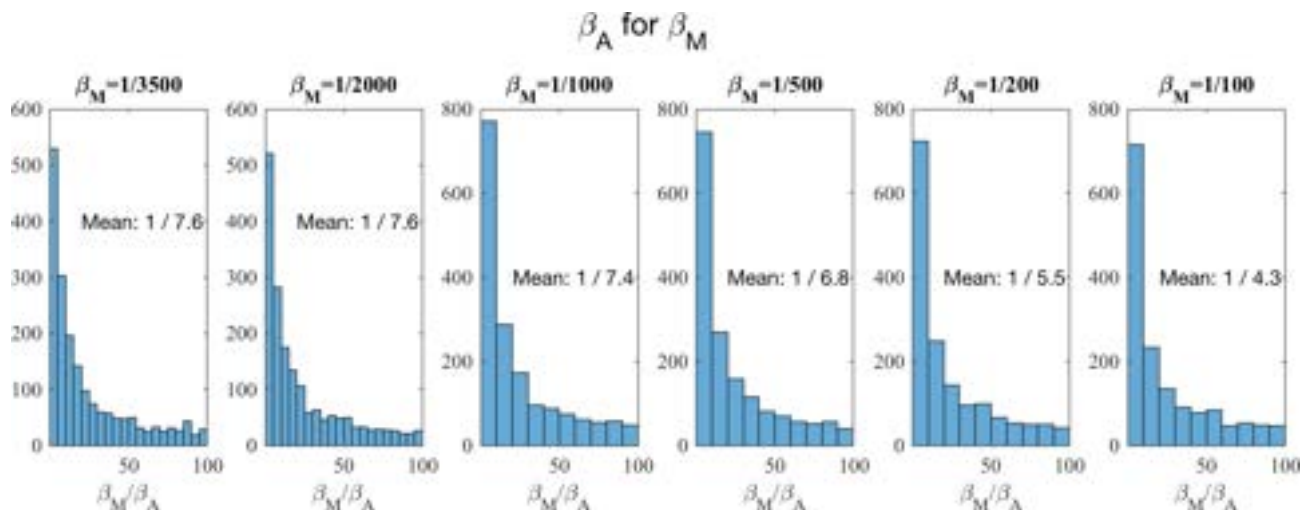


Figure 5.4. Ratios between the measured wall distortion and the applied soil distortion for buildings on unreinforced foundations. Buildings that don't become damaged, also don't follow the applied soil deformation and thus present high ratios.

Conclusions

This computational study has observed that:

- Masonry walls on unreinforced foundations are vulnerable to applied soil distortions. When free-field settlement profiles would show angular distortions of 1/500, the probability of fired-clay brick walls to exceed light damage has been computed at 20%.
- Masonry walls, typically calcium-silicate brick walls, on reinforced concrete foundations are significantly less vulnerable, with many models not exceeding light damage even at high values of applied ground distortion; at 1/500, the probability is estimated at 8%.
- Longer facades are more vulnerable; those with a length/height ratio around 4, exhibited about 50% more damage. Conversely, facades shorter than 5 metres or slender than the average ($L/H < 1$) show no damage.
- On masonry façades, the measured distortion that leads to damage is very similar between façades of different shapes and is better correlated to the strength properties of the façade. On average, a measured distortion of 1/3000 is associated with the exceedance of light damage with cracks wider than 2 millimetres.
- The applied distortion, of how the ground would deform without a building, must be transferred to the façades for these to deform and crack. Stiffer, shorter, slender, and stronger façades on more flexible soil, will resist this transfer are thus less vulnerable; while their counterpart will follow the applied distortion more easily and become damaged. This transfer factor varies between 5 to 10 (β_A/β_M) but can go up to 100 for the stiffer façades on flexible soil.
- A convex settlement shape, also called hogging, is more damaging on average than the concave sagging settlement profile; it is also more frequent in damage reports.
- Below an applied or measured distortion of 1/10.000, even masonry walls with existing cracks, will not exceed light damage with a larger probability than 10%. If walls were totally uncracked, this probability would be below 1%.
- When formulating a guideline to determine damage probability, the type of foundation and the length/height ratio of masonry walls will be key parameters to segregate limit values or threshold for damage as in Table 5.1.

Table 5.1. Reference values of applied distortion for various wall length/height ratios on different foundation types.

β_A Probability $\Psi \geq 2.5$	Unreinforced Foundation			Reinforced Foundation		
	$L/H \leq 1$	$1 < L/H \leq 2$	$2.5 \leq L/H \leq 4.5$	$L/H \leq 1$	$1 < L/H \leq 2$	$2.5 \leq L/H \leq 4.5$
10%	1/760	1/750	1/2300	>1/5	1/410	1/870
25%	1/140	1/250	1/1200	>1/5	1/120	1/440
50%	1/22	1/74	1/540	>1/5	1/31	1/210
Number of Models	772	1421	554	48	75	24

VI. References

- 1 **Boonpichetvong et al. (2004)**
M. Boonpichetvong, H. Netzel, J.G. Rots (2004). Numerical Analyses of Soil-Foundation-Building Interaction due to Tunnelling. 5th International PhD Symposium in Civil Engineering - London
- 2 **Nederlandse Cellenbeton Vereniging**
<https://www.cellenbeton.nl/fysiek.htm>
- 3 **Diana User's Manual -- Release 10.5, 2021**
<https://dianafea.com/manuals/d105/Diana.html>
- 4 **Voortgangsoverleg IMG-TNO-TU Delft, 23 November 2020.**
- 5 **Farrell et al. (2014)**
R. Farrell, R. Mair, A. Sciotti, A. Pigorini (2014). Building response to tunnelling. Soils and Foundations 2014; 54(3):269–279
- 6 **Giardina et al. (2013)**
G. Giardina, J.G. Rots, M.A.N. Hendriks (2013). Modelling of Settlement Induced Building Damage. TU Delft
- 7 **Korswagen et al. (2018)**
P.A. Korswagen, E. Meulman, M. Longo, J.G. Rots (2018). Crack Initiation And Propagation In Unreinforced Masonry Structures Subjected To Repeated Load And Earthquake Vibrations. 10th International Masonry Conference, Milan, Italy 2018
- 8 **Korswagen et al. (2019)**
P. Korswagen, M. Longo, E. Meulman, J.G. Rots (2019). Experimental and Computational Study of the Influence of Pre-Damage Patterns in Unreinforced Masonry Crack Propagation Due to Induced, Repeated Earthquakes. 13th North American Masonry Conference
- 9 **Korswagen et al. (2019)**
P.A. Korswagen, M. Longo, E. Meulman, J.G. Rots (2019). Crack initiation and propagation in unreinforced masonry specimens subjected to repeated in-plane loading during light damage. Bulletin of Earthquake Engineering <https://doi.org/10.1007/s10518-018-00553-5>
- 10 **Korswagen (2021)**
P.A. Korswagen (2021). InSAR Analyses of surface vertical settlements – Norg. TU Delft Memo 20210223 v2, on WP 2.3 IMG Project.
- 11 **Mair (2003)**
R.J. Mair (2003). Research on tunnelling-induced ground movements and their effects on buildings – Lessons from the Jubilee Line extension. In: Building response to tunnelling: Case studies from construction of the Jubilee Line extension, Eds. Burland J.B., Standing J.R. and Jardine F.M. CIRIA SP199 and Thomas Telford, London
- 12 **Ozer & Geurts (2021)**
I.E. Ozer, C.P.W. Geurts (2021). Literature Review: Effects of subsidence on buildings. 2020 R12073, Tno
- 13 **Pluymakers & Roholl (2021)**
M.P.D. Pluymakers, J.A. Roholl (2021). Effecten diepe bodemdaling en -stijging rondom de gasopslag Norg en het Groningenvelde. 2020 R12068, Tno
- 14 **Mariani et al. (2017)**
V. Mariani, F. Messali, M.A.N. Hendriks, J.G. Rots (2017). Numerical Modelling And Seismic Analysis Of Dutch Masonry Structural Components And Buildings. 16th World Conference on Earthquake, 16WCEE 2017

- 15 Schreppers et al. (2016)**
G.M.A. Schreppers, A. Garofano, F. Messali, J.G. Rots (2016). DIANA validation report for masonry modelling. DIANA FEA report 2016-DIANA-R1601 TU Delft Structural Mechanics Report CM-2016-17, 143 pp
- 16 Van Staalduin et al. (2018)**
P.C. Van Staalduin, K. Terwel, J.G. Rots (2018). Onderzoek naar de oorzaken van bouwkundige schade in Groningen Methodologie en case studies ter duiding van de oorzaken.. Delft University of Technology. Report number CM-2018-01, 11 July 2018 - Downloadable from www.NationaalCoordinatorGroningen.nl
- 17 Burland et al. (2001)**
J.B. Burland, J.R. Standing, F.M. Jardine (2001). Building response to tunnelling Case studies from construction of the Jubilee Line Extension, London. CIRIA Special Publication 200
- 18 Grondsoorten in Nederland**
<https://www.thinklink.com/scene/1040171602467094531>
- 19 Berkela - funderingen op staal**
<https://berkela.home.xs4all.nl/skelet/skelet%20fundering%20op%20staal.html>
- 20 Gaggero & Korswagen (2021)**
M.B. Gaggero, P.A. Korswagen (2021). Self-healing mortar for Dutch masonry - First Experimental study. TU Delft Report C31B69WP5-1 v20210225.
- 21 Rots et al. (2021)**
J.G. Rots, P.A. Korswagen, M. Longo (2021). Computational Modelling Checks Of Masonry Building Damage Due To Deep Subsidence. TU Delft Report, v5, 19 February 2021
- 22 van Dalen et al. (2021)**
J. van Dalen, H.J. Everts, P.C. van Staalduin (2021). Werkinstructie - Zettingen als gevolg van indirekte effecten van diepe bodemdaling. Instituut Mijnbouwschade Groningen (IMG)
- 23 Boscardin & Cording (1989)**
M.D. Boscardin, E.J. Cording (1989). Building response to excavation-induced settlement. Journal of Geotechnical Engineering, 115(1):1–21, 1989.
- 24 Kooi et al. (2021)**
H. Kooi, J.C. Landwehr, R.J. Stuurman, J.J. van Meerten, O. Levelt, M. Korff (2021). Indirecte schade-effecten van diepe bodemdaling en -stijging bij het Groningen gasveld en gasopslag Norg. Deltares, 11207096-002-BGS-0001, 30 augustus 2021
- 25 de Vent (2011)**
I. de Vent (2011). Prototype of a diagnostic decision support tool for Structural damage in masonry. Delft University of Technology, Faculty of Architecture ISBN: 978-90-8570-760-8
- 26 Nehrp (2012)**
Nehrp (2012). Soil-Structure Interaction for Building Structures. NIST GCR 12-917-21 U.S. Department of Commerce National Institute of Standards and Technology
- 27 Lourenço et al. (1995)**
P.B. Lourenço, J.G. Rots, J. Blaauwendraad (1995). Two approaches for the analysis of masonry structures: micro and macro-modeling. HERON. Vol. 40. No.4 ISSN 0046-7316
- 28 Korswagen et al. (2020)**
P.A. Korswagen, M. Longo, J.G. Rots (2020). Calcium silicate against clay brick masonry: an experimental comparison of the in-plane behaviour during light damage. Bulletin of Earthquake Engineering (2020) 18:2759–2781 <https://doi.org/10.1007/s10518-020-00803-5>
- 29 Simpson & Grose (1996)**

B. Simpson, W.J. Grose (1996). Discussion: The effect of ground movements on rigid masonry facades. Geotechnical Aspects of Underground Construction in Soft Ground, Mair & Taylor (eds)

30 Gazetas (1991)

G. Gazetas (1991). Formulas and Charts For Impedances Of Surface and Embedded Foundations. Journal of Geotechnical Engineering, Vol. 117, No. 9, September, 1991 ©ASCE, ISSN 0733-9410/91/0009-1363

31 Mylonakis et al. (2006)

G. Mylonakis, S. Nikolaou, G. Gazetas (2006). Footings under seismic loading: Analysis and design issues with emphasis on bridge foundations. Soil Dynamics and Earthquake Engineering 26 (2006) 824–853

32 Fib (2010)

Fib (2010). Fib Model Code for Concrete Structures 1st ed.. Fédération internationale du béton/International Federation for Structural Concrete, 2013.

33 Son & Cording (2007)

M. Son, E.J. Cording (2007). Evaluation of Building Stiffness for Building Response Analysis to Excavation-Induced Ground Movements. Journal of Geotechnical and Geoenvironmental Engineering 133(8)

34 Potts & Addenbrooke (1997)

D.M. Potts, T.I. Addenbrooke (1997). A structure's influence on tunnelling-induced ground movements. Proceedings of the Institution of Civil Engineers, Geotechnical Engineering 1997, 125, April, 109-125

35 EuroCode 6

EN 1996-1-1 (2005). Eurocode 6: Design of masonry structures. National Annex to NEN-EN 1996-1-1+A1.

36 Son & Cording (2005)

M. Son, E.J. Cording (2005). Estimation of Building Damage Due to Excavation-Induced Ground Movements. Journal Of Geotechnical and Geoenvironmental Engineering

Advice Memo: Damage sensitivity of Dutch Masonry Façades against Soil Deformations

Paul Korswagen & Jan Rots - TU Delft

Background

Between October 2021 and October 2022, TU Delft conducted a finite-element modelling study [6] where the effect of the deformation of the soil underneath masonry façades was investigated in terms of crack-based damage. In the report titled "Supporting analyses to determine probability of damage and fragility curves due to indirect subsidence effects", the intensity of soil distortion required to cause visible damage on various masonry buildings was observed to depend heavily on the geometry of the façade itself and the type of foundation underneath the masonry walls. In particular, a subset of buildings was observed to be especially well prepared to withstand soil deformations in comparison to the rest of the façades. For these robust buildings, higher hazard thresholds could be assumed without incurring in an elevated probability of damage. The present memo describes this robust typology of buildings and proposes a reasonable increase in the limiting values of soil deformation.

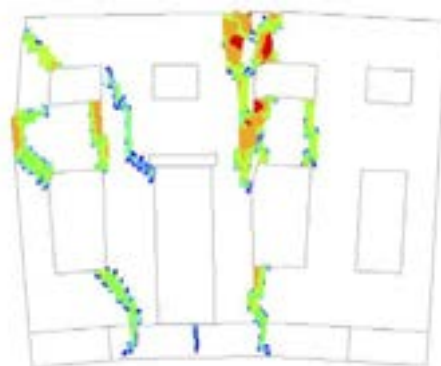


Figure 1. A fired-clay brick masonry façade on an unreinforced foundation subjected to hogging soil distortion and exhibiting cracks in the FE model.

Robust Façades

The study observed that long façades, with a length over height ratio greater than three, were especially prone to follow soil deformations and thus become damaged. In contrast, slender or shorter façades, when their length was not greater than 2 times their height, were able to accommodate much larger soil distortions before displaying cracks. Furthermore, reinforced (concrete) foundations, where steel rebar prevented excessive bending of the foundations, could limit the amount of distortion being transferred from the soil to the masonry superstructure, which consequently exhibited less damage.

In this light, masonry façades with a reinforced foundation and a low length-over-height ratio, could withstand soil distortions ten times larger than longer walls on unreinforced (masonry) foundations, before displaying cracks wider than two millimeters.

Current threshold for damage

Deltares [1] investigated the locations in the region of Groningen where the water table is likely to have decreased more than 2 cm. A lowering of the ground water table may lead to oxidation of peat, shrinkage/swelling of clay, and other soil phenomena which in turn can modify the shape of the soil surface and lead to damage in buildings. Also buildings founded on timber piles could be affected as the lowering of the water table could expose the timber piles to degradation phenomena.

The relationship between lowering of the water table and building damage is not yet thoroughly understood, much less quantified. What soil distortion or differential settlement could be expected for a given decrease of the water table will depend on the type and variability of the soil and the load provided by the building, among other factors. These should then also be linked to the probability of visible damage on the buildings.

A clear understanding of how these soil phenomena lead to soil distortions and consequent building damage will contribute to establishing safe thresholds against building damage.

Worse-case Scenarios

The threshold of 2 cm seems especially strict [2] and does not appear to be related to a probability of building damage. Indeed, because this value is strict, worst-case scenarios can be visualised, where unfavourable soil combinations and building conditions are examined in a modelling study to determine whether damage could be expected at all. Moreover, while these "worst" cases would not be able to reflect the probability of damage, they could provide insight into absolute lower limits for lowering of the groundwater table; see also the worst-case scenarios explored to determine whether deep-subsidence leads to damage [4].

Angular distortion vs differential settlement

It is also important to note in this memo, that many thresholds for building damage provided in literature [5] are set as differential settlement values. Yet, masonry façades are only damaged when a soil distortion or angular distortion occurs, since the differential settlement could lead to a small, rigid, in-plane tilt of the façades which does not translate to in-plane, crack-based damage. In contrast, the "bending" of the façade enforced by an angular distortion, is better correlated to the appearance of damage.

A study of bedjoint level measurements performed on masonry buildings with settlement damage [3] revealed that it is indeed possible for the masonry walls to be subjected to a relatively large differential settlement but not develop any distortion. Figure 2 presents the relationship between the measured angular distortion and differential settlement on these façades. Assuming a linear relationship, a differential settlement of 10 mm appears coupled with an angular distortion of 1/500; however, the scatter in the results, where the relationships are log-normally distributed, means that, with a 5% probability of exceedance, a differential settlement of 3.5 mm could already be present with a distortion of 1/500.

The apparent linear relationship between these parameters describing the soil deformation, suggests that other limits might also be related linearly.

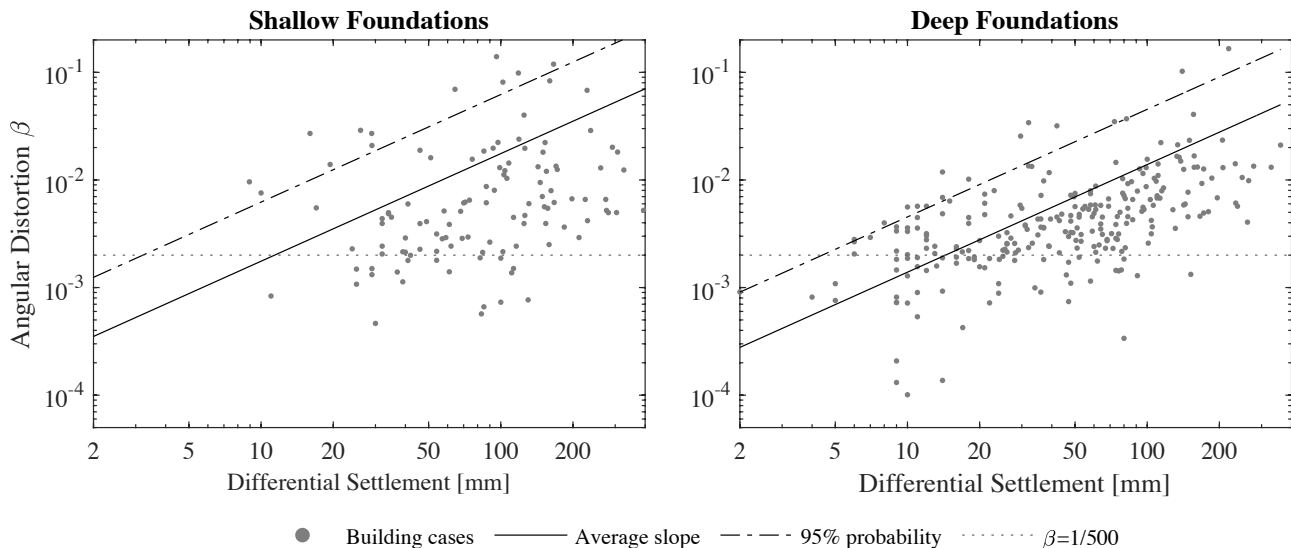


Figure 2. Relationship between the differential settlement and the angular distortion measured on the masonry façades from a database of 396 buildings [3].

Conclusion: compensation factor for robust buildings

Figure 3, adapted from [6], illustrates how calcium-silicate brick masonry façades on strong foundations are 3 to 10 times less susceptible to an applied angular soil distortion when compared against fired-clay brick masonry walls on unreinforced foundations. When the walls are slender (with a length-over-height ratio smaller than 2), the difference is more pronounced. For a probability of light damage larger than 10%, the more robust building typology is about 4 times less vulnerable.

In this context, it can be advised that this specific group of buildings, typically built after 1975 with calcium-silicate brick masonry walls with a $L/H \leq 2$ and including a reinforced concrete strip or beam foundation, be subjected to a more lenient threshold for the evaluation of indirect subsidence effects than the 2 cm proposed by Deltares. For freestanding houses with no more than three storeys, this critical threshold can be reasonably increased by a factor of four.

However, it is also strongly advised that the relationship between lowering of the ground water table, resulting soil distortion, and building damage be further investigated, where the worst-case method mentioned above could be a starting point.

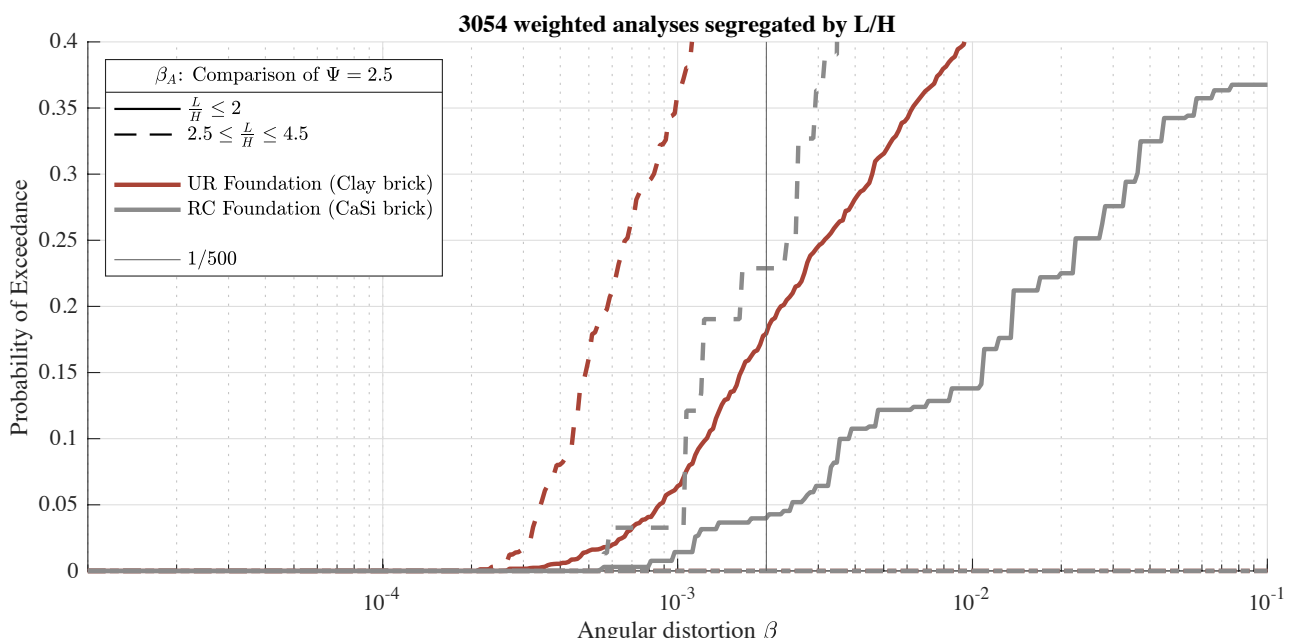


Figure 3. Relationship between the probability of reaching or exceeding crack-based damage with cracks in the order of 2 mm in width ($\Psi=2.5$ marks the transition from DS1 to DS2) and the applied angular soil distortion underneath the buildings' foundations.

References

1. H. Kooi, J.C. Landwehr, R.J. Stuurman, J.J. van Meerten, O. Leveld, M. Korff (2021). Indirecte schade-effecten van diepe bodemdaling en -stijging bij het Groningen gasveld en gasopslag Norg. Deltares, 11207096-002-BGS-0001, 30 augustus 2021.
2. Het invloedsgebied van grondwateronttrekkingen voor droogteschade, Advies Commissie Schade Grondwater, June 2019.
3. A. Prosperi, P.A. Korswagen, M. Korff, R. Schipper, J.G. Rots (2022). Empirical vulnerability and fragility curves for masonry buildings subjected to settlements. Engineering Structures (UNDER REVIEW)
4. Rots, J.G., Korswagen, P.A., Longo, M. (2021). Computational modelling checks of masonry building damage due to deep subsidence. Delft University of Technology. Report number 01, Version 05, February 18, 2021.
5. I.E. Ozer, C.P.W. Geurts (2021). Literature Review: Effects of subsidence on buildings. 2020 R12073, TNO.
6. P.A. Korswagen, M. Longo, J.G. Rots, A. Prosperi (2022). Supporting analyses to determine probability of damage and fragility curves due to indirect subsidence effects. Delft University of Technology. Final Version 2, October 3, 2022.

Schade aan gebouwen door diepe bodemdaling

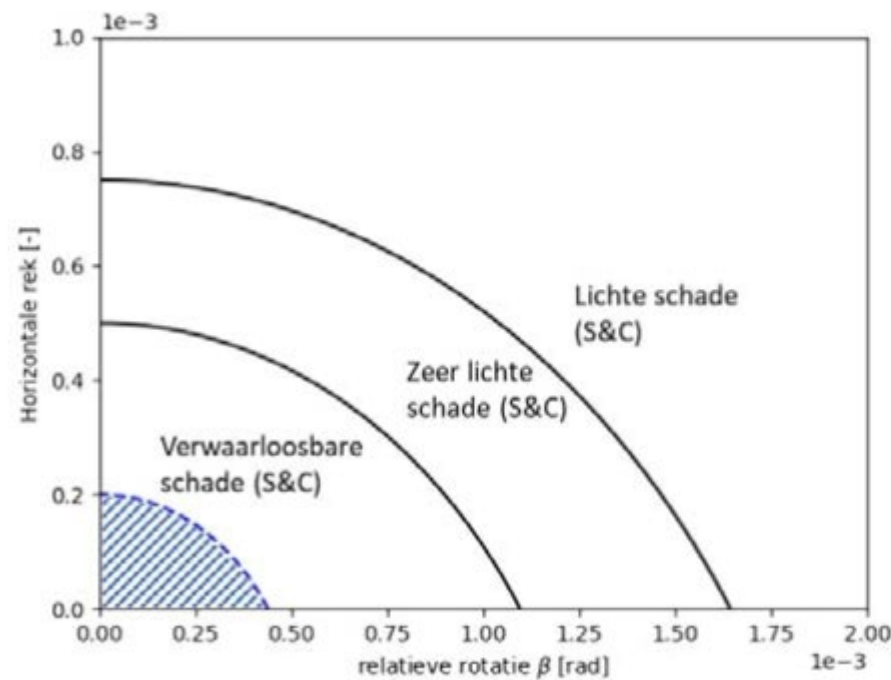
Concept rapportage TNO/TUD

Uitgevoerde activiteiten

- Bepalen ondergrenscriteria (TNO)
- Historie van bodemdaling (TNO)
 - Berekeningen van bodemdalingen NORG en Groningen
 - Berekeningen toetsen met ondergrenscriteria
- Modelberekeningen met een detailmodel van metselwerk (TUD)
- Overal notitie (TNO)

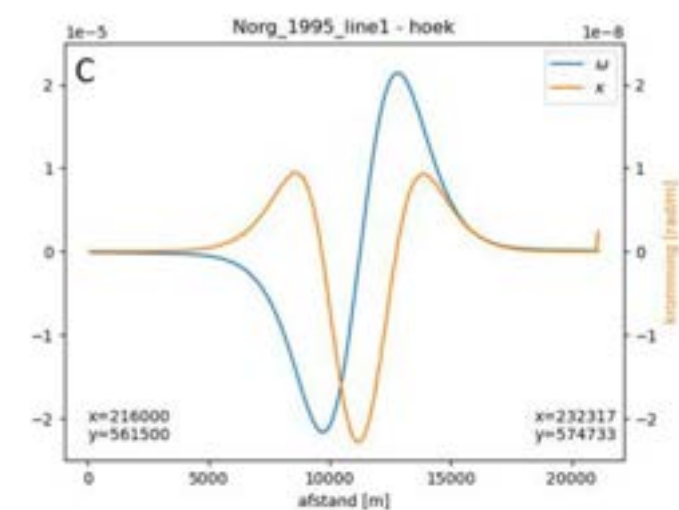
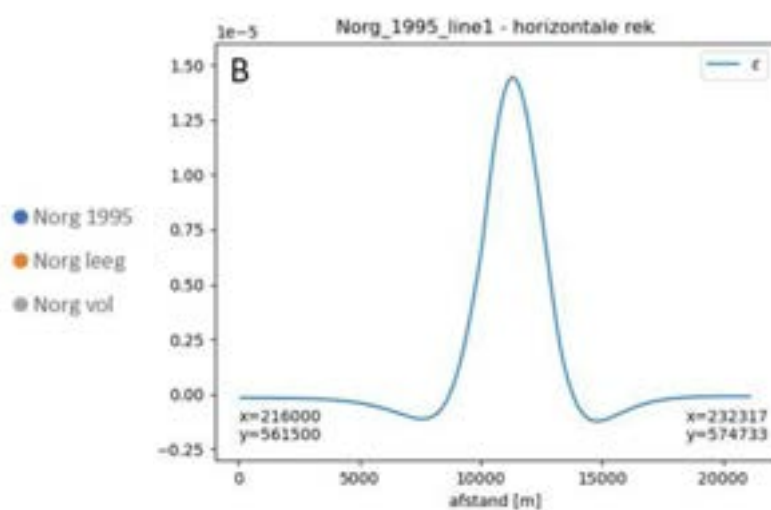
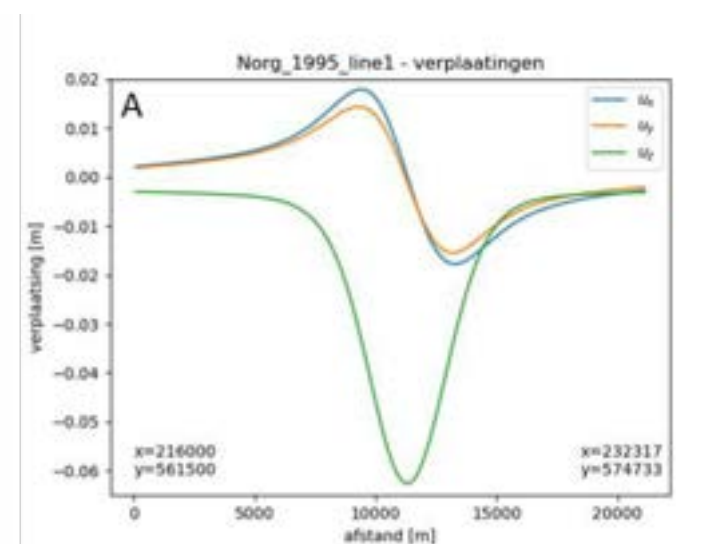
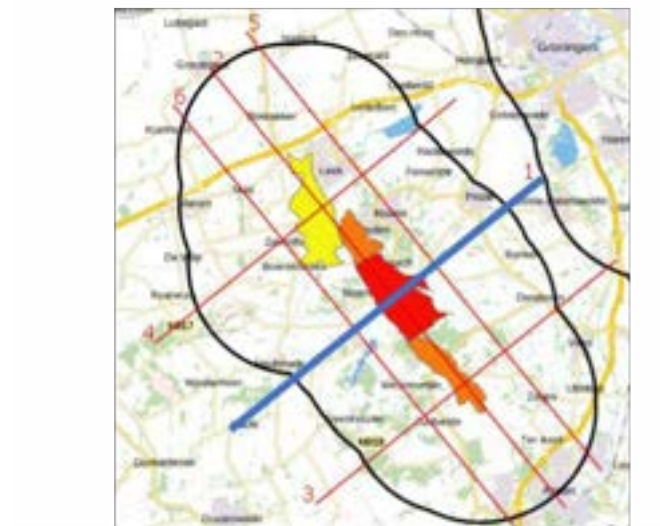
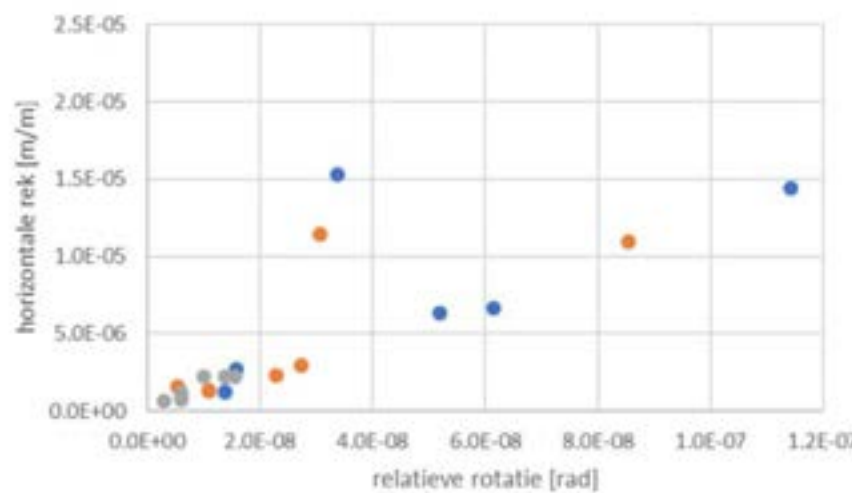
Bepalen ondergrenscriteria

Literatuurstudie
circa 25 studies



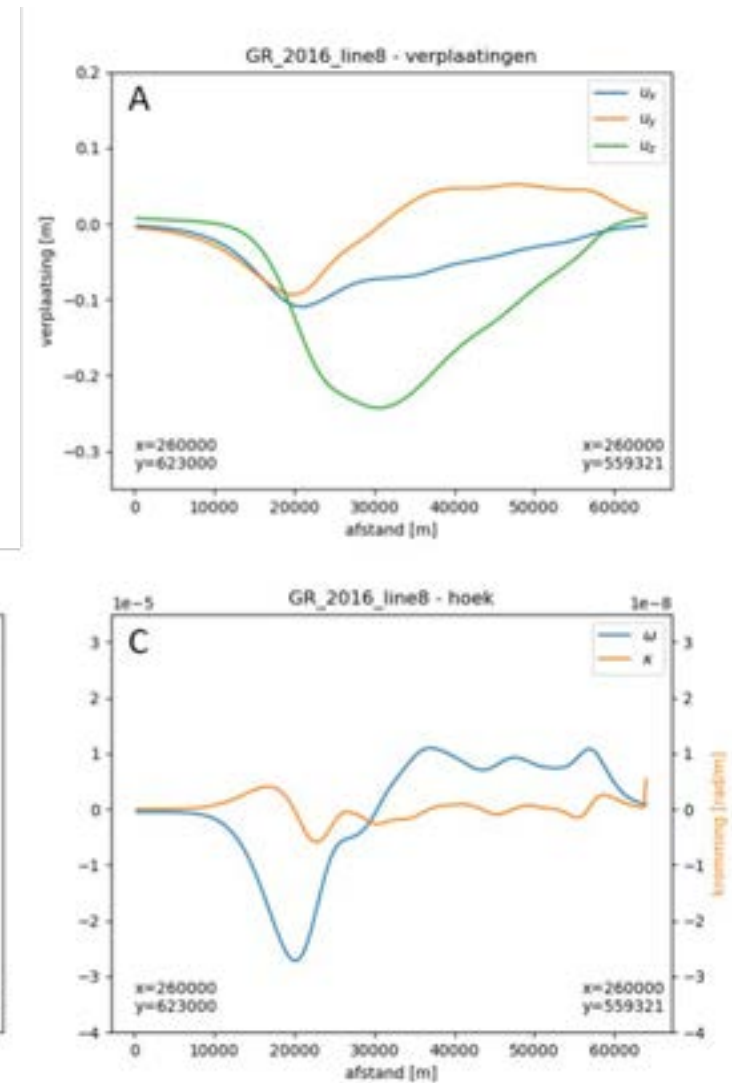
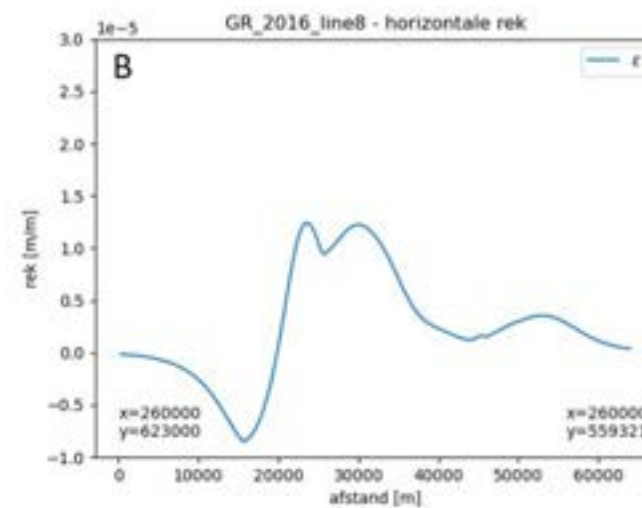
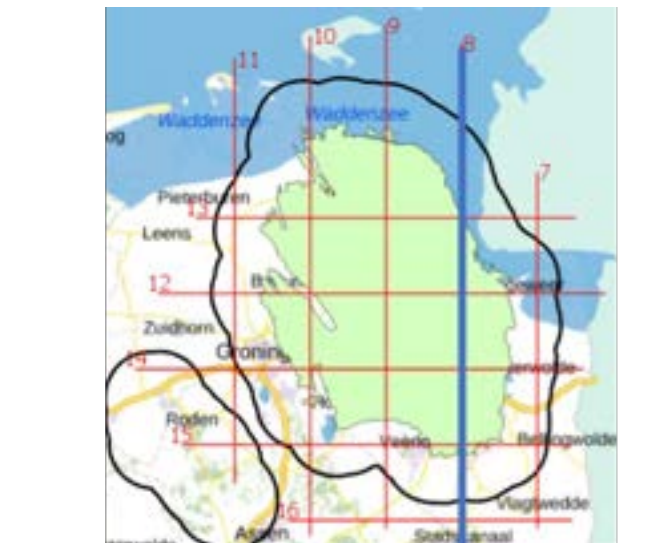
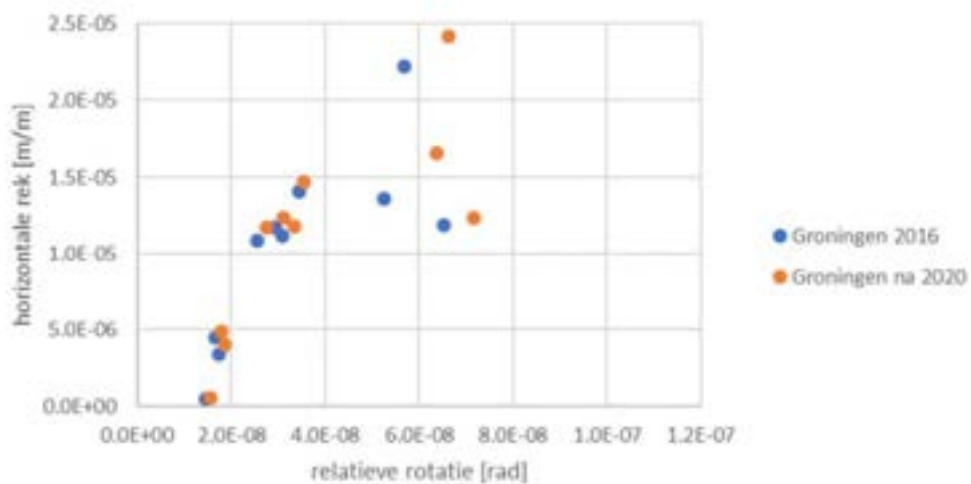
Bodemdaling

- NORG (max=1995)



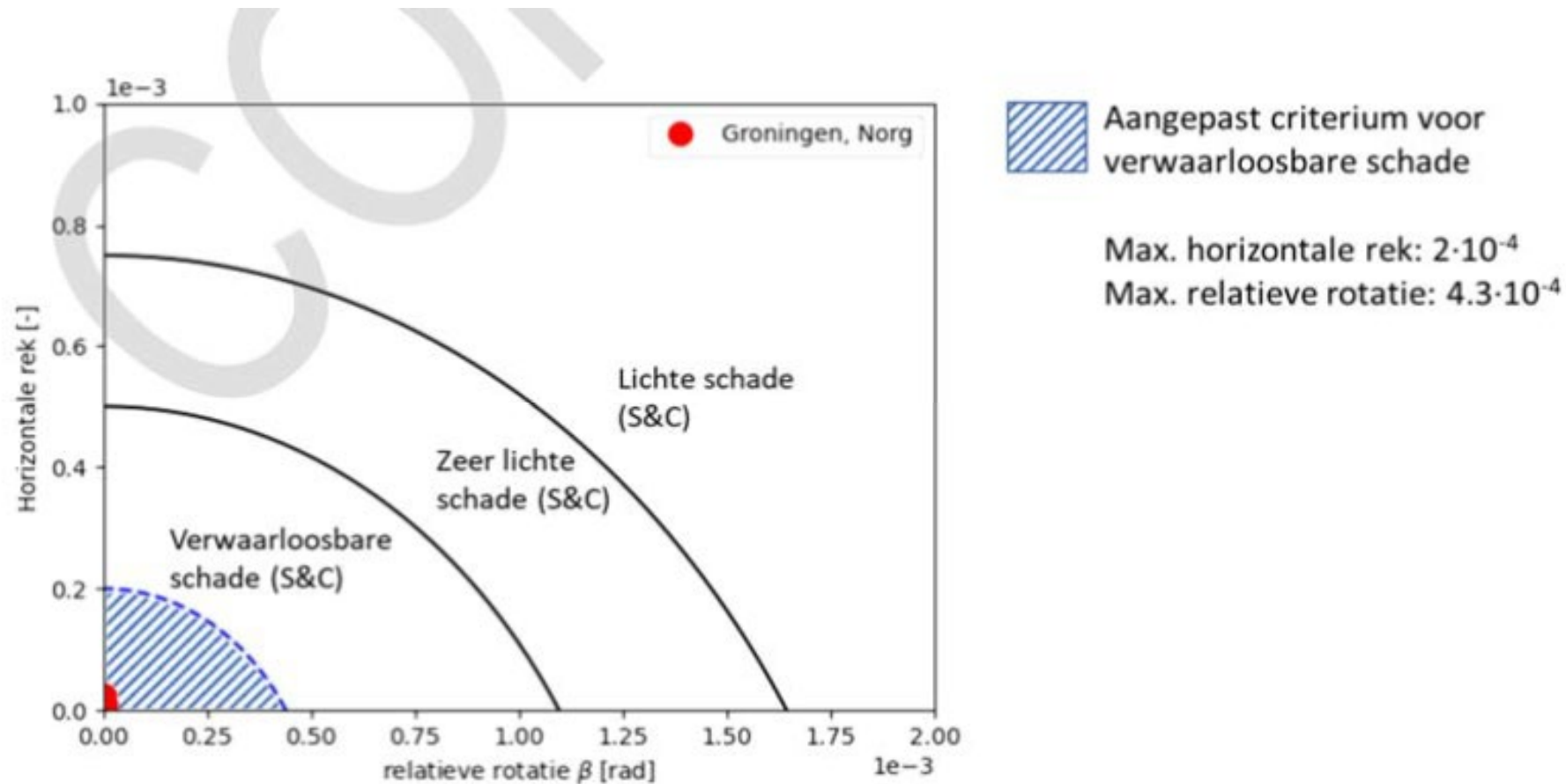
Bodemdaling

- Groningen



TNO: Er wordt geconcludeerd dat de diepe bodemdaling en -stijging ten gevolge van de activiteiten in het Groningenveld en de gasopslag Norg niet leiden of hebben geleid tot schade aan gebouwen.

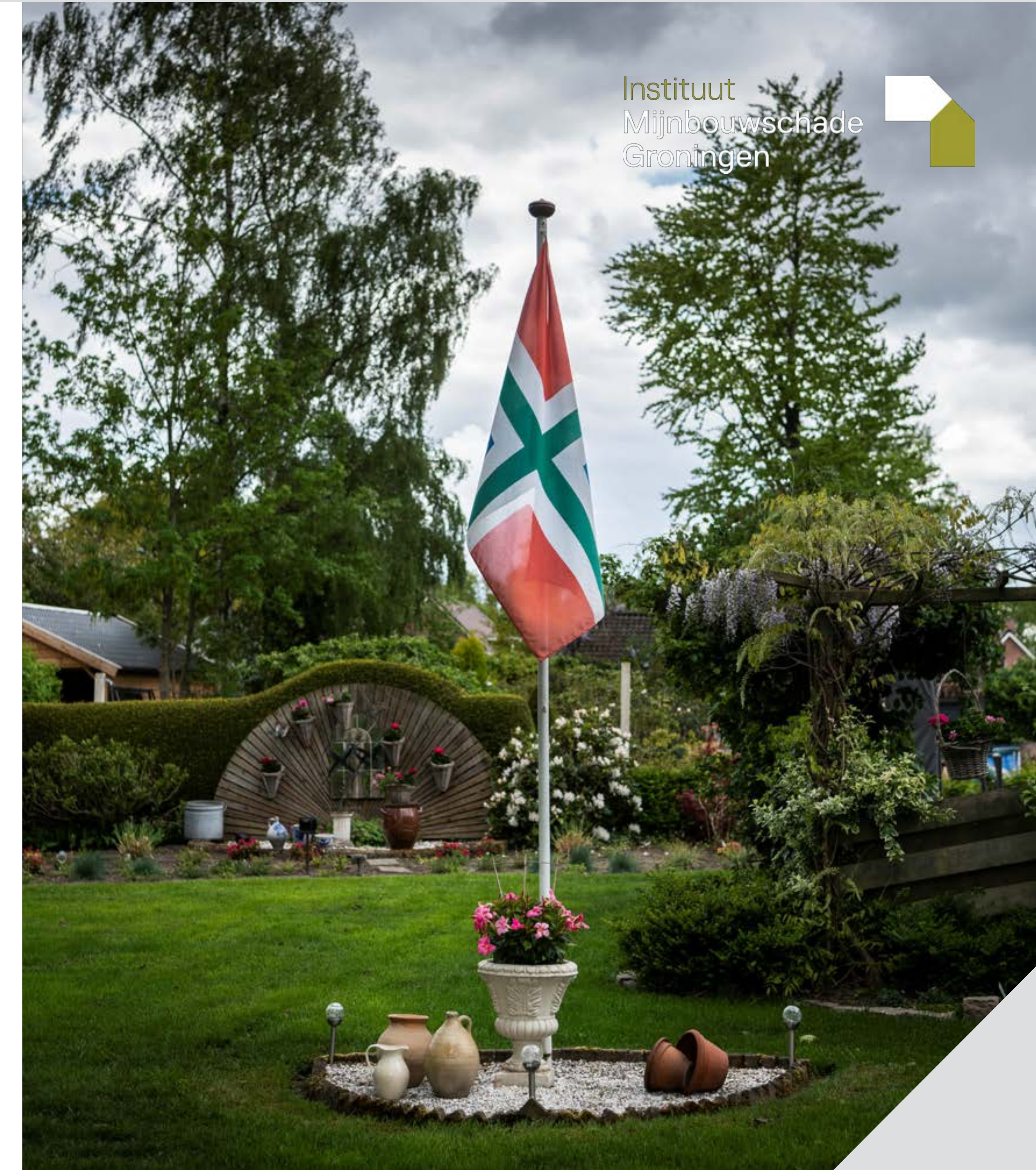
TUD: De resultaten ondersteunen de algemene bevinding dat schade door directe diepe bodemdaling bij Norg en het Groningerveld extreem onwaarschijnlijk is.

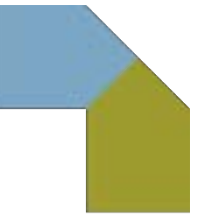


Heidag 2021 Blok 2

Diepe bodemdaling en stijging

5 februari 2021





Doelstellingen blok 2

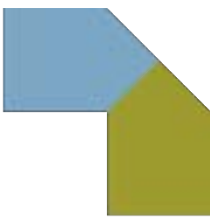
Diepe bodemdaling en stijging

- Aanleiding
- Conclusies TNO- TU Delft
- Impact bij toepassen van de conclusies
- Vraagstelling
- Vervolgstappen

Aanleiding – context (1)

- Het paneladvies van 2019 stelde: er kan niet uitgesloten worden dat er ook schade ontstaat door diepe bodemdaling. Het bewijsvermoeden is daarom, geografisch gezien, van toepassing in het gebied waar die diepe bodemdaling plaatsvindt.
- Op dat moment lagen er rapporten die het tegendeel stelden. Rapporten die ook bekend waren bij het panel van deskundigen. Desalniettemin is dit geconcludeerd en geadviseerd, niet als bijzin, maar explicet en inclusief een grensbepaling met buffer van 6 km.
- Dit advies is vervolgens onverkort extern gecommuniceerd (website, maatschappelijke organisaties, overleggen met lokale bestuurders, informatiebijeenkomsten).
- Na een bespreking met IMG wordt door deskundigen een andere koers gevaren die er op neer komt dat diepe bodemdaling niet meer als oorzaak van mijnbouwschade wordt erkend.

Aanleiding – context (2)



- In de zomer van 2020 ontstaat maatschappelijke onrust in de omgeving van de gasopslag Norg door een groot en groeiend aantal afwijzingen in korte tijd. Lokale bestuurders en belangenverenigingen trekken aan de bel en regionale media berichten hierover.
- Ook intern komen er signalen dat er divers met deze dossiers wordt omgegaan; deskundigen vragen om duidelijkheid; toetsing geeft aan dat het opvallend is dat er ineens veel meer nuldossiers in een bepaald gebied komen en ook vanuit zaakbegeleiding worden de signalen sterker dat eenduidigheid in handelen onder druk staat.
- het IMG besluit vervolgens de schadeafhandeling in dat gebied en een gebied in en rondom Pekela stil te leggen. De vragen die naar aanleiding daarvan gesteld worden zijn onder meer: hoe kan het bestuur besluiten hebben genomen die afwijken van het paneladvies? Waarom greep het bestuur pas in nadat er maatschappelijk onrust ontstond? Hoe is aan een bewoner uit te leggen dat hij niks krijgt en zijn buurman eerder nog meer dan 10.000 euro vergoeding.
- Na eerst gecommuniceerd te hebben dat het TNO-TU Delft rapport in december zou verschijnen is gecommuniceerd dat dit begin 2021 gaat worden. Bij monde van de burgemeesters van de gemeenten Noordenveld en Pekela neemt de onrust over en de kritiek op het IMG toe onder de inwoners van hun gemeenten. De brede verwachting lokaal is dat het IMG de deskundigen gaat corrigeren, de afwijzingen zal herzien en vervolgens schade als gevolg van diepe bodemdaling gaat vergoeden.

Rapport TNO TU Delft

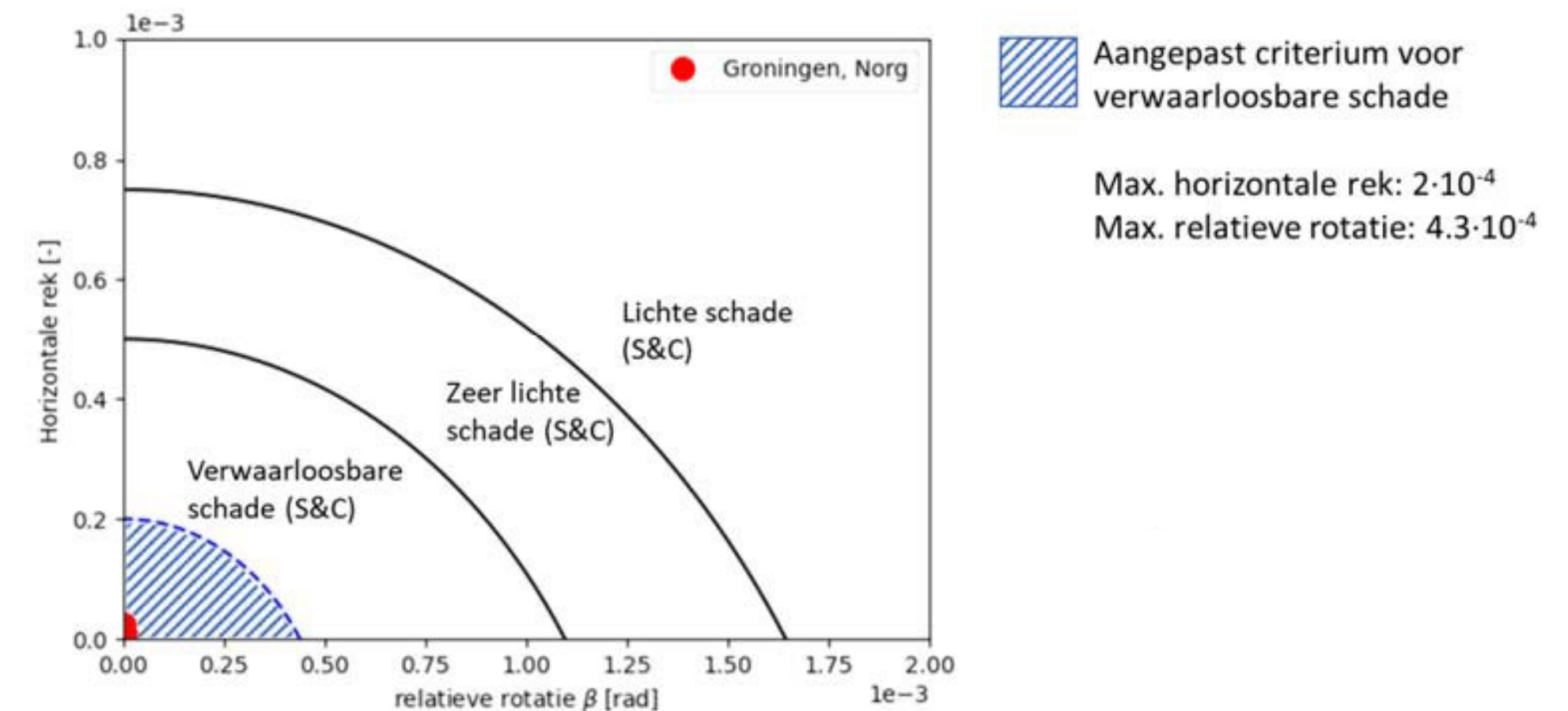
Scope: metselwerken, gevoeliger dan beton- en staalconstructies

Status: draft

Vervolg: nog een paar stappen te zetten om deze definitief te maken,
o.a. het toepassingsgebied bespreken.

Onderzoeken:

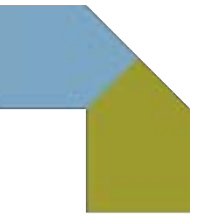
- Literatuuronderzoek criteria schade aan gebouwen;
- Modelberekeningen bodem- en stijging tgv Groningerveld en gasopslag Norg;
- Validatie bodembewegingen met satelliet waarnemingen;
- Modelstudies effect bodemdaling op gebouwen



Omvang impact

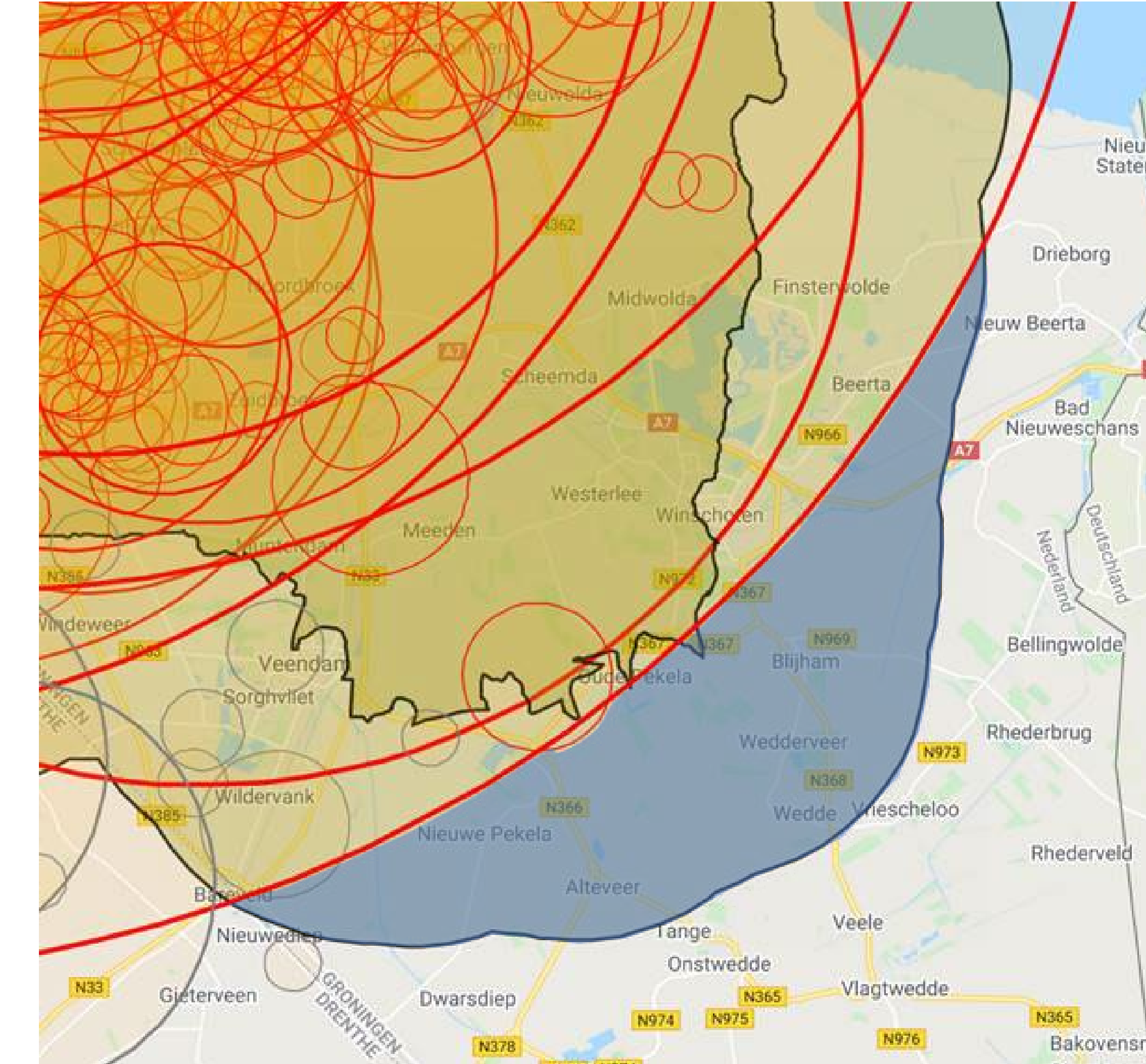
Uitgevoerde activiteiten t.b.v. Groningerveld en Gasopslag Norg

- Aantal ingediende en on hold dossiers
- Aantal afgehandelde dossiers
- Geschat omvang van het totaal aantal woningen in het effectgebied voor diepe bodemdaling.



Groningerveld

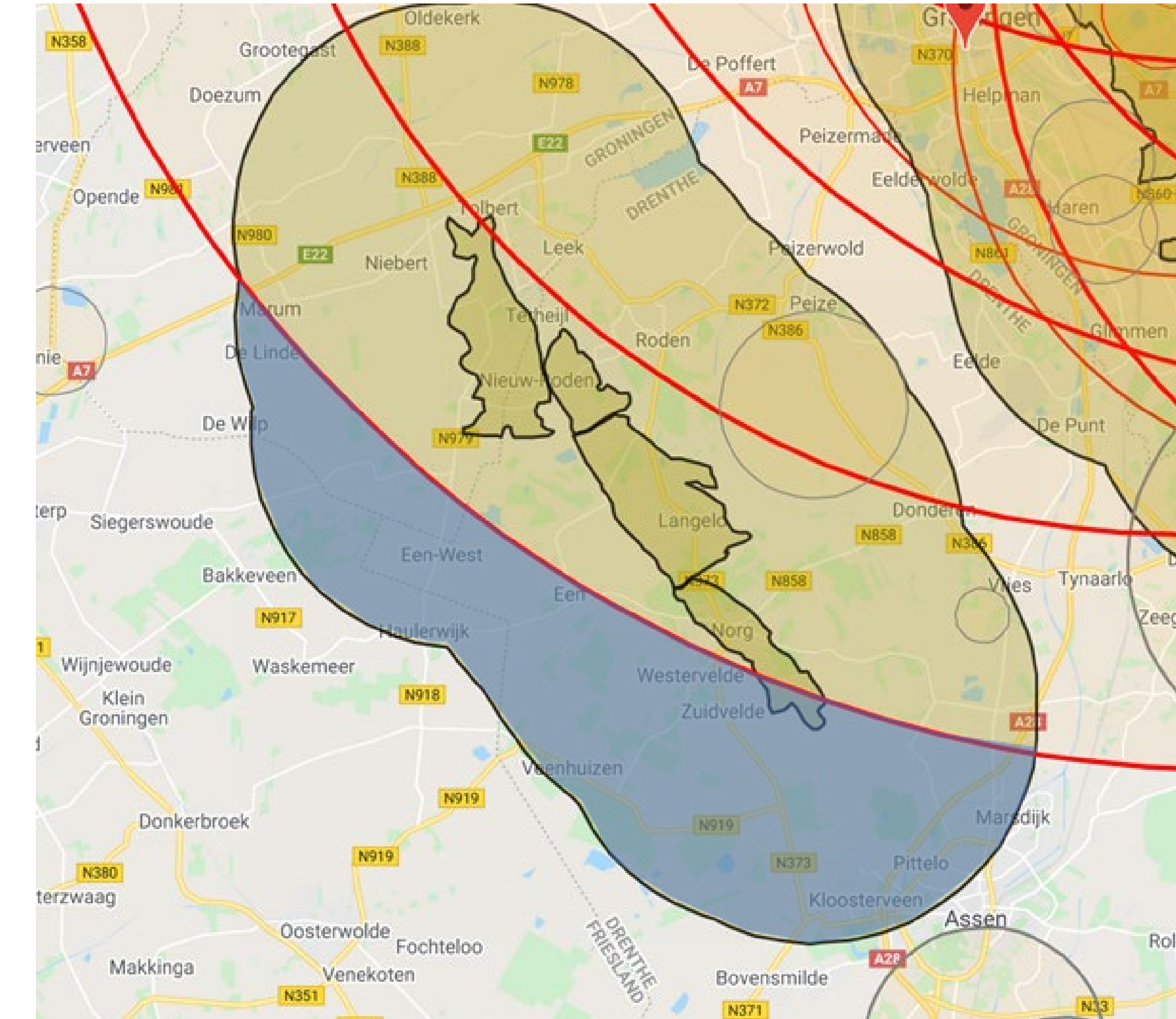
	#
Ingediend en on hold	1100
Afgehandelde dossiers	580
Totaal aantal adressen in de blauwe zone	Circa 6000



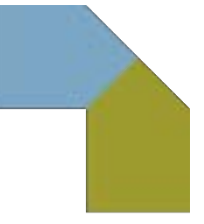
Outside 2mm/s contour and within the 6km contour of the Groningen gasfield

Gasopslag Norg

	#
Ingediend en on hold	340
Afgehandelde dossiers	170
Totaal aantal adressen in de blauwe zone	17500 (Assen 15500)

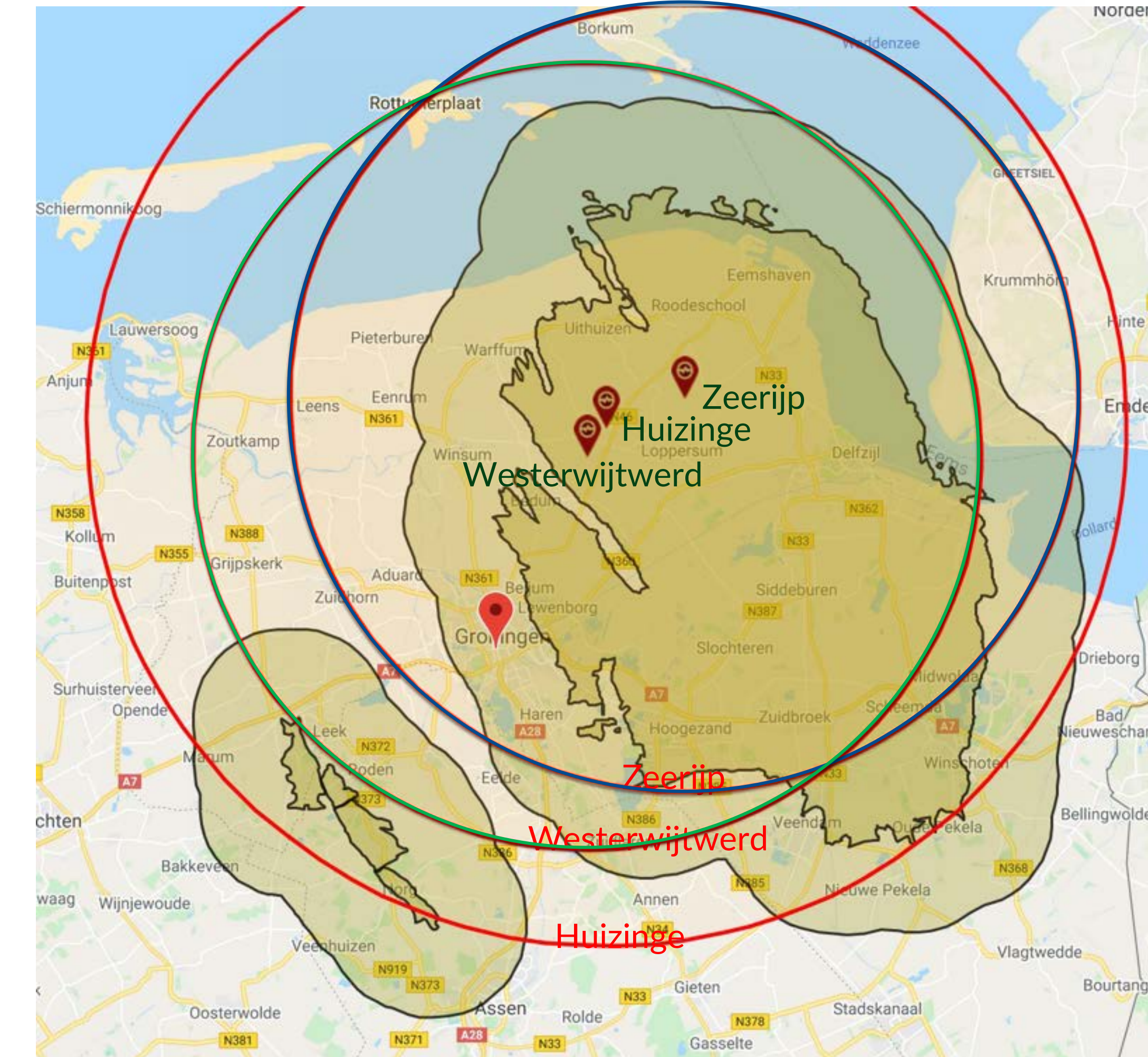


Outside 2mm/s contour and within the 6km contour of the Norg gasfield

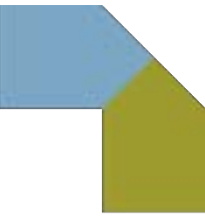


Overige impact

Contour 2mm/s	datum	contour
Huizinge	8/2012	Rood
Westerwijtwerd	5/2019	Groen
Zeerijp	1/2018	Blauw



2mm/s contour Huizinge, Westerwijtwerd; Zeerijp



Impact totaal

In onderstaande tabel is aangegeven het aantal adressen dat buiten de 2 mm/sec contour ligt, maar binnen het effectgebied van diepe bodemdaling (6km zone)

Locatie	Afgehandelde adressen	Ingediend en on hold	Potentieel aantal adressen incl on hold (buiten 2 mm/s contour)	Potentieel aantal adressen binnen 2 mm/s contour (zie toelichting)
Groningerveld	580	1100	5.500	??
Norg	170	340	17.250	??
Totaal aantal	750	1440	22.750	??
Schadevergoeding	7 M€	-	200M€ - 250M€	??

Toelichting laatste kolom: wijzigen omgang met diepe bodemdaling heeft ook impact op alle woningen binnen de 2mm/sec contour. Indien het effect diepe bodemdaling komt te vervallen is er geen aanleiding nieuwe vergoedingen toe te kennen aan situaties waarbij al schade vergoed is in het verleden en waarbij er nadien geen trillingen groter dan 2 mm/sec zijn geweest voor bodembeweging. Hetzelfde geldt voor nieuwbouw woningen, waarbij steeds de maatgevende aardbeving sinds de bouw van de woning in beschouwing genomen moet worden.

Vraagstelling

Op basis van het voorgaande formuleert het Panel de volgende twee alternatieve criteria:

De ligging van het gebouw of werk met de fysieke schade is op een afstand van minder dan 6 km buiten de begrenzing van het Groningenveld (of, zo de suggestie van het Panel, zoals verwoord in voetnoot 1 wordt gevolgd, buiten de begrenzing van de gasopslag Norg).

of

De topwaarde van de trilling van het maaiveld als gevolg van een aardbeving met epicentrum gelegen in het Groningenveld – bepaald op basis van wetenschappelijk gevalideerde rekenmodellen op basis van praktijkwaarnemingen – bedroeg in een periode van ten hoogste 30 jaar (gelijk aan de wettelijke verjaringstermijn) vóór de melding van de schade bij enige aardbeving meer dan 2 mm/s in combinatie met een overschrijdingskans6 van meer dan 1%. Dit is equivalent met een topwaard

- Laten we criterium twee, zoals door het panel geadviseerd vervallen op basis van de conclusies van het rapport?
- Handhaven we het criterium onverkort?
- Handhaven we het criterium, met de nuancering van het bewijsvermoeden, zoals aangegeven door de Hoge Raad.

Vervolgstappen

Hoe gaan we om met de adressen die op Hold staan:

- Overgangsregeling?
- Nieuwe inzichten direct toepassen?

Hoe hangt dit advies samen met :

- Zettingen / zakkingen
- Calculatiemodel
- Mestkelders

Communicatie op hoofdlijnen

Stap 1: informeren en bespreken advies TNO – TU Delft

Stap 2: communiceren besluitvorming IMG en implementatie van dat besluit

Stap 1: Informeren en bespreken

Boodschap:

IMG heeft, zoals bekend, TNO- TU Delft gevraagd te adviseren over de relatie tusen diepe bodemdaling – en stijging en mijnbouwschade aan gebouwen. Het adviesrapport is opgeleverd. Het IMG bespreekt dit rapport met verschillende belanghebbenden en zal daarna een bepalen of het dit advies zal overnemen en welk gevolg het hieraan zal geven. Het IMG zal hiervoor in toaal XX weken de tijd nemen.

Communicatie op hoofdlijnen

Acties stap 1

Extern

- 22/2 Bespreken rapport met burgemeesters Pekela en Noordenveld en gedeputeerde Drenthe.
- 22/2 Bespreken rapport met Dorpsbelangen Een
- 23/2 Brief naar aanvragers waarvan dossier on hold is gezet
- 23/2 Versturen rapport met begeleidende mail van Bas naar: lokale belangenverenigingen, GBB en GGB, lokale en regionale bestuurders, bestuurders regio-overleg en EZK.
- 23/2 Publicatie rapport op website, begeleid door een nieuwsbericht.
- 23/2 Bespreken met deskundigenparijen
- 23/2 Start bespreking rapport met GGB, GBB, lokale belangenverenigingen die zich melden, regio-overleg, EZK etc.

Intern

- 18/2 Nieuwsflits, kennisbank en instructies voor Serviceloket en ZB (toelichting, Q&A etc)
- 22/2 Nieuwsbericht PLEK

Communicatiemiddelen:

Extern: Presentatie in power point, nieuwsbericht en Q&A website, bericht mogelijk ondersteund door een animatie met toelichting diepe bodemdaling.

Intern: Bericht PLEK (ondersteund door animatie), interne nieuwsflits, Kennisbank, Q&A, instructies Serviceloket en ZB

Van: 5.1.2.e
Aan: Kortmann, prof.mr. S.C.J.J. (Bas); Buuren, prof. mr. P.J.J. van (Peter); 5.1.2.e @utwente.nl"; Giebels, prof.dr. E. (Ellen); Bouwes, mr. M.T. (Menno); Pagter, ing. J.K. de (Jan Kees); Houdijk, mr. J.N. (Hans);
Cc: 5.1.2.e 5.1.2.e 5.1.2.e 5.1.2.e 5.1.2.e
Onderwerp: Aantekeningen heisessie Blok 2
Datum: vrijdag 5 februari 2021 11:21:55
Bijlagen: [IMG presentatie heidag blok 2 versie def 05022021.pptx](#)

Aanwezig: Bas Kortmann, Peter van Buuren, Ellen Giebels, Menno Bouwes, Jan Kees de Pagter, Hans Houdijk, 5.1.2.e , 5.1.2.e en 5.1.2.e

- Peter opent;
- 5.1.2.e leidt in aan de hand van de presentatie (bijgevoegd);
- 5.1.2.e licht de aanleiding en context toe;
- 5.1.2.e licht de conclusies van het conceptrapport TNO TU Delft over diepe bodemdaling toe. Het richt zich nu op metselwerk; het wordt nog verbreed naar andere constructies (waarbij metselwerk het meest kwetsbaar is). Er wordt geen antwoord gegeven op effect grondwaterstand. In de grafiek staat 'verwaarloosbare schade': dat moet worden toegelicht. Diepe bodemdaling is geen aanleiding voor schade aan gebouwen;
- Impact Groningenveld: 1.100 aanvragen on hold, 580 aanvragen afgehandeld (gem. € 10.000 schade) en 6.000 adressen in het betreffende gebied (waarvan dus 2.000 bij ons bekend);
- Impact Norg: 340, 170 en 17.500;
- Van de afgehandelde dossiers is ongeveer 9% afgewezen: wordt nog nagekeken;
- Vraagstelling. Peter: het 6-km criterium is destijds door het panel Van Mierlo zekerheidshalve aangenomen; dit rapport geeft een nieuw inzicht, ik ben ervoor om dit criterium te laten vervallen. Menno: wij weten al langer dat diepe bodemdaling geen schade veroorzaakt, al sinds de jaren '80: wij wisten dat ook toen we het paneladvies Van Mierlo omarmden, er waren redenen om hier geen rekening mee te houden. Plus we hebben inmiddels al schade toegewezen. Plus bij infra en industrie, waartoe we nu ook bevoegd zijn, kan diepe bodemdaling wel tot schade leiden. Kortom; handhaaf het effectgebied maar kijk op een andere manier naar schade aan de randen, meer rekening houdend met andere factoren dan in de kern van het gebied. Ik mis nog in het rapport het effect op gebouwen die om andere reden kwetsbaar zijn. Jan Kees: ik voel ook voor het niet veranderen van grenzen en paneladvies: kijk naar wat dit betekent voor de toepassing van het bewijsvermoeden. Peter kan zich hier ook in vinden. Ellen: wat is dan de aanleiding geweest voor dit onderzoek, als we dit al wisten? Bas: reden voor onderzoek was dat er mensen waren die zeiden dat diepe bodemdaling wel tot schade kan leiden;
- Bas: we moeten duidelijk onderscheid maken tussen bewijsvermoeden en weerlegging van bewijsvermoeden. 6-km was het idee van de eenvoud. Plaatjes 7 en 8 zijn heel duidelijk: mijn idee is dat we het paneladvies/effectgebied handhaven en de weerlegging van het bewijsvermoeden nuanceren;
- 5.1.2.e : de vraag is hoe we dit uitleggen aan de bewoner? We gaan dan afwijzen, dus beter mea culpa, duidelijkheid geven, geen opname meer doen in Norg;
- 5.1.2.e: maar dit geldt niet voor andere werken dan gebouwen;
- Bas: het gaat niet alleen over deze twee gebieden, paneladvies geldt voor het hele gebied. Het nuanceren van het weerlegging van het bewijsvermoeden laat ons ruimte. Ook als we 6-km afschaffen, speelt de vraag of we nog een schadeopname gaan doen;

- Menno: ik vind het raar om op voorhand te zeggen dat het geen mijnbouwschade is, dus we komen niet opnemen. We hebben hier geen goede ervaring mee;
- Hans: ik heb wat moeite met te makkelijk mea culpa zeggen want dit is inderdaad geen nieuwe informatie. Met een aanpassing kan de hoeveelheid aanvragen in het buitengebied weer afnemen;
- Bas: in beginsel gaan we daar nog wel schadeopnames doen (maar vooraf duidelijk aangeven dat de kans bestaat dat het geen mijnbouwschade is);
- 5.1.2.e dit gaat tot grote verschillen leiden tussen mensen;
- Bas: de variant van het onverkort blijven toepassen van het paneladvies, heeft nu niet de voorkeur. Geen steun voor grote mea culpa. We handhaven het paneladvies en kijken naar nuancingering van het weerleggen van bewijsvermoeden. Vervolgens is de vraag hoe we komen van A naar B (overgangsrecht)?
- Jan Kees: de impact gaat verder dan de twee blauwe gebieden, bv ook woningen van 2019 in Zoutkamp;
- Menno: mensen moeten serieus de gelegenheid hebben om te reageren. Peter: dat zou kunnen met een zienswijze;
- Bas: als je zeker weet dat het niet wordt toegewezen, moet je geen verwachtingen wekken door een opname te doen. Mensen kunnen een zienswijze indienen, we moeten het wel goed uitleggen in het concept-besluit. Bij twijfel gaan we wel kijken;
- Menno: dit moet eerst goed verder doordacht en uitgewerkt worden om te voorkomen dat we later, zoals na de SMR, op zaken terug te moeten komen;
- Bas: we nemen nu geen definitieve beslissing, eerst deze uitwerking op papier. Andere vraag: hoe zou een 'overgangssituatie' er uit kunnen zien?
- 5.1.2.e : we kunnen werken met een overlastvergoeding;
- Bas: een echte overgangssituatie is niet aan de orde. Bovendien moeten we dit rapport eerst bespreken met een aantal partijen:
- 5.1.2.e klopt, met de MO's, gemeenten/gedeputeerde/dorpsbelangen Een etc.
- MT werkt de toepassing verder uit, inclusief een evt. overlastvergoeding (Bas, Ellen, 5.1.2.e en 5.1.2.e en zet plussen en minnen op een rij. Er wordt een nieuwe afspraak gepland.

verslag

Omschrijving	IMG	
Vergaderdatum en -tijd	Donderdag 17 december 2020, 12.30 – 16.00 uur	
Vergaderplaats	Webex	
Aanwezig:	Bas Kortmann (voorzitter), Ellen Giebels, Menno Bouwes, Jan Kees de Pagter, 5.1.2.e [REDACTED], Hans Houdijk, 5.1.2.e [REDACTED] [REDACTED]	
Afwezig:	Peter van Buuren (m.k.)	

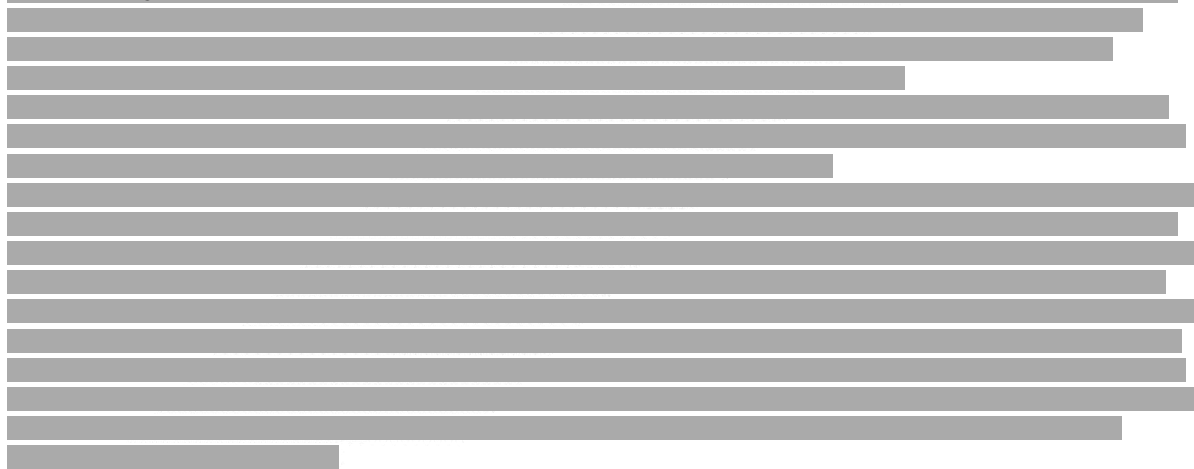
Cascadeplein 10
9726 AD Groningen

Antwoordnummer 3061
8000 WB Zwolle

0800 44 44 111
contact@schadedoormijnbouw.nl

1. Opening, vaststelling agenda en mededelingen

Buiten reikwijde



Buiten reikwijde



Buiten reikwijde





5. Nader advies TNO-TU Delft over diepe bodemdaling en -stijging

Bas Kortmann verwelkomt 5.1.2.e [REDACTED], civieltechnisch bouwkundig adviseur binnen het IMG. 5.1.2.e [REDACTED] begint met een korte toelichting op het proces. De ontvangen stukken zijn nog conceptstukken. Er wordt een tussenbericht gestuurd naar die aanvragers waartegen eerder is gezegd dat hun aanvraag rond half december weer zou worden opgepakt. 5.1.2.e [REDACTED] neemt ons, aan de hand van een korte presentatie, op hoofdlijnen mee door het advies. Het advies zal uitgebreid aan de orde komen tijdens de heidag in januari.

De conclusie is duidelijk: diepe bodemdaling als gevolg van mijnbouwactiviteiten leidt niet tot schade aan gebouwen. Menno Bouwes geeft aan dat deze conclusie de uitkomst van eerdere onderzoeken bevestigt; in de praktijk zien we vooral problemen ontstaan bij constructiefouten en/of achterstallig onderhoud: geldt de conclusie daar ook? 5.1.2.e [REDACTED] zegt dat is uitgegaan van metselwerk, een kwetsbare vorm van bouwen, en dat complexere situaties niet de basis van dit onderzoek vormen. Het is belangrijk dat de conclusie generiek getrokken kan worden en explicet in het advies wordt opgenomen; dit zal worden voorgelegd aan TNO/TU-Delft. Ook zal worden gevraagd explicet aandacht te besteden aan het effect van diepe bodemdaling op grondwaterstanden, waardoor schade kan ontstaan. Hans Houdijk vraagt zich af hoe dit advies past bij het paneladvies over het bewijsvermoeden en het effectgebied. Jan Kees de Pagter wijst op de eerdere presentatie van Dorpsvereniging Een waarin andere getallen staan: het is belangrijk deze verschillen te kunnen uitleggen. 5.1.2.e [REDACTED] weet dat daar gebruik is gemaakt van satellietdata. Een andere vraag is of diepe bodemdaling/-stijging het laatste zetje kan zijn, naast andere oorzaken, waardoor schade ontstaat. Plus de vraag van het effect van herhaalde grondbewegingen: ook deze punten worden mee teruggenomen naar de onderzoekers.

5.1.2.e [REDACTED] verwacht dat, ondanks dat de uitkomst congruent is met eerdere onderzoeken, het advies hard gaat landen. We hebben belang bij een gezaghebbend en duidelijk advies, inclusief consistentie formuleringen; daar moet nog een slag in worden gemaakt. Termen als 'verwaarloosbare schade' zien we liever niet, aldus 5.1.2.e [REDACTED]. Hans Houdijk wijst, ook in voorbereiding op de heidag, op een ander punt uit het recente onderzoek van Gronings Perspectief,



namelijk dat bewoners en professionals grote moeite hebben met wijzigende kaders. Tot slot zal aan TNO/TU-Delft worden gevraagd wanneer we het definitieve advies krijgen.



12. Rondvraag en sluiting



Buiten reikwijdte



Verslag

Omschrijving	IMG	Cascadeplein 10 9726 AD Groningen
Vergaderdatum en -tijd	Donderdag 22 april 2021 12.30 – 16.00 uur	Antwoordnummer 3061 8000 WB Zwolle
Aanwezig	Bas Kortmann (voorzitter), Peter van Buuren, Ellen Giebels (telefonisch), Menno Bouwes, Jan Kees de Pagter, [REDACTED] 5.1.2.e [REDACTED], Hans Houdijk, [REDACTED] 5.1.2.e [REDACTED], 5.1.2.e en [REDACTED] 5.1.2.e	0800 44 44 111 contact@schadedoormijnbouw.nl

Buiten reikwijdte

Buiten reikwijdte

Buiten reikwijdte

Buiten reikwijdte

3. Besluitvorming (adviezen) diepe bodemdaling, uniformiteit, mestkelders en eerste ideeën over een mogelijke forfaitaire afhandeling

Als eerste ligt het rapport Diepe bodemdaling van TNO en TU-Delft (definitieve versie van 9 maart 2021) voor. [REDACTED] 5.1.2.e meldt dat Deltares binnenkort zal adviseren dat bodemdaling indirect wel in bepaalde, afgebakende gebieden (binnen het gehele gebied dus niet alleen aan de randen) tot (zettings-)schade kan leiden. Deltares komt volgende week met een kaart waarop deze gebieden staan: in die gebieden zul je de schade wel moeten onderzoeken, voor deze specifieke gebieden blijft het bewijsvermoeden van toepassing. Er is voor zover bekend geen kennis beschikbaar in Nederland over het totale effect van de verschillende vormen van bodemdaling. Het bestuur besluit het rapport Diepe bodemdaling in beginsel over te nemen, het effectgebied wordt niet meer bepaald door het 6 km-criterium, enkel nog door de trillingssterkte van 2 mm/sec. Hierbij geldt dat er een paar uitzonderingen zijn, zoals de grondwaterrisico-locaties van Deltares en lokaties als wierden en terpen.

Buiten reikwijdte



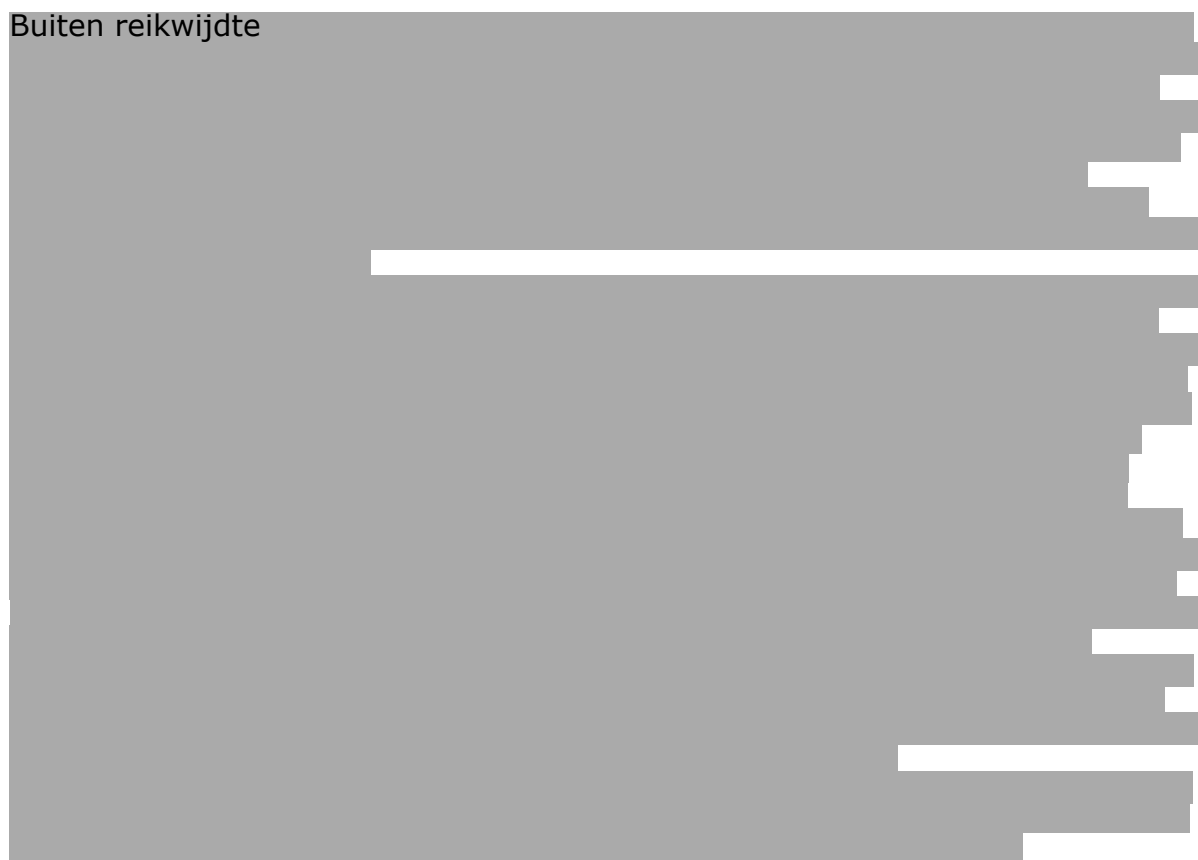
Buiten reikwijdte



Buiten reikwijdte



Buiten reikwijdte



Buiten reikwijdte





Buiten reikwijdte



Buiten reikwijdte

Buiten reikwijdte

Buiten reikwijdte

Buiten reikwijdte



Buiten reikwijdte

Buiten reikwijdte

Buiten reikwijdte

Buiten reikwijdte



Verslag

Omschrijving	Bestuursvergadering IMG
Vergaderdatum en -tijd	Woensdag 8 juni 2023, 12.30 – 16.00 uur
Vergaderplaats	Cascadeplein 6, Martinitoren
Aanwezig	Henk Korvinus (voorzitter), Menno Bouwes, Els van Schie, Paula van der Beek, Jan Wierenga, 5.1.2.e [REDACTED] Hans Houdijk, 5.1.2.e [REDACTED], 5.1.2.e [REDACTED], 5.1.2.e [REDACTED] (t/m agendapunt 5)
Afwezig m.k.	5.1.2.e [REDACTED]

Cascadeplein 10
9726 AD Groningen

Antwoordnummer 3061
8000 WB Zwolle

0800 44 44 111
contact@schadedoormijnbouw.nl





4. Aanvullend onderzoek n.a.v. peer review

TNO/TU Delft hebben naar aanleiding van de peer review nader onderzoek gedaan naar een aantal specifieke risicofactoren. Het nadere onderzoek van TNO/TU Delft is deze week mondeling toegelicht. Zij hebben het meest kwetsbare gebouw in het gebied uitgezocht (een langgerekt gebouw/boerderij gebouwd voor 1940) en gekeken of dit gebouw, als het in de lobben zou staan, schade zou kunnen hebben door diepe bodemdaling. Dit is niet het geval. Als we de uitkomsten op schrift hebben, zullen deze gedeeld worden met EZK. De vraag is of EZK dit nog aan de peers wil voorleggen, dit zal met EZK besproken worden.





Buiten reikwijdte



Intern gebruik

Cascadeplein 10
9726 AD Groningen

Antwoordnummer 3061
8000 WB Zwolle

0800 44 44 111
contact@schadedoormijnbouw.nl

MT IMG

Onderwerp	:	Directe effecten diepe bodemdaling
Datum	:	21-11-2023
Portefeuillehouder Bestuur	:	Jan Wierenga
Sponsor MT*	:	5.1.2.e
Contactpersoon (auteur)	:	5.1.2.e (BJA) / 5.1.2.e (SEH)
Doel**	:	ter besluitvorming
Vertrouwelijk	:	Nee

Onderdeel	Overleg gevoerd met	Standpunt van de betreffende afdeling	
		Akkoord (ja / nee)	Niet akkoord (toelichting)
Klantcontact- en dienstverlening	n.v.t. (indien besloten opnemen Q&A)		
Schade Expertise en Herstel			
Bestuurlijke & Juridische Zaken en Schadeafhandeling	Akkoord		
Regiebureau	n.v.t.		
Informatievoorziening	n.v.t.		
Communicatie	Akkoord		
Bedrijfsvoering: Financiële toets Personele toets	n.v.t.		

Moet worden geagendeerd in:	Advies
Bestuursvergadering	N.o.t.k.
Ondernemingsraad	Nee



1. Inleiding

Binnenkort worden de resultaten van een follow-up studie naar directe effecten van diepe bodemdaling gepubliceerd. Deze studie is een vervolg op een eerdere studie van TU Delft en TNO (2020) en de peer review op deze studie door Movares (2021). In deze notitie worden de belangrijkste uitkomsten van de follow-up studie van TU Delft en TNO benoemd. Deze rapporten worden openbaar gemaakt. Met EZK is besproken dat Movares na publicatie hierop een review zal houden. In deze notitie wordt voorgesteld hoe de uitkomsten van deze studie geadresseerd kunnen worden in de schadebeoordeling.

2. Voorstel en conclusie

De follow-up studie van TU Delft en TNO geeft aan dat schade als gevolg van directe effecten van diepe bodemdaling in de voormalige lobjes uitgesloten kan worden (conform de eerdere studie). In het effectgebied voor trillingen (de 'Huizinge cirkel') is er in twee deelgebieden (rond Warffum en Bedum) een zeer geringe kans van 1:800 of kleiner op schade voor woningen met gemetselde funderingen. Het gaat om een kleine groep gebouwen in de kern van het effectgebied.

De gebouwen staan in de kern van het effectgebied, waar het bewijsvermoeden al van toepassing is. Dit betekent dat voor elke schade eerst een evidente autonome oorzaak vastgesteld moet worden. Is deze er niet dan wordt de schade vermoed mijnbouwschade te zijn en wordt deze schade vergoed. Voor schades waarbij er een evident autonome andere oorzaak vastgesteld is, moet de vervolgvraag gesteld worden of bodembeweging de schade toch kan hebben veroorzaakt of verergerd. In het beoordelingskader wordt bij trillingen dit uitgesloten als de kans op verergering kleiner dan 1% is. Dit beleid is akkoord bevonden door de afdeling bestuursrechtspraak van de Raad van State. Voorgesteld wordt om deze norm ook voor eventuele verergering door diepe bodemdaling te hanteren. Aangezien de schade kans hierop bij diepe bodemdaling 1:800 of kleiner is, geldt ook hier dat als er een autonome oorzaak is vastgesteld, de schade niet door diepe bodemdaling kan zijn ontstaan of verergerd. Voor trillingen ligt dit anders en dat leggen wij nu uit.

Wanneer trillingen de grenswaarden drie keer overschrijden is de kans op schade ten minste 30%. Bij veel gebouwen is in de twee gebieden zijn de grenswaarden drie keer overschreden en dient de schade volledig vergoed te worden. Bij overschrijding tussen één en drie keer de limiet bepaalt de deskundige of trillingen de autonome schade hebben kunnen verergeren. Vaak leidt dit tot een schadevergoeding vanwege het niet kunnen uitsluiten van verergering.

Samengevat betekent dit als directe effecten van diepe bodemdaling al schade hebben veroorzaakt uit het huidige beleid volgt dat die schade moet worden vergoed. Hetzij omdat de deskundige geen evidente oorzaak heeft kunnen aanwijzen, hetzij omdat de hoogte van de trillingen al zorgt voor een schadevergoeding omdat niet kan worden uitgesloten dat trillingen de schade hebben ontstaan of verergerd.

Het MT wordt gevraagd om akkoord te gaan met de voorgestelde werkwijze.

3. Achtergrond

Uit het advies van het Panel van deskundigen (22 januari 2019) volgde de volgende geografische criteria voor het bepalen van het effectgebied waarbinnen het bewijsvermoeden van toepassing is: (1) het gebouw ligt op een afstand van minder dan 6 kilometer van het Groningenveld of de Gasopslag Norg; of (2) ter plaatse is een trillingssnelheid van minimaal 2 mm/s (1% overschrijdingskans) berekend.



In 2020 heeft het Instituut de TU Delft en TNO om advies gevraagd te adviseren over de effecten van de diepe bodemdaling en -stijging die optreedt door de mijnbouwactiviteiten uit het Groningenvelde en de gasopslag Norg. Op basis van deze studie is geconcludeerd dat diepe bodemdaling niet direct leidt tot schade aan gebouwen.¹ Vervolgens heeft het IMG besloten dat het zes kilometer gebied is komen te vervallen bij het bepalen van de toepasselijkheid van het bewijsvermoeden.

In opdracht van de Staatssecretaris van Economische Zaken en Klimaat heeft Movares een peer review uitgevoerd op de studie van TU Delft en TNO uit 2021. In 2022 is Movares met de uitkomst van het peer review gekomen. Hieruit volgt dat de resultaten van TU Delft en TNO in principe niet onjuist zijn, maar dat er wel een aantal onzekerheden zijn betreffende het onderzoek. In reactie hierop hebben TU Delft en TNO een follow-up studie uitgevoerd, gericht op de opmerkingen uit het peer review van Movares. Na publicatie van de follow-up zal Movares een tweede review verrichten.

4. Resultaat

Met de follow-up studie van TU Delft en TNO zijn de eventuele onzekerheden uit de eerdere studie besproken en onderzocht. De eerdere resultaten worden niet weersproken en in de twee gebieden waar het bewijsvermoeden niet langer van toepassing is (het zes kilometer gebied), is het niet aannemelijk dat directe effecten van diepe bodemdaling tot schade aan gebouwen leidt. De kans op schade is namelijk kleiner dan 1:10.000. Dit betekent dat minder dan één gebouw schade kan hebben als gevolg van deze directe effecten. Hetzelfde geldt voor het huidige effectgebied. Het generiek uitsluiten van directe bodemdaling in het gehele effectgebied is echter niet mogelijk, omdat er twee gebieden rond Warffum en Bedum zijn, waarbij – gelet op de ondergrond en type bouwstijl/fundering – de kans op schade wel groter dan 1:10.000 is. Het gaat hier om een groep woningen met een gemetselde fundering waarbij de kans op schade 1:800 of kleiner kan zijn. Binnen deze groep gebouwen is de kans op schade alsnog zeer klein en is de kans op schade door andere schademechanismen groter. Dit betekent dat de kans dat er een gebouw is met schade door directe effecten van diepe bodemdaling in feite nog steeds zeer gering is.

De follow-up studie biedt logischerwijs geen antwoord op een aantal aspecten en actuele ontwikkelingen binnen de taak van het Instituut. Aan TU Delft en TNO wordt een update van de studie verzocht om bodemdaling veroorzaakt door kleine gasvelden, de gasopslag Grijpskerk en mogelijke toekomstige bodemdaling te bespreken.

5. Wat betekent de follow-up studie voor de huidige beoordelingswijze?

Op het moment dat er schade is die naar zijn aard door mijnbouwactiviteiten kan zijn ontstaan, dan is het bewijsvermoeden van toepassing en wordt daar het huidige beoordelingskader op toegepast. Uit het beoordelingskader volgt dat wanneer er geen autonome oorzaak is, de schade geheel wordt vergoed. Als er wel een autonome oorzaak voor de schade is aan te wijzen, dan moet de deskundige beoordelen of trillingen niet alsnog van invloed zijn op het ontstaan of verergeren van de schade of kosten van herstel. Uit het door de afdeling bestuursrechtspraak geaccordeerde beleid van het IMG volgt dat uitgesloten kan worden dat een autonome schade toch is ontstaan of verergerd als de kans kleiner is dan 1%. De kans op schade door directe effecten van diepe bodemdaling bij een gebouw is 1:800 of kleiner. Dit betekent als de deskundige een autonome oorzaak aanwijst, directe effecten de schade niet alsnog hebben kunnen veroorzaken of verergeren. Dezelfde grenswaarde hanteert het IMG voor trillingen. De

¹ Er kan wel sprake zijn van indirekte effecten van diepe bodemdaling (IEDB), hiervoor heeft het Instituut Deltares om advies gevraagd.



voorgestelde werkwijze zal de beoordeling van schades in de gebieden hetzelfde waarborgen als bij trillingen.

Bij veel gebouwen in de gebieden is een trillingssnelheid berekend waarbij de grenswaarden met een factor 3 zijn overschreden. Hierbij is de kans dat de schade is ontstaan of verergerd door trillingen ten minste 30%. Bij overschrijding van drie keer de limiet van trillingen wordt de schade vergoed. Dit is overigens vaak al het geval bij één keer overschrijding van de limiet van trillingen, omdat verergering dan vaak niet kan worden uitgesloten door de deskundigen.

Het betreft de gebieden binnen de (volledig dikgedrukte) zwarte lijnen op de onderstaande kaart.

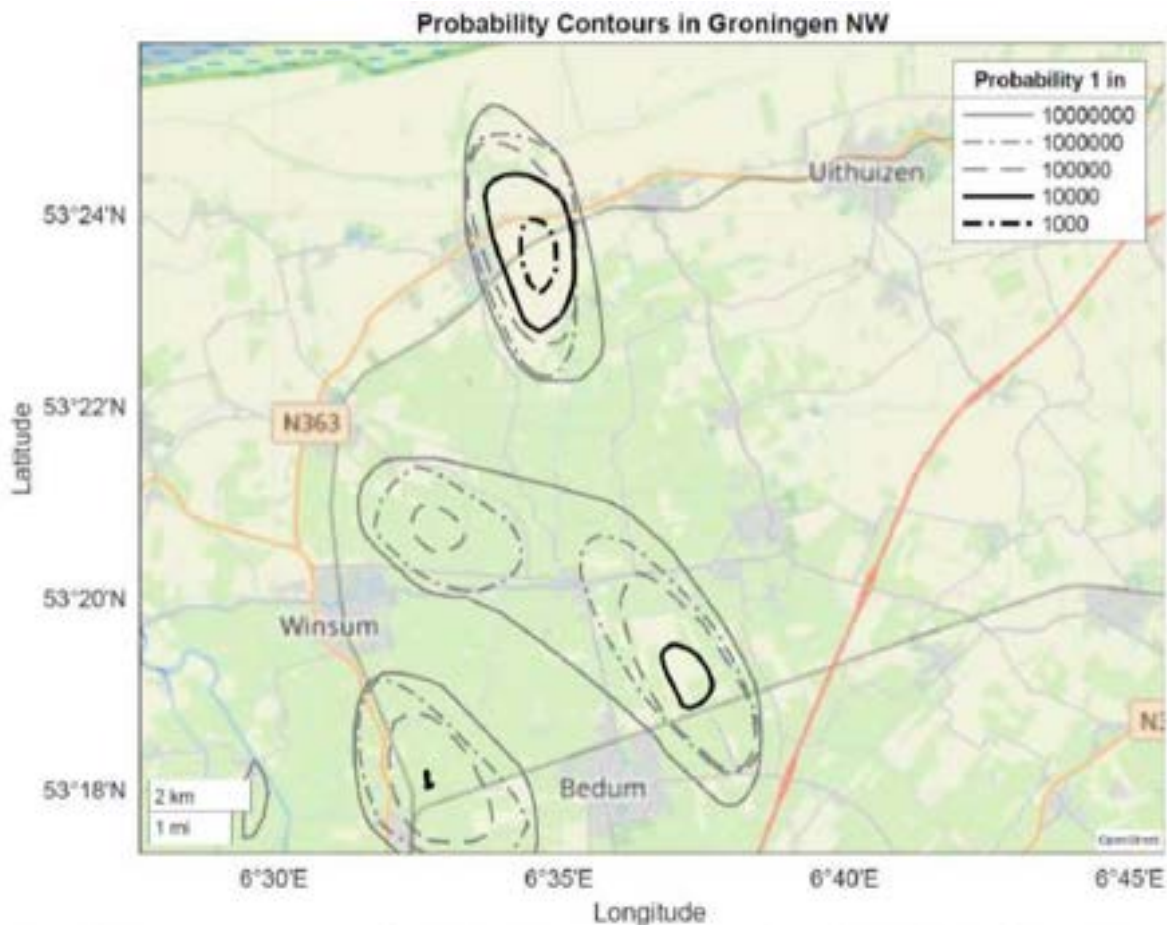


Figure J.13. Probability contours in the NW of Groningen for light damage ($\Psi=1$) of buildings with unreinforced masonry structures.

Figure 2: The solid lines envelope the areas in which the probability of minor damage (crack widths below 0.1 mm) for a building with a masonry foundation, as a result of deep subsidence, is greater than 1 in 10,000.



Communicatie

De resultaten uit het onderzoek geven geen aanleiding om tussentijds de wijze van beoordelen aan te passen. Daarnaast worden definitieve conclusies pas getrokken als de Movares (de peer-reviewers) de reactie van TNO beoordeeld heeft. Voor de bewoner wijzigt de regeling vooralsnog niet. De communicatie kan voor nu beperkt worden ingezet.

EZK heeft de reactie van TNO ontvangen en overlegt met de peer-reviewers. Wij nemen contact op met de Tijdelijke werkgroep Een, mailen de reactie van TNO aan ze. Als daar behoefte aan is nodigen we hen uit voor een overleg. Enkele dagen later wordt een bericht op Plek en de website geplaatst. Betrokken gemeenten en de provincie worden via de stakeholdermanager geïnformeerd. EZK is akkoord met deze werkwijze.

Verslag

Omschrijving	Bestuursvergadering IMG			
Vergaderdatum en -tijd	Donderdag 23 november 2023, 12.30 – 14.15 uur			
Vergaderplaats	Cascadeplein 6, Korenbeurs			
Aanwezig	Henk Korvinus (voorzitter), Menno Bouwes, Jan Wierenga, Sylvia Wortmann, Olivier de Bruijne, 5.1.2.e 5.1.2.e 5.1.2.e B 5.1.2.e 5.1.2.e .			

Afwezig	Els van Schie
---------	---------------



3. Eindrapport TNO/TU Delft

Het aanvullende rapport van TNO/TU Delft naar aanleiding van de peer review is gereed. De implicaties worden kort toegelicht door 5.1.2.e.

In de gebieden waar geen trillingen plaatsvinden, blijkt uit het aanvullende onderzoek dat schade is uit te sluiten. Binnen het gebied met trillingen zijn 2 gebieden aan te wijzen waar mogelijk wel een



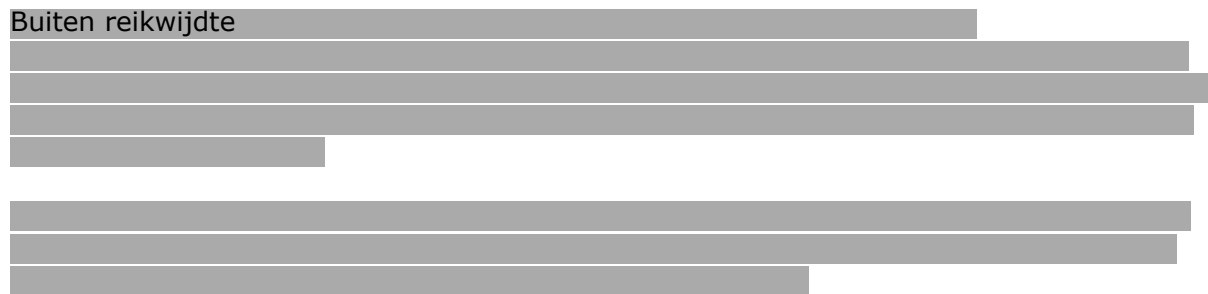
kans op schade is. Aangezien hier al het bewijsvermoeden geldt, wordt de schade die kan ontstaan al meegenomen in de huidige wijze van beoordelen/werken.

EZK wil de peer reviewers de conclusies voorleggen. De betrokken bewonersvereniging zal geïnformeerd worden alvorens het rapport openbaar te maken, met communicatie van de conclusies en de betekenis hiervan.





Buiten reikwijdte



Buiten reikwijdte

